

# INTEGRAL PULSE FREQUENCY MODULATION WITH TECHNOLOGICAL AND BIOLOGICAL APPLICATIONS

Electrical      Howard C. Lee, B.Sc.(Eng.Phys.) (Manitoba), M.Eng.      Ph.D.

## ABSTRACT

The present work is concerned with the theory and applications of integral pulse frequency modulation (IPFM). It essentially comprises three parts. In the first part, IPFM is studied by means of a spectral analysis. Single-signed IPFM is shown to be equivalent to a well-known method of modulation. A general method for spectral analysis of IPFM is developed, and the spectral characteristics of the output pulse train for a class of modulating signals comprising one or more sinusoids are examined in detail. Useful criteria are derived for synthesizing the modulators.

The second part is concerned with the application of IPFM to analogue computation. A method for implementing multipliers using IPFM is formulated and studied. In addition, a method of pulse frequency modulation originally proposed by Goldberg can be represented approximately in terms of single-signed IPFM, and is utilized to implement a divider.

In the third part, single-signed IPFM is used to investigate neural communication in the afferent pathway of the monosynaptic spinal reflex (MSR) in physiological systems. The signal transmission system, comprising many sensory units and neural paths in parallel, is modelled and statistically analyzed. The analysis takes into consideration the distribution of the spindle stretch thresholds, the dispersion of conduction speeds in the afferents, the effects of spatial distribution of synaptic inputs, and the noise introduced by the sensory encoding process. The results of the analysis show that the multiplicity of similar sensory units and of neural paths with different properties, is essential for fidelity of information transmission.

# INTEGRAL PULSE FREQUENCY MODULATION WITH APPLICATIONS

Howard C. Lee, B.Sc. (Eng.Phys.) (Manitoba), M.Eng.

INTEGRAL PULSE FREQUENCY MODULATION  
WITH TECHNOLOGICAL AND BIOLOGICAL APPLICATIONS

by

Howard Chong Lee, B.Sc.(Eng.Phys.) (U. of Man.), M.Eng.

A thesis submitted to the Faculty of Graduate Studies and Research  
in partial fulfillment of the requirements for the degree of  
Doctor of Philosophy.

Department of Electrical Engineering,  
McGill University,  
Montreal, Quebec,

July, 1969.

## ABSTRACT

The present work is concerned with the theory and applications of integral pulse frequency modulation (IPFM). It essentially comprises three parts. In the first part, IPFM is studied by means of a spectral analysis. Single-signed IPFM is shown to be equivalent to a well-known method of modulation. A general method for spectral analysis of IPFM is developed, and the spectral characteristics of the output pulse train for a class of modulating signals comprising one or more sinusoids are examined in detail. Useful criteria are derived for synthesizing the modulators.

The second part is concerned with the application of IPFM to analogue computation. A method for implementing multipliers using IPFM is formulated and studied. In addition, a method of pulse frequency modulation originally proposed by Goldberg can be represented approximately in terms of single-signed IPFM, and is utilized to implement a divider.

In the third part, single-signed IPFM is used to investigate neural communication in the afferent pathway of the monosynaptic spinal reflex (MSR) in physiological systems. The signal transmission system, comprising many sensory units and neural paths in parallel, is modelled and statistically analyzed. The analysis takes into consideration the distribution of the spindle stretch thresholds, the dispersion of conduction speeds in the afferents, the effects of spatial distribution of synaptic inputs, and the noise introduced by the sensory encoding process. The results of the analysis show that the multiplicity of similar sensory units and of neural paths with different properties, is essential for fidelity of information transmission.

## ACKNOWLEDGEMENTS

I wish to express my sincere thanks to Dr. J.H. Milsum for his valuable guidance and encouragement during the research and the writing of this thesis.

I also wish to thank the following :

The J.W. McConnell Foundation for the award of a McConnell Memorial Fellowship ;

Mr. M.J. Korenberg for checking most of the algebra and proof-reading ;

Messrs. D. Cheung, J.C. Chang, M. Cheng and Mrs. J. Brown for assistance in preparing the diagrams ;

Miss C.S. Holland and Mr. R.E. Kearney for proof-reading ;

Dr. C.A. Laszlo for reading part of Chapter IV ;

Mrs. T. Hyland and Miss L. Smith for their excellent work in typing the thesis.

Finally, I wish to express my very special appreciation to my wife, Elaine, for her patience and assistance in preparing this thesis.

This project was supported by the National Research Council and the Medical Research Council of Canada.

TABLE OF CONTENTS

			<u>Page</u>
ABSTRACT			i
ACKNOWLEDGEMENTS			ii
TABLE OF CONTENTS			iii
ABRIDGED LIST OF SYMBOLS			vi
CHAPTER	I	INTRODUCTION	1
	1.1	General Background	1
	1.2	Previous Works Related to Integral Pulse Frequency Modulation	4
	1.3	Outline of the Thesis	5
	1.4	Claim of Contributions	7
CHAPTER	II	FUNDAMENTALS OF INTEGRAL PULSE FREQUENCY MODULATION	9
	2.1	Introduction	9
	2.2	Definitions and Assumptions	9
	2.3	A Functional Model of the Modulator	13
	2.4	The Equivalence of Continuous Pulse Frequency Modulation to S - S IPFM	19
	2.5	Implementation of IPFM	22
	2.6	Demodulation	28
CHAPTER	III	SPECTRAL ANALYSIS OF INTEGRAL PULSE FREQUENCY MODULATION	34
	3.1	Introduction	34
	3.2	Spectral Analysis of Single-Signed Integral Pulse Frequency Modulation	35
	3.2.1	Formulating the Approach	35
	3.2.2	Single-Tone Modulation	40
	3.2.3	Multitone Modulation	51
	3.2.4	Recapitulation	54
	3.3	Synthesis Criteria for S - S IPFM	56
	3.3.1	The Approach	56
	3.3.2	A Synthesis Criterion for Single-Tone Modulation	58
	3.3.3	A Synthesis Criterion for Multi-Tone Modulation	67
	3.4	Double-Signed Integral Pulse Frequency Modulation	74

		<u>Page</u>
	3.4.1	An Approximate Model of the Modulator 74
	3.4.2	Spectral Analysis 75
	3.4.3	Choice of Modulator Threshold 82
	3.5	Discussion and Conclusions 84
CHAPTER	IV	APPLICATION OF INTEGRAL PULSE FREQUENCY MODULATION TO ANALOGUE MULTIPLICATION AND DIVISION 87
	4.1	Introduction 87
	4.2	Multipliers Using IPFM 88
	4.2.1	Theory 88
	4.2.2	Implementation 92
	4.3	Dividers Using Goldberg's PFM 94
	4.3.1	Representation of Goldberg's PFM in Terms of S - S IPFM 96
	4.3.2	Theory and Implementation of the Dividers 99
	4.4	Results of a Computer Simulation Study 102
	4.5	Discussion and Conclusion 105
CHAPTER	V	APPLICATION OF INTEGRAL PULSE FREQUENCY MODULATION TO THE ANALYSIS OF A NEURAL COMMUNICATION SYSTEM 107
	5.1	Introduction 107
	5.2	The Monosynaptic Spinal Reflex 108
	5.3	Information Flow in the Afferent Limb of the Monosynaptic Spinal Reflex 114
	5.4	Modelling the Neural Encoder 117
	5.5	A Model of the Muscle-to-Motoneuron Communication Link 127
	5.6	Statistical Analysis of the Muscle-to-Motoneuron Communication System 134
	5.6.1	Statistical Formulation 134
	5.6.2	The Signal and Noise Components of the "Spatially and Temporally" Summated EPSP 138
	5.6.3	Significance of the Analytical Results 143
	5.6.4	Variation in the Waveform of the Quantal EPSP 154
	5.7	Computer Simulation Study 157
	5.7.1	Method 157
	5.7.2	Results and Discussions 166
	5.8	Discussion and Conclusions 182

CHAPTER	VI	CONCLUSION	188
	6.1	Summary of Results	188
	6.2	Areas for Further Research	192
APPNEDIX	A	AN ALTERNATIVE DERIVATION OF A MATHE- MATICAL EXPRESSION OF THE OUTPUT IMPULSE TRAIN FOR SINGLE-SIGNED INTEGRAL PULSE FREQUENCY MODULATION (S - S IPFM)	196
APPENDIX	B	DERIVATION OF A MODEL FOR THE NEURAL ENCODER FROM A PARTICULAR NEURON MODEL	199
REFERENCES			204

ABRIDGED LIST OF SYMBOLS

$a$	Threshold of the integral pulse frequency modulator.
$A(\omega)$	Amplitude characteristic of the linear element whose impulse responses represent the pulses in the integral pulse frequency modulated pulse train.
$b_i$	A positive constant representing the size of the quantal excitatory postsynaptic potential at the output of the $i^{\text{th}}$ path.
$b$	A random variable corresponding to $b_i$ .
$c_i$	The dynamic gain of $C_i(s)$ at the frequency $\omega_1$ of the sinusoidal component of the change in muscle length.
$c$	A random variable corresponding to $c_i$ .
$C_i(s)$	The transfer function representing the linearized dynamics which relate the change in muscle length to the resulting change of summated generator current in the primary nerve endings of the spindle in the $i^{\text{th}}$ path.
$c_{oi}$	The static gain of $C_i(s)$ .
$c_o$	A random variable corresponding to $c_{oi}$ .

- d Magnitude of the output impulses from the integral pulse frequency modulator.
- $D(k, n), D(k, n_1, \dots, n_M)$   $D(k, n) = \frac{2}{k\omega_0} J_n(\beta)$  is the amplitude of a spectral component in the frequency-modulated sinusoidal carrier  $e_k(t)$  with single-tone modulation ;  $D(k, n_1, \dots, n_M)$  is that with  $M$ -tone modulation.
- D-S IPF Double-signed integral pulse frequency.
- D-S IPFM Double-signed integral pulse frequency modulation.
- $e_k(t)$  A frequency modulated sinusoidal carrier whose derivative is proportional to the  $k^{\text{th}}$  constituent of the noise component in the integral pulse frequency modulated impulse train. See Equations (3-8) to (3-12).
- $E(k, n), E(k, n_1, \dots, n_M)$   $E(k, n)$  is the amplitude of a spectral component in the  $k^{\text{th}}$  constituent  $\mu_k(t)$  of the noise component in the output pulse train of single-signed integral pulse frequency modulation with single-tone modulation ;  $E(k, n_1, \dots, n_M)$  is that with  $M$ -tone modulation.
- EPSP Excitatory postsynaptic potential.
- $E_r(k, n)$   $E(k, n)$  for rectangular output pulses.

FM	Frequency modulated.
h	Height of rectangular pulse.
Im	Imaginary part of.
IPFM	Integral pulse frequency modulation.
$J_n(\beta)$	Bessel function of the first kind with order $n$ and argument $\beta$ .
m	Ratio of the cutoff frequency $\omega_c$ of the low-pass filter and the maximum significant frequency $\omega_{\max}$ of the modulating signal ; $m = \omega_c / \omega_{\max}$ . For single-tone modulation in single-signed IPFM, $m = \omega_c / \omega_1$ where $\omega_1$ is the frequency of the sinusoidal component of the modulating signal.
MSR	Monosynaptic spinal reflex.
MN	Motoneuron.
$N(t)$	Noise component.
$N_{1 \min}, N'_{1 \min}$	$N_{1 \min}$ is a positive number related to the minimum significant frequency of the noise component for single-tone modulation in single-signed IPFM. It is given by Equation (3-70) for $k = 1$ . $N'_{1 \min}$ is that for multitone modulation.

$q_i$	The increase of the summated generator current in the primary nerve endings of the spindle in the $i^{\text{th}}$ path due to constant $\gamma$ -efferent activity.
$q$	A random variable corresponding to $q_i$ .
$P_2(t)$	Quantizer output.
$P(s)$	Transfer function of a linear system whose impulse response is the output pulse in IPFM.
$Q(\omega)$	The phase characteristic of $P(s)$ .
$\text{Re}$	Real part of .
S-S IPF	Single-signed integral pulse frequency.
S-S IPFM	Single-signed integral pulse frequency modulation.
$S(t)$	Signal component.
$t_i$	Emission time of $i^{\text{th}}$ pulse ; $t_0 = 0$ .
$U$	Amplitude of sinusoidal component in the modulating signal.
$X_0$	The biasing constant in the modulating signal of S-S IPFM. Also a constant representing average stretch of muscle length.

$x(t)$ 

Modulating signal in integral pulse frequency modulation,  
i.e. input of the modulator.

 $x^*(t)$ 

Output pulse train.

 $z(t)$ 

$$z(t) = \int_0^t x(t) dt .$$

 $\alpha$ -MN

$\alpha$ - motoneuron.

 $\beta$ 

Modulating index:  $\beta = \frac{k\omega_o U}{\omega_1} = \frac{k2\pi}{\omega_1} \cdot \frac{U}{a}$  ,

$$\beta_1 = \frac{\omega_o U}{\omega_1}$$

$$\beta_m = \frac{k\omega_o U}{\omega_m} .$$

 $\gamma_1$ 

$\gamma_1 = k\omega_o X_o + n\omega_1$  , spectral frequency of the noise component in single-tone modulation.

 $\gamma_M$ 

Spectral frequency of the noise component in  $M$ -tone modulation.

 $\theta$ 

Phase angle of sinusoidal component in the modulating signal.

 $\theta_i, \theta$ 

Phase angle of  $C_i(s)$  at the frequency  $\omega_1$  where  $C_i(s)$  is the transfer function representing the linearized dynamics relating the change in muscle length and the resulting change of summated generator current in the

primary nerve endings of the spindle in the  $i^{\text{th}}$  path.  $\theta$  is the corresponding random variable.

$\mu_k(t), \mu_{Mk}(t), \mu_{rMk}(t)$

A constituent of the noise component in the output pulse train.

$\tau$

Pulse width ; dummy variable .

$\tau_i, \tau$

The transmission time from spindle to the pulse generating site of the  $\alpha$ -motoneuron ; for the  $i^{\text{th}}$  path ;  $\tau$  is the corresponding random variable.

$\varphi_1$

Phase angle ;  $\varphi_1 = n\theta - \beta \sin \theta$

$\Phi_x(j\omega)$

Characteristic function of the probability density of the random variable  $x$  .

$\omega_0$

$\omega_0 = 2\pi/a$  , where  $a$  is the threshold of the modulator.

$\omega_1$

Angular frequency of the sinusoidal component in the modulating signal. It is also the angular frequency of the sinusoidal change in muscle length.

$\omega_m$

Angular frequency of a sinusoidal component in a multitone signal.

## CHAPTER 1

### INTRODUCTION

#### 1.1 General Background

Signals in many communication and control systems are in the form of a pulse sequence. This form of the signal may either be used to gain technical and economical advantages, or arise as a result of the intrinsic properties of the system. Thus pulses of fixed size and shape have been employed to overcome the problem of noise accumulation in long distance communications, while the neural pulses in biological systems constitute a naturally evolved intrinsic method of information transmission.

There are numerous methods for representing a message by a pulse train.<sup>1,2</sup> However, they can be grouped into two basic categories, depending on whether the pulses are synchronous or asynchronous. While synchronous methods are generally popular in engineering applications, asynchronous methods have been preferred in some specialized systems, and furthermore seem to have been generally favoured by nature. In particular, one class of asynchronous methods called pulse frequency modulation has been applied to investigations in telemetry, automatic control, bio-electronics, and physiology by an increasing number of workers.<sup>4-26</sup> The present thesis is concerned with the theory and applications of one particular type of pulse frequency modulation.

By pulse frequency modulation (PFM), we mean the class of methods which convert a message signal into a train of pulses having identical size and shape but possibly different signs; further, the pulse frequency which is defined as the inverse of the spacing between adjacent pulses, is varied as some function of the signal magnitude.

Several schemes of PFM have been proposed in the literature. In one of the earlier schemes, the pulse train is derived from a frequency modulated continuous carrier. The message signal first modulates a sinusoidal wave and then a standard pulse is generated for each complete oscillation of the modulated carrier. This method has been known in the literature as "pulse frequency modulation" or "continuous pulse frequency modulation".<sup>1-3</sup> To avoid confusion with the term defined in the previous paragraph, we shall call this particular scheme "continuous pulse frequency modulation" (CPFM). In CPFM, the deviation from the unmodulated carrier frequency is approximately proportional to the magnitude of the message signal.

Another scheme was proposed earlier by Goldberg.<sup>27,28</sup> In this method, the modulating signal is first made positive by a fixed bias and then compared with a positive ramp signal having a pre-specified slope. When the two signals are equal, a standard pulse is emitted and the ramp is reset to zero at the same instant. Then the whole process is repeated. The pulse frequency of the train produced by this method is inversely proportional to the sampled signal magnitude.

Recently, a simple but interesting scheme called integral pulse frequency modulation (IPFM) was proposed by Li and Meyer.<sup>8,9</sup> In this method, a pulse is initiated at the instant  $t_1$  when the magnitude of the time integral of the modulating signal reaches a pre-specified threshold value. The sign of the pulse is the sign of the integral at  $t_1$ . After the pulse has been initiated, the integrator is reset to zero and the whole process is repeated. The resulting pulse train is "in phase" with the modulating signal in the sense that both the pulse and the modulating signal have the same sign at the pulse emission time. Usually the pulse frequency is approximately proportional to the modulating signal magnitude.

The invention of IPFM has motivated the proposal of three other schemes of pulse frequency modulation (PFM). In Clark's method, the interval between pulses is determined by the instantaneous value of the modulating signal at the beginning of the pulse just prior to the interval under consideration.<sup>13</sup> In fact, the pulse frequency is made linearly proportional to the sampled signal magnitude. The other two schemes are generalizations of IPFM. One of them was proposed by Pavlidis, and is called sigma pulse frequency modulation ( $\Sigma$ PFM).<sup>16</sup> In one version of this scheme, the integrator in IPFM is replaced by a first order time-invariant low-pass filter so that a pulse is emitted when the output of the filter reaches a pre-specified threshold value. The third method, proposed by Blanchard, is a further generalization called functional pulse frequency modulation (FPFM).<sup>18</sup> In this method, the modulator emits a pulse when a functional of the modulating signal reaches the threshold value. The frequency of the pulse train produced by these latter two schemes is in general a nonlinear dynamic function of the modulating signal.

From among the schemes of PFM described above, integral pulse frequency modulation (IPFM) appears to possess the greatest number of valuable properties. Its modulator and demodulator are simple to implement. It has good immunity against both input and channel noises. It combines some of the better features of pulse code modulation with the analogue features of frequency modulation. It can easily encode both discrete and continuous input signals. It tends to reduce redundancy in the sense that a pulse is emitted only when that is necessary. In addition to these properties which are valuable for engineering applications in communication and control systems, IPFM has other important characteristics which are useful for biological investigations: As a very important parti-

cular case, single - signed IPFM is functionally similar to neural pulse modulation in neuro-physiological systems. In comparison with the other PFM schemes, IPFM is more versatile than both CPFM and the schemes proposed by Goldberg and Clark. In comparison with  $\Sigma$ PFM and FPFM, it is less sophisticated than these latter for modelling neural elements, but is mathematically more tractable than the generalized schemes. Thus, IPFM is a simple but versatile method of asynchronous pulse modulation. Its importance for engineering and biological investigations is evidenced by the number of works reported in the literature. In the present thesis, IPFM is analyzed and applied to both engineering and neuro-physiological investigations.

## 1.2 Previous Works Related to Integral Pulse Frequency Modulation

Integral pulse frequency modulation (IPFM) was first defined in 1959 by Li and Meyer as a result of search for a suitable model of the pulse-generating mechanism in sensory receptors of the nervous system.<sup>22</sup> It was subsequently incorporated into linear feedback control systems. Li<sup>8</sup> and recently Blanchard and Jury<sup>17,18</sup> have analyzed the stability of such systems, while Meyer<sup>9</sup> has established the existence and characteristics of various types of sustained oscillations in them. Farrenkopf et al have applied IPFM to attitude control of space craft and found it superior to certain other common on-off control schemes.<sup>10</sup> Ciscato and Mariani have used it to accomplish adaptive sampling, thereby improving signal sampling efficiency.<sup>11</sup>

IPFM has also been investigated as a method of information transmission. Li has studied the "approximate frequency response" (i.e. describing functions) of the

modulator and examined the effect of Gaussian channel noise on the output pulse train.<sup>8</sup> Recently, Blanchard,<sup>18</sup> and Bombi and Ciscato<sup>19</sup> have investigated the input noise filtering properties of the modulator. For demodulation, Li has proposed the use of a time-invariant low-pass filter,<sup>8</sup> and Blanchard has suggested the use of a Lagrangian interpolation method as an alternative.<sup>18</sup>

In addition to these engineering investigations, IPFM has been applied to the study of physiological systems. Li and Jones have analyzed feedback systems which simulated the basic dynamic structure of reciprocal innervation in neuro-muscular systems.<sup>8,23</sup> Partridge has studied the frequency response of the muscle by stimulating its efferent nerve with a pulse train from an integral pulse frequency modulator.<sup>25</sup> Furthermore, assuming single-signed IPFM as the actual neural pulse generating mechanism, Partridge has also investigated signal distortion introduced by the neural encoding process,<sup>24</sup> while more recently, Bayly has examined the spectral characteristics of pulse frequency modulation in the nervous system.<sup>26</sup>

### 1.3 Outline of the Thesis

In Chapter II, some of the fundamentals of integral pulse frequency (IPFM) are reviewed and re-examined. IPFM is here precisely defined and the validity of a functional model of the modulator is established. Continuous pulse frequency modulation (CPFM) is then shown to be equivalent to single-signed integral pulse frequency modulation (S - S IPFM). A new and versatile method for hardware implementation of IPFM is presented. Then, demodulation using analogue and digital filters is discussed.

In Chapter III, IPFM is studied by means of a spectral analysis. A general method for spectral analysis of S - S IPFM is developed. The spectral characteristics of pulse trains produced by modulating signals comprising one or more sinusoids are examined in detail. Then, by using the results obtained, useful criteria for synthesizing the modulator are derived. Finally, the spectral characteristics of a pulse train produced by double-signed IPFM are examined in detail, and the results are utilized to derive a criterion for selecting the modulator threshold.

Chapter IV is concerned with the application of IPFM to analogue computation. A method for implementing multipliers using IPFM is formulated and studied. The method of pulse frequency modulation originally proposed by Goldberg is shown to be representable by an S - S IPFM model, and is then used to formulate a method of analogue division. Lastly, the results of a computer simulation study are shown to verify the feasibility of the proposed methods.

In Chapter V, S - S IPFM is used to investigate the functional significance of the multiplicity of sensory units and neural paths employed in peripheral neural communication in physiological systems. In particular, the transmission of signals in the afferent limb of the monosynaptic spinal reflex (MSR) of the neuro-muscular system is examined for the present purpose. The pertinent features of the MSR are first briefly reviewed. Then, the afferent limb of the MSR is modelled and statistically analyzed, taking into consideration the variations of properties in the multiplicity of neural elements and paths. Finally, the results of a computer simulation study are presented and discussed.

Lastly, Chapter VI concludes with a summary of the main results. Areas for further research are suggested and briefly discussed.

#### 1.4 Claim of Contributions

In the author's belief, the present work contributes knowledge to both engineering and physiology. The major contributions claimed are :

1. Single-signed integral pulse frequency modulation (S - S IPFM) is shown to be equivalent to continuous pulse frequency modulation (CPFM). This demonstration effectively broadens the knowledge of IPFM in the sense that what is known about CPFM is applicable to S - S IPFM, and vice versa. (Chapter II).
2. A general method for the spectral analysis of integral pulse frequency modulation (IPFM) is developed. In particular, the analysis presented in the present work makes possible a better understanding of the information transfer characteristics of IPFM. Useful criteria are derived for synthesizing the modulators. (Chapter III).
3. A method for implementing analogue multipliers is formulated using IPFM. Goldberg's method of pulse frequency modulation

is shown to be approximately representable in terms of S - S IPFM, and is utilized to implement an analogue divider. (Chapter IV).

4. The functional significance of the multiplicity of sensory units and neural paths employed in peripheral neural communication in physiological systems is established through a statistical study of the afferent limb of the monosynaptic spinal reflex (MSR). In particular, it is shown that the variation in the transmission times of the afferent paths, plus subsequent summation of afferent pulse trains in the  $\alpha$  - motoneuron, together constitute a low-pass filter whose characteristic is needed for accurate demodulation. In general, the multiplicity of similar sensory units and of neural paths with different properties is found to be essential for fidelity of information transmission. (Chapter V) .

## CHAPTER II

### FUNDAMENTALS OF INTEGRAL PULSE FREQUENCY MODULATION

#### 2.1 Introduction

The fundamentals of integral pulse frequency modulation (IPFM) essential for subsequent analyses are presented in this chapter. We shall define IPFM precisely and state the assumptions. A functional model of the modulator will be described and then shown to be an exact representation of the modulator input - output relations. This model will be used for subsequent analyses throughout the present work. We shall show next that continuous pulse frequency modulation (CPFM) is equivalent to a particular subclass of IPFM, namely, the single-signed IPFM. Although both IPFM and CPFM have been known for more than nine years, it appears that this equivalence has not been established before. A new and versatile method for implementing the integral pulse frequency (IPF) modulator will then be described. This method is similar to the generation of neural pulses in the nervous system. Finally, demodulation of IPFM using analogue and digital filters will be discussed.

#### 2.2 Definitions and Assumptions

Recently several types of modified integral pulse frequency modulation (IPFM) have been discussed in the literature.<sup>19,24</sup> However, they appear to have rather restricted applications and are little different from the unmodified version originally defined by Li and Meyer.<sup>8,9</sup> Thus, these modified IPFM will not be considered in the present work. In the following, we shall be concerned only with the well-known unmodified version defined below.

IPFM is defined as the encoding process which converts a bounded integrable signal  $x(t)$  into a pulse train with the following properties :

1. If the pulses are numbered sequentially by the positive integers,  $i = 1, 2, 3, \dots$ , then the emission time  $t_i$  of the  $i$ th pulse is determined by the criterion

$$\left| l(i-1, i) \right| \equiv \left| \int_{t_{i-1}}^{t_i} x(t) dt \right| = a \quad (2-1)$$

$i=1, 2, 3, \dots$

where  $t_0 = 0$  and "a" is a pre-specified positive constant called the modulator threshold. The input signal  $x(t)$  is assumed integrable for all intervals  $(t_{i-1}, t_i)$ .

2. The sign  $q_i$  of the  $i$ th pulse is the sign of  $l(i-1, i)$ .
3. The  $i$ th pulse is completely characterized by  $q_i p(t-t_i)$  where  $p(t)$  is a pre-specified function describing the pulse shape and size. For  $\tau > 0$ ,

$$p(t) \neq 0, \quad 0 \leq t \leq \tau$$

$$\equiv 0, \quad \text{otherwise .}$$

If the pulse is an impulse of strength  $d$ , then  $p(t) = d \cdot U_0(t)$  where  $U_0(t)$  is the unit - impulse function. We will call " $\tau$ " the pulse width and  $p(t)$  the "pulse - shape function".

4. The pulses do not overlap. This condition implies that the pulse width is less than the minimum possible  $(t_i - t_{i-1})$  for all  $i$ . The assumption that the input signal is bounded makes it always possible to fulfill this condition.

The encoding process defined above is illustrated in Figure 2-1. The modulator has the input signal  $x(t)$  and the output pulse train  $x^*(t)$ . The output pulse has been assumed to be rectangular. The modulating signal  $x(t)$  is integrated, with the initial condition of the integrator set to zero at  $t = 0$ . When the absolute value of the integral  $I(t)$  reaches the pre-specified threshold value  $a$  at time  $t_1$ , the modulator emits at this time a pulse. The sign of the pulse is the sign of the integral at  $t_1$  (which is positive in this example). At the instant when the pulse is initiated, the integrator is reset to zero. Then the whole cycle is repeated.

When the output of the modulator consists of both positive and negative pulses as shown in Figure 2-1, the modulation is known as double-signed IPFM (D-S IPFM). When the output contains pulses with one sign only, the modulation is called single-signed IPFM (S-S IPFM). To achieve D-S IPFM, the input  $x(t)$  of the modulator must have both positive and negative values. On the other hand, to achieve S-S IPFM, it is necessary that either  $I(i-1, i) = a$  or  $I(i-1, i) = -a$  for all  $i$ . To satisfy this requirement, it is sufficient, although not necessary, that either  $x(t) \geq 0$  or  $x(t) \leq 0$  for all  $t$ . Hence, a message signal with both positive and negative values can be encoded by S-S IPFM provided a suitable biasing constant is added.

In defining integral pulse frequency modulation (IPFM) we have assumed that the modulating signal is bounded and integrable in any finite interval. Thus signals containing impulse functions are not allowed. However, the modulating signal can be either continuous or piece-wise continuous. As an example, the input can be rectangular pulses, provided the modulator threshold  $a$  and the output pulse shape are so chosen that the output pulses do not overlap.

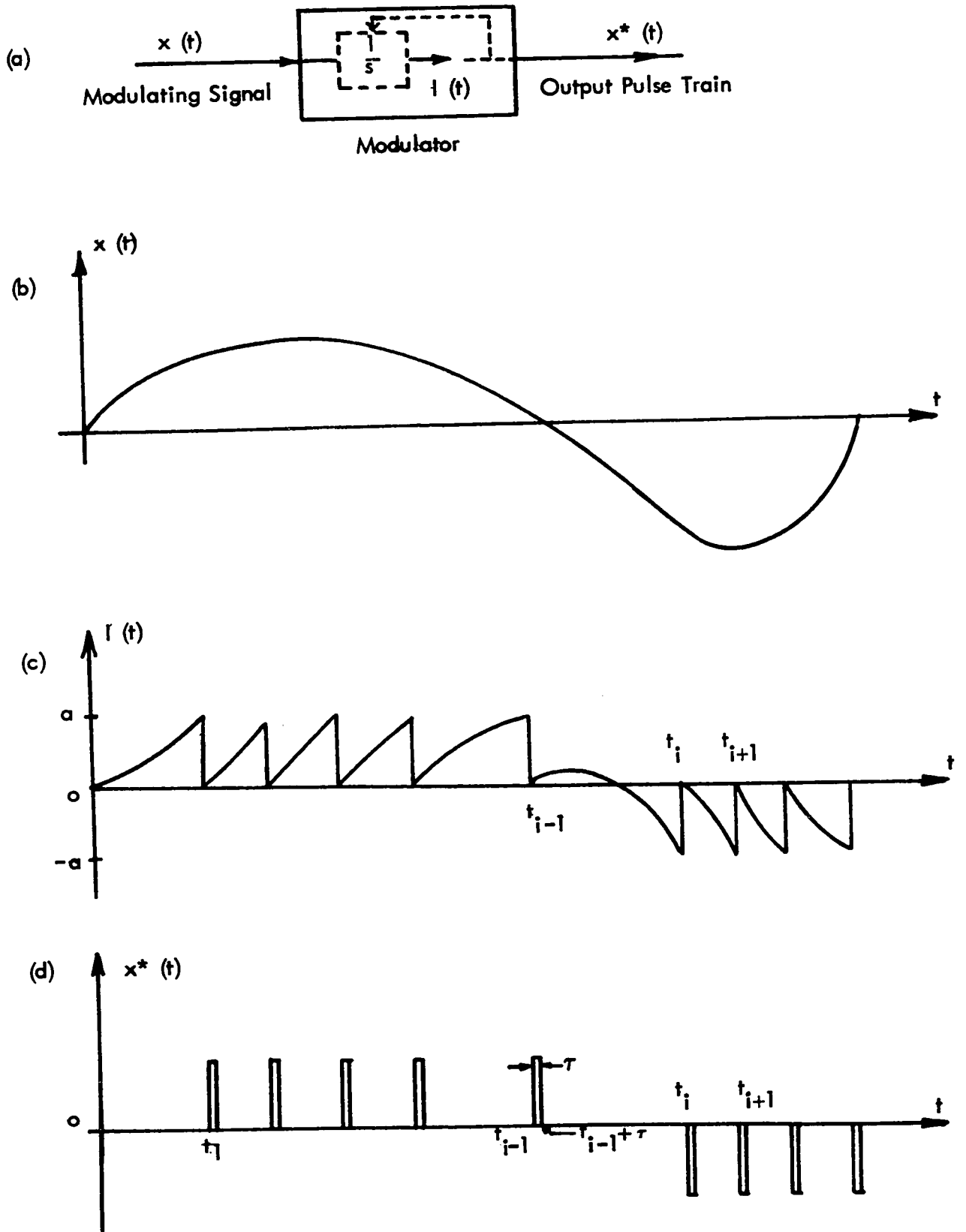


FIGURE 2-1. ILLUSTRATING THE PROCESS OF INTEGRAL PULSE FREQUENCY MODULATION. (IPFM).

Furthermore, we should note that all output pulses have the same pre-specified shape and size described by a given function  $p(t)$ . Hence, the output of the modulator is completely characterized by the sequence of pulse emission times  $t_1, t_2, \dots, t_i, \dots$ , and the sequence of pulse signs  $q_1, q_2, \dots, q_i, \dots$ . In the next section, we shall use this fact to show that the modulator can be represented exactly by a functional model.

### 2.3 A Functional Model of the Modulator

In order to facilitate analysis, it is desirable to represent the input - output relations of the integral pulse frequency (IPF) modulator by a model. We shall call such a model a "functional model".

A functional model of the IPF modulator is shown in Figure 2-2. It is essentially Meyer's "equivalent network",<sup>9</sup> and comprises an integrator, a uniform quantizer with hysteresis, a differentiator, and a linear system described by a transfer function  $P(s)$ . The transfer characteristic of the quantizer is shown in Figure 2-3. The quan-

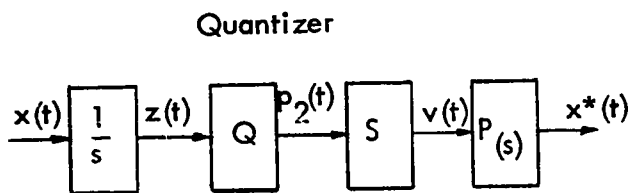


FIGURE 2-2. A FUNCTIONAL MODEL OF THE INTEGRAL PULSE FREQUENCY (IPF) MODULATOR.

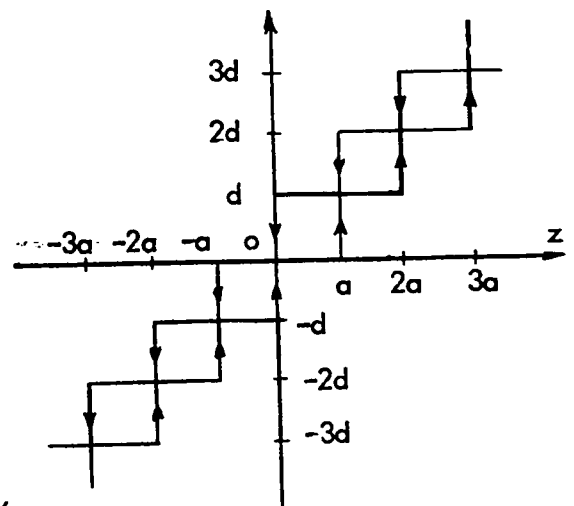


FIGURE 2-3. TRANSFER CHARACTERISTIC OF THE QUANTIZER Q WITH HYSTERESIS.

tizing level  $a$  is equal to the modulator threshold. The arrows in the transfer characteristic indicate the only paths along which  $p_2$  can vary as  $z$  is changed. When  $z$  is increasing,  $p_2$  can increase from one discrete value to another only by following the upward arrows. When  $z$  is decreasing,  $p_2$  can decrease from one discrete value to another only by following the downward arrows. Thus the quantizer converts  $z(t)$  into a staircase function  $p_2(t)$  with uniform step size  $d$ . When  $p_2(t)$  is differentiated by the differentiator, a train of impulses with equal strength  $d$  is produced. Consequently, the output of the modulator is a train of pulses with identical size and shape specified by the impulse response of the linear system  $P(s)$  and the impulse strength  $d$ . An example of the signals at various points in the block diagram of the model (Figure 2-2) is shown in Figure 2-4. Note that at any instant  $t_i$  when an impulse is generated by differentiating the step function, the integrator output  $z(t_i)$  is necessarily equal to  $ma$ , where  $m$  is an integer.

Since the functional model will be used as a basic tool for analysis throughout the present work, we shall now show that the model exactly represents the input - output relations of the IPF modulator. We shall achieve this objective by proving that both the modulator and its model have exactly the same output for the same arbitrary bounded integrable input signal.

It has been pointed out in the previous section that for a given pulse-shape function  $p(t)$  known a priori, the output of the modulator is completely characterized by the pulse emission times  $t_i$  and their signs  $q_i$ ,  $i = 1, 2, 3, \dots$ . Hence, assuming that the model's output pulse shape and size can be made identical to  $p(t)$  by appropriate choice of  $d$  and  $P(s)$ , both the modulator and the model will have the same output, pro-

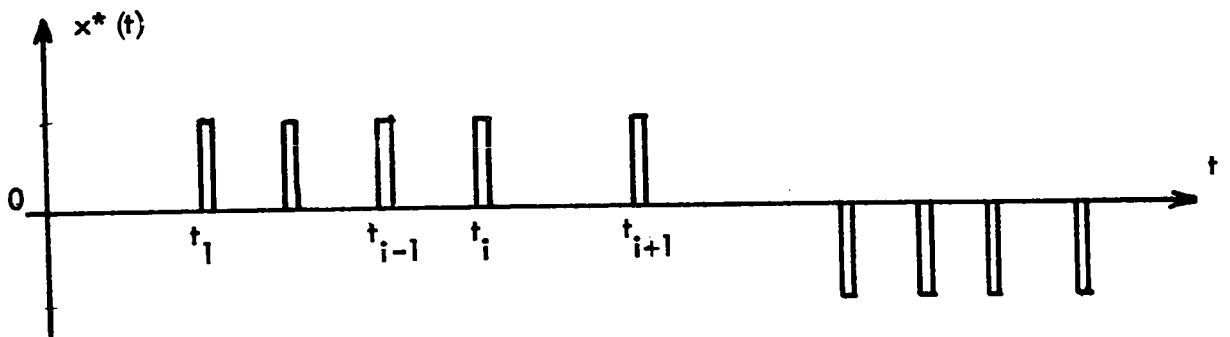
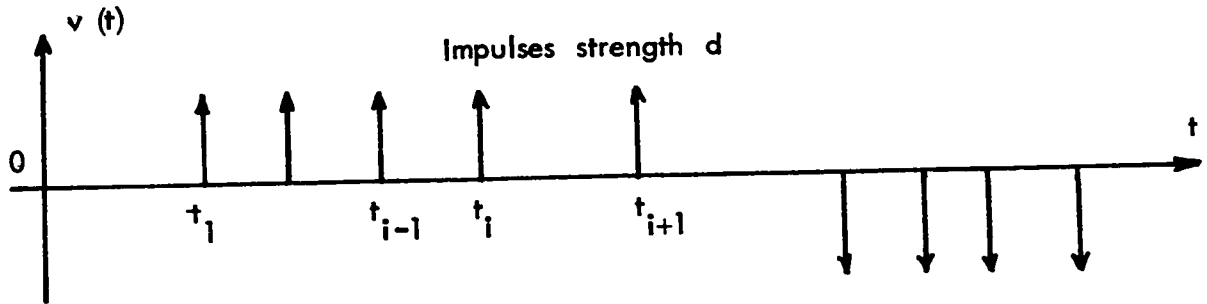
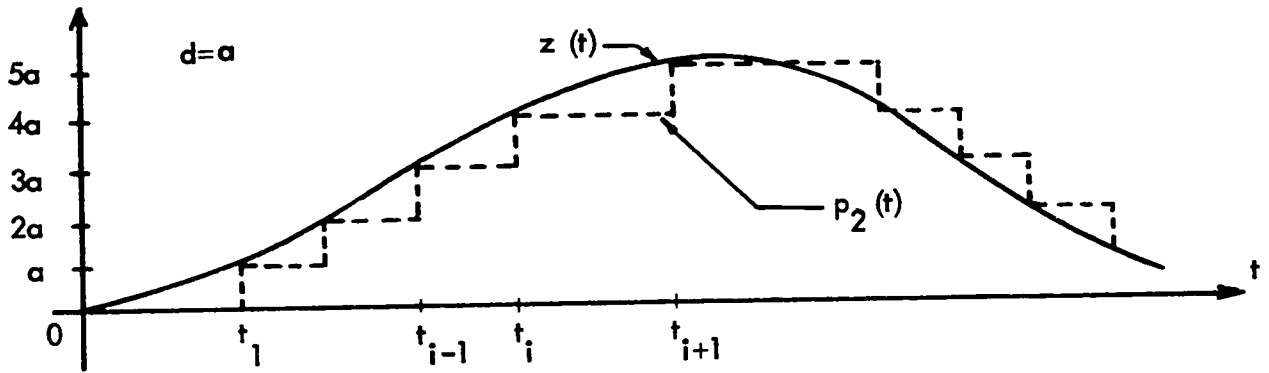
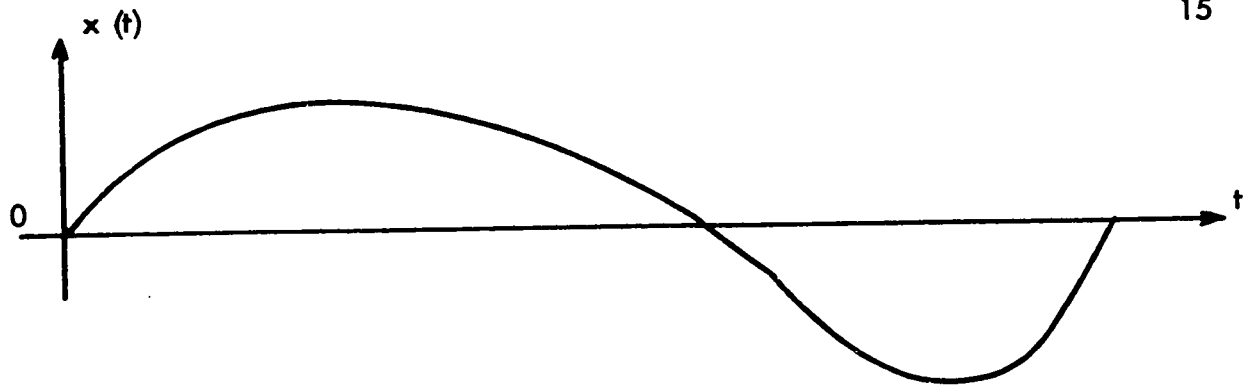


FIGURE 2-4. SIGNALS AT VARIOUS POINTS IN THE FUNCTIONAL MODEL OF THE MODULATOR.

vided they both emit pulses of the same polarity at the same instant of time. Thus, we proceed as follows.

Let  $x(t)$  be an arbitrary bounded integrable modulating signal applied to the modulator and its model at  $t = 0$ . Then, by definition, the modulator will emit its first pulse at  $t = t_1$  when

$$\left| I(0, 1) \right| = \left| \int_0^{t_1} x(t) dt \right| = a.$$

The pulse is positive if  $I(0, 1) = a$ , or negative if  $I(0, 1) = -a$ . Now, let the pulse emission time of the model be defined as the instant at which the impulse is applied to the linear system  $P(s)$ . As specified by the transfer characteristic of the quantizer,  $p_2(t)$  will change by a step  $d$  when the integrator output  $z(t)$  reaches either the value  $a$  or the value  $-a$  from the zero initial value. An impulse is generated by the differentiator at the instant when the step occurs. Hence, the model will emit its first impulse and thus its first pulse at  $t_1'$  when

$$\left| z(t_1') \right| = \left| \int_0^{t_1'} x(t) dt \right| = a.$$

Since the sign of the impulse is the sign of the step change, the output pulse is positive if  $z(t_1') = a$ , or negative if  $z(t_1') = -a$ . Clearly,  $z(t_1') = I(0, 1)$  and thus  $t_1' = t_1$  for both positive and negative pulses. Therefore, both the modulator and its model emit the first pulse with the same sign at the same instant of time.

The coincidence of all subsequent pulses can be similarly proven. Thus let us assume, for the present, that both the modulator and its model emit the  $(i-1)$ th pulse

at  $t_{i-1}$ . By definition the  $i$ th pulse will be emitted by the modulator at  $t_i$  when Equation (2-1) is satisfied. The pulse is positive if  $l(i-1, i) = a$ , or negative if  $l(i-1, i) = -a$ . Since the model also emits a pulse at  $t_{i-1}$ , as pointed out above we must have  $z(t_{i-1}) = m a$ , where  $m$  is an integer. Hence,  $p_2(t)$  will change by a step when  $z(t)$  reaches either the value  $ma + a$  or the value  $ma - a$ . And thus the model will emit the  $i$ th pulse at  $t_i'$  when

$$z(t_i') = ma \pm a$$

$$\text{i.e. } \left| z(t_i') - z(t_{i-1}') \right| = a \quad (2-2)$$

Since  $z(t) = \int_0^t x(t) dt$ , Equation (2-2) can be re-written as

$$\left| \int_{t_{i-1}'}^{t_i'} x(t) dt \right| = a \quad (2-3)$$

The pulse is positive if the step change in  $p_2(t)$  is positive, that is, if  $z(t_i') - z(t_{i-1}') = a$ . Otherwise, the pulse is negative. Keeping this point in mind and comparing Equation (2-3) with Equation (2-1), we have  $t_i' = t_i$  for both the positive and the negative pulses. Therefore, both the modulator and its model emit the  $i$ th pulse with the same polarity at the same instant  $t_i$ , provided that they have emitted the  $(i-1)$ th pulses coincidentally. Since their first pulses have been shown to be coincident, the output pulse train of the model must coincide with that of the modulator. Therefore, the modulator and its model have identical output for any arbitrary bounded integrable input signal. That is, the functional model shown in Figure 2-2 represents exactly the input - output relations of the modulator.

We have assumed in the above proof that the output pulse shape and size can be matched exactly by appropriate choice of the parameter  $d$  and the linear system  $P(s)$  in the model. Clearly we can choose  $d$  and  $P(s)$  independently without affecting the sign and emission time of the pulse. Hence, the above assumption is valid, provided the pulse-shape function  $p(t)$  can be considered as the impulse response of a linear system.

The model shown in Figure 2-2 is applicable for both D-S IPFM and S-S IPFM, but can be simplified if the modulation is single-signed. For this case,  $z(t)$  is a monotonic function of time because either  $x(t) \geq 0$  or  $x(t) \leq 0$  for all  $t \geq 0$ . Hence  $z(t)$  traverses either the upward or the downward path of the quantizer transfer characteristic only. This simplified model for S-S IPFM with positive pulses is shown in Figure 2-5.

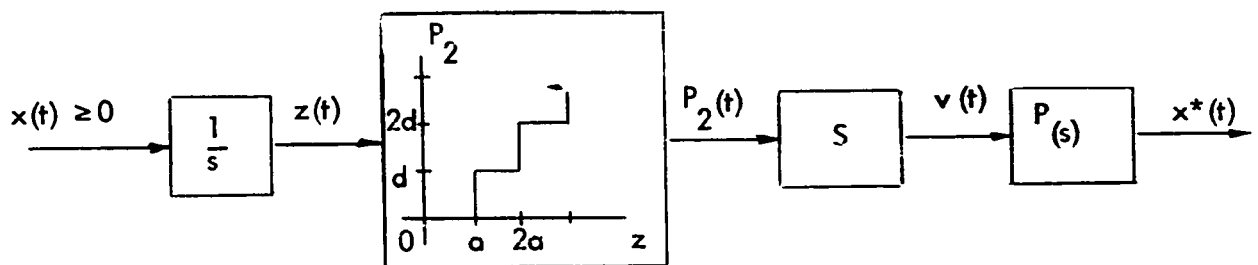


FIGURE 2-5. A MODEL FOR THE SINGLE-SIGNED INTEGRAL PULSE FREQUENCY (S-S IPF) MODULATOR.

Concerning the block diagram of the model, we should emphasize that the diagram is used only for analysis and it should not be confused with the actual implementation of IPFM. Clearly, it is not feasible to implement S-S IPFM using Figure 2-5

directly since both the integrator and the quantizer must theoretically have infinite dynamic range. Methods of implementation will be described in Section 2.5 after we establish the equivalence of continuous pulse frequency modulation to S - S IPFM in the next section.

#### 2.4 The Equivalence of Continuous Pulse Frequency Modulation (CPFM) to S - S IPFM

It was pointed out in Section 2.2 that a necessary condition for achieving single-signed integral pulse frequency modulation (S - S IPFM) is that either

$$\int_{t_{i-1}}^{t_i} x(t) dt \geq 0$$

or

$$\int_{t_{i-1}}^{t_i} x(t) dt \leq 0$$

for all  $i$ . This condition is sufficiently satisfied provided either  $x(t) \geq 0$  or  $x(t) \leq 0$  for all  $t \geq 0$ . The input signal can be represented as a sum of two components. That is, for a modulator emitting positive output pulses, we have

$$x(t) = X_0 + f(t) \geq 0 \quad (2-4)$$

where  $X_0$  is a positive constant and  $f(t)$  is a function of time with both positive and negative values. Without loss of generality, we define  $X_0$  as a biasing constant added to a message signal  $f(t)$ . Substituting Equation (2-4) into Equation (2-1) and noting that in this case the integral is always non-negative, we have the following criterion for pulse

emission in S - S IPFM :

$$\int_{t_{i-1}}^{t_i} (X_o + f(t)) dt = a. \quad (2-5)$$

The pulse emission times  $t_i$ ,  $i = 1, 2, 3, \dots$ , determined from this relation completely characterize the output of the modulator, since the output pulses are all positive and the pulse-shape function is known a priori.

We have stated earlier that a method of asynchronous pulse modulation known as "continuous pulse frequency modulation" (CPFM) or "pulse frequency modulation"<sup>1-3</sup> can be shown to be equivalent to S - S IPFM. In CPFM, a pulse train is derived from a sinusoidal carrier which has been frequency modulated by the message signal. The pulse train is produced by generating a standard pulse for each complete oscillation of the modulated carrier. We now show the equivalence of CPFM to S - S IPFM as follows.

Let the message signal  $f(t)$  in S - S IPFM be the input to the analogue frequency modulator at  $t = 0$ . Then, the modulated sinusoidal carrier is given by<sup>2</sup>

$$e(t) = E \sin(\omega_c t + C_o + b \int_0^t f(t) dt), \quad (2-6)$$

where  $E$ ,  $C_o$ ,  $\omega_c$ , and  $b$  are constants.  $E$  and  $C_o$  are respectively the amplitude and the initial phase angle of the carrier, while  $\omega_c$  is the unmodulated carrier frequency.

Equation (2-6) can be re-written as

$$\begin{aligned} e(t) &= E \sin \left[ \int_0^t (\omega_c + bf(t)) dt + C_o \right] \\ &= E \cos C_o \cdot \sin \left[ \int_0^t (\omega_c + bf(t)) dt \right] \\ &\quad + E \sin C_o \cdot \cos \left[ \int_0^t (\omega_c + bf(t)) dt \right]. \end{aligned} \quad (2-7)$$

If a standard pulse is generated when  $e(t) = E \sin C_0$  for each complete oscillation of the modulated carrier  $e(t)$ , the  $i$ th pulse will be emitted at  $t_i$  when

$$\int_0^{t_i} (\omega_c + bf(t)) dt = i 2\pi, \quad (2-8)$$

$$i = 1, 2, 3, \dots$$

Let  $t_{i-1}$  be the emission time of the  $(i-1)$ th pulse. Then, Equation (2-8) can be re-written in the format of Equation (2-5). Thus

$$\begin{aligned} \int_{t_{i-1}}^{t_i} (\omega_c + bf(t)) dt &= i 2\pi - \int_0^{t_{i-1}} (\omega_c + bf(t)) dt \\ &= i 2\pi - (i-1) 2\pi = 2\pi. \end{aligned}$$

$$\text{i.e.} \quad \int_{t_{i-1}}^{t_i} \left( \frac{\omega_c}{b} + f(t) \right) dt = \frac{2\pi}{b}. \quad (2-9)$$

Equation (2-9) is the criterion for pulse emission in CPFM. If  $\omega_c$  and  $b$  are so chosen such that  $\frac{\omega_c}{b} = X_0$  and  $\frac{2\pi}{b} = a$ , Equations (2-9) and (2-5) become identical. Therefore, for these values of the modulator parameters, the pulse emission times in CPFM are identical to those in S-S IPFM. Consequently, CPFM is equivalent to S-S IPFM.

Although CPFM and IPFM have been known since the 1940's and 1959 respectively, it appears that the equivalence of CPFM to S-S IPFM has not been established before. This demonstration effectively broadens the knowledge on IPFM in the sense that what is known about CPFM is applicable to S-S IPFM and vice versa. Furthermore, knowledge of this equivalence will hopefully prevent repetition of past work occurring in future.

## 2.5 Implementation of IPFM

Integral pulse frequency modulation (IPFM) can be implemented in a variety of ways. A method using analogue computer hardware has been described by Li.<sup>8</sup> Implementation by electronic hardware can be accomplished using the method of continuous pulse frequency modulation described in the previous section. In addition, Inose and Yasuda have proposed an electronic encoder which implements S - S IPFM approximately.<sup>29</sup> Another approach to implementing IPFM is to use incremental encoders. As an example, the shaft speed of a motor can be encoded into a train of identical pulses using an incremental tachometer. Referring to Figure 2-2, the shaft speed is the modulating signal  $x(t)$ , the shaft position is the output  $z(t)$  of the integrator, and the incremental encoder corresponds to the remainder of the block diagram. In the following, we shall describe a new and versatile method which resembles neural pulse generation.

The feedback system shown in Figure 2-6 is proposed for implementing S - S IPFM. This system will be extended later to implement D - S IPFM. The modulator can be constructed using common electronic hardware components. It requires only two amplifiers, one integrator, one comparator such as the Schmitt trigger, and one pulse generator such as the monostable multi-vibrator.

The operation of the modulator is illustrated in Figure 2-7. The modulating signal  $x(t)$  is applied at  $t = 0$ , with all other signals in the system initially set to zero. Until the first pulse is emitted, the output of the integrator is

$$I(t) = \int_0^t K_1 x(t) dt .$$

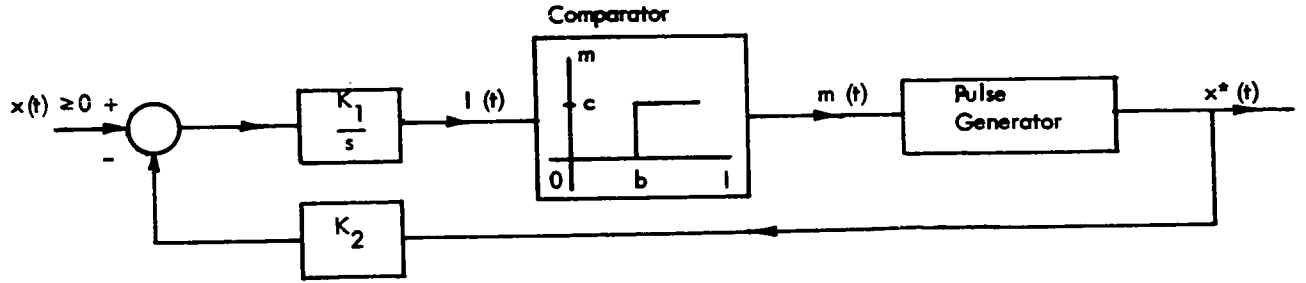
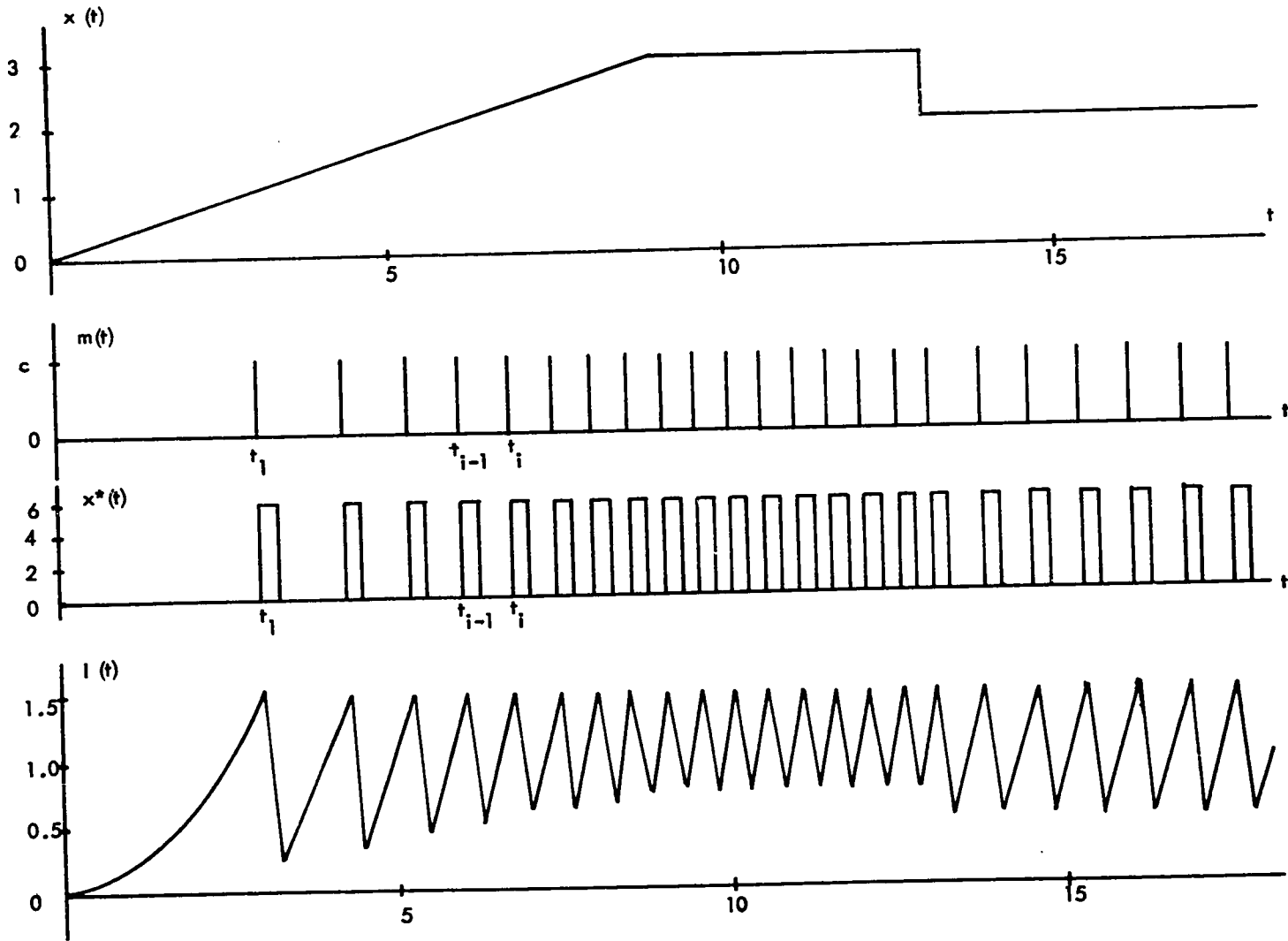


FIGURE 2-6. A SINGLE-SIGNED INTEGRAL PULSE FREQUENCY (S - S IPF) MODULATOR.



Modulator Parameters :  $K_1 = K_2 = 1$ ,  $b = a = 1.5$  ; Pulse Width,  $\tau = 0.25$  .

FIGURE 2-7. ILLUSTRATING THE OPERATION OF THE S - S IPF MODULATOR.

When  $I(t) = b$  at some time  $t = t_1$ , the input to the pulse generator is abruptly changed from  $m = 0$  to  $m = c$ . Thus, the pulse generator is triggered to emit a standard pulse. Now this output pulse is fed back negatively to the input to cause  $I(t)$  to decrease towards zero. Thus,  $m$  is reset to zero and the trigger to the pulse generator is removed. Since the feedback signal is non-zero only during the output pulse,  $I(t)$  will increase again to the value  $b$  to trigger the second pulse, and so on.

In order to show that the method under consideration implements S - S IPFM, let us examine the criterion by means of which the pulses are emitted. First, we define the pulse emission time as the instant at which the pulse generator receives the trigger. Thus, as shown above, the first pulse is emitted at  $t_1$  when the following criterion is satisfied.

$$I(t_1) = \int_0^{t_1} K_1 x(t) dt = b.$$

i.e. 
$$\int_0^{t_1} x(t) dt = b / K_1. \quad (2-11)$$

As to the subsequent pulses, the  $i$ th pulse will be emitted at  $t_i$

when

$$I(t_i) = K_1 \int_{t_{i-1}}^{t_i} (x(t) - K_2 x^*(t)) dt + I(t_{i-1}) = b, \quad (2-12)$$

$$i = 2, 3, 4, \dots$$

where  $t_{i-1}$  is the emission time of the  $(i-1)$ th pulse. Since the  $(i-1)$ th pulse is emitted at  $t_{i-1}$ ,  $I(t_{i-1})$  must be equal to  $b$ . Hence, Equation (2-12) becomes

$$\int_{t_{i-1}}^{t_i} x(t) dt = \int_{t_{i-1}}^{t_i} K_2 x^*(t) dt. \quad (2-13)$$

Assuming that the output pulses do not overlap, then, in the interval  $(t_{i-1}, t_i)$ , there is exactly one pulse in  $x^*(t)$ , namely, the  $(i-1)$ th pulse. Thus, if the area of the pulse is  $A$ , Equation (2-13) simplifies to,

$$\int_{t_{i-1}}^{t_i} x(t) dt = K_2 A \quad (2-14)$$

$i = 2, 3, 4, \dots$

Equations (2-11) and (2-14) are the criteria used by the feedback system for pulse emission and can be made identical to Equation (2-1) which is the criterion for pulse emission in IPFM. Clearly, if we set  $K_2 A = \frac{b}{K_1} = a$ , Equations (2-11) and (2-14) combined together will be identical to Equation (2-1). Therefore, the system shown in Figure 2-6 can implement S - S IPFM exactly.

In the above discussion, we have implicitly assumed that there is sufficient negative feedback to remove the trigger to the pulse generator in a small fraction of the duration of the output pulse. For rectangular output pulses, this condition implies that  $K_2 h > x(t)$  for all  $t \geq 0$ , where  $K_2$  is the gain in the feedback path and  $h$  is the height of the pulse. In practice, the upper bound of the modulating signal will be less than  $K_2 h$  because the components have inherent dynamics and thus do not exhibit the ideal transfer characteristics assumed.

The above method of implementing S - S IPFM is versatile and has other potentially useful applications. The system of Figure 2-6 has four independent adjustable parameters,  $K_1$ ,  $K_2$ ,  $b$ , and  $A$ . The parameters  $K_1$  and  $b$  control only the emission

of the first pulse, while  $K_2$  and  $A$  control all subsequent pulse emissions. When the output pulse shape and size are pre-specified, the threshold of the modulator can be easily changed by adjusting  $K_2$ . Now, if the output pulse is rectangular and a sampling gate is inserted in the feedback path as shown in Figure 2-8, the threshold of the modulator will vary linearly with the amplitude of the sampled signal  $y(t)$ . This latter feature may prove to be valuable if IPFM is used in an adaptive control system.<sup>12,30</sup> It may also be useful for implementing optimized pulse frequency controls.<sup>14</sup> Furthermore, the feedback system in Figure 2-6 can be considered as a reasonable model of the neural encoder. (See Chapter V). Thus, with the threshold easily controllable by a time-varying function, the system can be usefully applied to model neural elements with time-varying thresholds.

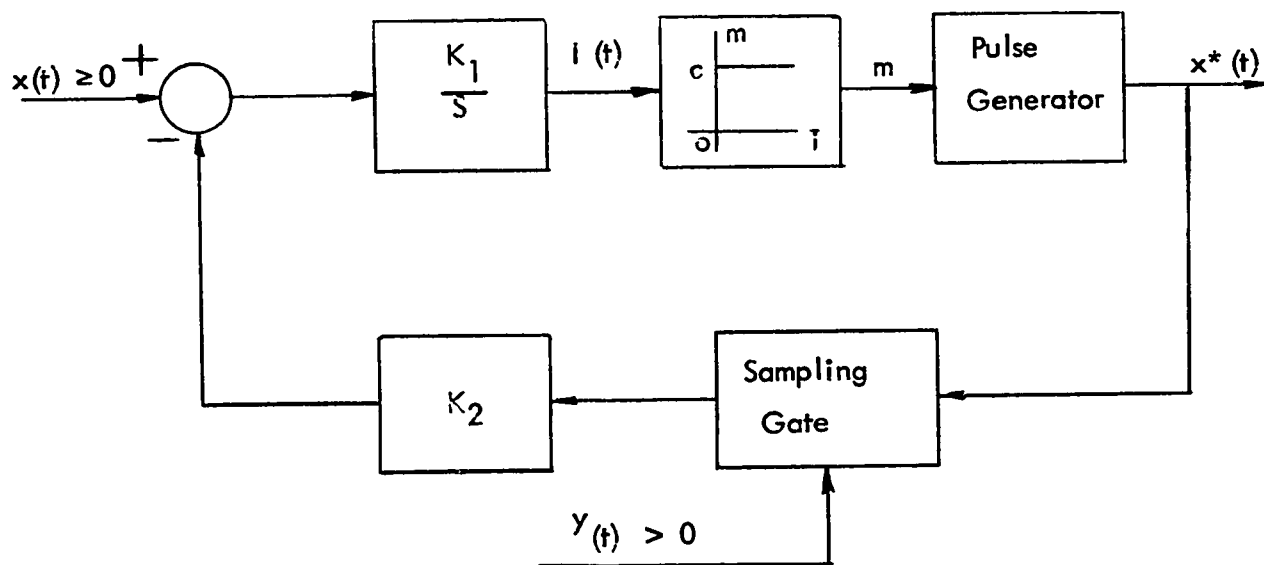


FIGURE 2-8. S - S IPF MODULATOR WITH TIME-VARYING THRESHOLD.

The feedback system of Figure 2-6 can be extended as in Figure 2-9 to implement D - S IPFM. The principle of operation of the resultant system is similar to that described above for S - S IPFM. When  $I(t)$  is positive and equal to  $b$ , Pulse Generator 1 is triggered to emit a positive standard pulse while Pulse Generator 2 has zero output. When  $I(t) = -b$ , Pulse Generator 2 emits a negative standard pulse while Pulse Generator 1 similarly has zero output. Following the procedure for analysing the single-signed modulator, it can be demonstrated that the system shown in Figure 2-9 can be represented by the model in Figure 2-2, provided that we set  $K_2 A = b / K_1$ , where  $A$  is the area of the pulse.

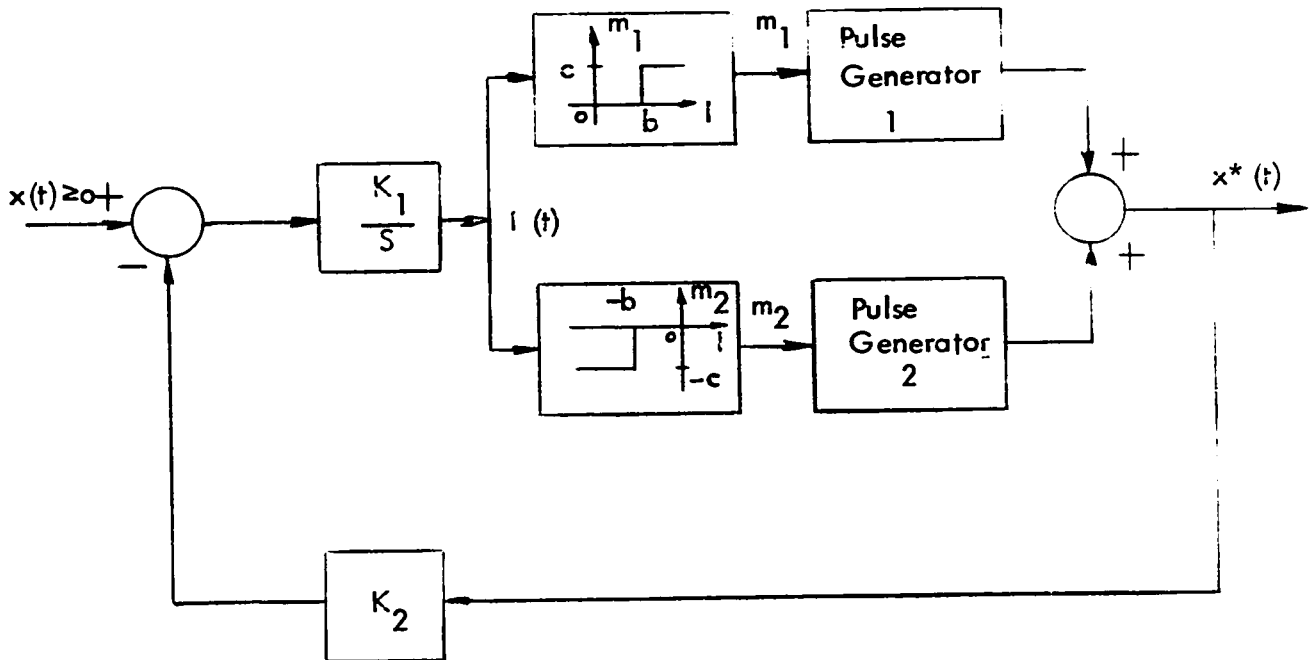


FIGURE 2-9. IMPLEMENTATION OF D - S IPFM .

## 2.6 Demodulation

There are two general methods for demodulating an integral pulse frequency (IPF) modulated pulse train. One method recently proposed by Blanchard is based on the Lagrangian interpolation formula,<sup>18</sup> and is essentially a numerical method for computing an approximation of the modulating signal. In its practical version, the computed approximation is simply the instantaneous pulse frequency multiplied by the modulator threshold  $a$  with the proper sign attached. Thus, if  $t_i$  and  $q_i$  are respectively the emission time and the sign of the  $i$ th pulse, then the demodulated signal is

$$\hat{x}(t) = \sum_{i=1} \frac{q_{i+1} a}{t_{i+1} - t_i} [U_{-1}(t - t_i) - U_{-1}(t - t_{i+1})] \quad (2-15)$$

where  $a$  is the threshold of the modulator and  $U_{-1}(t)$  is the unit step function. The resulting signal is a staircase function of time.

The other general method was proposed by Li.<sup>8</sup> Through a qualitative argument, he concluded that a linear time-invariant low-pass filter should be used for demodulation. This method has proved effective when the pulse frequency is much higher than the modulating signal frequency. However, the use of a low-pass filter to demodulate a single-signed IPF modulated pulse train was actually established long ago for continuous pulse frequency modulation,<sup>32</sup> which we have now shown to be equivalent to S-S IPFM. The detection of an analogue frequency modulated signal by a cycle counter is also based on this method.<sup>33,34</sup> Compared with Blanchard's method, Li's method is simpler to implement and appears to be more effective in practice. In the following we shall examine some aspects of this latter method of demodulation.

Consider the system shown in Figure 2-10. The pulse train from the modulator is to be demodulated by a linear low-pass filter described by the transfer function  $H(s)$ . Let  $g(t)$  be the unit impulse response of  $P(s)H(s)$ . Then, for zero initial conditions at  $\tau = 0$ , the demodulated output of the system is

$$\hat{x}(\tau) = \int_0^{\tau} v(t) g(\tau - t) dt. \quad (2-16)$$

But  $v(t)$  is an impulse train given by

$$v(t) = d \sum_{i=1} q_i U_0(t - t_i) \quad (2-17)$$

where  $U_0(t)$  is the unit impulse function;  $d$  is the strength of the impulse;  $q_i$  and  $t_i$  are respectively the sign and emission time of the  $i$ th pulse. Substituting Equation (2-17) into Equation (2-16) and simplifying, we have

$$\hat{x}(\tau) = d \sum_{i=1} q_i \cdot g(\tau - t_i) \quad (2-18)$$

From Equation (2-18) we see that the demodulated output is a linear summation of pulse responses of the filter  $H(s)$  (or alternatively the impulse responses of  $P(s) \cdot H(s)$ ). It is interesting to note that this characteristic is similar to both the temporal summation of postsynaptic potentials in the neuronal membrane and the summation of twitch responses in the muscle.

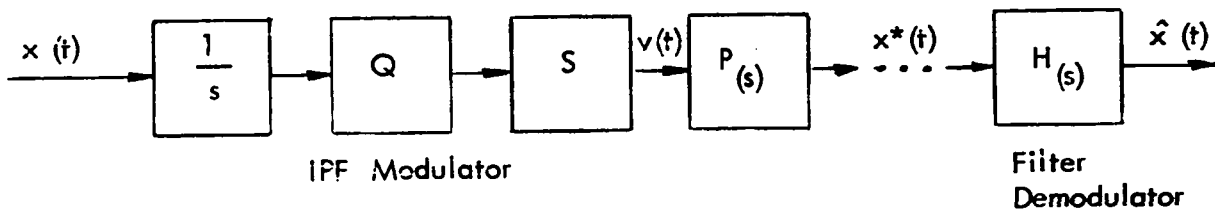


FIGURE 2-10. A COMMUNICATION SYSTEM USING IPFM .

The unit impulse response  $g(t)$  of  $P(s) \cdot H(s)$  can be approximated by a series of rectangular pulses as shown in Figure 2-11. Thus,

$$g(t) \approx \sum_{k=1}^K [U_{-1}(t-T_{k-1}) - U_{-1}(t-T_k)] \cdot g_k \equiv g^*(t), \quad (2-19)$$

where  $g_k = \frac{g(T_{k-1}) + g(T_k)}{2}, k = 1, 2, 3, \dots K;$

and  $T_k$  are as defined in the diagram.

Substituting Equation (2-19) into Equation (2-18), we have

$$\hat{x}(\tau) \approx \sum_{i=1}^K \sum_{k=1}^K d q_i g_k [U_{-1}(\tau-t_i - T_{k-1}) - U_{-1}(\tau-t_i - T_k)] \quad (2-20)$$

When the IPF modulated pulse train is single-signed, Equation (2-20) can be automatically computed by a network consisting of pulse delay units and pulse generators<sup>35, 36</sup>

as shown in Figure 2-12. The delay times are given by

$$D_k = T_k - T_{k-1}, k = 1, 2, \dots K-1.$$

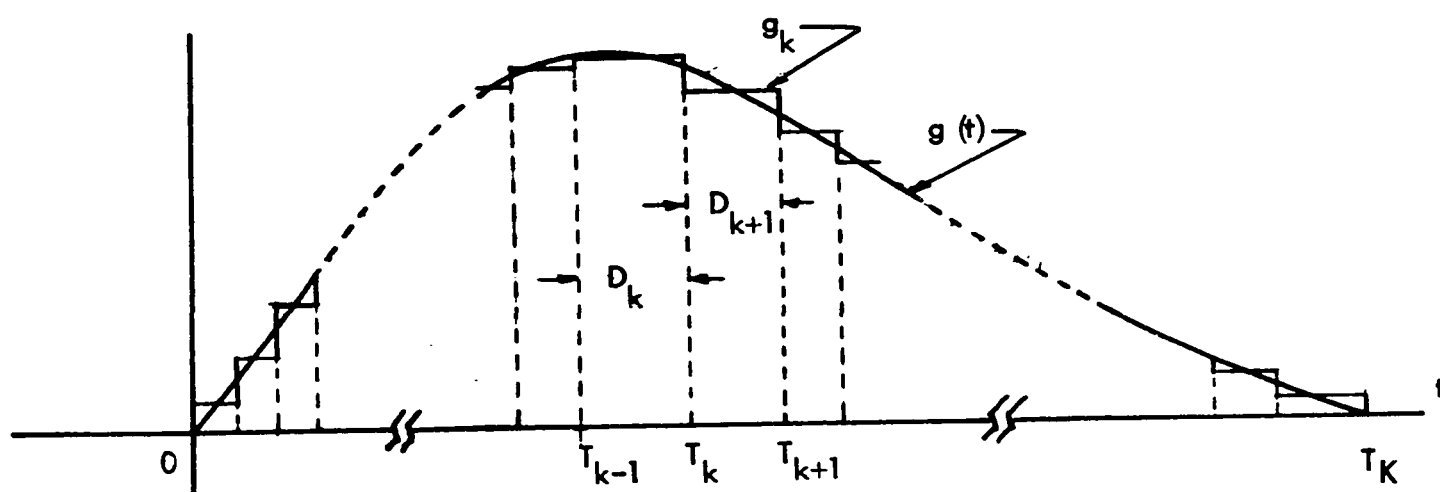


FIGURE 2-11. APPROXIMATING THE PULSE RESPONSE BY A STAIRCASE FUNCTION.

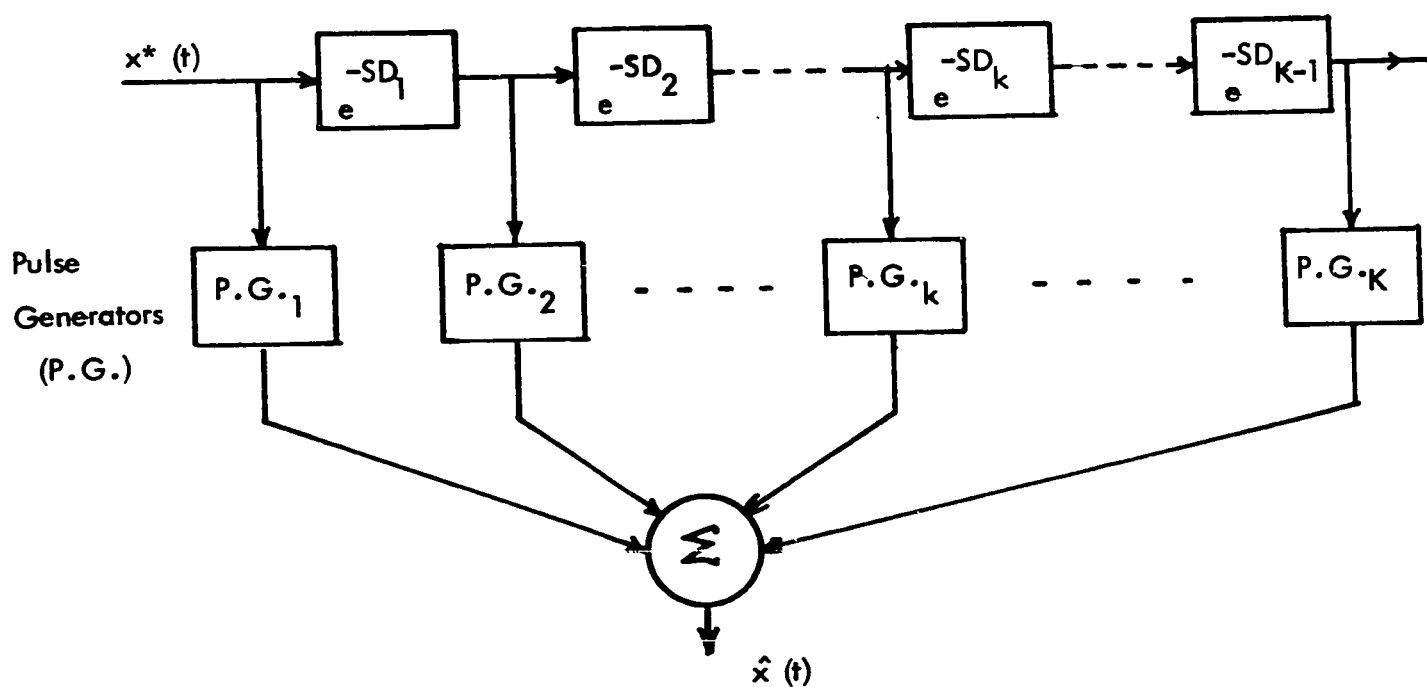


FIGURE 2-12. A NETWORK FOR IMPLEMENTING EQUATION (2-20) FOR SINGLE-SIGNED PULSE TRAINS.

The pulse generators are triggered sequentially by the input pulse as the latter propagates through the delay line. The  $k$ th generator P.G.<sub>k</sub> emits a rectangular pulse with width  $D_k$  and height  $dg_k$ . The outputs from the generators are added instantaneously to produce the output of the network. For a single pulse input, the network generates the approximate pulse response  $g^*(t)$  given by Equation (2-19). When the input is a pulse train, the pulse responses are added together as in Equation (2-20) to produce an approximation of the modulating signal.

The delay times  $D_k$  have been assumed to be unequal for generality, but to simplify construction, they could well be made all equal. However, for the same degree of approximation of the pulse response  $g(t)$ , less network elements are needed if  $T_k$  and thus  $D_k$  are chosen optimally without this constraint.

There is an upper bound for the delay times. A triggered pulse generator such as the monostable multivibrator cannot respond to a subsequent trigger before the output pulse is completed. Since the generator must emit a pulse for each pulse input and since the output pulse width of the  $k$ th generator is equal to the  $k$ th delay time  $D_k$ , the maximum delay time must be less than the minimum of all the input pulse intervals,  $t_{i+1} - t_i$ .

The network shown in Figure 2-12 can be extended to demodulate double-signed IPF modulated pulse trains. As shown in Figure 2-13, two networks similar to that shown in Figure 2-12 are connected in parallel. The upper network is sensitive only to positive input pulses while the lower network is sensitive only to negative input pulses. Otherwise, the two networks are identical.

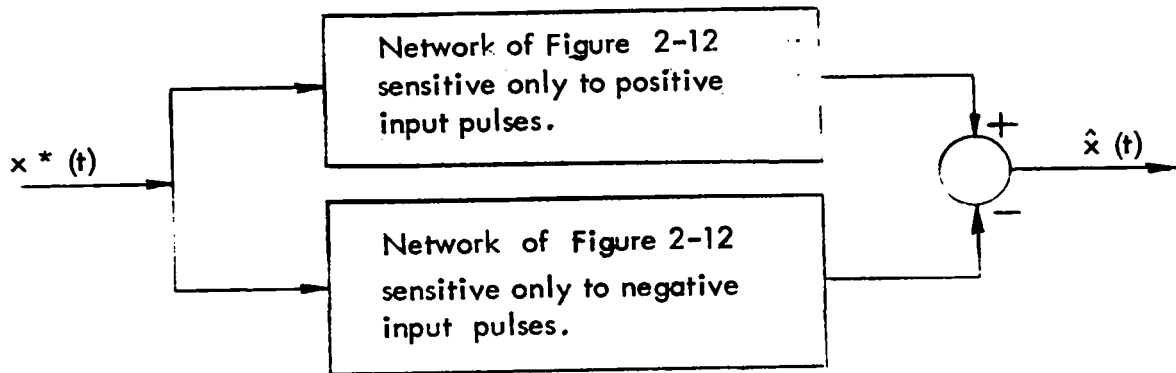


FIGURE 2-13. A NETWORK FOR IMPLEMENTING EQUATION (2-20) FOR DOUBLE-SIGNED PULSE TRAINS.

The network shown in Figure 2-12 is a particular form of real-time digital filter.<sup>37</sup> This particular form is possible because the IPF modulated pulse train comprises pulses of fixed size and shape. Although the network is more complex than the analogue filter for demodulating IPFM, it has the inherent advantageous properties of the digital filters. It offers a greater degree of accuracy and freedom in filter realization, since certain realization problems akin to negative elements do not arise. Furthermore, it may be more compact and economical than the analogue filters in the low frequencies where the size of analogue components becomes appreciable.

In the above discussion we have implicitly assumed that the IPF modulator has been properly designed so that a low-pass filter can recover the modulating signal with little error. In the next chapter, we shall examine through a spectral analysis the effects on the output pulse train due to both the modulator parameters and the characteristics of the modulating signal.

CHAPTER IIISPECTRAL ANALYSIS OF INTEGRAL PULSE FREQUENCY MODULATION3.1 Introduction

Although integral pulse frequency modulation (IPFM) has been applied to engineering and neurophysiological investigations by a number of workers,<sup>8-11,17-19,22-26</sup> its information transfer characteristics have not been adequately explored, apparently because of the difficulty in obtaining a mathematically tractable expression for the output pulse train.<sup>18</sup> There are only a few reported works in this area. Li has examined the "approximate frequency response" (i.e. describing functions) of the modulator.<sup>8</sup> Blanchard,<sup>18</sup> Bombi and Ciscato,<sup>19</sup> have studied the input noise filtering properties. In addition to these, Fitch<sup>32</sup> and Panter<sup>1</sup> have investigated the spectral characteristics of continuous pulse frequency modulation (which we have shown to be equivalent to single-signed IPFM) with a sinusoidal modulating signal. More recently, during the final preparation of this thesis, Bayly<sup>26</sup> has reported a similar spectral analysis of single-signed IPFM in a study of pulse frequency modulation in the nervous system.

In the present chapter a spectral analysis of IPFM will be developed and the results will be applied to derive some useful formulae for synthesizing the modulators. Although the spectral characteristics of S - S IPFM with sinusoidal excitation have been investigated before, the method of analysis to be presented below is new and more general. The new approach may hopefully lead to better insight of the information transfer characteristics of IPFM.

In the subsequent analysis, a number of symbols is employed to shorten lengthy mathematical expressions. Therefore, the reader may find the abridged list

of symbols helpful in reading this chapter.

### 3.2 Spectral Analysis of Single-Signed Integral Pulse Frequency Modulation

#### 3.2.1 Formulating the Approach

We have shown in Chapter II that the input - output relations of a single-signed integral pulse frequency (S - S IPF) modulator can be exactly represented by a functional model. For convenience of analysis this model can be re-drawn as shown in Figure 3-1, in which the quantizer has been represented as the parallel combination of a linear gain and a nonlinear element  $N$ .<sup>2</sup> The linear gain is defined as the ratio of the output impulse magnitude  $d$  and the modulator threshold  $a$ , while the transfer characteristic of  $N$  is specified by the periodic function  $p_1(z)$  shown in Figure 3-2.

Let the modulating signal  $x(t)$  in Figure 3-1 be bounded and integrable for any finite time  $t \geq 0$ . Then, the output of the integrator is

$$z(t) = \int_0^t x(t) dt, \quad (3-1)$$

and the quantizer output is

$$p_2(t) = \frac{d}{a} z(t) - p_1(z(t)). \quad (3-2)$$

Thus, the impulse train is

$$v(t) = \frac{dp_2(t)}{dt} = \frac{d}{a} \cdot \frac{dz(t)}{dt} - \frac{dp_1(z)}{dz} \frac{dz(t)}{dt}, \quad (3-3)$$

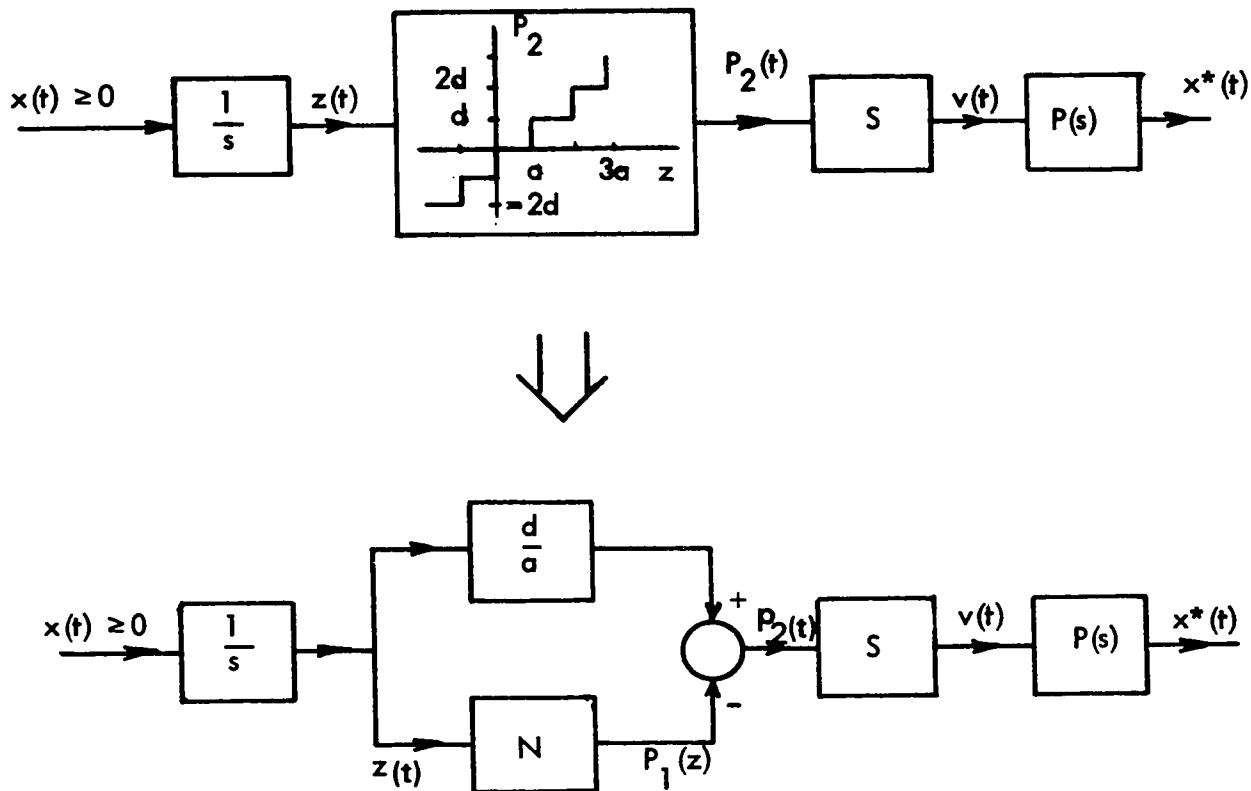


FIGURE 3-1. EQUIVALENT REPRESENTATION OF THE SINGLE-SIGNED INTEGRAL PULSE FREQUENCY (S - S IPF) MODULATOR.

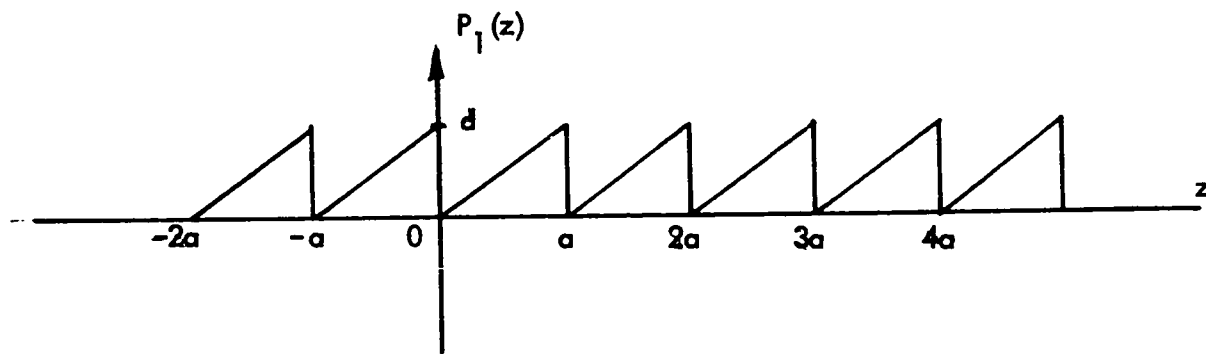


FIGURE 3-2. THE TRANSFER CHARACTERISTIC OF THE NONLINEAR ELEMENT N .

provided that both  $z(t)$  and  $p_1(z)$  are differentiable. By Equation (3-1),  $z(t)$  is clearly differentiable, and

$$\frac{dz(t)}{dt} = x(t). \quad (3-4)$$

The function  $p_1(z)$  is also differentiable, since it can be represented by the Fourier series

$$p_1(z) = \frac{d}{a} \left[ \frac{a}{2} - \sum_{k=1}^{\infty} \frac{2}{k\omega_0} \sin k\omega_0 z \right], \quad (3-5)$$

$$\text{where } \omega_0 = \frac{2\pi}{a},$$

and since, according to the theory of distributions,<sup>39</sup> any Fourier series can be differentiated term by term. Thus,

$$\frac{dp_1(z)}{dz} = -\frac{d}{a} \sum_{k=1}^{\infty} \frac{2}{k\omega_0} \frac{d}{dz} \sin k\omega_0 z. \quad (3-6)$$

Therefore, substituting Equations (3-4) and (3-6) into Equation (3-3) and simplifying, we have for the output impulse train,

$$v(t) = \frac{d}{a} \left[ x(t) + \sum_{k=1}^{\infty} \frac{2}{k\omega_0} \frac{d}{dt} \sin k\omega_0 z(t) \right] \quad (3-7)$$

which converges in the sense of distribution to a generalized function;<sup>39</sup> namely, a time sequence of impulse functions, even though it does not converge in the classical sense. This expression for the output impulse train can be alternatively derived using another approach as shown in Appendix A.

The first term in Equation (3-7) is proportional to the modulating signal  $x(t)$  and is defined here as the signal component of the output impulse train. The remaining terms are nonlinear functions of  $x(t)$  and represent the noise component of the output impulse train since they are not wanted in demodulation. The noise component is produced by the modulator internally in the encoding process. Specifically, it is generated by the nonlinear characteristic of the quantizer as illustrated in Figure 3-3, which is derived from Figure 3-1.

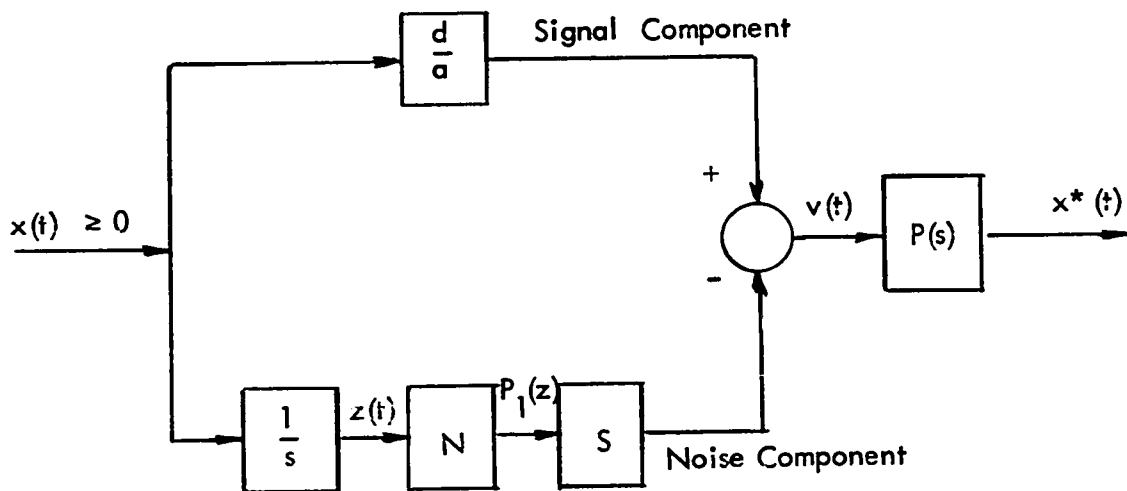


FIGURE 3-3. AN EQUIVALENT REPRESENTATION OF THE S - S IPF MODULATOR SHOWING THE SIGNAL AND NOISE COMPONENTS.

In order to facilitate subsequent analysis, we define a function  $e_k(t)$  such that

$$e_k(t) = \frac{2}{k\omega_0} \sin k\omega_0 z(t). \quad (3-8)$$

Using this function we can re-write Equation (3-7) as

$$v(t) = \frac{d}{dt} \left[ x(t) + \sum_{k=1}^{\infty} \frac{d}{dt} e_k(t) \right]. \quad (3-9)$$

The function  $e_k(t)$  can be shown to be a frequency-modulated (FM) sinusoidal carrier. As noted in Section 2.4, the modulating signal  $x(t)$  for S-S IPFM with positive output pulses is in general given by

$$x(t) = X_0 + f(t) \geq 0, \quad t \geq 0 \quad (3-10)$$

where  $X_0$  is a biasing constant and  $f(t)$  is a message signal. Therefore, the output of the integrator in Figure 3-1 is

$$z(t) = \int_0^t x(t) dt = X_0 t + \int_0^t f(t) dt. \quad (3-11)$$

Substituting this into Equation (3-8), we have

$$e_k(t) = \frac{2}{k\omega_0} \sin \left[ k\omega_0 X_0 t + k\omega_0 \int_0^t f(t) dt \right] \quad (3-12)$$

which clearly shows that  $e_k(t)$  is a sinusoidal carrier frequency-modulated by  $f(t)$ .

In the subsequent analysis, we shall utilize the fact that  $e_k(t)$  is an FM wave in order to take advantage of the well-developed theory of continuous carrier-frequency modulation. We shall first express the FM wave  $e_k(t)$  in terms of its spectral components and then substitute the resulting expression into Equation (3-9) to derive

a spectral representation of  $v(t)$ . Finally, we shall obtain an expression of the output pulse train  $x^*(t)$  by considering the pulse-shaping element  $P(s)$  as a filter and modifying the amplitude and phase of each spectral component of  $v(t)$  according to the amplitude and phase characteristics of  $P(j\omega)$ . This basic approach will be applied to investigate the signal and noise spectral characteristics of the output pulse trains for the class of modulating signals consisting of one or more sinusoids.

### 3.2.2 Single-Tone Modulation

#### (a) Mathematical Expression for the Output Pulse Train

Consider first the case in which the modulating signal is

$$x(t) = X_0 + U \cos(\omega_1 t + \theta) \geq 0, \quad (3-13)$$

where  $U$ ,  $\omega_1$ , and  $\theta$  are constant. Thus, the output of the integrator is

$$z(t) = X_0 t + \frac{U}{\omega_1} \sin(\omega_1 t + \theta) - C, \quad (3-14)$$

where  $C = (U \sin \theta) / \omega_1$ . Substituting this into Equation (3-8), we have

$$e_k(t) = \frac{2}{k\omega_0} \sin [k\omega_0 (X_0 t - C) + \beta \sin(\omega_1 t + \theta)] \quad (3-15)$$

where the modulation index,  $\beta = k\omega_0 U / \omega_1$ . It is well known<sup>1</sup> that the FM carrier  $e_k(t)$  can be expanded in terms of Bessel functions. Thus, using the identity<sup>38</sup>

$$e^{j\beta \sin t} = \sum_{n=-\infty}^{\infty} J_n(\beta) e^{jnt}, \quad (3-16)$$

we have

$$\begin{aligned}
e_k(t) &= \frac{2}{k\omega_o} \operatorname{Im} \left\{ e^{jk\omega_o(X_o t - C)} e^{j\beta \sin(\omega_1 t + \theta)} \right\} \\
&= \frac{2}{k\omega_o} \operatorname{Im} \left\{ e^{jk\omega_o(X_o t - C)} \sum_{n=-\infty}^{\infty} J_n(\beta) e^{jn(\omega_1 t + \theta)} \right\} \\
&= \sum_{n=-\infty}^{\infty} D(k, n) \sin(\gamma_1 t + \varphi_1), \tag{3-17}
\end{aligned}$$

where  $D(k, n) = \frac{2}{k\omega_o} J_n(\beta),$  (3-18)

$$\gamma_1 = k\omega_o X_o + n\omega_1, \tag{3-19}$$

$$\varphi_1 = n\theta - \beta \sin \theta, \tag{3-20}$$

$$\beta = \frac{k\omega_o U}{\omega_1} = \frac{k 2\pi}{\omega_1} \cdot \frac{U}{a}, \tag{3-21}$$

$a$  is the modulator threshold, and

$J_n$  is the  $n$ th order Bessel function of the first kind.

Substituting Equations (3-13) and (3-17) into Equation (3-9) and simplifying, we obtain the following expression for the output impulse train.

$$v(t) = \frac{d}{a} [X_o + U \cos(\omega_1 t + \theta)] + R \tag{3-22}$$

where

$$R = \frac{d}{a} \sum_{k=1}^{\infty} \sum_{n=-\infty}^{\infty} D(k, n) \gamma_1 \cos(\gamma_1 t + \varphi_1). \tag{3-23}$$

Now let the output pulse shape be specified by the function  $p(t)$  whose Fourier transform is

$$P(j\omega) = A(\omega) e^{jQ(\omega)}, \tag{3-24}$$

where  $A(\omega)$  and  $Q(\omega)$  are real functions of  $\omega$ , and  $A(\infty) = Q(0) = 0$ . Then, the amplitude and phase characteristics of the pulse-shaping element  $P(s)$  are given by  $A(\omega)$  and  $Q(\omega)$  respectively. Thus when  $v(t)$  is applied to  $P(s)$ , the amplitude and phase of each sinusoidal component of  $v(t)$  will be modified according to  $A(\omega)$  and  $Q(\omega)$  respectively. Therefore, the output pulse train is

$$x^*(t) = \frac{d}{dt} \left\{ X_0 A(0) + U A(\omega_1) \cos [\omega_1 t + \theta + Q(\omega_1)] \right\} + N(t) \quad (3-25)$$

where

$$N(t) = \frac{d}{dt} \sum_{k=1}^{\infty} \sum_{n=-\infty}^{\infty} E(k,n) \cos [\gamma_1 t + \varphi_1 + Q(\gamma_1)] , \quad (3-26)$$

$$E(k,n) = D(k,n) \gamma_1 A(\gamma_1) , \quad (3-27)$$

$D(k,n)$ ,  $\gamma_1$ , and  $\varphi_1$  are defined in Equations (3-18) to (3-20).

### (b) Characteristics of the Signal and Noise Components

The first two terms of Equation (3-25) constitute the signal component of the output pulse train while the last term represents the noise component. The signal component is proportional to the modulating signal  $x(t)$  filtered by the pulse-shaping element  $P(s)$ . This latter observation is also valid for any other admissible modulating signal, since the signal component of the output impulse train, as we have shown in Section 3.2.1, is proportional to the modulating signal. Based on this observation, we can derive some of the necessary properties of the output pulse shape.

Consider a modulating signal comprising more than one sinusoid, or more generally, a band of frequencies. The amplitude and phase of these frequency components

in the output pulse train are modified by  $P_{(j\omega)}$ , and as a result, the signal component of the output pulse train may be distorted if  $P_{(j\omega)}$  is not appropriately chosen. For the case that no distortion has been introduced, the signal component is

$$S(t) = \lambda_1 x(t - \alpha), \quad (3-28)$$

where  $\alpha \geq 0$  and  $\lambda_1 > 0$  are constants. Equation (3-28) implies that the system function of the pulse-shaping element is given by

$$P_{(j\omega)} = \lambda_1 e^{-j\alpha\omega} \quad (3-29)$$

in the frequency band of the modulating signal. Therefore, it is necessary that the pulse shape be chosen to satisfy Equation (3-29) at least approximately in the frequency band of the modulating signal in order that the distortion introduced by it may be negligible. One pulse shape which can satisfy this requirement is that of the commonly used rectangular pulse. For a rectangular pulse with height  $h$  and width  $\tau$ ,

$$\begin{aligned} P_{(j\omega)} &= h \cdot \frac{1 - e^{-j\omega\tau}}{j\omega} \\ &= h\tau \cdot \frac{\sin \omega\tau/2}{\omega\tau/2} e^{-j\omega\tau/2} \\ &= h\tau e^{-j\omega\tau/2} [1 - (\omega\tau)^2/24 + \dots]. \end{aligned} \quad (3-30)$$

When  $0 < \omega\tau < 1$ ,

$$P_{(j\omega)} \approx h\tau e^{-j\omega\tau/2} \quad (3-31)$$

with a maximum error of less than 6% in the amplitude frequency characteristic.

Hence, the distortion introduced by the rectangular pulse shape will be small, provided

that  $\tau < 1 / \omega_{\max}$  where  $\omega_{\max}$  is the maximum frequency of the modulating signal. In subsequent discussions, we shall assume that the output pulse shape is properly chosen and has no significant detrimental effect on the signal component.

Now, we turn to the noise component of the output pulse train. As shown by Equation (3-26) its spectrum theoretically has an infinite band-width, and thus many of its frequencies lie in the frequency band of the modulating signal, contaminating the signal component of the output pulse train. In particular, the noise frequencies,  $\omega_1 = k\omega_o X_o + n\omega_1$ , even coincide with the message signal frequency  $\omega_1$  whenever  $\omega_o X_o / \omega_1$  is an integer. In order that the modulating signal may be recovered with negligible error from the pulse train, the signal component must be effectively separated from the noise component. Thus, in the following we shall examine the noise spectral characteristics with this particular point in mind.

In order to facilitate subsequent analysis, let the expression of the noise component be re-written as

$$N(t) = \frac{d}{a} \sum_{k=1}^{\infty} \mu_k(t) \quad (3-32)$$

where 
$$\mu_k(t) = \sum_{n=-\infty}^{\infty} E(k,n) \cos [ (k\omega_o X_o + n\omega_1)t + n\theta - \beta \sin \theta + Q(k\omega_o X_o + n\omega_1) ], \quad (3-33)$$

and

$$E(k,n) = \frac{2}{k\omega_o} \cdot J_n(k\omega_o U / \omega_1) \cdot (k\omega_o X_o + n\omega_1) \cdot A(k\omega_o X_o + n\omega_1). \quad (3-34)$$

Furthermore, without loss of generality, let  $d = a$  in Equation (3-32) and the expression

of the output pulse train. Also, let  $\mu_k(t)$  be called the  $k$ th constituent of the noise component. Then, Equation (3-33) shows that each constituent,  $\mu_k(t)$ , theoretically has a double infinity of spectral components, with one at the center frequency  $k\omega_o X_o$ , infinitely many at the upper side frequencies  $k\omega_o X_o + n\omega_1$ , and infinitely many at the lower side frequencies  $k\omega_o X_o - n\omega_1$ , where  $n = 1, 2, 3, \dots$ . Thus, each constituent of the noise component has an infinite set of spectral components, while we see from Equation (3-32) that the spectrum of  $N(t)$  is composed of infinitely many such sets whose center frequencies are harmonically related. If the frequencies of all spectral components from different sets are different, the amplitude or power spectrum of  $N(t)$  is simply the superposition of the corresponding spectra of all  $\mu_k(t)$ . However, if  $\omega_o X_o / \omega_1$  is a rational number, some spectral components from different sets will have the same frequencies. In particular, if  $k\omega_o X_o / \omega_1$  is an integer for all values of  $k$ , the spectral components from all  $\mu_k(t)$  will constitute an identical set of frequencies. For these latter cases, all spectral components with common frequency contribute to the amplitude of the spectrum of  $N(t)$  at that frequency and the phase angles of these components must be taken into consideration when either the amplitude or power spectrum of  $N(t)$  is being determined.

Although the noise component  $N(t)$  of the output pulse train theoretically has infinitely many infinite sets of spectral components, the number of spectral components with sufficient power to be practically significant is in general finite. The average power  $w(k,n)$  of each noise spectral component is equal to  $E^2(k,n) / 2$ , where  $E(k,n)$  is given by Equation (3-34). The output pulse shape is generally such that  $A(\omega)$  is bounded by  $\frac{K}{\omega^i}$  for  $\omega$  large, where  $i \geq 1$  and  $K$  is a positive constant. Thus for  $n$  and  $k$  sufficiently large,

$$w(k, n) \leq 2 \left[ \frac{J_n(k\omega_0 U / \omega_1) \cdot K}{k\omega_0 \cdot (k\omega_0 X_0 + n\omega_1)^{i-1}} \right]^2, \quad i \geq 1. \quad (3-35)$$

Since  $|J_n(\beta)| \leq 1$  and  $J_n(\beta)$  approaches zero rapidly for  $\beta > n$  as  $\beta$  increases, it is clear from Equation (3-35) that when  $n$  and  $k$  are sufficiently large, the average power of these high frequency noise spectral components will then become negligibly small. Therefore, the "complete" noise spectrum, in practice, can be placed in a bounded frequency band. This property is important for demodulating the pulse train because the signal component will be effectively separated from  $N(t)$  if the "complete" noise spectrum can be re-located outside the frequency band of the modulating signal. In the next sub-section, we shall consider the rectangular output pulse train as an example.

### (c) The Rectangular Output Pulse Train

When the output pulse is rectangular with height  $h$  and width  $\tau$ , the system function,  $P(j\omega)$ , of the pulse-shaping element is given by Equation (3-30). Thus, its amplitude and phase characteristics are respectively given by

$$A(\omega) = h \tau \cdot \frac{\sin \omega \tau / 2}{\omega \tau / 2} \quad (3-36)$$

and

$$Q(\omega) = -\omega \tau / 2. \quad (3-37)$$

Substituting these into Equations (3-25) to (3-27) and setting  $d = a$  without loss of generality, we obtain the following expression for the rectangular output pulse train.\*

---

\* This expression differs slightly from the different expressions obtained by Panter,<sup>1</sup> Fitch,<sup>32</sup> and Bayley.<sup>40</sup> The discrepancy is due to a small difference in defining the pulse train.

$$x^*(t) = X_o h \tau + U h \tau \left[ \frac{\sin \omega_1 \tau / 2}{\omega_1 \tau / 2} \right] \cos (\omega_1 t + \theta - \omega_1 \tau / 2) + N(t) \quad (3-38)$$

In this case, the noise component  $N(t)$  is given by

$$N(t) = \sum_{k=1}^{\infty} \mu_{rk}(t), \quad (3-39)$$

where

$$\mu_{rk}(t) = \sum_{n=-\infty}^{\infty} E_r(k,n) \cos (\gamma_1 t + \varphi_1 - \gamma_1 \tau / 2), \quad (3-40)$$

$$E_r(k,n) = 2h \cdot D(k,n) \cdot \sin \gamma_1 \tau / 2, \quad (3-41)$$

$D(k,n)$ ,  $\varphi_1$ , and  $\gamma_1$  are as defined in Equations (3-18) to (3-20).

Assuming  $0 < \omega_1 \tau < 1$ , we have, for the signal component,

$$S(t) = h \tau [X_o + U \cos(\omega_1 (t - \tau) + \theta)] \quad (3-41a)$$

which is proportional to the delayed modulating signal. In the following, we shall examine the noise spectral characteristics in detail, with the objective to demonstrate that the noise bandwidth is in practice finite.

Consider a spectral component of the  $k$ th constituent,  $\mu_{rk}(t)$  of the noise component. By Equation (3-41), the amplitude of a spectral component with frequency  $\gamma_1 = k \omega_o X_o + n \omega_1$  is

$$\left| E_r(k,n) \right| = \left| 2h D(k,n) \sin \gamma_1 \tau / 2 \right|. \quad (3-42)$$

As shown in Equation (3-17),  $\left| D(k,n) \right|$  is the amplitude of the spectral components of

the FM carrier  $e_k(t)$ . Therefore, Equation (3-42) shows that, for any given  $k$ , the amplitude spectrum of  $\mu_{rk}(t)$  is equal to the amplitude spectrum of  $2h e_k(t)$  multiplied by  $\left| \sin \gamma_1 \tau / 2 \right|$  and furthermore, it is bounded by the spectrum of  $2h e_k(t)$  since  $\left| E_r(k,n) \right| \leq \left| 2h D_{(k,n)} \right|$  for all  $k$  and  $n$ . Since the average power of the spectral component is  $E_r^2(k,n) / 2$ , the power spectrum of  $\mu_{rk}(t)$  is similarly bounded by the power spectrum of  $2h e_k(t)$ .

In order to facilitate subsequent analysis, we now introduce some definitions.

In the theory of carrier frequency modulation, a spectral component is defined to be "significant" if its amplitude is not less than some fraction of the amplitude of the unmodulated carrier.<sup>1</sup> Thus, the "significant" spectral components of the FM wave  $2h e_k(t)$  are those for which

$$\left| 2h D_{(k,n)} \right| \geq \lambda \frac{4h}{k \omega_o} \quad (3-43)$$

where  $\lambda$  is an appropriately chosen small positive constant which is usually equal to 0.01.

In addition, the frequencies of the "significant" spectral components are said to be "significant" and the range between the maximum and the minimum significant frequencies is defined to be the "significant" bandwidth of the FM signal. For the present analysis, it is reasonable to define the "significant" spectral components of the  $k$ th constituent,  $\mu_{rk}(t)$  of the noise component similarly. Thus, a spectral component of  $\mu_{rk}(t)$  is defined

to be significant if

$$\left| E_r(k,n) \right| \geq \lambda \frac{4h}{k \omega_o} \quad (3-44)$$

or equivalently, if its average power

$$\frac{E_r^2}{2}(k, n) \geq \frac{1}{2} \left( \frac{4h \lambda}{k \omega_0} \right)^2 . \quad (3-45)$$

Furthermore, we define the significant frequencies and bandwidth of  $\mu_{rk}(t)$  in the same way as for those of the FM signals.

It is well known that the significant bandwidth of a sinusoidal carrier which is frequency modulated by an amplitude-bounded signal is finite.<sup>1</sup> Since the amplitude spectrum of  $\mu_{rk}(t)$  is bounded by that of the FM wave  $2h e_k(t)$ , the significant bandwidth of  $\mu_{rk}(t)$  must also be finite. Furthermore, for  $\omega_1 \neq 0$ , there is only a finite number of significant spectral components in each  $\mu_{rk}(t)$ .

Now consider the total average power  $W_{1k}$  of each  $\mu_{rk}(t)$ . By Parseval's theorem,

$$W_{1k} = \sum_{n=-\infty}^{\infty} \frac{E_r^2}{2}(k, n) \quad (3-46)$$

Using Equations (3-18) and (3-41), we obtain from this expression,

$$\begin{aligned} W_{1k} &= \frac{1}{2} \left( \frac{4h}{k \omega_0} \right)^2 \sum_{n=-\infty}^{\infty} J_n^2(\beta) \sin^2 \gamma_1 \tau / 2 \\ &\leq \frac{1}{2} \left( \frac{4h}{k \omega_0} \right)^2 \sum_{n=-\infty}^{\infty} J_n^2(\beta) \end{aligned} \quad (3-47)$$

$$\text{But } \sum_{n=-\infty}^{\infty} J_n^2(\beta) = 1 \quad (3-48)$$

Hence,

$$W_{1k} \leq \frac{1}{2} \left( \frac{4h}{k \omega_0} \right)^2 = 2 \left( \frac{h a}{k \pi} \right)^2 , \quad (3-49)$$

since  $\omega_0 = 2\pi/a$ . Thus, the total average power of each  $\mu_{rk}(t)$  is bounded from above by an upper bound which varies as  $(\frac{ha}{k})^2$ , where  $h$  is the pulse height and  $a$  is the modulator threshold.

Finally, we apply the results obtained above to demonstrate that the noise bandwidth is practically finite. By Equation (3-45), each of the "insignificant" spectral components of the first constituent,  $\mu_{r1}(t)$  of the noise component has an average power less than  $\frac{1}{2} \left( \frac{4h\lambda}{\omega_0} \right)^2$ . Clearly, if  $k > 1/\lambda$  in Equation (3-49),

$$W_{1k} < \frac{1}{2} \left( \frac{4h\lambda}{\omega_0} \right)^2. \quad (3-50)$$

Thus, the total average power of  $\mu_{rk}(t)$  for  $k > 1/\lambda$  is less than the average power of a significant spectral component of  $\mu_{r1}(t)$ . Hence, it is reasonable to neglect those  $\mu_{rk}(t)$ 's for which  $k > 1/\lambda$ . In other words, if  $K_1$  is the greatest integer not exceeding  $1/\lambda$ , only the first  $K_1$   $\mu_{rk}(t)$ 's of the noise component have sufficient power to be practically significant.

Based on the results obtained above, the noise component  $N(t)$  can be accurately represented by the following approximate relations.

$$N(t) \approx \sum_{k=1}^{K_1} \mu_{rk}(t) \quad (3-51)$$

where

$$\mu_{rk}(t) \approx \sum_{n=-N_k}^{N_k} E_r(k,n) \cos(\gamma_1 t + \phi_1 - \gamma_1 \tau/2)$$

where  $N_k$  is the largest integer for which the spectral frequencies of  $\mu_{rk}(t)$  remain signi-

ficant. Therefore, the significant bandwidth of  $N_k(t)$  is practically finite. In subsequent discussions, the frequencies  $\omega_k = k \omega_o X_o + n \omega_1$ , where  $|n| \leq N_k$  and  $1 \leq k \leq K_1$ , will be referred to as the "significant" noise frequencies.

### 3.2.3 Multitone Modulation

In practical problems, the message signal usually consists of more than one frequency. Thus, a more common modulating signal is

$$x(t) = X_o + \sum_{m=1}^M U_m \cos(\omega_m t + \theta_m), \quad (3-52)$$

where  $X_o$ ,  $U_m$ ,  $\omega_m$  and  $\theta_m$  are constant; and  $M$  is any positive integer. Assuming  $x(t) \geq 0$ , the analysis presented above for single-tone modulation can be directly extended to cover this more general case. By a development similar to that used for single-tone modulation, a series expansion of the FM wave  $e_k(t)$  can be shown to be

$$e_k(t) = \sum_{n_1=-\infty}^{\infty} \sum_{n_2=-\infty}^{\infty} \dots \sum_{n_M=-\infty}^{\infty} D_{(k, n_1, n_2, \dots, n_M)} \sin(\omega_M t + \phi_M), \quad (3-53)$$

where

$$D_{(k, n_1, \dots, n_M)} = \frac{2}{k \omega_o} \prod_{m=1}^M J_{n_m}(\beta_m), \quad (3-54)$$

$$\omega_M = k \omega_o X_o + \sum_{m=1}^M n_m \omega_m, \quad (3-55)$$

$$\varphi_M = \sum_{m=1}^M (n_m \theta_m - \beta_m \sin \theta_m), \quad (3-56)$$

$$\beta_m = k \omega_o U_m / \omega_m. \quad (3-57)$$

Then, following the steps used for deriving Equations (3-25) to (3-27), we can obtain an expression of the output pulse train in terms of its spectral components. Thus,

$$x^*(t) = \frac{d}{a} \left[ X_o A(o) + \sum_{m=1}^M U_m A(\omega_m) \cdot \cos(\omega_m t + \theta_m + Q(\omega_m)) \right] + N(t), \quad (3-58)$$

where the noise component of the output pulse train is now given by

$$N(t) = \frac{d}{a} \sum_{k=1}^{\infty} H_{Mk}(t), \quad (3-59)$$

$$H_{Mk}(t) = \sum_{n_1=-\infty}^{\infty} \cdots \sum_{n_M=-\infty}^{\infty} E_{(k, n_1, \dots, n_M)} \cdot \cos[\gamma_M t + \varphi_M + Q(\gamma_M)], \quad (3-60)$$

$$E_{(k, n_1, \dots, n_M)} = D_{(k, n_1, \dots, n_M)} \cdot \gamma_M \cdot A(\gamma_M), \quad (3-61)$$

and all other symbols are as defined previously.

The spectral characteristics of the output pulse train for this general case are qualitatively similar to those discussed previously for single-tone modulation. In particular, as shown by Equations (3-58) to (3-60), the spectra of the signal and noise components overlap as they do in single-tone modulation. The noise spectrum similarly has a theoretically infinite bandwidth, but its significant bandwidth can be shown to be finite

by the same argument used in Sub-section 3.2.2 (b). For this general case, if we assume as before  $A(\omega) \leq \frac{K}{\omega^i}$  for  $\omega$  large, where  $i \geq 1$ ; then the average power of each noise spectral component will be bounded by

$$2 \left[ \frac{K \prod_{m=1}^M J_{n_m}(\beta_m)}{k \omega_0 \gamma_M^{i-1}} \right]^2$$

when the frequency  $\gamma_M = k \omega_0 X_0 + \sum_{m=1}^M n_m \omega_m$  is sufficiently high. Clearly, those noise spectral components corresponding to sufficiently large values of  $k, n_1, \dots, n_M$  have negligible average power and thus can be neglected in practice.

When the output pulses are rectangular with height  $h$  and width  $\tau$ , an expression of the output pulse train can be readily obtained by substituting Equations (3-36) and (3-37) into Equations (3-58) to (3-61). Thus,

$$x^*(t) = \frac{d h \tau}{a} \left[ X_0 + \sum_{m=1}^M U_m \cdot \frac{\sin \omega_m \tau / 2}{\omega_m \tau / 2} \cdot \cos(\omega_m t + \theta_m - \omega_m \tau / 2) \right] + N(t) \quad (3-62)$$

where now the noise component  $N(t)$  is given by

$$N(t) = \frac{d}{a} \sum_{k=1}^{\infty} \mu_{rMk}(t) \quad (3-63)$$

$$\mu_{rMk}(t) = \sum_{n_1=-\infty}^{\infty} \dots \sum_{n_M=-\infty}^{\infty} E_r(k, n_1, \dots, n_M) \cos[\gamma_M t + \phi_M - \gamma_M \tau / 2] \quad (3-64)$$

$$E_r(k, n_1, \dots, n_M) = 2h \cdot D(k, n_1, \dots, n_M) \cdot \sin \gamma_M \tau / 2 \quad (3-65)$$

As in the case of single-tone modulation, the signal component is essentially proportional to the delayed modulating signal if  $0 < \omega_{\max} \tau < 1$ , where  $\omega_{\max}$  is the maximum sinusoidal frequency of the modulating signal. The spectral characteristics of the noise component  $N(t)$  can be examined using the procedure developed in the previous section. As an example, we shall show below that the significant amplitude spectrum of each constituent,  $\mu_{rMk}(t)$  of  $N(t)$  is bounded.

Consider a spectral component of  $\mu_{rMk}(t)$  with the frequency

$$\omega_M = k \omega_o X_o + \sum_{m=1}^M n_m \omega_m. \quad \text{From Equation (3-65), its amplitude is}$$

$$\left| E_r(k, n_1, \dots, n_M) \right| \leq \left| 2h \cdot D(k, n_1, \dots, n_M) \right|, \quad (3-66)$$

where  $\left| D(k, n_1, \dots, n_M) \right|$  is, as shown by Equation (3-53), the amplitude of the corresponding spectral component of the FM wave  $e_k(t)$ . Since this relation holds for all values of  $k, n_1, \dots,$  and  $n_M$ , the amplitude spectrum of  $\mu_{rMk}(t)$  must be bounded by the amplitude spectrum of  $e_k(t)$ . Furthermore, as noted previously, a sinusoidal carrier which is frequency-modulated by an amplitude-bounded signal has a significant spectrum with finite bandwidth. Hence, the significant spectrum of the constituent  $\mu_{rMk}(t)$  of the noise component also has a finite bandwidth.

#### 3.2.4 Recapitulation

In the present section, we have developed a new and general method for the spectral analysis of single-signed integral pulse frequency modulation. This method is appli-

cable to any modulating signal  $x(t) \geq 0$  for which the FM wave  $e_k(t) = \frac{2}{k \omega_0} \sin k \omega_0 z(t)$ , where  $z(t) = \int_0^t x(t) dt$ , can be expressed in terms of its spectral components. A spectral representation of the output impulse train  $v(t)$  is derived by substituting the expression for  $e_k(t)$  into Equation (3-9) which is repeated here for convenience.

$$v(t) = \frac{d}{a} \left[ x(t) + \sum_{k=1}^{\infty} \frac{d}{dt} e_k(t) \right] \quad (3-9)$$

The expression for the output pulse train is then obtained by considering the linear pulse-shaping element  $P(s)$  as a filter whose input is the impulse train  $v(t)$ . The spectral characteristics of the output pulse train for a class of modulating signals comprising one or more different sinusoids have been examined. The main characteristics are :

1. The pulse train contains a signal component and a noise component whose spectra in general overlap each other.
2. The signal component is proportional to the modulating signal modified by the frequency characteristics of the pulse-shaping element.
3. The noise component is produced internally by the modulator. Its spectrum theoretically has an infinite bandwidth ; however, in practice, its significant bandwidth is finite.
4. The noise component may be considered as a sum of constituents  $\mu_{Mk}(t)$  each of which theoretically comprises an infinite number of spectral components distributed about the center frequency  $k \omega_0 X_0 = k 2 \pi X_0 / a$ , where  $X_0$  is the biasing constant of the modulating signal,  $a$  is the modulator threshold, and  $k$  is a positive integer. When the output pulses are rectangular with

height  $h$  and width  $\tau$ , the amplitude and power spectra of  $\mu_{rMk}(t)$  are bounded respectively by the amplitude and power spectra of the FM wave  $2h e_k(t)$ .

### 3.3 Synthesis Criteria for S - S IPFM

#### 3.3.1 The Approach

We have shown above that the spectra of the signal and noise components of the output pulse train generally overlap. Therefore, if the noise power in the signal frequency band is high compared to the power of the signal component, it may be difficult to recover the modulating signal with negligible error. Fortunately, however, the bandwidth of the noise component in practice is finite, and furthermore, the center frequencies  $k \omega_o X_o$  of the constituents  $\mu_k(t)$  of the noise component, can be shifted by changing the value of  $\omega_o X_o = 2\pi X_o / a$ , since  $a$  is the modulator threshold and  $X_o$  is the biasing constant of the modulating signal. Thus the noise spectrum can be re-located outside the signal frequency band to separate the signal component from the noise component so that the modulating signal can be recovered by filtering. This latter situation is illustrated in Figure 3-4 for an output impulse train. In this example, the noise spectral power is less than 1% of the average power of the signal component when the frequency is less than 4. Clearly, in this case, the modulating signal can be recovered by filtering the impulse train with a low-pass filter having a cut-off frequency equal to 3. In the present section, we shall develop some criteria for selecting  $\omega_o X_o$  so that the pulse train can be demodulated with an acceptable noise content. Our attention will be focused mainly on the rectangular pulse train since it is most commonly used in engineering systems.

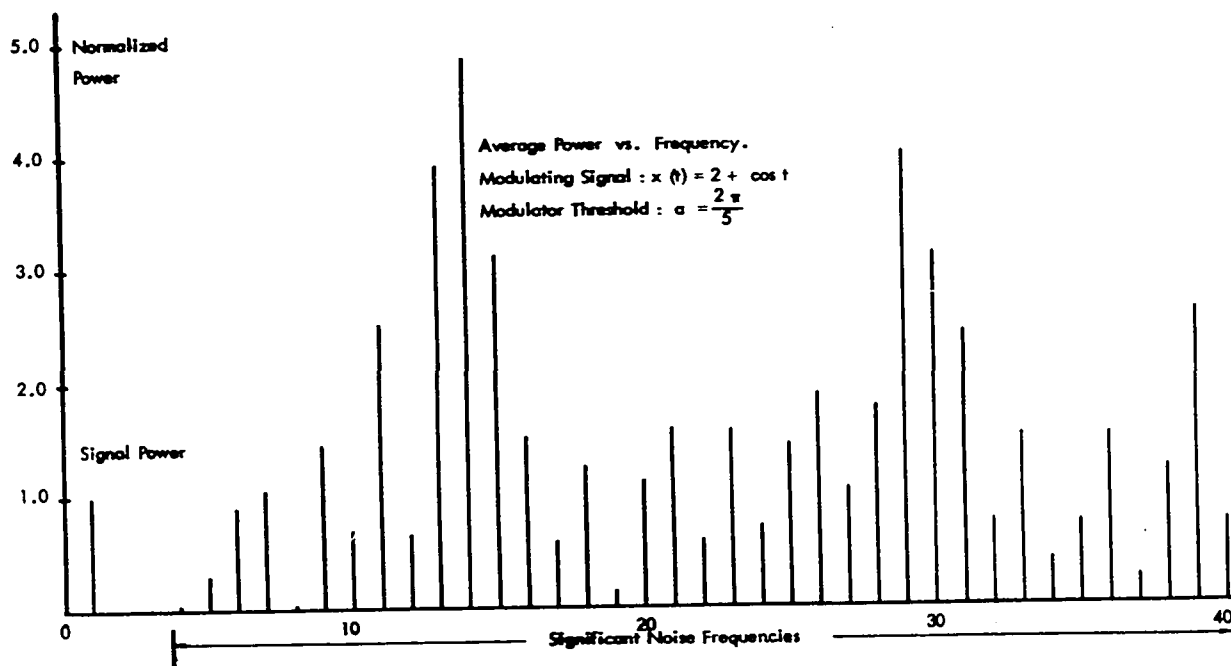


FIGURE 3-4. THE POWER SPECTRUM OF AN OUTPUT IMPULSE TRAIN FROM AN S-S IPF MODULATOR.

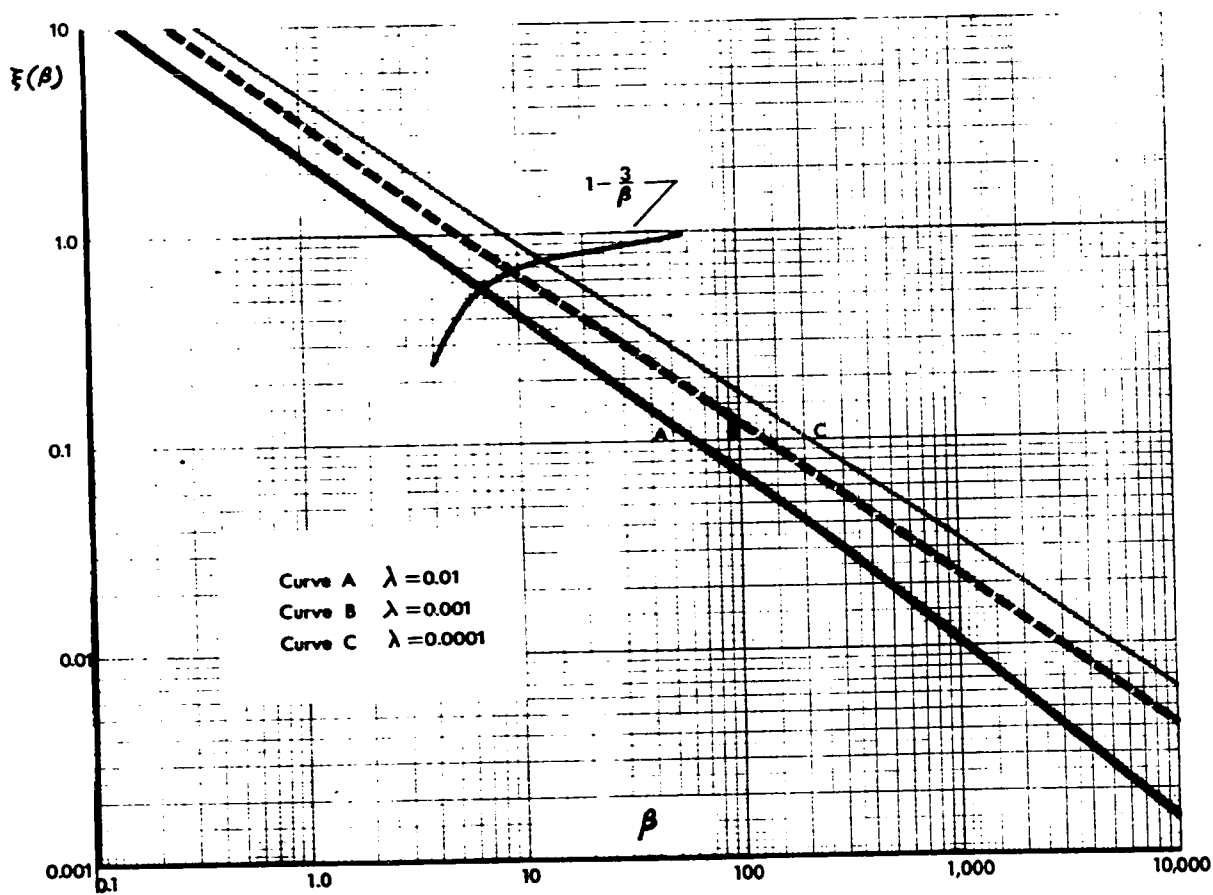


Fig.3-5. Variation of  $\Xi(\beta)$  vs.  $\beta$ .  
 (Replotted from Ref. 42)

Since the significant bandwidth of the noise component is finite, one reasonable way to effectively separate the signal and noise spectra is to choose such values of  $\omega_o X_o$  that the minimum significant frequency of the noise component is greater than the maximum significant frequency in the modulating signal. However, this minimum significant noise frequency is difficult to determine. Instead, we shall achieve the above objective by using a lower bound of the significant noise frequencies.

For a rectangular pulse train, we have shown that the amplitude spectrum of its noise component is composed of the spectra of  $\mu_{rk}(t)$ , and that the amplitude spectrum of each  $\mu_{rk}(t)$  is bounded by that of the FM wave  $2 h e_k(t)$ , if the modulating signal consists of one or more sinusoids. Thus, the minimum significant frequency of  $\mu_{rk}(t)$  is not less than the minimum significant frequency of the corresponding FM wave  $2 h e_k(t)$ , and the absolute minimum significant frequency for all  $\mu_{rk}(t)$ 's is necessarily not less than its counterpart for all the corresponding FM waves. Therefore, a useful criterion for choosing  $\omega_o X_o$  can be derived from the stipulation that the absolute minimum significant frequency for all the related FM waves be greater than the maximum frequency of the modulating signal.

### 3.3.2 A Synthesis Criterion for Single-tone Modulation

#### (a) Derivation

Consider, for the present, the case in which the modulating signal consists of only one sinusoid with amplitude  $U$  and frequency  $\omega_1$ . Let the output pulses be rectangular with height  $h$  and width  $\tau$ . Then, for this case, the significant frequencies of the related FM wave  $2 h e_k(t)$  are given by  $k \omega_o X_o + n \omega_1$ , where the integers

$k$  and  $n$  take on those values for which the following inequality is satisfied.

$$|2h \cdot D_{(k,n)}| \geq \lambda \cdot \frac{4h}{k\omega_0} \quad (3-67)$$

where  $D_{(k,n)}$  is defined by Equation (3-18) and  $\lambda$  is a positive constant usually set arbitrarily equal to 0.01. Using the definition of  $D_{(k,n)}$ , we can simplify Equation (3-67) to obtain the relation

$$|J_n(\beta)| \geq \lambda \quad (3-68)$$

where  $\beta = k\omega_0 U / \omega_1$ .

In order to find the minimum significant frequency of the FM wave  $2h e_k(t)$ , we must find a minimum value of  $n$  such that Equation (3-68) is satisfied for the given  $k$  and  $\lambda$ . There are two possible situations:

1.  $k$  is sufficiently large so that Equation (3-68) is not satisfied for any value of  $n$ ; and
2.  $k$  is sufficiently small so that Equation (3-68) is satisfied for at least one value of  $n$ .

In the first situation,  $2h e_k(t)$  has no significant frequency and thus the corresponding noise spectral components bounded by its spectrum are negligible. Hence, this situation has no significant consequence on our criterion for choosing  $\omega_0 X_0$ . In the second situation, we can find the minimum significant frequency of  $2h e_k(t)$  as follows.

Consider the variation of  $J_n(\beta)$  when  $n$  is varied while  $\beta$  is treated as an independent parameter. For  $n \geq \beta$ ,  $J_n(\beta)$  will decrease monotonically

towards zero at a rate which increases rapidly with  $\beta$ .<sup>41</sup> Therefore, for each value of  $\beta$ , there exists a smallest positive value  $N_{k \min}$  of  $n$  such that  $|J_n(\beta)| < \lambda$  for all  $|n| > N_{k \min}$ , since  $J_{-n}(\beta) = (-1)^n J_n(\beta)$ .<sup>38</sup> Consequently, in accordance with Equation (3-68), the minimum significant frequency of  $2h e_k(t)$  for a given value of  $k$  is

$$\omega_{k \min} = k \omega_o X_o - N_{k \min} \omega_1 \quad (3-69)$$

The number  $N_{k \min}$  depends on both  $\beta$  and  $\lambda$ , and can be determined for any admissible values of  $\beta$  and  $\lambda$  by computing  $J_n(\beta)$  with  $n$  increasing from  $n \approx \beta$ . If  $\lambda$  is considered as an independent parameter, the relation between  $N_{k \min}$  and  $\beta$  is given by

$$N_{k \min} = [1 + \xi(\beta)] \beta \quad (3-70)$$

where  $\xi(\beta)$  is given graphically in Figure 3-5 as a function of  $\beta$  for  $\lambda = 0.01$ ,  $0.001$ , and  $0.0001$ . Note that  $\xi(\beta)$  represents change in the significant bandwidth of  $2h e_k(t)$  as  $\beta$  is varied, since  $2 N_{k \min} \omega_1 = 2 k \omega_o U [1 + \xi(\beta)]$ .

We now search for the absolute minimum significant frequency  $\omega_{\min}$  of all related FM waves  $2h e_k(t)$ , where  $k$  takes on all admissible values. Substituting Equation (3-70) into Equation (3-69), we have

$$\omega_{k \min} = k \omega_o X_o - [1 + \xi(\beta)] \beta \omega_1,$$

and since  $\beta = k \omega_o U / \omega_1$ ,

$$\omega_{k \min} = k \omega_o [X_o - (1 + \xi(\beta)) U]. \quad (3-71)$$

Since our objective is to find a proper value of  $\omega_0 X_0$  so that  $\omega_{k \min} > \omega_1 > 0$  for all admissible values of  $k$  and since  $k$  is a positive integer, we must have, in Equation (3-71), the inequality,

$$X_0 - [1 + \xi_{(\beta)}] U > 0 \quad (3-72)$$

As shown in Figure 3-5,  $\xi_{(\beta)}$  decreases monotonically as  $\beta$  increases. Thus,  $X_0 - [1 + \xi_{(\beta)}] U$  increases monotonically with  $\beta$  and hence with  $k$ . It is clear, therefore, from Equation (3-71) that  $\omega_{k \min}$  increases monotonically with  $k$ , and the absolute minimum significant frequency,  $\omega_{\min}$  of all FM waves  $2 h e_k(t)$  occurs when  $k = 1$ . Thus,

$$\omega_{\min} = \omega_0 [X_0 - (1 + \xi_{(\beta_1)}) U], \quad (3-73)$$

or from Equation (3-69),

$$\omega_{\min} = \omega_0 X_0 - N_{1 \min} \omega_1, \quad (3-74)$$

where  $N_{1 \min}$  is determined using Equation (3-70) and graphs such as those shown in Figure 3-5 for  $\beta = \beta_1 = \omega_0 U / \omega_1$ .

Therefore, when  $\omega_{\min} > \omega_1$ , the spectra of the signal and noise components of the pulse train are practically separated. However, if a low-pass filter with a cut-off frequency  $\omega_c$  is to be the demodulator, it is desirable to have  $\omega_{\min} > \omega_c$ .

Thus, from Equation (3-74), we have

$$\omega_0 X_0 - N_{1 \min} \omega_1 > \omega_c. \quad (3-75)$$

And, for  $\omega_c = m \omega_1$ , this inequality can be re-written as

$$\frac{\omega_o X_o}{\omega_1} > N_1 \min + m, \quad (3-76)$$

where  $m > 1$ .

Equation (3-76) is our criterion for choosing the value of  $\omega_o X_o = 2 \pi X_o / a$ , where  $a$  is the modulator threshold and  $X_o$  is the biasing constant for the modulating signal. It should be noted that this criterion is valid only if the inequality given in Equation (3-72) is satisfied for  $\beta = \beta_1 = \omega_o U / \omega_1$ .

The left hand side of Equation (3-76) can be shown to be equal to the number of output pulses per period  $T$  of the modulating signal  $x(t)$ . Recall that the criterion for pulse emission in S-S IPFM is

$$\int_{f_{i-1}}^{f_i} x(t) dt = a. \quad (3-77)$$

This indicates that the area under the curve  $x(t)$  between two consecutive pulse-emission times is  $a$ . Since the total area under the curve  $x(t)$  in one period  $T = 2 \pi / \omega_1$  is

$$\int_{t_i}^{t_i+T} x(t) dt = X_o T + \int_{t_i}^{t_i+T} U \cos(\omega_1 t + \theta) dt = X_o T, \quad (3-78)$$

the number of pulses per period is

$$\frac{X_o T}{a} = \frac{X_o 2 \pi}{a \omega_1} = \frac{\omega_o X_o}{\omega_1}. \quad (3-79)$$

Therefore, Equation (3-76) simply states that  $\omega_o X_o$  should be so selected that the number of pulses per modulating signal period is greater than  $N_{1 \text{ min}} + m$ .

The number  $N_{1 \text{ min}}$  can be readily determined if  $\beta_1$  is known, because  $N_{1 \text{ min}}$  can then be found directly using Equation (3-70) and graphs such as those shown in Figure 3-5. However, the assumption that  $\beta_1$  is known implies that  $\omega_o$  has been pre-specified, since  $\beta_1 = \omega_o U / \omega_1$ . In this case, the modulator threshold  $a$  is given, and hence we can only choose  $X_o$  to satisfy the criterion for separating the signal and noise spectra. Thus, from Equation (3-76) we must have

$$X_o > (N_{1 \text{ min}} + m) \omega_1 / \omega_o. \quad (3-80)$$

The values of  $X_o$  satisfying this relation will also automatically satisfy the requirement given by Equation (3-72), since by Equation (3-80),

$$X_o - [1 + \xi(\beta_1)] U > (N_{1 \text{ min}} + m) \omega_1 / \omega_o - [1 + \xi(\beta_1)] U$$

which can be simplified to yield

$$X_o - [1 + \xi(\beta_1)] U > m \omega_1 / \omega_o,$$

where the right-hand side is clearly greater than zero.

When the modulator threshold,  $a$ , is to be determined with the modulating signal biasing constant  $X_o$  given, the problem must be solved in a different way. Substituting Equation (3-70) with  $k = 1$  into Equation (3-76) and simplifying, we have

$$\frac{X_o}{U} - 1 - \frac{m}{\beta_1} > \xi(\beta_1) \quad (3-81)$$

Both the left-hand side and the right-hand side of this inequality are functions of  $\beta_1$ . Hence we can plot them on the same graph and then read from the graph the values of  $\beta_1$  for which this inequality is satisfied. The appropriate modulator threshold,  $a$ , can then be determined using the definition,  $\beta_1 = \omega_o U / \omega_1 = 2 \pi U / a \omega_1$ . The values of  $a$  determined this way will also satisfy the requirement given by Equation (3-72), since Equation (3-81) can be re-written as

$$X_o - [1 + \xi(\beta_1)] U > \frac{m U}{\beta_1}, \quad (3-82)$$

where the right-hand side is obviously positive.

As an example, let the modulating signal be  $x(t) = 2 + \cos t$  and let the demodulator be an ideal low-pass filter with cutoff frequency  $\omega_c = 3$ . Then, the left-hand side of Equation (3-81) becomes  $1 - 3 / \beta_1$  which is plotted in Figure 3-5, where the graphs for  $\xi(\beta)$  are now interpreted with  $\beta = \beta_1$ . Clearly, for the case that  $\lambda = 0.01$ , Equation (3-81) is satisfied provided  $\beta_1 \geq 7$ . Therefore, the modulator threshold necessary for separating the signal and noise components must be not greater than  $2 \pi / 7$ .

#### (b) The Residual Noise Power

We have established above a criterion for selecting  $\omega_o X_o$  so that the significant noise frequencies are above the cutoff frequency of the demodulator. Since the

bandwidth of the noise component is theoretically infinite, it is impossible to completely isolate the signal spectrum from the noise spectrum. Thus there is a certain amount of residual noise power within the signal frequency band due to the "insignificant" spectral components of the noise. It is desirable that this residual noise power be known. At any frequency  $\omega_N$ , the noise power is equal to the sum of contributions from the spectral components of all  $\mu_{rk}(t)$  with the same frequency; that is, the average noise power is

$$W_t = \frac{1}{2} \left( \sum_{k=1}^{\infty} E_k \cos \eta_k \right)^2 + \frac{1}{2} \left( \sum_{k=1}^{\infty} E_k \sin \eta_k \right)^2 \quad (3-83)$$

where  $E_k$  and  $\eta_k$  are respectively the amplitude and phase of the spectral components with frequency  $\omega_N$ . Although  $W_t$  can be evaluated approximately by truncating the series at  $k = K_1$  where  $K_1$  is the greatest integer not exceeding  $1/\lambda$ , it is unwieldy for analysis. As an alternative, a useful measure of the maximum residual noise power at any frequency within the pass band of the demodulator will be derived in the following.

We have shown in Section 3.2.2 that the power spectrum of the constituent  $\mu_{rk}(t)$  of the noise component is bounded by that of the related FM wave  $2h e_k(t)$ . As noted there, the amplitudes of the significant spectral components of  $2h e_k(t)$  are not less than  $4h\lambda/k\omega_o$ . Therefore, the average power of any "insignificant" spectral component of  $\mu_{rk}(t)$  is bounded from above by

$$W_{bk} = \frac{1}{2} \left( \frac{4h\lambda}{k\omega_o} \right)^2. \quad (3-84)$$

Thus, if  $\omega_o X_o$  has been selected to satisfy the criterion given by Equation (3-76), a

reasonable measure of the maximum possible noise power at any frequency  $\omega_N$  less than the cutoff frequency  $\omega_c$  of the demodulator is

$$W_b = \sum_{k=1}^{\infty} W_{bk} = \frac{4}{3} \left( \frac{\pi h \lambda}{\omega_o} \right)^2, \quad (3-85)$$

since<sup>31</sup>

$$\sum_{k=1}^{\infty} \frac{1}{k^2} = \frac{\pi^2}{6}. \quad (3-86)$$

It should be noted that  $W_b$  is a conservative measure of the residual noise power especially at lower values of  $\omega_N$ , since the actual residual noise power at those frequencies may be much less than  $W_b$ . This latter observation is based on the fact that the average power of the insignificant spectral components of  $2 h e_k(t)$  decreases monotonically with frequency for the frequencies less than  $\omega_{k \min}$ .

Using the measure of residual noise power obtained above, we can obtain an estimate of the signal - to - noise ratio of the demodulated signals at the modulating signal frequency  $\omega_1$ . As shown in Equation (3-42), the signal amplitude is essentially  $U h \tau$ , provided the pulse width  $\tau$  is such that  $0 < \omega_1 \cdot \tau < 1$ . Thus, the average power of the signal is  $\frac{1}{2} (U h \tau)^2$ . Assuming that the demodulator is an ideal low-pass filter with cutoff frequency  $\omega_c$  and that the noise power is constant in the pass-band of the filter, we obtain the following estimate of the signal - to - noise ratio

$$S/N = \frac{3}{8 \omega_c} \left( \frac{\omega_o U \tau}{\pi \lambda} \right)^2 \quad (3-87)$$

Letting  $\tau = \alpha / \omega_1$  where  $0 < \alpha < 1$ , and substituting  $\omega_0 = 2\pi / \alpha$ , we have

$$S/N = \frac{3}{2\omega_c} \cdot \left(\frac{\alpha U}{\alpha \lambda \omega_1}\right)^2, \quad (3-88)$$

where  $\alpha$  is the modulator threshold,  $\lambda$  is a small positive constant used in determining the significant frequencies,  $U$  and  $\omega_1$  are respectively the amplitude and frequency of the modulating sinusoid. It is interesting to note that this signal - to - noise ratio is independent of the biasing constant,  $X_0$  of the modulating signal, provided  $X_0 \omega_0$  satisfies the criterion given in Equation (3-76). This result is reasonable, because the amplitude of the signal frequency is independent of  $X_0$  while the amplitudes of the noise spectral components depend on  $X_0$  only through  $\sin[(k\omega_0 X_0 + n\omega_1)\tau/2]$  which is bounded by unity. It is also interesting to note that the signal - to - noise ratio is proportional to the square of the amplitude - frequency ratio,  $U / \omega_1$  of the modulating signal, but is inversely proportional to the square of the modulator threshold.

### 3.3.3 A Synthesis Criterion for Multitone Modulation

In the last sub-section, we have derived a synthesis criterion for single-tone modulation, which can be expressed in terms of the minimum number of pulses per modulating signal period. This criterion, Equation (3-76), was derived by first establishing that the significant frequencies of the noise component in the output rectangular pulse train are bounded from below by the minimum significant frequency of the corresponding FM wave  $2h e_1(t)$ , where  $e_1(t)$  is defined by Equation (3-17) with  $k=1$ . In a similar way, we can also now derive a similar criterion for multitone modulation.

Let us assume, for the present, that the significant frequencies of the noise component in multitone modulation are bounded from below by the minimum significant frequency  $\omega'_{1 \min}$  of the corresponding FM wave  $2 h e_1(t)$ , where  $e_1(t)$  is here defined by Equation (3-53) for  $k = 1$ . Then in analogy with Equation (3-74) this minimum significant frequency can be expressed as

$$\omega'_{1 \min} = \omega_o X_o - N'_{1 \min} \omega_{\max} \quad (3-89)$$

where  $\omega_{\max}$  is the maximum significant frequency of the message signal, and  $N'_{1 \min}$  is a positive number. As in the case of single-tone modulation, we require that  $\omega'_{1 \min}$  be greater than the cut-off frequency  $\omega_c$  of the demodulating low-pass filter. Thus, for  $\omega_c = m \omega_{\max}$  where  $m > 1$ , we require

$$\omega_o X_o - N'_{1 \min} \omega_{\max} > m \omega_{\max},$$

which can be re-written as

$$\frac{\omega_o X_o}{\omega_{\max}} > N'_{1 \min} + m. \quad (3-90)$$

This expression is our synthesis criterion for multitone modulation. This criterion is similar to the criterion for single-tone modulation, Equation (3-76), and states that the parameters  $\omega_o$  and  $X_o$  should be so selected that the number of pulses per period of the maximum significant frequency in the message signal is greater than  $N'_{1 \min} + m$ .

Now, with the criterion so obtained, it remains for us to show that (a) the significant frequencies of the noise component are, as assumed above, bounded from below by the minimum frequency,  $\omega_{1 \min}^1$ , of  $2 h e_1(t)$ , and (b) the number  $N_{1 \min}^1$  can be determined. In order to establish these points, we only need to prove that the minimum significant frequency,  $\omega_{k \min}^1$  of  $2 h e_k(t)$  is greater than  $\omega_{1 \min}^1$  for all  $k > 1$ , since the significant amplitude spectrum of the noise constituent,  $\mu_{rMk}(t)$ , is bounded by that of  $2 h e_k(t)$ , as we have shown in Sub-section 3.2.3. We shall first demonstrate the validity of this for a specific multitone signal, and then generalize the result.

Consider the periodic message signal  $f(t)$  shown in Figure 3-6. The modulating signal,  $X_o + f(t) \geq 0$ , is of the form given by Equation (3-52), since  $f(t)$  can be expressed in a Fourier series. Thus, as we have shown in Sub-section 3.2.3, the amplitude spectrum of the  $k$ th constituent of the noise component in the output rectangular pulse train is bounded by the amplitude spectrum of the corresponding FM wave  $2 h e_k(t)$ . By Equations (3-10) to (3-12),

$$2 h e_k(t) = \frac{4 h}{k \omega_o} \cdot \sin [k \omega_o X_o t + \zeta(t)], \quad (3-91)$$

where

$$\zeta(t) = k \omega_o \int_0^t f(t) dt.$$

This frequency-modulated (FM) wave can be expressed in terms of its spectral components. Using the result from Reference 42, we obtain

$$2 h e_k(t) = \frac{4 h}{k \omega_o} \sum_{n=-\infty}^{\infty} \frac{\beta' \cdot \sin [\pi \alpha (\beta' - n)]}{\pi (\beta' - n) (\beta' \alpha - n \alpha + n)} \cdot \sin (k \omega_o X_o + n \nu) t, \quad (3-92)$$

where  $\nu$  and  $D$  are respectively the repetition frequency and the maximum amplitude of the signal  $f(t)$  shown in Figure 3-6. Further,  $\beta' = k \omega_o D / \nu$  is the modulation index,  $\alpha$  is a parameter of the given  $f(t)$ , whose value lies between zero and one, and all other symbols are as defined previously.

Equation (3-92) can be utilized to determine the minimum significant frequency and the significant bandwidth of  $2 h e_k(t)$  as a function of  $\beta'$ . The significant frequencies of the present signal are those for which

$$\left| \frac{\beta' \cdot \sin [\pi \alpha (\beta' - n)]}{\pi (\beta' - n) (\beta' \alpha - n \alpha + n)} \right| \geq \lambda, \quad (3-93)$$

where  $\lambda$  is a small positive constant. When  $\alpha = 0.5$ , i.e. when the modulating signal for  $e_k(t)$  is a square wave, the variation of bandwidth as a function of modulation index  $\beta'$  for  $\lambda = 0.01$  and  $0.001$ , is as shown in Figure 3-7, wherein the ordinate is defined as

$$\xi'(\beta') = \frac{\text{bandwidth} - 2 k \omega_o D}{2 k \omega_o D}. \quad (3-94)$$

Defining the minimum significant frequency of  $2 h e_k(t)$  as

$$\omega'_{k \min} = k \omega_o X_o - N'_{k \min} \omega_{\max}, \quad (3-95)$$

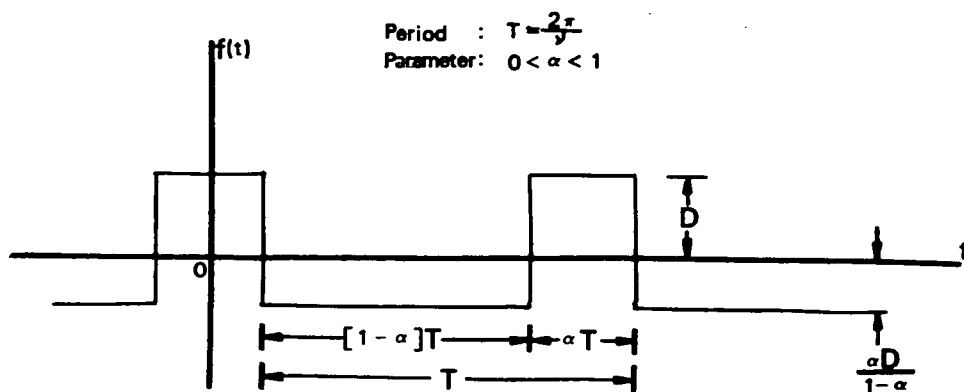


Fig. 3-6. A Message Signal for S-S IPFM

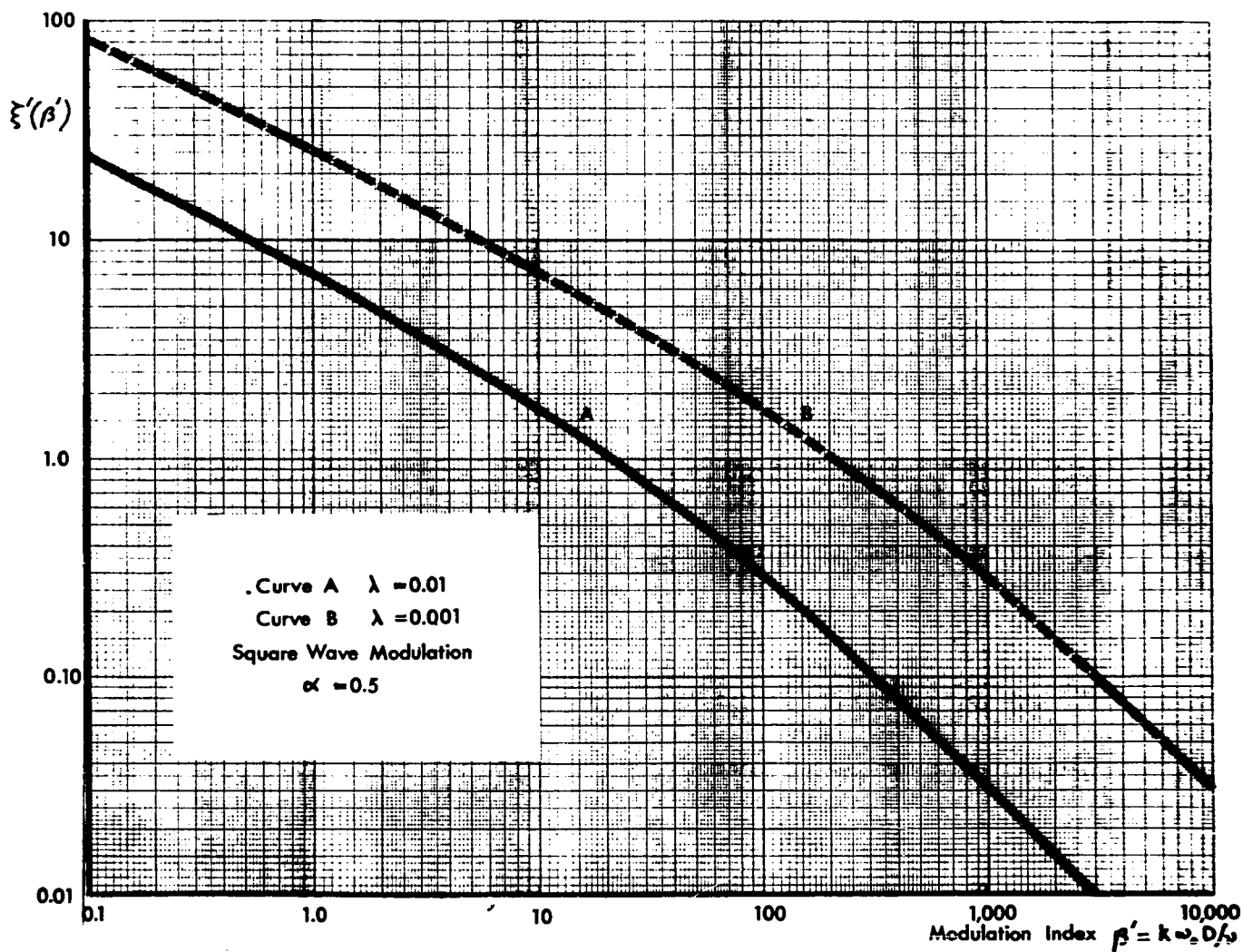


Fig. 3-7. Variation of bandwidth with modulation index.  
 (Replotted from Ref. 42)

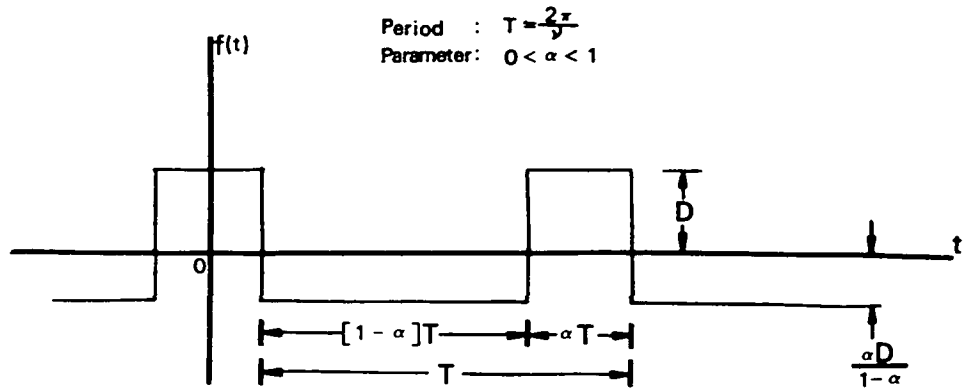


Fig. 3-6. A Message Signal for S-S IPFM

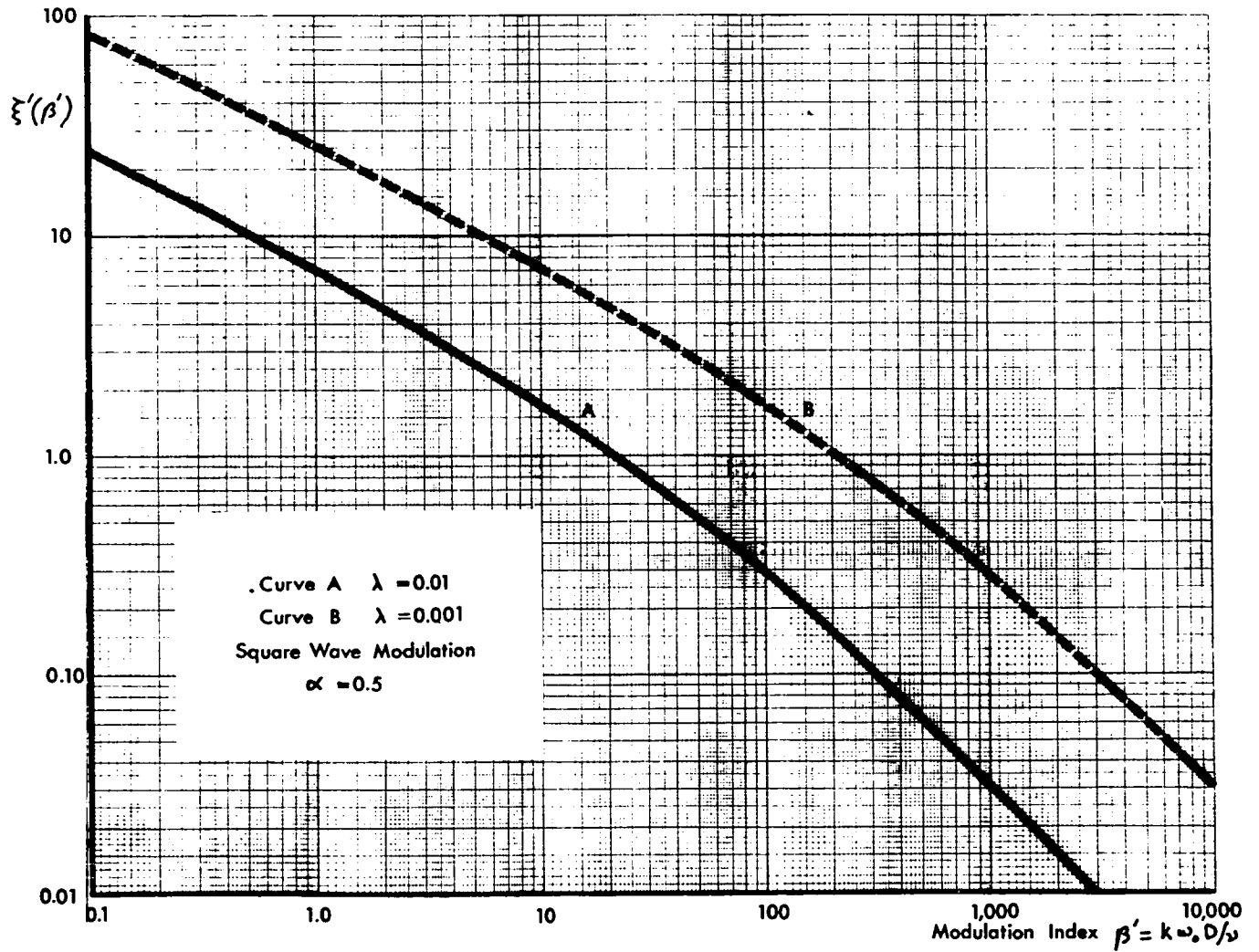


Fig. 3-7. Variation of bandwidth with modulation index.  
 (Replotted from Ref. 42)

where  $\omega_{\max}$  is the maximum significant frequency of the message signal  $f(t)$ , and  $N'_{k \min}$  is a positive constant, then we can re-write Equation (3-94) as

$$\xi'(\beta') = \frac{N'_{k \min} \omega_{\max} - k \omega_o D}{k \omega_o D}, \quad (3-96)$$

since the amplitude spectrum of the FM wave produced by a symmetrical modulating signal is symmetrical.<sup>43</sup> Hence, from Equations (3-95) and (3-96), we have

$$\omega'_{k \min} = k \omega_o [X_o - D(1 + \xi'(\beta'))]. \quad (3-97)$$

This equation is of the same form as Equation (3-71) which has been used in deriving the synthesis criterion which has been used in deriving the synthesis criterion for single-tone modulation. Therefore, using the argument which follows Equation (3-71), we can show that  $\omega'_{1 \min} < \omega'_{k \min}$  for all  $k > 1$ . Further, as in the case of single-tone modulation, the number  $N'_{1 \min}$  can be determined by using the graph of  $\xi'(\beta')$ . Thus, from Equation (3-96),

$$N'_{1 \min} = \frac{\omega_o D}{\omega_{\max}} \cdot [1 + \xi'(\beta'_1)] \quad (3-98)$$

where  $\beta'_1 = \omega_o D / \nu$ .

In the preceding paragraphs we have demonstrated that the synthesis criterion, given in Equation (3-90), for multi-tone modulation is applicable to one particular modulating signal. We shall now show that this criterion is applicable to some

more general modulating signals of the form given by Equation (3-52). Thus, consider the following approximate formula which is commonly used to estimate the significant bandwidth of an FM signal.<sup>1</sup>

$$\text{Bandwidth} \approx 2 (\Delta F + 2 \omega_{\max}), \quad (3-99)$$

where  $\Delta F$  is the maximum deviation of frequency, and  $\omega_{\max}$  is as defined above. For the FM wave  $2 h e_k(t)$ ,  $\Delta F = k \omega_o D_m$ , where  $D_m$  is the maximum amplitude of the message signal. Thus, assuming the amplitude spectrum of  $2 h e_k(t)$  to be symmetrical, we can express its minimum significant frequency as

$$\omega'_{k \min} \approx k \omega_o \left[ X_o - D_m \left( 1 + \frac{2}{\beta_m} \right) \right], \quad (3-100)$$

where  $\beta_m = k \omega_o D_m / \omega_{\max}$ . By comparing this expression with Equation (3-97) and noting that  $2 / \beta_m$  also decreases monotonically with  $\beta_m$ , it is clear that  $\omega'_{1 \min} < \omega'_{k \min}$  for all  $k > 1$ . Therefore, the criterion given by Equation (3-90) is also applicable for a general signal, provided the amplitude spectrum of  $2 h e_k(t)$  is symmetrical. In this case, the number  $N'_{1 \min}$  can be determined by comparing Equation (3-89) with Equation (3-100) for  $k = 1$ . Thus,

$$N'_{1 \min} \approx \frac{\omega_o D_m}{\omega_{\max}} + 2. \quad (3-101)$$

In summary, we have derived above a synthesis criterion for S - S IPFM with multitone modulation. This criterion, given in Equation (3-90), states that the modulator threshold  $\alpha = 2 \pi / \omega_o$  and the biasing constant  $X_o$  should have such values to

yield more than  $N_{1\min}' + m$  pulses per period of the highest significant frequency  $\omega_{\max}$  in the message signal. The number  $N_{1\min}'$  can be determined using Equation (3-98) and graphs such as the one in Figure 3-7, if the modulating signal is a biased square wave. For a general modulating signal which produces a symmetrical amplitude spectrum in  $2 \text{ h e}_k(t)$ ,  $N_{1\min}'$  is given by the approximate relation in Equation (3-101). The number,  $m$ , is given by  $m = \omega_c / \omega_{\max}$ , where  $\omega_c$  is the cutoff frequency of the demodulating filter, and  $\omega_{\max}$  is the highest significant frequency of the message signal.

### 3.4 Double-Signed Integral Pulse Frequency Modulation

#### 3.4.1 An Approximate Model of the Modulator

As we have shown in Chapter II, a double-signed integral pulse frequency (D - S IPF) modulator can be represented by the model shown in Figure 2-2. This model contains a uniform quantizer with hysteresis. Because of the functional complexity introduced by the hysteresis in the quantizer, the spectral characteristics of the output pulse train from this modulator can not be mathematically analyzed at present. However, such an analysis becomes possible if an approximate representation of the modulator is utilized. We believe the results thus obtained will give a reasonably good description of the spectral characteristics of double-signed integral pulse frequency modulation (D - S IPFM), provided that the number of output pulses is approximately equal to the number of pulses in the D - S IPF modulated pulse train, as we shall show in the next paragraph.

For the present purpose, we represent the D - S IPF modulator approximately as shown in Figure 3-8 . In this approximate representation, the only change is that the quantizer is considered to be without hysteresis ; the other components and quantizer characteristics are identical with those of the model shown in Figure 2-2. A typical output pulse train from this approximate model, together with the pulse train from the corresponding D - S IPF modulator with the same input, are shown in Figure 3-9. The two pulse trains are very similar, and in fact, if the pulses marked A and B are removed from the pulse train,  $\hat{x}(t)$ , generated by the approximate model, then the two trains are identical. Pulses A and B are generated after the derivative of  $z(t)$ , or equivalently, after the modulating signal  $x(t)$ , has changed its sign. In general, the approximate model generates one additional pulse each time after  $x(t)$  changes sign and then retains the same sign until the threshold of the modulator is reached. As an example, a sinusoidal signal with sufficient amplitude to produce more than 4 pulses per cycle in the D - S IPF modulated pulse train will produce 2 additional pulses per cycle in the output of the approximate model. Thus, provided the number of additional pulses is small compared with the total number of pulses in the pulse train, the approximate model shown in Figure 3-9 can be used with negligible error for analyzing D - S IPFM.

### 3.4.2 Spectral Analysis

Now, we proceed to obtain a spectral representation for the output pulse trains of this approximate model of the D - S IPF modulator. Since this approximate model is identical with the model for a S - S IPF modulator (Figure 3-1), the method

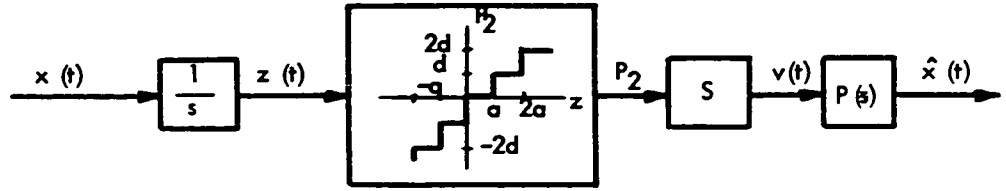
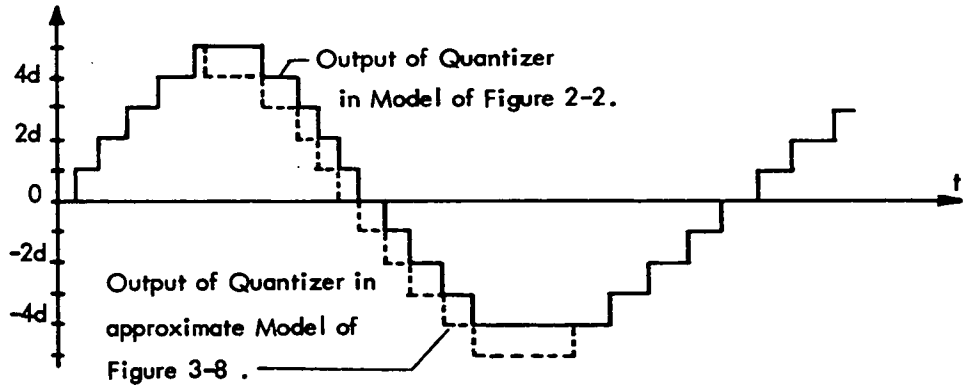
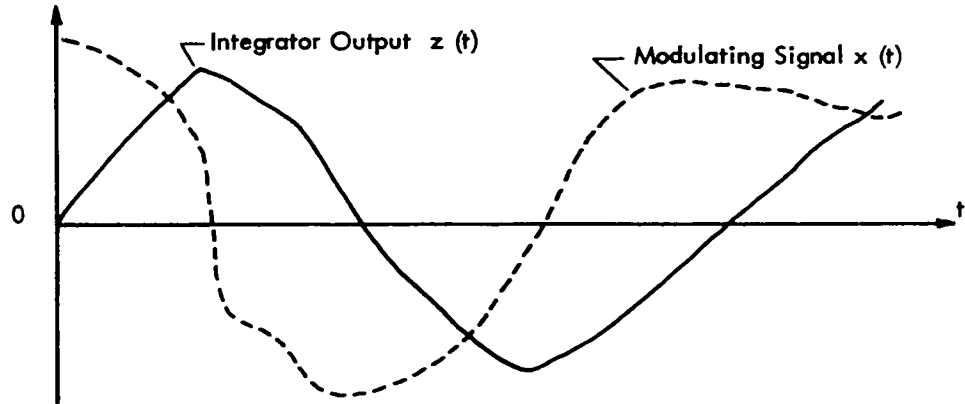
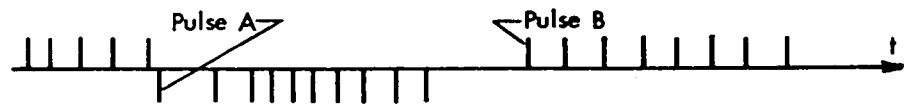


FIGURE 3-8. AN APPROXIMATE MODEL OF THE D-S IPF MODULATOR.



Pulse Train from a D - S IPF Modulator



Pulse Train from approximate Model of the Modulator

FIGURE 3-9. COMPARISON OF SIGNALS FROM A D-S IPF MODULATOR AND ITS APPROXIMATE MODEL.

of analysis developed in Section 3.2 for S - S IPFM is applicable to the present problem. In fact, if the biasing constant,  $X_o$ , is set equal to zero in the equations describing the S - S IPF modulated pulse trains, the resulting expressions will represent the output of the approximate model for the D - S IPF modulator. Hence, for single-tone modulation with the modulating signal,

$$x(t) = U \cos(\omega_1 t + \theta), \quad (3-102)$$

an expression for the output pulse train  $\hat{x}(t)$  can be readily obtained from Equations (3-25) to (3-27). Thus,

$$\hat{x}(t) = \frac{d}{a} \cdot U \cdot A(\omega_1) \cos[\omega_1 t + \theta + Q(\omega_1)] + \hat{N}(t), \quad (3-103)$$

where

$$\hat{N}(t) = \frac{d}{a} \sum_{k=1}^{\infty} \sum_{n=-\infty}^{\infty} \frac{2}{k \omega_o} \cdot J_n(\beta) \cdot n \omega_1 \cdot A(n \omega_1) \cdot \cos[n \omega_1 t + n \theta + Q(n \omega_1) - \beta \sin \theta], \quad (3-104)$$

and other symbols are as defined previously.

Similarly, expressions for the output pulse trains produced by multitone modulation can be obtained using Equations (3-58) to (3-61).

Equations (3-103) and (3-104) represent the output pulse train in terms of its spectral components. It is clear, from Equation (3-103), that the pulse train contains a signal component which is proportional to the modulating signal modified by the frequency

characteristics of the pulse-shaping element,  $P(s)$ . Further, the pulse train contains a noise component,  $\hat{N}(t)$ , which, as shown by Equation (3-104), has a theoretically infinite bandwidth with its spectral frequencies located at  $n\omega_1$ , where  $|n| = 1, 2, 3, \dots$ . Note that the noise spectral component at zero frequency has zero amplitude; and note further, that the remaining noise spectral components are the fundamental and higher harmonics of the modulating signal. The noise component has the following additional characteristics:

1. The amplitude spectrum depends on the phase angle  $\theta$  of the modulating signal. In particular, the spectrum contains only the even harmonics of the modulating signal whenever

$$\theta = \sin^{-1} \left[ \frac{\omega_1}{\omega_0 U} \cdot (2m + 1) \frac{\pi}{2} \right], \quad (3-105)$$

and it contains only the odd harmonics whenever

$$\theta = \sin^{-1} \left[ \frac{\omega_1}{\omega_0 U} \cdot m\pi \right] \quad (3-106)$$

where  $m$  is any integer.

In order to establish this result, we re-write Equation (3-104) to represent  $\hat{N}(t)$  in terms of positive frequencies only. Thus,

$$\hat{N}(t) = \frac{d}{a} \cdot \sum_{k=1}^{\infty} \frac{2}{k\omega_0} \cdot \sum_{n=1}^{\infty} \left\{ J_n(\beta) \cdot n\omega_1 \cdot A(n\omega_1) \cdot \cos[n\omega_1 t + n\theta + Q(n\omega_1) - \beta \sin \theta] + \right.$$

$$(-1)^{n+1} \cdot J_n(\beta) \cdot n \omega_1 \cdot A(n \omega_1) \cdot \cos [n \omega_1 t + n \theta + Q(n \omega_1) + \beta \sin \theta] \Big\} , \quad (3-107)$$

since  $J_{-n}(\beta) = (-1)^n J_n(\beta)$  and since  $A(-\omega) = A(\omega)$  and  $Q(-\omega) = -Q(\omega)$  for a real pulse-shaping element,  $P(s)$ . By using the identities,

$$\cos x + \cos y = 2 \cos \left( \frac{x+y}{2} \right) \cdot \cos \left( \frac{x-y}{2} \right)$$

and

$$\cos x - \cos y = 2 \sin \left( \frac{x+y}{2} \right) \sin \left( \frac{y-x}{2} \right) ,$$

Equation (3-107) can be simplified to yield

$$\begin{aligned} \hat{N}(t) = & \sum_{n=1}^{\infty} B_{2n} \sin [2n \omega_1 t + 2n \theta + Q(2n \omega_1)] \\ & + B_{2n-1} \cos [(2n-1) \omega_1 t + (2n-1) \theta + Q(2n \omega_1 - \omega_1)] , \end{aligned} \quad (3-108)$$

where

$$B_{2n} = \frac{4d}{a} \cdot \frac{2n \omega_1}{\omega_o} \cdot A(2n \omega_1) \cdot \sum_{k=1}^{\infty} \frac{J_{2n}(\beta)}{k} \sin(\beta \sin \theta) , \quad (3-109)$$

$$B_{2n-1} = \frac{4d}{a} \cdot \frac{(2n-1) \omega_1}{\omega_o} \cdot A(2n \omega_1 - \omega_1) \cdot \sum_{k=1}^{\infty} \frac{J_{2n-1}(\beta)}{k} \cdot \cos(\beta \sin \theta) . \quad (3-110)$$

Now, by noting that  $\beta = k \omega_o U / \omega_1$ , it is clear from Equation (3-110) that whenever Equation (3-105) is satisfied,  $B_{2n-1} = 0$  and thus  $\hat{N}(t)$  contains only the even harmonics of the modulating signal. Similarly, whenever Equation (3-106) is satisfied,  $B_{2n} = 0$  and  $\hat{N}(t)$  contains only the odd harmonics of the modulating signal.

2. The amplitude spectrum of the noise component is bounded by a curve which is proportional to the amplitude characteristic of the cascade of the last two elements in the model of the D - S IPF modulator.

In order to establish this result, let us consider the series

$$F_{2n} = \sum_{k=1}^{\infty} \frac{J_{2n}(\beta)}{k} \sin(\beta \sin \theta) \quad (3-111)$$

which is in the expression for  $B_{2n}$  given in Equation (3-109).

It is known that <sup>44</sup>

$$J_n(\beta) \approx \left(\frac{2}{\pi\beta}\right)^{1/2} \cos\left(\beta - \frac{\pi}{4} - n\frac{\pi}{2}\right), \quad (3-112)$$

for  $\beta$  large. Hence,

$$|F_{2n}| \leq \sum_{k=1}^{\infty} \left(\frac{2}{\pi\beta}\right)^{1/2} \frac{1}{k}, \quad (3-113)$$

and substituting  $\beta = k\omega_0 U / \omega_1$ , we have

$$|F_{2n}| \leq \left(\frac{2\omega_1}{\omega_0 U \pi}\right)^{1/2} \sum_{k=1}^{\infty} \frac{1}{k^{3/2}} \quad (3-114)$$

By using Cauchy's integral test, <sup>40</sup> the sum in Equation (3-114) can be shown to be bounded as follows .

$$2 < \sum_{k=1}^{\infty} \frac{1}{k^{3/2}} < 3 \quad (3-115)$$

Therefore,

$$|F_{2n}| < 3 \cdot \left( \frac{2\omega_1}{\omega_0 U \pi} \right)^{1/2} \quad (3-116)$$

Using this result, we have from Equation (3-109),

$$|B_{2n}| < \frac{1}{a} \cdot \left( \frac{2\omega_1}{\omega_0 U \pi} \right)^{1/2} \cdot \frac{2n\omega_1}{\omega_0} \cdot A(2n\omega_1), \quad (3-117)$$

$n = 1, 2, 3, \dots$

By a similar development, we derive from Equation (3-110),

$$|B_{2n-1}| < \frac{1}{a} \cdot \left( \frac{2\omega_1}{\omega_0 U \pi} \right)^{1/2} \cdot \frac{(2n-1)\omega_1}{\omega_0} \cdot A(2n\omega_1 - \omega_1); \quad (3-118)$$

$n = 1, 2, 3, \dots$

Now, Equations (3-117) and (3-118) can be combined into one expression. Thus, defining  $|B_n|$  as the amplitude of the spectral component of  $\hat{N}(t)$  for  $n = 1, 2, 3, \dots$ , we have

$$|B_n| < \frac{1}{a\omega_0} \cdot \left( \frac{2\omega_1}{\pi\omega_0 U} \right)^{1/2} \cdot n\omega_1 \cdot A(n\omega_1). \quad (3-119)$$

This relation shows that the amplitude spectrum of  $\hat{N}(t)$  is bounded by a curve which is proportional to the amplitude characteristic of a system whose transfer function is  $sP(s)$ .

Therefore, this proves the result initially stated above.

### 3.4.3 Choice of Modulator Threshold

We have noted above that the spectral frequencies of the noise component in a D - S IPF modulated pulse train are the fundamental and higher harmonics of the modulating signal. It is clear, from this observation, that for a modulating signal comprising more than one frequency, the noise spectrum always significantly overlaps the signal spectrum. Hence, it is impossible to recover the modulating signal without distortion from the attending noise frequencies, if a low-pass filter is to be the demodulator. Fortunately, this distortion can be reduced to an acceptable level by proper choice of the modulator threshold  $\alpha$ , as we shall now demonstrate for the case of a rectangular output pulse train.

When the output pulses are rectangular with height  $h$  and width  $\tau$ ,  $A(\omega)$  and  $Q(\omega)$  in the expressions related to the output pulse train are given by Equations (3-36) and (3-37) respectively. Hence, from Equation (3-103) the signal component of the pulse train is

$$S(t) \approx \frac{d}{\alpha} \cdot h \tau \cdot U \cos(\omega_1 t + \theta - \omega_1 \tau/2), \quad (3-120)$$

if  $0 < \omega_1 \tau < 1$ . Further, from Equation (3-119) we obtain the following inequality for the amplitude of the noise spectral component at the frequency  $n \omega_1$ .

$$|B_n| < \frac{1}{\alpha} \frac{2d}{\omega_0} \left[ \frac{2\omega_1}{\pi \omega_0 U} \right]^{1/2} \cdot 2h \cdot \sin(n \omega_1 \tau/2). \quad (3-121)$$

Now, consider the ratio of average power

$$\rho_n = \frac{\text{average power of noise at frequency } n\omega_1}{\text{average power of signal component}} = \left| \frac{B_n}{S(t)} \right|^2 \quad (3-122)$$

By Equations (3-120) and (3-121) ,

$$\rho_n < \left[ \frac{2.4}{\omega_0 U \tau} \cdot \sin(n\omega_1 \tau/2) \right]^2 \cdot \frac{2\omega_1}{\pi \omega_0 U} \quad (3-123)$$

Let  $\omega_1 \tau = \alpha$  where  $0 < \alpha < 1$  , and substitute  $\omega_0 = 2\pi/\alpha$  into Equation (3-123) .

Then, after simplification, we have

$$\rho_n < \frac{1}{2} \cdot \left[ \frac{1.2}{\alpha \pi} \right]^2 \cdot \left[ \frac{\omega_1 \alpha}{U} \right]^3 \cdot (1 - \cos n\alpha) \quad (3-124)$$

This relation shows that the noise-to-signal power ratio  $\rho_n$  is bounded by a curve which varies with frequency as  $1 - \cos n\alpha$  , where  $n = 1, 2, 3, \dots$  . In particular, note that this ratio at the modulating signal frequency is given by  $\rho_1$  . Further, it is clear from Equation (3-124) that  $\rho_n$  can be made arbitrarily small by choosing an appropriately small value for the modulator threshold  $\alpha$  .

Equation (3-124) can be utilized to establish a criterion for choosing the modulator threshold  $\alpha$  . Let the demodulator be an ideal low-pass filter with cutoff frequency  $\omega_c = m\omega_1$  where  $m > 1$  . Then, the signal-to-noise ratio of the demodulated signal is

$$S/N = \left[ \sum_{n=1}^N \rho_n \right]^{-1} \quad (3-125)$$

where  $N$  is the largest integer not greater than  $m$  .

Using Equation (3-124) in this equation, we obtain

$$S/N > \frac{1}{\epsilon}, \quad (3-126)$$

where

$$\epsilon = \frac{1}{2} \left[ \frac{1}{\alpha \pi} \right]^2 \cdot \left[ \frac{\omega_1 \alpha}{U} \right]^3 \cdot \left[ N - \sum_{n=1}^N \cos n \alpha \right]. \quad (3-127)$$

Therefore, for a given desired lower bound on the  $S/N$  of the demodulator output, the required value of the modulator threshold  $\alpha$  can be determined by using Equation (3-127).

The criterion that we have just derived is for the case of single-tone modulation. A similar criterion for multitone modulation, cannot be derived at present. However, the criterion given by Equations (3-126) and (3-127) can be profitably used to choose the modulator threshold for a general modulating signal by considering  $\omega_1$  as the highest significant frequency in the modulating signal.

### 3.5 Discussion and Conclusions

In the present chapter, we have developed a general method for spectral analysis of integral pulse frequency modulation (IPFM). In this method, the modulating signal  $x(t)$  is first incorporated into a function described by Equation (3-8), since this provides a systematic approach to derive a spectral description of the output pulse train. Then, this function is represented in terms of its spectral components and the resulting ex-

pression is substituted into Equation (3-9) to yield an expression for the output impulse train. Finally, the spectral representation of the output pulse train of the modulator is derived by considering the linear pulse-shaping element  $P(s)$  as a filter which modifies the spectral components of the impulse train.

Using this method, we have examined in detail the spectral characteristics of IPFM for a class of modulating signals comprising one or more sinusoids. Several useful results have been derived from this analysis. In particular, we have shown that the modulating process introduces a noise component in the output pulse train, whose amplitude spectrum always overlaps that of the signal component. Further, we have derived criteria for selecting the modulator threshold  $a$  and the biasing constant  $X_0$ . For single-signed (S - S) IPFM, the criterion can be expressed in terms of the number of pulses per period of the highest significant frequency component in the message signal.

In the analysis of double-signed (D - S) IPFM, we have assumed that the modulator can be represented sufficiently accurately by a model involving a quantizer without hysteresis. This satisfactory agreement has been demonstrated by means of an example in Section 3.4.1, wherein the output pulse train from this approximate representation is very similar to a D - S IPF modulated train, provided the two trains have about the same number of pulses. However, it is desirable that this approximation be quantitatively evaluated in further investigations.

The synthesis criteria that we have derived in the present analysis are useful for the design of an integral pulse frequency modulator. They can be useful also for the

design of the averaging type FM discriminators, since this type of discriminator demodulates a continuous FM wave by first converting it into a S - S IPF modulated pulse train and then filtering the result with a low-pass network.<sup>33,34</sup>

## CHAPTER IV

### APPLICATION OF INTEGRAL PULSE FREQUENCY MODULATION TO ANALOGUE MULTIPLICATION AND DIVISION

#### 4.1 Introduction

In some control and industrial systems, it is desirable to multiply a continuous signal by a frequency-modulated pulse train. For example, the amount of material per unit time moving on a feeder conveyor can be computed if the weight of the material is multiplied by the velocity of the conveyor, where the former signal is measured by analogue load sensors while the latter can be conveniently represented by a frequency-modulated pulse train originating from an incremental encoder. As another example, the power of a rotating shaft can be similarly determined, since the torque of the shaft is usually measured by an analogue torque transducer, and the shaft speed can be readily encoded into an integral pulse frequency modulated train as we have noted in Section 2.5. Hence, in view of the potential usefulness, it is of interest to investigate the feasibility of implementing analogue multiplication by means of integral pulse frequency modulation (IPFM).

Numerous analogue multiplication methods have been reported in the literature.<sup>3,45,46</sup> Some multipliers, such as the Hall - effect multiplier, directly implement a physical law, while some others, such as the logarithmic or quarter-square multipliers, utilize nonlinear circuit elements and/or special function generators. Of particular interest is the class of multipliers which operate by a combination of modulation methods. In this class of multipliers, various dual modulation schemes involving pulse width modulation as well as amplitude, phase, and frequency modulation of sinusoidal carriers or

pulse trains have been used.<sup>3</sup> However, up to this time, IPFM apparently has not been applied to implement analogue multiplication.

In this chapter, methods for implementing analogue multipliers and dividers using pulse frequency modulation are formulated and studied. Single-signed IPFM (S - S IPFM) is employed to formulate a method of analogue multiplication. A method of pulse frequency modulation originally proposed by Goldberg<sup>27,28</sup> is then represented approximately by an S - S IPFM model, and further this method is utilized to formulate a method of analogue division. Finally, the results of a computer simulation study are shown to verify the feasibility of the proposed methods.

## 4.2 Multipliers Using IPFM

### 4.2.1 Theory

It is well known from sampled data theory that the process of sampling a signal  $y(t)$  is the same as multiplying it by a train  $x^*(t)$  of identical rectangular pulses of unit height.<sup>47</sup> Thus, the output of the sampler, which we denote by  $y^*(t)$ , may be expressed mathematically as

$$y^*(t) = y(t) \cdot x^*(t) \quad (4-1)$$

Now, consider the situation in which the sampling pulse train  $x^*(t)$  is produced by a single-signed integral pulse frequency (S - S IPF) modulator. Based on the results obtained in Chapter III,  $x^*(t)$  can be represented as the sum of a signal com-

ponent  $S(t)$  and a noise component  $N(t)$ . Thus, Equation (4-1) can be re-written as

$$y^*(t) = y(t) \cdot S(t) + y(t) \cdot N(t) . \quad (4-2)$$

When the sampling pulses are sufficiently narrow,  $S(t)$  is almost linearly proportional to the input  $x(t)$  of the S - S IPF modulator. Indeed, if the sampling pulses become impulses, then  $S(t) = \alpha x(t)$ , where  $\alpha$  is a proportionality constant, and the output of the sampler contains a component which is proportional to the product  $x(t) y(t)$ . Therefore, multiplication of two signals,  $x(t)$  and  $y(t)$ , can be accomplished by the arrangement shown in Figure 4-1, provided that the signal component,  $y(t) S(t)$  of  $y^*(t)$  can be recovered with negligible error by the filter.

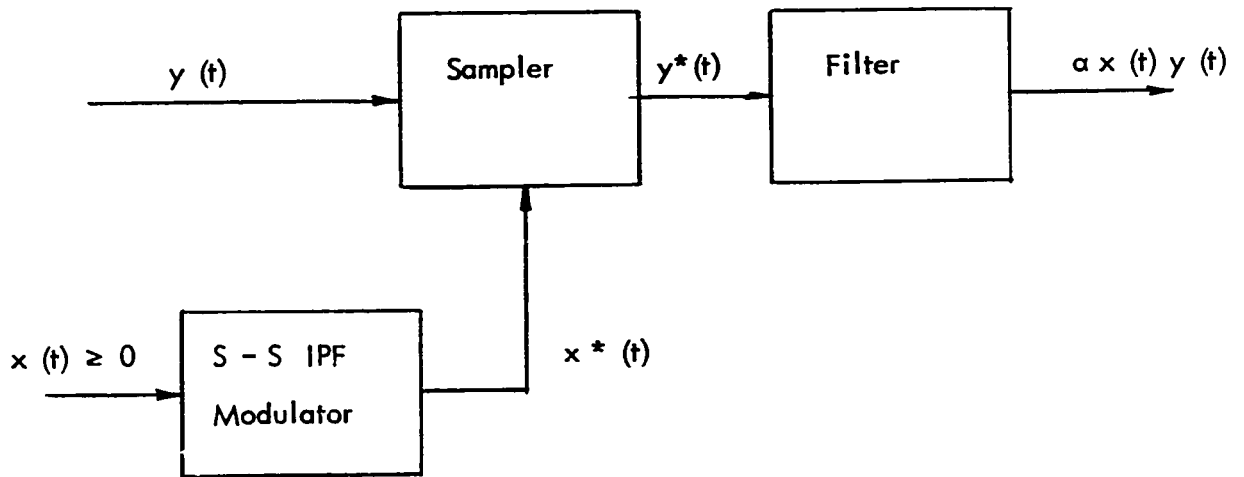


FIGURE 4-1. A METHOD OF ANALOGUE MULTIPLICATION USING IPFM .

We shall now show that the signal component of  $y^*(t)$  can, in fact, be recovered with negligible error by a low-pass filter. Consider first the simpler cases in which either  $x(t)$  or  $y(t)$  is constant. When  $x(t)$  is constant, say  $x(t) = X$ , the sampling pulse train  $x^*(t)$  from the S-S IPF modulator can be readily shown to be periodic with period  $a/X$ , where  $a$  is the modulator threshold. Hence, by the sampling theorem, the signal  $X \cdot y(t)$  can, in principle, be recovered completely by a low-pass filter with cutoff frequency  $\omega_c$ , provided that the power spectrum of  $y(t)$  is zero for frequencies greater than  $\omega_c$ , and provided that the modulator threshold  $a$  is selected to yield the sampling frequency  $\frac{2\pi X}{a} > 2\omega_c$ . For the other case in which  $y(t)$  is constant, the output of the sampler is simply a S-S IPF modulated pulse train. As we have shown in Chapter III, the signal component of this pulse train can be recovered with negligible error by a low-pass filter also, provided that the S-S IPF modulator threshold and the biasing constant in  $x(t)$  are properly selected. Therefore, for both of these simpler cases, the proposed method for multiplication is feasible.

Now, consider the more general situation in which  $x(t)$  is a multitone signal as described by Equation (3-52), and  $y(t)$  is a sinusoid given by

$$y(t) = U_y \cos \nu t . \quad (4-3)$$

For this case, the sampling pulse train  $x^*(t)$  is described by Equations (3-62) to (3-64) with  $h d = 1$ . Substituting these equations and Equation (4-3) into Equation (4-1) and simplifying, we have

$$y^*(t) = \frac{\tau}{a} \cdot U_y \cos \nu t \cdot \left[ X_o + \sum_{m=1}^M U_m \cdot \frac{\sin \omega_m \tau / 2}{\omega_m \tau / 2} \cdot \cos (\omega_m t + \theta_m - \omega_m \tau / 2) \right] + N^s(t) , \quad (4-4)$$

where

$$N'(t) = \frac{U}{2ah} \cdot \sum_{k=1}^{\infty} \sum_{n_1=-\infty}^{\infty} \dots \sum_{n_M=-\infty}^{\infty} E_r(k, n_1, \dots, n_M) \cdot \quad (4-5)$$

$$\left\{ \cos [(\gamma_M - \nu)t + \phi_M - \gamma_M \tau/2] + \cos [(\gamma_M + \nu)t + \phi_M - \gamma_M \tau/2] \right\}$$

and all other symbols are as defined previously.

The first bracketed term of Equation (4-4) is the signal component of  $y^*(t)$  and is almost linearly proportional to the product  $x(t) y(t)$  for a sufficiently small pulse width  $\tau$ .

The noise component, as represented by  $N'(t)$ , has spectral characteristics similar to those of the noise component  $N(t)$  in  $x^*(t)$ . Indeed, the amplitude spectrum of  $N'(t)$  is a composition of two individual spectra :

- (i) the spectrum of  $N(t)$  multiplied by  $\frac{U}{2}$  and shifted downward in frequency by  $\nu$ , and
- (ii) the spectrum of  $N(t)$  multiplied by  $\frac{U}{2}$  and shifted upward in frequency by  $\nu$ .

Since the significant bandwidth of  $N(t)$  is finite, the significant bandwidth of  $N'(t)$  is also finite, and thus the signal and noise spectra of  $y^*(t)$  can be practically separated by proper choice of the modulator threshold  $a$  and the biasing constant  $X_0$  in  $x(t)$ . Therefore, the product,  $x(t) y(t)$ , can be recovered with negligible error by low-pass filtering  $y^*(t)$ .

The above analysis can be immediately extended to demonstrate the feasibility of the proposed method of analogue multiplication for the case in which both  $x(t)$  and  $y(t)$  are multitone signals of the form given by Equation (3-52). Since an arbitrary signal can be closely approximated by a multitone signal, the arrangement shown in Figure 4-1 can be used to implement multiplication of arbitrary signals, provided that the parameters  $a$  and  $X_0$  of the S - S IPF modulator have properly chosen values. The synthesis criteria derived in Section 3.3 may be profitably used here for the selection of  $a$  and  $X_0$ . It should be noted, however, that the bandwidth of the signal and noise components of  $y^*(t)$  depend on both  $x(t)$  and  $y(t)$ . The maximum significant frequency of the signal component is equal to the sum of the maximum significant frequencies of  $x(t)$  and  $y(t)$ , while the minimum significant frequency of  $N'(t)$  is smaller than that of  $N(t)$ . Hence, the selection of the parameters  $a$  and  $X_0$  of the modulator must take these points into consideration.

#### 4.2.2 Implementation

Analogue multipliers based on the theory presented above can be readily implemented using commonly available electronic hardware. The block diagram of a two-quadrant multiplier is shown in Figure 4-2. In this diagram,  $f(t)$  and  $g(t)$  are the signals to be multiplied, while  $X_0$  is a biasing constant in the input,  $x(t)$ , of the S - S IPF modulator. Sampling is performed by the electronic switch. Because the sampling pulse train  $x^*(t)$  contains a signal component which is proportional to  $X_0$ ,

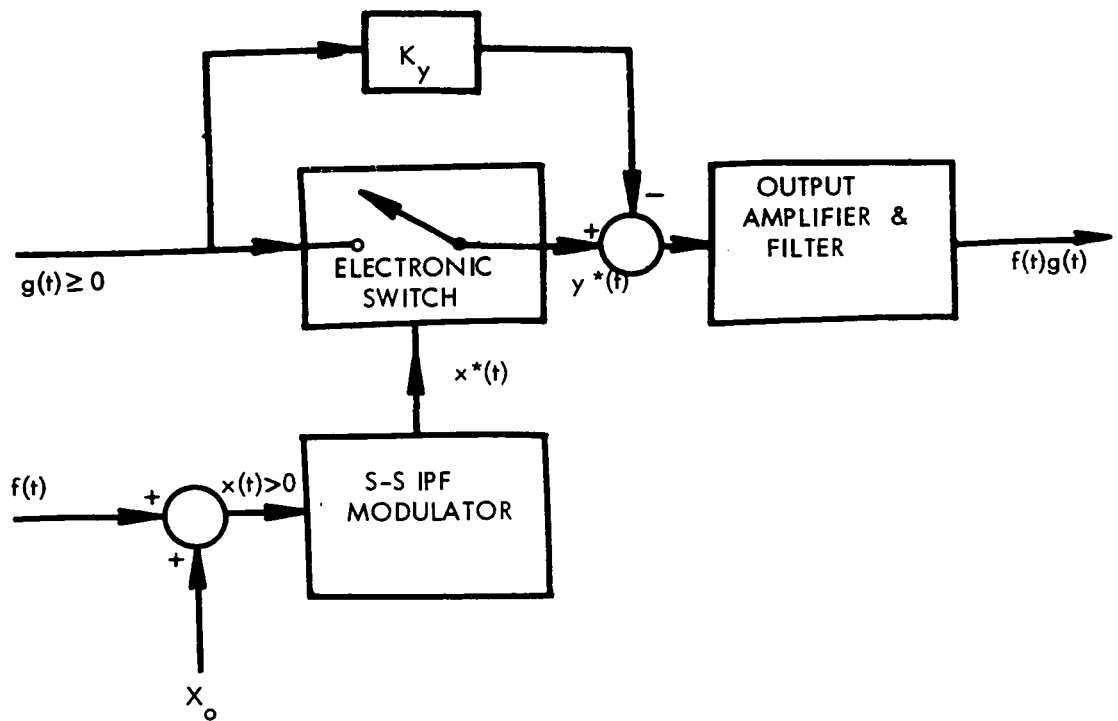


FIG. 4-2. BLOCK DIAGRAM OF A TWO-QUADRANT MULTIPLIER

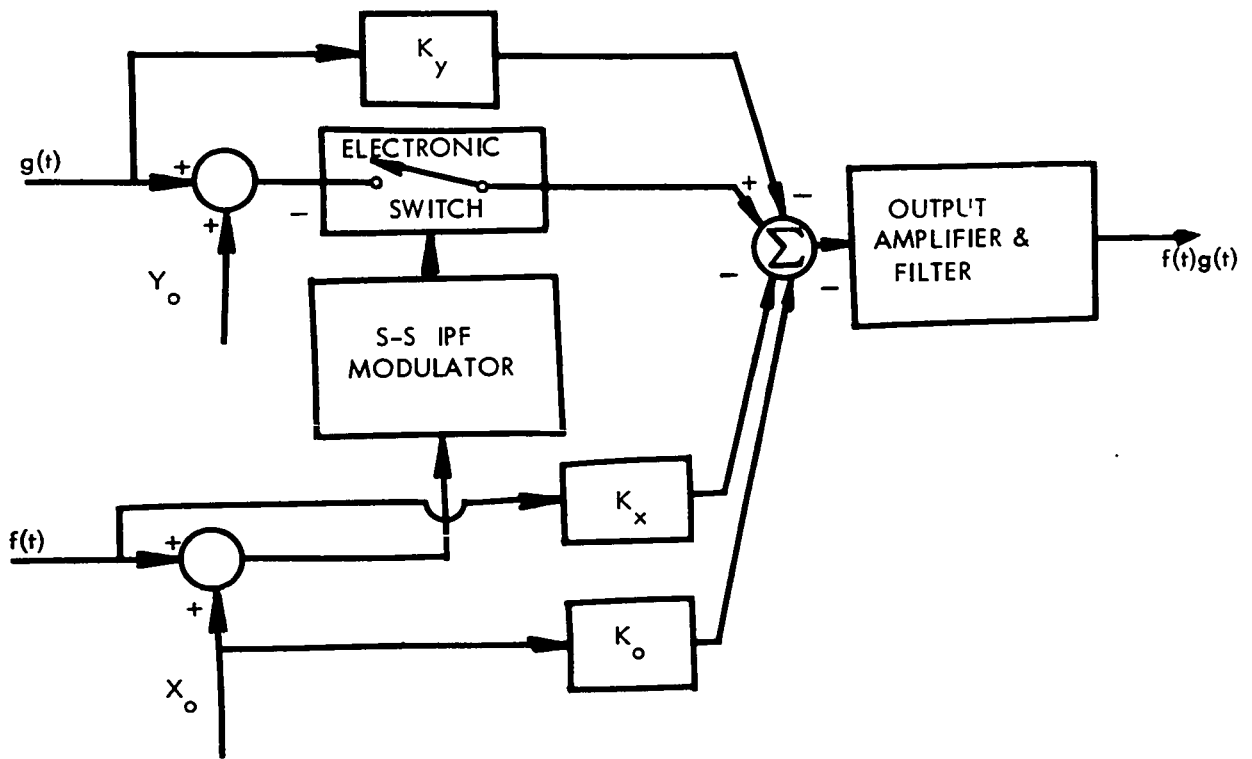


FIG: 4-3. BLOCK DIAGRAM OF A FOUR-QUADRANT MULTIPLIER.

the attenuator  $K_y$  must be adjusted so that the unwanted product  $X_o g(t)$  is zero at the output of the multiplier. The output block contains an amplifier to compensate for the attenuation introduced by pulse frequency modulation and amplitude sampling. The S - S IPF modulator can be implemented as described in Section 2.5, and for the other components of the multiplier, well known electronic circuits or building blocks can be used.<sup>3</sup>

The two-quadrant multiplier can be extended as shown in Figure 4-3 to accomplish four-quadrant multiplication. In this case, a biasing constant  $Y_o$  is added to the signal  $g(t)$  which may now have both positive and negative values. The attenuators  $K_x$  and  $K_o$  are to be adjusted so that the additional unwanted products  $Y_o X_o$  and  $Y_o f(t)$  are zero at the output of the multiplier.

#### 4.3 Dividers Using Goldberg's PFM

One of the earlier methods of pulse frequency modulation (PFM) was proposed by Goldberg.<sup>27,28</sup> (See also Section 1.1). In Goldberg's method, the pulse train is generated by the process shown in Figure 4-4. The modulating signal  $u(t)$  contains a biasing constant so that either  $u(t) > 0$  or  $u(t) < 0$  for all  $t$ . The ramp signal,  $r(t)$ , is generated internally in the modulator and has a constant slope  $m$  whose sign is the same as that of  $u(t)$ . The signals  $u(t)$  and  $r(t)$  are compared. Whenever  $u(t) = r(t)$ , a standard pulse is emitted by the modulator and the ramp is reset to zero at the same instant. Goldberg's method of PFM can be utilized to implement analogue dividers. As a first

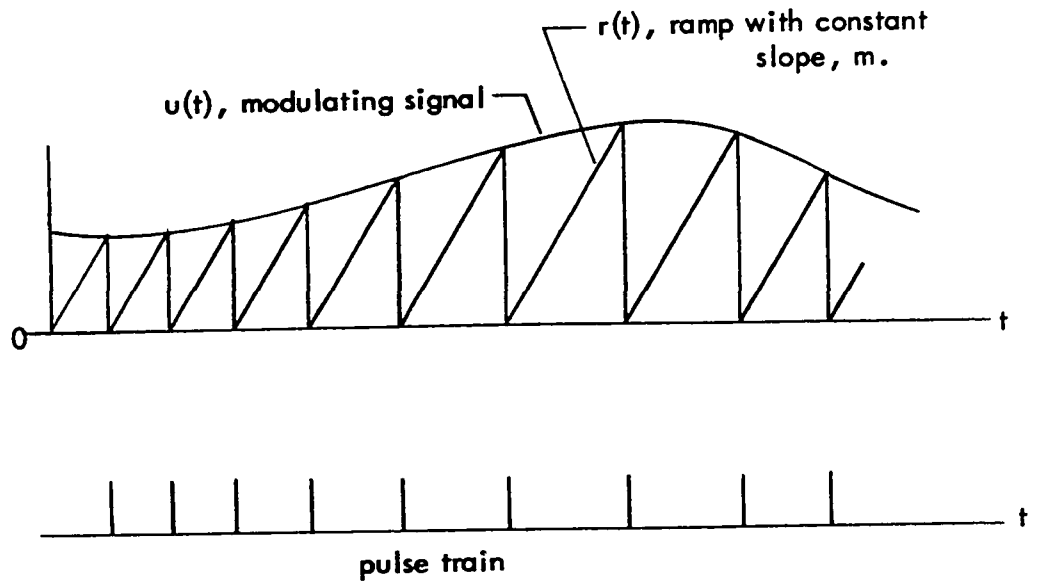


FIGURE 4 - 4. ILLUSTRATING GOLDBERG'S METHOD OF PFM

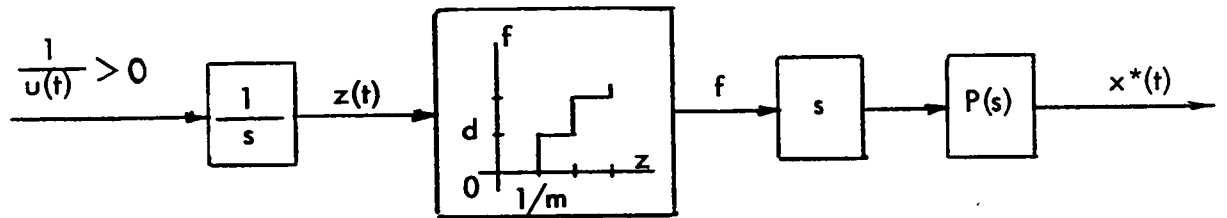


FIGURE 4 - 5. REPRESENTATION OF GOLDBERG'S MODULATOR BY AN S - S IPF MODULATOR

step to establish this result, we shall now show that this method can be approximately re-presented in terms of S - S IPFM .

#### 4.3.1 Representation of Goldberg's PFM in Terms of S - S IPFM

Let  $t'_{i-1}$  and  $t'_i$  be respectively the pulse-emission times of the  $(i-1)$  th and the  $i$ th pulses from Goldberg's modulator. Further, without loss of generality, let  $m > 0$  and  $u(t) > 0$  for all  $t$ . Then, for  $t'_{i-1} < t \leq t'_i$  where  $i = 1, 2, 3, \dots$ , the ramp signal given by

$$r(t) = m(t - t'_{i-1}) . \quad (4-6)$$

Since  $r(t'_i) = u(t'_i)$ , we have from Equation (4-6)

$$t'_i = t'_{i-1} + \frac{u(t'_i)}{m} . \quad (4-7)$$

This relation shows that the pulse interval is linearly proportional to the sampled amplitude of the modulating signal  $u(t)$ . In particular, if  $u(t) = E_0 = \text{constant}$ ,

$$t'_i = t'_{i-1} + \frac{E_0}{m} . \quad (4-8)$$

Now, consider a S - S IPF modulator whose input is  $\frac{1}{u(t)}$ . From Equation (2-1) we have

$$\int_{t'_{i-1}}^{t'_i} \frac{dt}{u(t)} = a \quad (4-9)$$

where  $t'_{i-1}$  and  $t'_i$  are the pulse-emission times of the  $(i-1)$  th and the  $i$ th pulses

respectively, and  $a$  is the modulator threshold. For the particular case in which  $u(t) = E_0$ , we have from Equation (4-9),

$$t_i = t_{i-1} + a E_0 \quad (4-10)$$

Comparing this result with Equation (4-8), we see that the pulse train from an S - S IPF modulator can be made identical to that generated by Goldberg's method if we set the S - S IPF modulator threshold  $a$  equal to  $\frac{1}{m}$ . Hence, for this particular case of  $u(t) = \text{constant}$ , Goldberg's modulator can be represented by an S - S IPF modulator with the threshold  $a = \frac{1}{m}$  and input  $\frac{1}{u(t)}$  as shown in Figure 4-5. We shall now show that this representation is approximately valid for a general signal, provided that the slope  $m$  of the ramp signal in Goldberg's modulator is sufficiently large.

Let the block diagram in Figure 4-5 be called the approximate model of Goldberg's modulator, and let the emission time of its  $i$ th pulse be  $t_i$ . Then, applying the mean-value theorem<sup>40</sup> to the integral in Equation(4-9) and setting  $a = \frac{1}{m}$ , we have

$$t_i = t_{i-1} + \frac{u(q_i)}{m} \quad (4-11)$$

where  $t_{i-1} \leq q_i \leq t_i$ . Now, by assuming  $t_{i-1} = t'_{i-1}$ , the error introduced by the approximate model into the emission time of the  $i$ th pulse is

$$e_i = t'_i - t_i = \frac{u(t'_i) - u(q_i)}{m} \quad (4-12)$$

This result shows that the error is negligible, provided that  $|u(t'_i) - u(q_i)| \ll m$ . Therefore, for  $m$  sufficiently large, Goldberg's modulator can be represented by the approximate model with negligible error.

In utilizing the approximate model for analysis of Goldberg's PFM, it is desirable to know an upper bound of the error for a given modulating signal  $u(t)$  and a given value of  $m$ . Hence, we shall now derive such an upper bound in terms of  $m$  and the maximum slope of  $u(t)$ .

Let  $u(t)$  be expanded in a Taylor series about  $t'_{i-1}$ . Then successively substituting  $t = t'_i$  and  $t = q_i$  in the expansion, and utilizing the resulting two series in Equation (4-12), we obtain

$$e_i = \frac{1}{m} \left\{ (t'_i - q_i) u'(t'_{i-1}) + [(t'_i - t'_{i-1})^2 - (q_i - t'_{i-1})^2] \frac{u''(t'_{i-1})}{2!} + \dots \right\} \quad (4-13)$$

where  $u'$  denotes the first derivative of  $u(t)$ ,  $u''$  the second derivative, and so on.

Now, we assume that

(i) the second and higher order derivatives of  $u(t)$  at  $t = t'_{i-1}$

are negligible for all  $i$ , and

(ii)  $|u'(t)| \leq K$  for all  $t$ , where  $K$  is a positive constant.

Then, by noting that  $|t'_i - q_i| \leq |t'_i - t'_{i-1}|$ , Equation (4-13) can be simplified to yield the relation

$$\left| \frac{e_i}{t'_i - t'_{i-1}} \right| \leq \frac{K}{m}, \quad (4-14)$$

for all  $i$ .

The left-hand side of Equation (4-14) is the magnitude of the error normalized with respect to the pulse interval. Equation (4-14) shows that this normalized error of pulse emission times introduced by the approximate model is bounded by a constant which is linearly proportional to the maximum slope of the modulating signal  $u(t)$ , but inversely proportional to the slope of the ramp signal. Therefore, if  $u(t)$  is given and thus  $K$  can be estimated, then an upper bound of the normalized error can be determined for a given value of  $m$ , the slope of the ramp signal in Goldberg's modulator. Further, Equation (4-14) can be utilized to choose a value of  $m$  for which the approximate model of Goldberg's modulator can be meaningfully utilized. For example, if  $u(t) = E + U \sin(\omega t + \theta) > 0$  and a maximum normalized error of 0.01 is desired, then  $m = 100 \omega U$ .

It should be noted that Equation (4-14) has been derived with the assumption that the second and higher order derivatives are negligible at the initial point of each pulse interval. This assumption implies that  $u(t)$  in all pulse intervals can be closely represented by a linear function. This latter approximation can be made if the bound  $\frac{K}{m}$  is small.

#### 4.3.2 Theory and Implementation of the Divider

Consider the system shown in Figure 4-6. As we have just shown above, Goldberg's modulator can be closely represented by an S - S IPF modulator provided that the slope  $m$  of the ramp signal in Goldberg's modulator is sufficiently large. Thus, the system in Figure 4-6 is practically equivalent to that shown in Figure 4-7 when  $m$  is sufficiently large. Now, based on the theory presented in Sub-section 4.2.1, the output

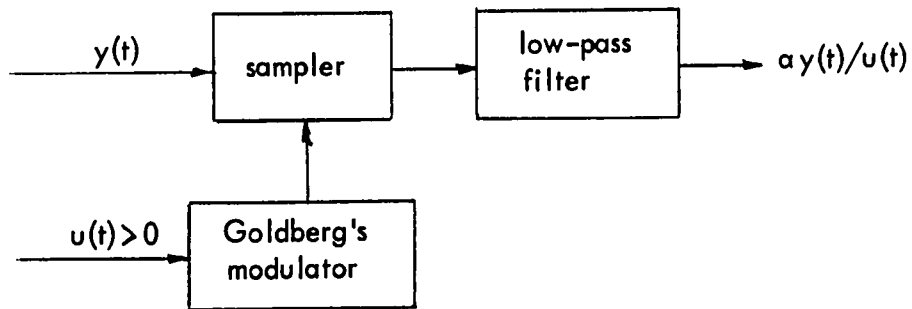


FIG. 4 - 6. A METHOD OF ANALOGUE DIVISION USING GOLDBERG'S PFM

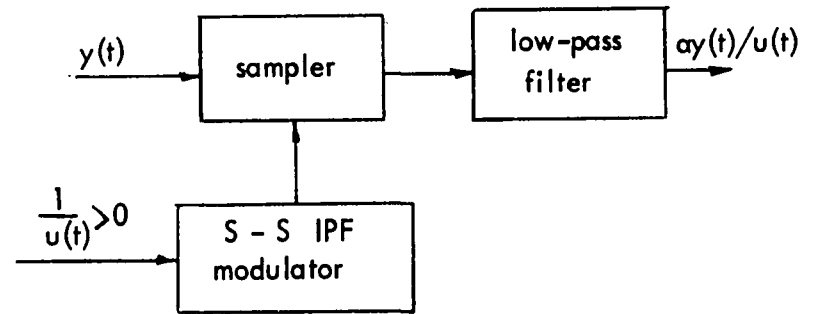


FIG. 4 - 7. A SYSTEM EQUIVALENT TO THAT OF FIG. 4 - 6

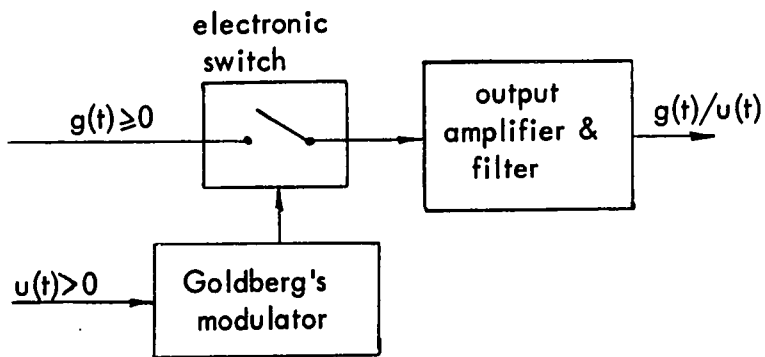


FIG. 4 - 8. ONE-QUADRANT DIVIDER USING GOLDBERG'S PFM

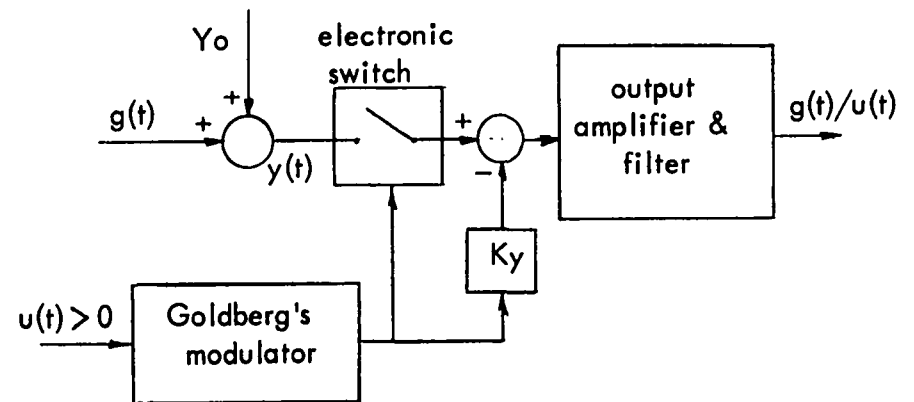


FIG. 4 - 9. TWO-QUADRANT DIVIDER USING GOLDBERG'S PFM

of the low-pass filter in Figure 4-7 is proportional to the quotient  $\frac{y(t)}{u(t)}$ . Since the systems in Figures 4-6 and 4-7 are practically equivalent, the system in Figure 4-6, therefore, can be utilized to implement analogue division.

The block diagram of a one-quadrant divider using Goldberg's PFM is shown in Figure 4-8. In this figure, the signal  $g(t) \geq 0$  is to be divided by  $u(t) > 0$ . The electronics switch performs sampling and the output amplifier compensates for the attenuation introduced by pulse frequency modulation and sampling.

The one quadrant divider can be extended as shown in Figure 4-9 to achieve two-quadrant division. Here, the signal  $g(t)$  is biased by a constant  $Y_0$  so that  $y(t) = Y_0 + g(t) \geq 0$ . Because the output of the sampler contains a component which is proportional to the unwanted quotient  $\frac{Y_0}{u(t)}$ , the attenuator  $K_y$  is included and is to be adjusted so that this unwanted quotient is zero at the output of the divider. It should be noted that the output of  $K_y$ , after passing through the output amplifier and filter, becomes a signal which is proportional to  $\frac{1}{u(t)}$ , since Goldberg's modulator can be closely represented by the S - S IPF model shown in Figure 4-5.

The various blocks of the proposed dividers can be implemented using well-known electronic circuits and / or commonly available building blocks.

#### 4.4 Results of a Computer Simulation Study

A digital computer simulation study has been performed with the objective to verify the feasibility of the proposed methods of analogue multiplication and division. The typical results are shown in Figures 4-10 and 4-11. In Figure 4-10, the output of the multiplier is compared with the true value of the product. The multiplier output follows the true value closely, but lags the latter by a considerable amount. The lag is introduced by the output filter which, for this case, is a slightly under-damped second order system with the break frequency equal to  $6 \text{ rad / sec}$  and the damping ratio equal to  $0.9$ . This break frequency is only about twice the frequency of one of the two sinusoidal components in the product and thus the phase lag introduced into this sinusoidal component is about  $45^\circ$ . The amount of lag can be reduced by increasing the break frequency of the filter; however, if the cutoff characteristic of the filter is not changed, the average pulse frequency of the train from the S - S IPF modulator must be increased in order that the output noise content may be kept at the same low level.

The output of the divider is compared with the true value of the quotient in Figure 4-11. The output of the divider also follows the true value closely, but lags the latter by a considerable amount for the same reason given above in the discussion of the result for the multiplier. The output filter employed in this case is a second order system with a damping ratio of  $0.9$  and a break frequency of  $12 \text{ rad / sec}$ . The ramp signal in Goldberg's modulator has a slope of  $100 \text{ units / sec}$ .

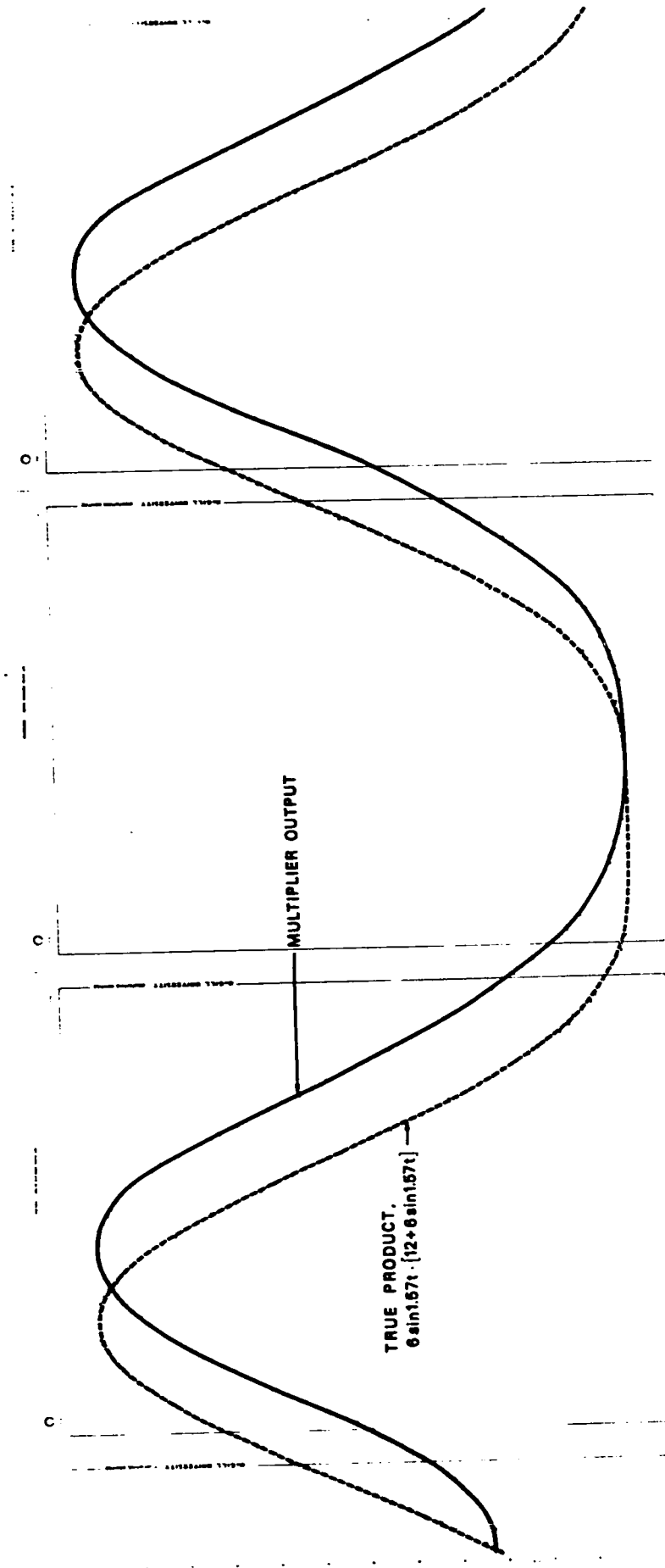


FIG.4-10. MULTIPLIER OUTPUT COMPARED WITH TRUE PRODUCT

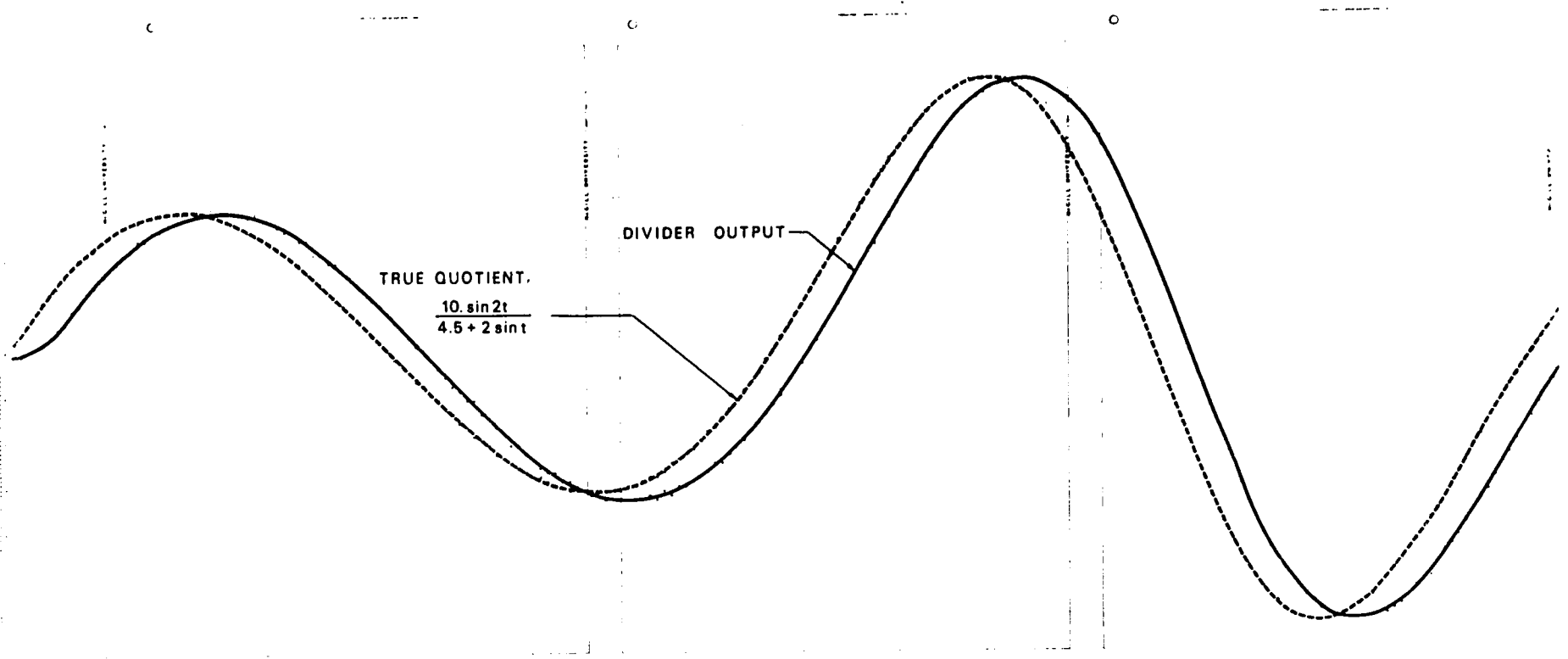


FIG.4-11. DIVIDER OUTPUT COMPARED WITH TRUE QUOTIENT

#### 4.5 Discussion and Conclusion

In this chapter, we have successfully applied IPFM to analogue computation. In particular, we have formulated a method for implementing analogue multipliers using IPFM. Further, we have shown that Goldberg's method of pulse frequency modulation (PFM) can be closely represented in terms of  $S - S$  IPFM, provided that the slope of the ramp signal in the modulator is sufficiently large. This method of PFM is then utilized to implement analogue dividers. The feasibility of these methods of analogue multiplication and division has been studied theoretically and by digital computer simulation.

The multiplier using IPFM is similar to one of the commonly used multipliers, namely, the self-excited time-division multiplier.<sup>3,45</sup> They both operate by amplitude modulation of a pulse train which is generated by means of a feedback system. (See Section 2.5 of this thesis and Reference 3, Figure 7 - 14). However, both the pulse-width and pulse frequency of the train in the self-excited time-division multiplier vary with one of its inputs, whereas the width of the pulses in the multiplier using IPFM remains constant. The multiplier using IPFM appears to have all the advantages possessed by the time-division multiplier. Further, it may be more accurate and versatile than the latter, since it employs pulses of fixed width. Indeed, the multiplier using IPFM would offer more advantages if a number of signals located at widely separated places is to be multiplied by one common signal and the resulting products are to be utilized at the corresponding locations. It would be of interest to compare the performance of the multiplier using IPFM with the commonly used multipliers by constructing prototypes; however, this proposal would form a project by itself and is outside the scope of the present work.

The method of analogue division using Goldberg's PFM has some significant limitations. Firstly, it can only implement one-quadrant and two-quadrant division. Further, the input of Goldberg's modulator in the divider cannot contain any biasing constant and thus the performance of the divider is sensitive to the characteristic of the input signal. However, the proposed dividers are simple to implement and may be profitably employed for special purpose computation.

CHAPTER VAPPLICATION OF INTEGRAL PULSE FREQUENCY MODULATION TO THE  
ANALYSIS OF A NEURAL COMMUNICATION SYSTEM5.1 Introduction

In the peripheral nervous system of an animal, information is transmitted by trains of electrical pulses, called action potentials, via multitudes of nerve fibers. The pulses themselves in any single fiber are essentially identical, but their repetitive frequency may vary. In particular, pulse frequencies in the individual afferent fibers of many sensory organs have been found to vary as some function of stimulus intensity. Thus, it has been generally recognized that pulse frequency is one of the information carriers in the nervous system and that the corresponding neural pulse generating mechanism in a single fiber operates according to some form of pulse frequency modulation.<sup>48,49</sup>

Single-signed integral pulse frequency modulation (S - S IPFM) was proposed in 1959 as a mathematical model of the neural generating mechanism,<sup>22</sup> and since then it has been applied to a number of neurophysiological studies. Li and Jones have analyzed S - S IPFM feedback control systems whose operation resembles that of the neuro-muscular system with reciprocal innervation incorporated.<sup>8,23</sup> Partridge has studied the frequency response of the muscle by stimulating its efferent nerve with a pulse train from an integral pulse frequency modulator.<sup>25</sup> Furthermore, by assuming S - S IPFM as the actual neural pulse generating mechanism, Partridge has also investigated signal distortion introduced by the neural encoding process,<sup>24</sup> while more recently, Bayly has examined the spectral characteristics of pulse frequency modulation in the nervous system.<sup>26</sup>

In the present chapter, we shall apply S-S IPFM to investigate the transmission of signals in a particular multi-unit multipath neural communication system, namely, the afferent limb of the monosynaptic spinal reflex (MSR). We shall start by briefly reviewing the pertinent features of the MSR. Then, the afferent limb of the MSR will be modelled and statistically analyzed, taking into consideration the variations of properties in the multiplicity of neural elements and pathways.

We assume, in the subsequent presentation, that the reader has some basic knowledge of neurophysiology, in addition to his knowledge of analysis. Those not familiar with neurophysiology may acquire some of the required background by reading Chapters 2, 4, 6 and 7 in Reference 50.

50-52

## 5.2 The Monosynaptic Spinal Reflex

The monosynaptic spinal reflex (MSR) is a basic sub-system in most neuromuscular control systems of an animal. Its principal features for a mammal are illustrated in the highly simplified and conventional representation shown in Figure 5-1, in which only one of each of the various main functional components is shown. In reality, however, the MSR consists of many similar elements acting more or less in parallel.

One of the principal components of the MSR is the muscle spindle which is a few millimeters long and is located within the muscle itself. It comprises a bundle of from 2 to 10 intrafusal muscle fibers surrounded by a connective tissue capsule whose ends are attached to the sheaths of the surrounding regular or extrafusal muscle fibers.

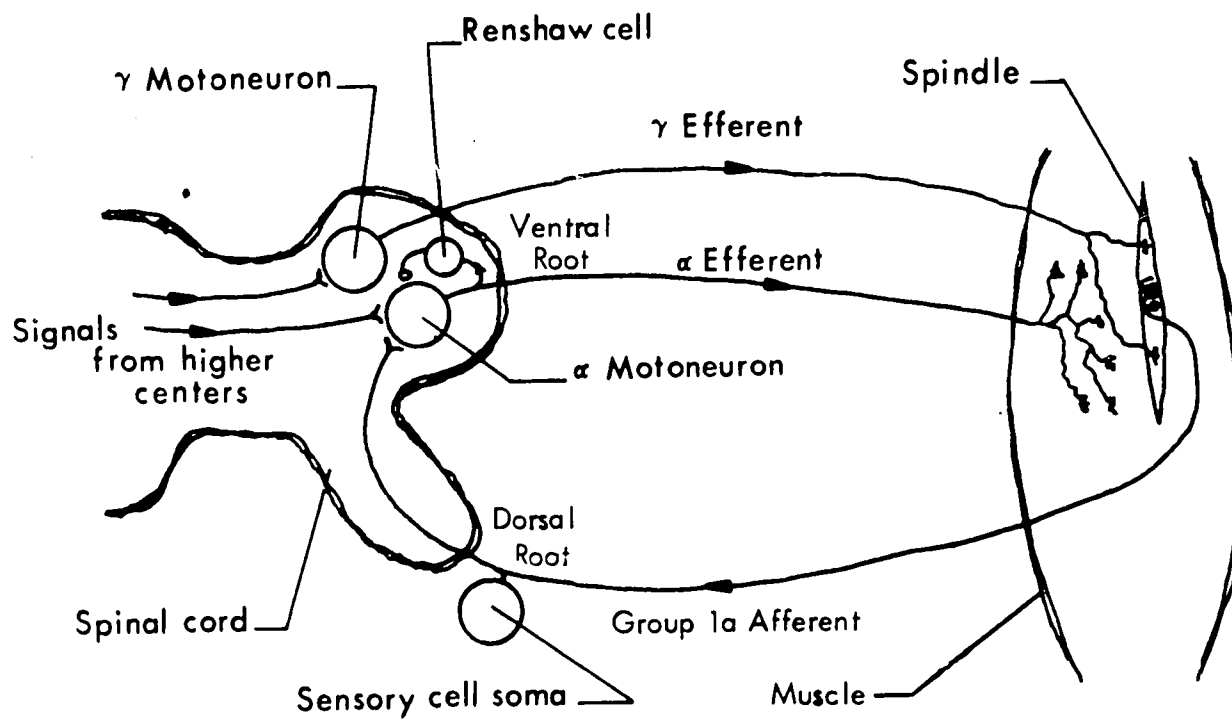


FIGURE 5-1. NEURAL PATHWAYS OF THE MONOSYNAPTIC SPINAL REFLEX.

The long, slender ends of the intrafusal fibers are striated and contractile, whereas the central or equatorial region is unstriated and probably cannot contract, but instead become stretched whenever the spindle is stretched.

The spindle is supplied by three main types of nerve fibers. It has up to fifteen  $\gamma$ -efferent fibers, one Group Ia afferent fiber, and from one to several Group II afferent fibers. The  $\gamma$ -efferent fibers originate from the  $\gamma$ -motoneurons in the spinal cord and their branches innervate the contractile polar regions of the intrafusal muscle fibers. The peripheral end of the Ia afferent fiber branches inside the capsule of the spindle and terminates as the so-called primary endings that encircle the equatorial region of the intrafusal muscle fibers. The Ia afferent enters the spinal cord via the dorsal root and sends branches directly to the  $\alpha$ -motoneurons ( $\alpha$ -MN's) that innervate the same muscle in which the spindle is located. The peripheral endings of the Group II afferent fibers terminate on both sides of the equatorial region of the intrafusal muscle fibers, but their central endings in the spinal cord do not terminate on the  $\alpha$ -MN's directly. Hence, these latter nerve fibers are not directly relevant to the MSR, and thus they are not shown in Figure 5-1 and will not be included in subsequent discussions.

The muscle spindle is attached in parallel to the extrafusal fibers of the muscle. Therefore, stretching the muscle tends to increase the length of the spindle and thus to extend the equatorial region of the intrafusal fibers. As a result, the primary nerve endings are distorted and then, as generally believed, produce electric currents called generator currents. These currents spread electrotonically into the adjacent regions of the parent axon and summate there to produce the so-called generator potential. Whenever the membrane potential at the pulse generating site of the Ia axon reaches threshold value,

an action potential is generated in this afferent fiber which conducts it to the  $\alpha$  - MN in the spinal cord. The spindle thus monitors the length of the muscle, encodes the information into a neural pulse train, and then transmits it via the Ia afferent nerve fiber to the  $\alpha$  - MN.

In addition to the mechanical input derived from the change in muscle length, the spindle has another input which is derived from the neural pulse trains in the  $\gamma$  - efferents. These pulse trains cause contraction of the polar regions of the intrafusal fibers and tend to decrease the overall length of the spindle. Hence, if the surrounding muscle does not contract simultaneously, the equatorial region of the intrafusal fibers will be extended, producing the same series of subsequent events described above for the mechanical input. However, in this case the spindle does not operate as a feedback monitor; instead, it operates as a relay station and a summer, since it converts the  $\gamma$  - efferent pulse trains into generator currents, summates these generator currents with those derived from the mechanical input, and then converts the result into an afferent pulse train.

The afferent pulse train from each spindle excites the  $\alpha$  - MN directly through synaptic contacts and evokes voltage changes called quantal excitatory postsynaptic potentials (EPSP's) in the postsynaptic membrane of the  $\alpha$  - MN.<sup>58</sup> These quantal EPSP's spread electrotonically into the adjacent regions of the neuronal membrane and summate there with the quantal postsynaptic potentials (PSP's) caused by other synaptic inputs such as those from higher centers and other neurons. It should be noted, however, that the other synaptic inputs may be excitatory or inhibitory.

Whenever the summated PSP at the pulse generating site of the  $\alpha$  - MN reaches the threshold value, an action potential is generated in the  $\alpha$  - efferent axon

which conducts it to the muscle. The  $\alpha$  - efferent axon branches in the muscle, making connections with a number of extrafusal fibers. Thus, a pulse in it activates a number of muscle fibers which then contract in unison to produce a unit contractile response of the whole muscle. The  $\alpha$  - MN together with its axon and the set of extrafusal fibers it innervates is known as a motor unit.

We have noted earlier that the monosynaptic spinal reflex (MSR), in reality, consists of many similar elements acting more or less in parallel. Let us now consider this aspect with particular reference to the representation of information. Consider first the efferent limb of the MSR. The muscle, often comprising thousands of extrafusal fibers, receives information from a lesser number of  $\alpha$  - motoneurons ( $\alpha$  - MN's) via the  $\alpha$  - efferent axons. The cat soleus, for example, consists of about 25,000 extrafusal fibers grouped as about 150 motor units. However, the state of the muscle can be described in terms of its terminal force and length changes, and this state is produced as the net result of the motor unit contractions. Since the contractions of the motor units are dependent upon the efferent activities, information is thus represented in this case by the ensemble of pulse trains in the  $\alpha$  - efferent axons.

In the afferent limb of the MSR, information is transmitted by the spindles to the  $\alpha$  - MN's in the spinal cord. There are many spindles distributed at random throughout the belly of the muscle. (As an example, the cat soleus has about 55 spindles). When the muscle is stretched, the spindles tend to generate pulse trains in their afferent nerve fibers, and both the pulse frequency and the number of active nerve fibers tend to increase with the stretch amplitude. Since the muscle spindles are attached in parallel

to the extrafusal muscle fibers, it is reasonable to consider some dynamic function of the change in muscle length as the information transmitted to the  $\alpha$  - MN's. Clearly, in this case also, information is represented by an ensemble of pulse trains.

From the above description, we see that neural communication in both the efferent and afferent limbs of the MSR is mediated respectively by many motor units and by many sensory units, over many parallel paths. We call this property of the communication systems the multi-unit multipath characteristic. This characteristic is not restricted to the monosynaptic spinal reflex (MSR) above, but is a property common to other sensory and motor systems.<sup>48,52</sup>

We can usefully ask why the method of neural communication has evolved to this present form involving a multiplicity of units and pathways. Clearly the redundant structures provide reliability, some degree of which is essential for survival. However, does the multi-unit multipath characteristic have in addition any functional significance in the transfer of information? Recent experimental evidence indicates that the answer is affirmative.<sup>53,54</sup> In the following, we shall investigate this problem theoretically, by mathematical analysis and computer simulation. Our attention will be restricted to the transmission of information from the muscle to the  $\alpha$  - motoneuron in the afferent limb of the MSR. Clearly, the MSR is a closed-loop feedback system. Since the effects of feedback unnecessarily complicate the analysis of signal transmission, we shall assume in the present investigation that the ventral root is cut to open the loop, while the efferent pulse trains may still be generated artificially by electrical stimulation.

### 5.3 Information Flow in the Afferent Limb of the Monosynaptic Spinal Reflex

As noted above, in the afferent limb of the MSR information is transmitted by the spindles to the  $\alpha$  - motoneurons ( $\alpha$  - MN's) in the spinal cord. Let us now consider the flow of information and examine the pertinent characteristics of the transmission paths.

Consider first the flow of information to a single  $\alpha$  - MN. It is well known that an  $\alpha$  - MN receives information from many sources (Ref. 50) Chapter 6). However, for our analysis we are concerned only with the information conveyed to it by the monosynaptic nerve fibers arising from the spindles in the muscle which it innervates. Thus, the  $\alpha$  - MN in the present analysis can receive signals originating from only three possible sources, namely, the applied muscle stretch, the  $\alpha$  - efferent pulse trains, and the  $\gamma$  - efferent pulse trains. From the present viewpoint, the other inputs to it are irrelevant and may be considered as noise if they are included in the analysis.

The flow of information to an  $\alpha$  - MN via monosynaptic afferent fibers can be illustrated as shown in Figure 5-2. The applied stretch and the  $\alpha$  - efferent pulse trains produce change of muscle length which is coupled mechanically to the spindles, while the  $\gamma$  - efferent pulse trains stimulate the spindles directly. The information contained in these input signals is encoded by the spindles into pulse trains which are conducted to the  $\alpha$  - MN by the afferent fibers. It should be noted that in the spinal cord a single  $\alpha$  afferent axon breaks into many branches making synaptic contact with many postsynaptic cells and conversely many synaptic knobs on a single  $\alpha$  - MN derive from many different parent afferent axons (Ref. 50, Chapter 6). This overlapping innervation is recently

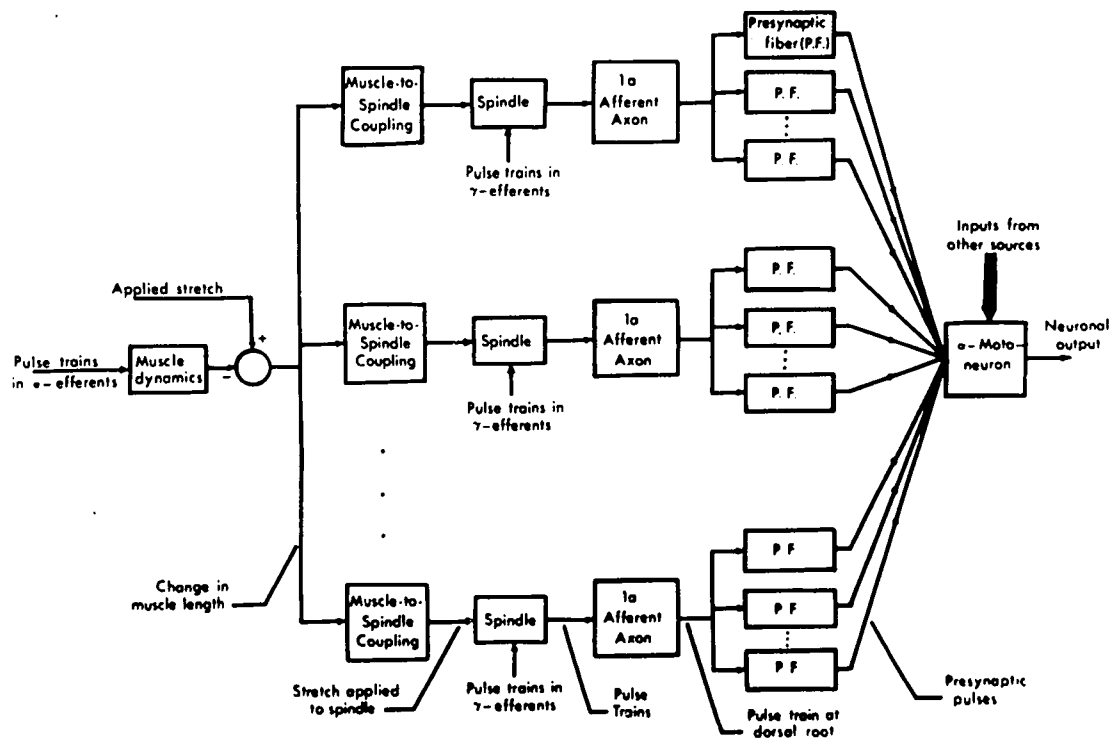


FIGURE 5-2. THE FLOW OF INFORMATION IN THE AFFERENT LIMB OF THE MONOSYNAPTIC SPINAL REFLEX.

found to be almost complete over the  $\alpha$  - motoneuron pool and the homonymous muscle spindles for the cat gastrocnemius.<sup>55</sup>

The number of parallel paths for information transmission to the  $\alpha$  - MN is equal to the number of monosynaptic knobs on the neuronal soma-dendritic complex. Each path in this multipath system has its own intrinsic properties different from its neighbours. The spindles are known to have different stretch-thresholds for pulse generation and this variation is believed to be caused partly by the variance in the intrinsic sensitivity of the spindles, but mainly by their spatial distribution in the muscle so that some spindles are more readily excited by the applied stretch than the others (Ref.50,Chapter 4). Thus, output pulse trains of different spindles are generally different for a given change in muscle length. Furthermore, the pulse trains are conducted to the  $\alpha$  - MN by afferent fibers whose conduction velocities vary from one fiber to another. A final additional variation occurs at the neuronal membrane. A recent experimental finding indicates that the excitatory postsynaptic potential (EPSP), resulting from spatial and temporal summation, presumably at the soma of the  $\alpha$  - MN is an information carrying signal.<sup>53</sup> Thus if the soma, or preferably the pulse-generating site which is generally believed to be the axon hillock, is considered as the point where the quantal EPSP's summate, then the quantal EPSP's produced at this site by single synaptic inputs at different locations on the neuronal membrane will be different. Since there is evidence that the monosynaptic knobs are randomly distributed throughout the soma-dendritic complex of the  $\alpha$  - MN,<sup>56-58</sup> the quantal EPSP's produced at the pulse-generating site are different. In other words, the "neuronal transfer dynamics" relating a single presynaptic neural pulse to the resulting postsynaptic subthreshold neuronal response at the pulse generating site varies from one path of information transmission to another.

Consider now the complete afferent limb of the MSR as a communication system. Clearly, the flow of information to any one of the  $\alpha$  - MN in the motoneuron pool innervating the muscle can be represented as shown in Figure 5-2. Thus, if the subsystem shown in Figure 5-2 is defined as a communication link in the MSR, the afferent limb of the MSR can be considered as a system of such links in parallel. The number of links in the system is, of course, equal to the number of  $\alpha$  - motoneurons ( $\alpha$  - MN) in the motoneuron pool. However, because of overlapping innervation in the pool, the number of "spindles" in different links may be different and furthermore the total number of spindles actually existing in the muscle is not equal to the sum of all "spindles" used in the representation of the MSR. It should be noted also that the change in muscle length is a signal common to all communication links in the representation.

Since the afferent limb of the MSR is composed of a number of similar communication links in parallel, the transmission properties of the whole system can be derived from the properties of a single link. Thus, in the following, we shall consider signal transmission in a single communication link only.

#### 5.4 Modelling the Neural Encoder

In our brief review of the MSR, we have noted that pulse initiation in the Ia afferent axon is preceded by the production of the so-called generator currents in the primary nerve endings, and that an afferent pulse is generated whenever the depolarization by these currents at the pulse generating site reaches threshold value. As a first step in obtaining a complete mathematical model of a communication link in the afferent limb of

the MSR, we now consider the problem of representing the neural pulse generating mechanism which converts the summated generator current into the afferent pulse train. In subsequent discussions, we shall call this mechanism the "neural encoder", or more briefly, the "encoder".

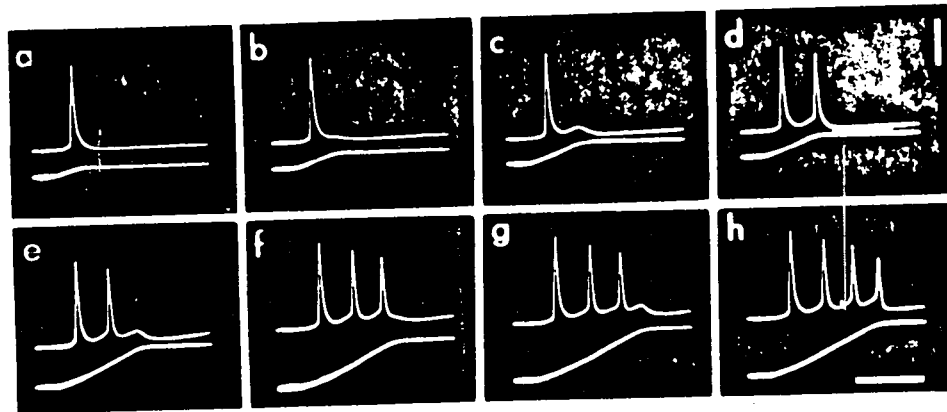
At present the exact operating principle of the neural encoder is unknown. However, some characteristics of its method of pulse generation and its terminal relations are known qualitatively. We shall first present these characteristics and then show that most of these are also exhibited by single-signed integral pulse frequency modulation.

1. Method of Pulse Generation : The records shown in Figure 5.3 illustrate several features in the generation of afferent pulses. The lower traces in these records indicate extension of the spindle, while the upper traces illustrate the changes of potential which is presumably proportional to the membrane potential at the pulse-generating site of the afferent axon, when the spindle is stretched at a constant rate to different final amplitudes. In (a) the stretch is just over threshold for eliciting one single pulse. With somewhat greater extension in (b), a slight increase in potential occurs in the aftermath of the pulse. With further increase in extension, the amplitude of this so-called prepotential increases proportionally and at a specific amplitude of stretch, a second pulse is generated in (d). As the stretch is increased, the same sequence of events is repeated, producing an afferent pulse train such as the one shown in (i). From these records we can observe the following characteristics of pulse generation.

- (a) Each pulse is preceded by a prepotential which is dependent upon the applied stretch.

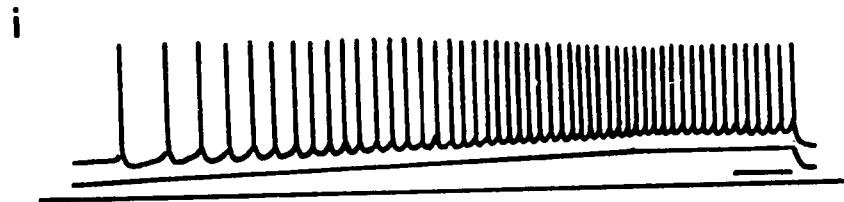
Upper traces : Changes of potential.

Lower traces : Extension of spindle.



Horizontal bar : 20 m sec .

Vertical bar : 2 m V .

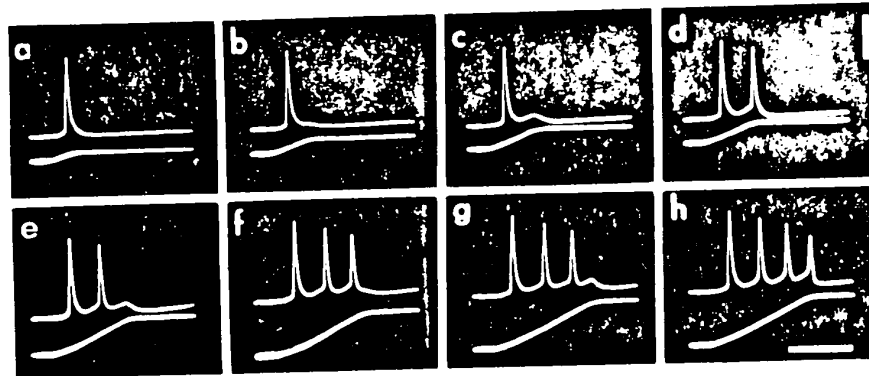


Horizontal bar : 50 m sec .

FIGURE 5-3. RECORDINGS ILLUSTRATING PULSE GENERATION IN THE  $I_a$  AFFERENT OF THE FROG SPINDLE.  
(FROM REFERENCES 64 AND 65) .

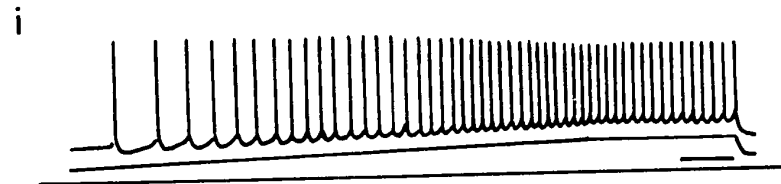
Upper traces : Changes of potential.

Lower traces : Extension of spindle.



Horizontal bar : 20 m sec.

Vertical bar : 2 m V .



Horizontal bar : 50 m sec.

FIGURE 5-3. RECORDINGS ILLUSTRATING PULSE GENERATION IN THE I<sub>a</sub> AFFERENT OF THE FROG SPINDLE.  
(FROM REFERENCES 64 AND 65) .

- (b) A pulse is generated whenever the membrane potential reaches a threshold value .
- (c) After the pulse is generated, the membrane is repolarized and the potential is brought back to a certain value below the point at which the pulse arose .
- (d) As the stretch amplitude becomes greater, the repolarization phase between individual pulses becomes less complete, resulting in a base line shift of membrane potential towards greater depolarization for the duration of the stretch . The prepotentials and the pulses appear superimposed upon a sustained potential .
- (e) The threshold for pulse generation appears to increase with this sustained potential .

2. Terminal Relations : There is very little known about the functional relations between the output pulse train and the summated generator current at the input of the neural encoder . However, there are known relationships between output pulse frequency and stretch amplitude or generator potential, and from these we shall infer some terminal relations .

- (a) When the primary nerve endings are depolarized by an applied direct current (DC), the afferent pulse frequency is constant and appears to be proportional to the strength of the current over a significantly wide range . <sup>61,62</sup>

- (b) Within normal physiological range, the static relation between afferent pulse frequency and generator potential is essentially linear.<sup>63,65</sup> Generator potential in these cases was measured with one electrode on the nerve which was placed in oil, while the grounding electrode was placed near the spindle lying in the Ringer's solution. Thus, the measured generator potential is linearly proportional to the current flowing along the nerve fiber. Therefore, afferent pulse frequency can reasonably be considered as linearly proportional to the summated generator current.
- (c) For the dynamic case of a ramp stretch of the spindle, both afferent pulse frequency and generator potential in the steady state are linearly proportional to the stretch.<sup>64,65</sup> Thus, afferent pulse frequency is linearly proportional to generator potential also when the generator potential follows a ramp function. As in the static case, because of the method for measuring generator potential, afferent pulse frequency can also be considered to vary linearly with the summated generator current in this dynamic case.

Now, with these known characteristics which we have listed for the neural encoder, we consider the problem of modelling the encoder. Our objective is to obtain a physiologically reasonable and yet mathematically tractable model. From among the various known methods of pulse frequency modulation, including those utilized in neuron models but not explicitly developed,<sup>21,66,67</sup> single-signed integral pulse frequency modu-

lation (S - S IPFM) appears to be the most suitable for our present purpose. We have shown in Chapter III a spectral representation of the output pulse train for S - S IPFM. In the following, we shall show that S - S IPFM satisfies most of the known characteristics of the neural encoder listed above.

1. Method of Pulse Generation : A method for implementing S - S IPFM exactly has been shown in Chapter II. For convenience, the block diagram of this modulator and the diagram illustrating its operation are shown here again in Figure 5-4. We can easily see that the method of pulse generation in this feedback system is similar to that of the neural encoder if we make the following analogies : the input  $x(t)$  represents the summated generator current at the pulse generating site ; the summing point represents the membrane property known as temporal summation ; the integrator represents the subthreshold current-voltage characteristic of the membrane ; the integrator output  $I(t)$  represents the membrane potential, excluding the action potential ; the threshold device represents the threshold mechanism of the nerve membrane ; the pulse generator represents the pulse generating mechanism in the first segment of the axon ; the output pulse train  $x^*(t)$  represents the afferent axonal pulse train ; and finally the negatively feedback pulse represents the repolarizing ionic current.

As shown in Figure 5-4(b), the output  $I(t)$  of the integrator is very similar to the record of neural potential shown in Figure 5-3(i) if the action potentials are removed from this latter diagram. In particular, the "prepotentials" appear superimposed upon a sustained "potential" which is proportional to the input  $x(t)$ . We can show this feature mathematically as follows .

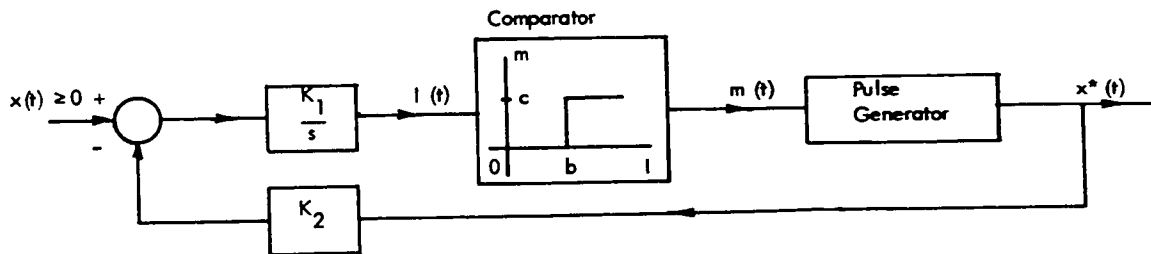


FIGURE 5-4a. A SINGLE-SIGNED INTEGRAL PULSE FREQUENCY (S - S IPF) MODULATOR.

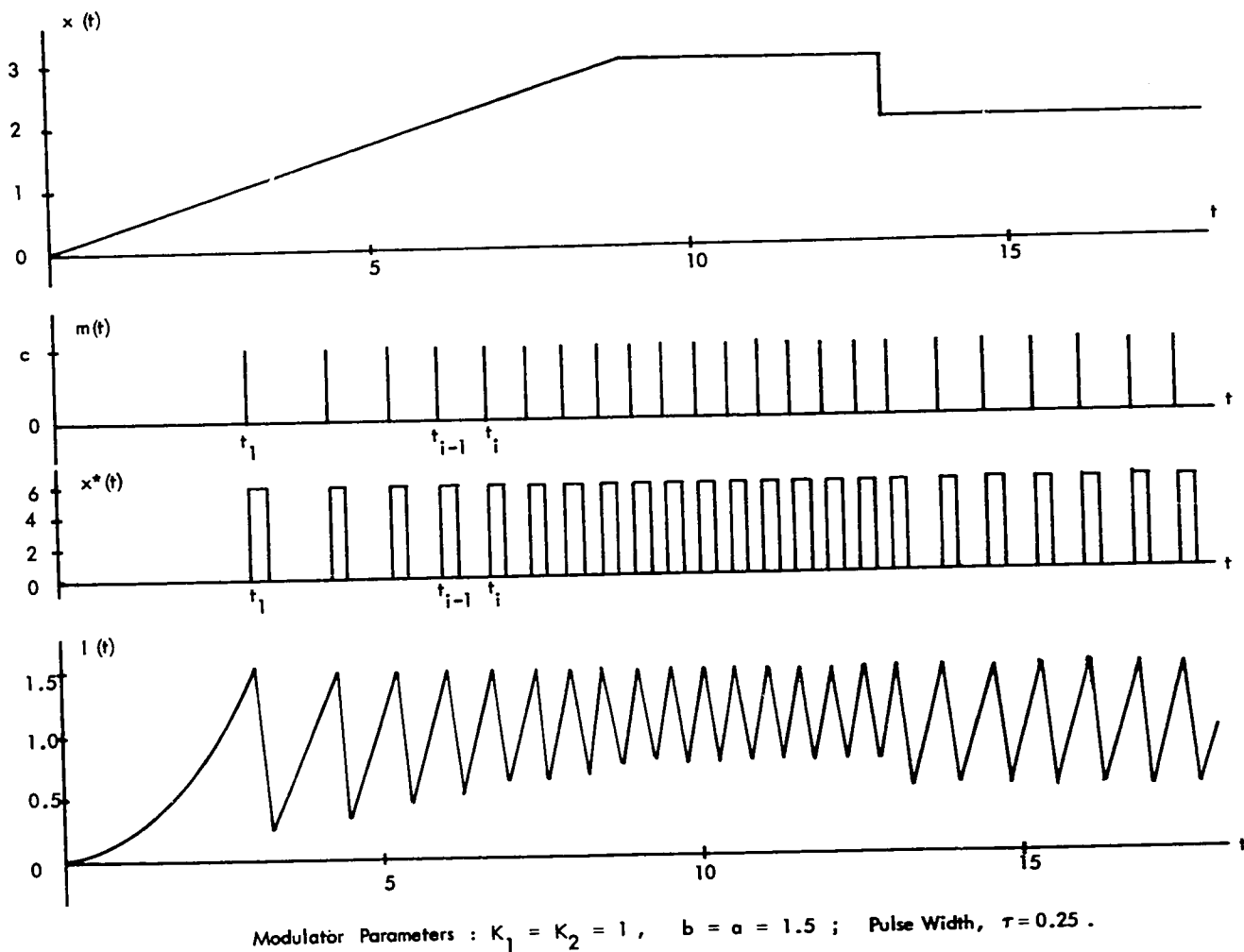


FIGURE 5-4b. ILLUSTRATING THE OPERATION OF THE S - S IPF MODULATOR.

Let  $x(t) = Ct$  for  $T \geq t \geq 0$ , where  $C$  and  $T$  are positive constants.

Then, for  $t_i \geq t \geq t_{i-1}$ , where  $t_i$  and  $t_{i-1}$ ,  $i = 1, 2, \dots$ , denote the pulse emission times of the  $i$ th and  $(i-1)$ th pulses respectively, we have

$$I(t) = K_1 \left[ \int_{t_{i-1}}^t x(t) dt - \int_{t_{i-1}}^t K_2 x^*(t) dt \right] + b. \quad (5-1)$$

As shown in Chapter II, in order that  $S - S$  IPFM be implemented exactly, we must have

$K_2 A = \frac{b}{K_1}$ , where  $A$  is the area of the output pulse. Hence, if  $\tau$  is the duration of the pulse, then replacing  $t$  by  $t_{i-1} + \tau$  we have from Equation (5-1),

$$I(t_{i-1} + \tau) = K_1 C \left[ t_{i-1} \tau + \frac{\tau^2}{2} \right] \quad (5-2)$$

Without loss of generality, if the output pulse is assumed rectangular,  $I(t_{i-1} + \tau)$  can be easily seen to be the minimum value of each "prepotential". Clearly, Equation (5-2) shows that the minimum of the "propotential" increases linearly with time, giving the appearance that the "prepotentials" are superimposed upon a sustained potential. We can similarly show that this feature holds also for a constant input,  $x(t)$ .

In our comparison of the membrane potential with  $I(t)$ , we have found it necessary to remove the action potentials from the neural record. This should not be a cause for objection, since the depolarizing phase of the action potential only serves as a trigger for the axonal pulse while the repolarizing phase serves as resetting mechanism of the membrane, the effect of which we have represented by the negative feedback in the  $S - S$  IPFM implementation.

There are two important features of the neural encoder, which S - S IPFM does not possess. Firstly, we have compared the integrator with the subthreshold current-voltage characteristic of nerve membrane at the pulse generating site. It is well known that the subthreshold nerve membrane can be approximately represented by a "leaky integrator". Thus, for a sufficiently small constant current at the pulse generating site, the neural encoder will not generate any afferent pulse, while the integral pulse frequency (IPF) modulator will generate an output pulse train with low pulse frequency. We can make the modulator a more realistic model of the neural encoder by replacing the integrator with a "leaky integrator" or other linear system of higher order ; but then, the resulting model becomes mathematically unwieldy for our present purpose. It is interesting to note that a rather elaborate mathematical model of the neuron developed by Roberge<sup>67</sup> can be shown to be equivalent to the modified IPF modulator we have just suggested. (See Appendix B).

The second feature of pulse generation not exhibited by the modulator shown in Figure 5-4(a) is the variation of threshold with the "sustained potential". However, as we have shown in Section 2.5, this feature can be incorporated into the modulator very simply by the arrangement shown in Figure 2-8. For our present purpose of analyzing signal transmission in the afferent limb of the MSR, we shall assume that the threshold of the neural encoder remains constant in order to obtain mathematical tractability.

2. Terminal Relations : There are presently only two known relations between the afferent pulse train and the summated generator current for the neural encoder in the afferent axon. These can be incorporated in one statement : the afferent pulse frequency

is linearly proportional to the amplitude of the input current if the current is either a step or a ramp. We can show that the output pulse frequency of the IPF modulator is constant and linearly proportional to the amplitude of the input step immediately from the criterion for pulse emission given by Equation (2-1). For S - S IPFM with positive pulses, Equation (2-1) can be re-written as

$$\int_{t_{i-1}}^{t_i} x(t) dt = a \quad (5-3)$$

When the input  $x(t) = K$  for  $t > 0$ , where  $K$  is a positive constant, we have the pulse frequency

$$f_i(t) = \frac{1}{t_i - t_{i-1}} = \frac{K}{a}, \quad t_i < t < t_{i+1}, \quad i = 1, 2, 3, \dots, \quad (5-4)$$

which establishes the stated relation. When  $x(t)$  is a ramp, the output pulse frequency of the IPF modulator is also approximately a ramp, provided we assume that pulse frequency can be considered a continuous variable as neuro-physiologists normally do. Let  $x(t) = Kt$  for  $t \geq 0$ , where  $K$  is a positive constant. Then, from Equation (5-3) we have

$$f_i = \frac{K}{a} [t_i + t_{i-1}] / 2. \quad (5-5)$$

This result indicates that pulse frequency at time  $t_i$  is linearly proportional to the average of two consecutive pulse emission times  $t_{i-1}$  and  $t_i$ . Clearly the relation between pulse frequency and the input is approximately linear.

We have shown above that S - S IPFM exhibits most of the known properties of the neural encoder. In addition, there is other evidence that S - S IPFM is a physiologically reasonable model. The "decoding" method used by the neuromuscular system is somewhat similar to that of IPFM. Since the subthreshold nerve membrane is generally considered linear, the quantal excitatory postsynaptic potentials produced by a single afferent pulse train summate linearly at the motoneuron membrane. Further, it is well known that the tetanus response of the muscle is the temporal summation of the so-called twitch responses elicited by  $\alpha$  - efferent stimulation. In analogy to these results, we have shown in Section 2.6, that demodulation of IPFM is a linear temporal summation of the pulse responses of the demodulating low-pass filter. It should be noted, however, that temporal summation occurring at the muscle is somewhat nonlinear,<sup>68</sup> whereas temporal summation in demodulating IPFM is strictly linear.

As final supporting evidence for choosing S - S IPFM as a model of the neural encoder, we cite the fact that neural pulse trains have been commonly processed either by low-pass filtering or by obtaining their instantaneous pulse frequencies,<sup>53,69</sup> with the usual implicit assumption that neural signals can be meaningfully demodulated in these ways. These two methods are also employed to demodulate IPFM as we have described in Chapter II.

### 5.5 A Model of the Muscle-to-Motoneuron Communication Link

From the discussion given in Section 5.3, we see that a typical path in the afferent limb of the monosynaptic spinal reflex (MSR) consists of the muscle, the coupling

between the muscle and the spindle, a spindle, an afferent nerve fiber, and the neuronal transfer dynamics relating presynaptic pulse to the resulting postsynaptic neuronal response at the pulse-generating site of the  $\alpha$  - motoneuron ( $\alpha$  - MN). We shall first obtain a model for this typical path and then formulate a multipath model for signal transmission from the muscle to the  $\alpha$  - MN .

Let us first model the muscle and the spindle. Although these components have been extensively studied,<sup>69-77</sup> there is no generally accepted mathematical model for them either individually or in combination, and in particular there is no available model suitable for our present purpose. Because of their complex functional behaviour and the lack of knowledge on some important details, we are forced to take the following somewhat qualitative approach.

As noted previously, pulse initiation in the Ia afferent of the spindle is preceded by production of the so-called generator currents which are believed to be caused by distortion of the primary nerve endings located in the equatorial region of the intrafusal muscle fibers.<sup>51</sup> We also recall that the distortion of the primary nerve endings arises when the equatorial region is extended from the resting length either by stretching the spindle through an increase of muscle length, or by contracting the polar regions of the intrafusal muscle fibers through  $\gamma$ -efferent stimulation. Based on these observations, we may represent the combination of the whole muscle and one of its spindles by a single unit as shown in Figure 5-5. In this diagram, block M represents the dynamics of the whole muscle when it is subjected to the applied stretch and / or  $\alpha$  - efferent stimulation. The output of M then corresponds to the stretch applied to the spindle under consideration. Note, however, that M therefore contains a factor representing the muscle - to - spindle

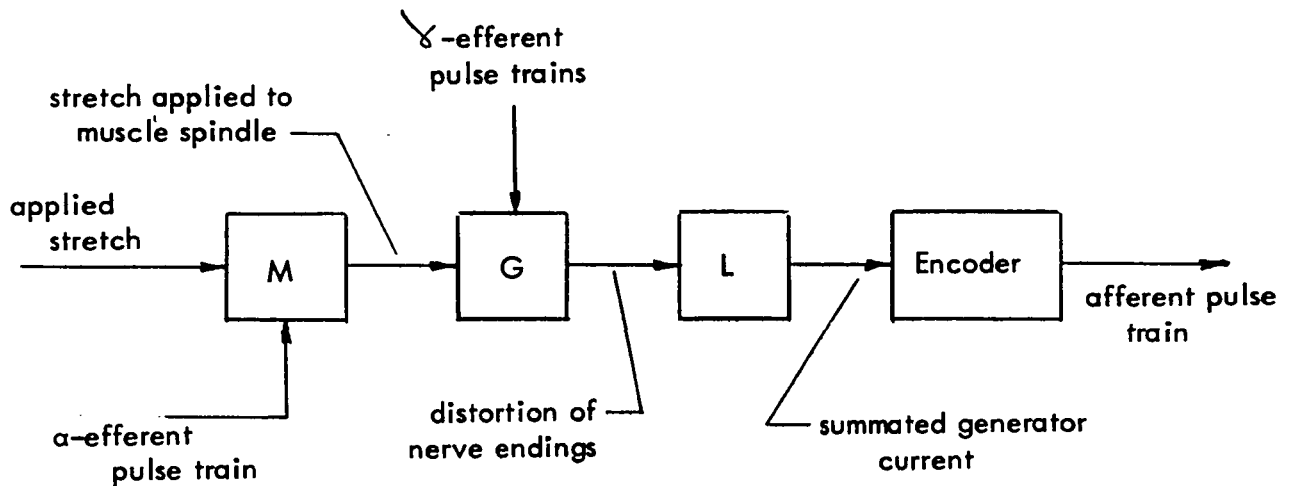


FIGURE 5 - 5. BLOCK DIAGRAM OF THE WHOLE MUSCLE AND ONE OF ITS SPINDLES.

mechanical coupling which varies from one path to another.  $G$  represents the mechanical dynamics of the intrafusal fibers of the spindle when they are stretched by the change in muscle length and / or stimulated by the  $\gamma$ -efferent pulse trains. Its output corresponds to the distortion of primary nerve endings.  $L$  represents the transduction process by means of which the distortion of nerve endings is converted into the summed generator current at the pulse generating site of the afferent axon. Finally, the block entitled "encoder" represents the neural encoder which we have modelled with a single-signed integral pulse frequency (S - S IPF) modulator in the previous section.

Blocks  $M$ ,  $G$  and  $L$  in this general representation of the whole muscle and one of its spindles are nonlinear and at present cannot be determined. In order to simplify the problem, we consider the special case in which

- (i) the  $\gamma$ -efferent pulse frequency is either zero or constant at a sufficiently high rate to produce a constant summed generator current ; and

- (ii) the  $\alpha$  - efferent pulse frequency is either zero or constant at a sufficiently high rate to produce a constant muscle contraction.
- (iii) The muscle length is made to vary sinusoidally about a suitable mean length so that the muscle spindle fires continuously.

Given these constraints, the only time-varying input for the muscle and spindle assembly is the applied stretch, and the resulting afferent pulse frequency is known to vary almost sinusoidally,<sup>71,72</sup> if it is considered as a continuous variable. The afferent pulse train is represented in our block diagram by the output of the block entitled "encoder" which we have modelled using a S - S IPF modulator. When the input of the modulator is a biased sinusoid, the output pulse frequency can be shown to vary almost sinusoidally also. Thus, let the input be

$$x(t) = X_0 + U \cos(\omega t + \theta) \geq 0, \quad t \geq 0 \quad (5-6)$$

where  $X_0$ ,  $U$ ,  $\omega$  and  $\theta$  are constant. Then, using Equation (5-3) we have

$$X_0 \cdot \Delta_i + \frac{U}{\omega} \left\{ \sin(\omega t_i + \theta) - \sin[\omega(t_i - \Delta) + \theta] \right\} = a, \quad (5-7)$$

where  $\Delta_i = t_i - t_{i-1}$ . When  $\Delta_i$  is small compared with the period of the input signal, Equation (5-7) can be simplified to yield the pulse frequency,

$$f_i = \frac{1}{\Delta_i} \approx \frac{1}{a} [X_0 + \cos(\omega t_i + \theta)] = \frac{x(t_i)}{a}. \quad (5-8)$$

This result clearly verifies the stated relation given above. Therefore, for this special case under consideration, we can consider that, in our representation of the muscle and one of its spindles, block M, G and L lumped together constitute a linear system. Consequently, we can model the muscle and one of its spindles as shown in Figure 5-6, wherein the S - S IPFM modulator represents the encoder, and C (s) represents the linearized dynamics relating the change in muscle length to the resulting change in summated generator current. The efferent inputs are now represented by two constants, g and q; where g represents the decrease in muscle length produced by the constant  $\alpha$  - efferent activities and q represents the increase in summated generator current produced by the constant  $\gamma$  - efferent activities.

Now we consider the modelling of the remaining two components, namely, the afferent fiber and the neuronal transfer dynamics, of the path of information transmission. The afferent fiber conducts the pulses without affecting their size and shape, and thus can be modelled by a pure time-delay whose delay time  $\tau$  is equal to the time required to conduct a pulse from the spindle to the synapse at the motoneuron. The neuronal transfer dynamics relating the pre-synaptic pulse and the postsynaptic neuronal response at the axon hillock can be represented by a linear element whose pulse response has practically the same shape and size as the quantal EPSP. As an example, if the transfer function H (s) of the linear element is

$$H (s) = \frac{b}{1 + \tau s} \quad (5.9)$$

then the Laplace transform of the pulse response is given by  $\frac{bP'(s)}{1 + \tau s}$  where P (s) is the Laplace transform of the presynaptic pulse. It should be noted that there is a small delay

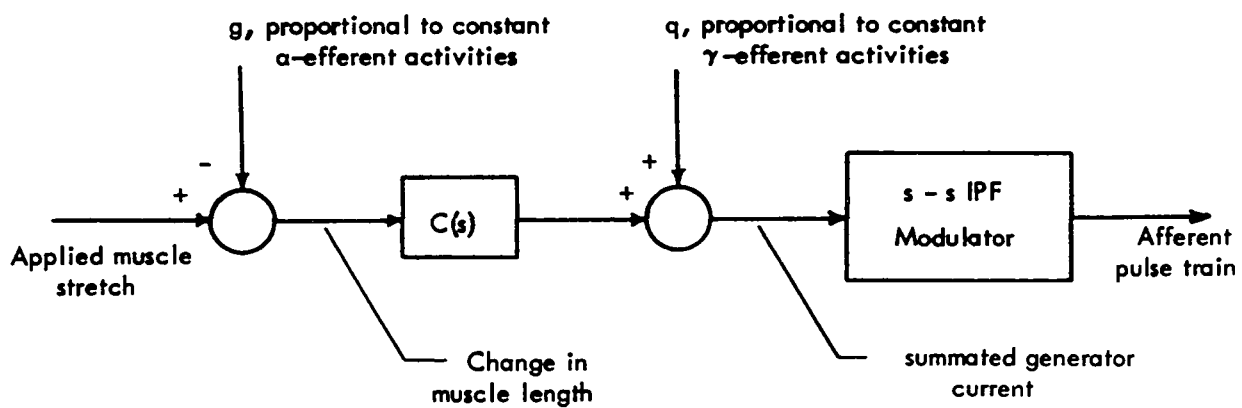


Fig. 5-6. A Linearized Model of the Whole Muscle and one of its Spindles

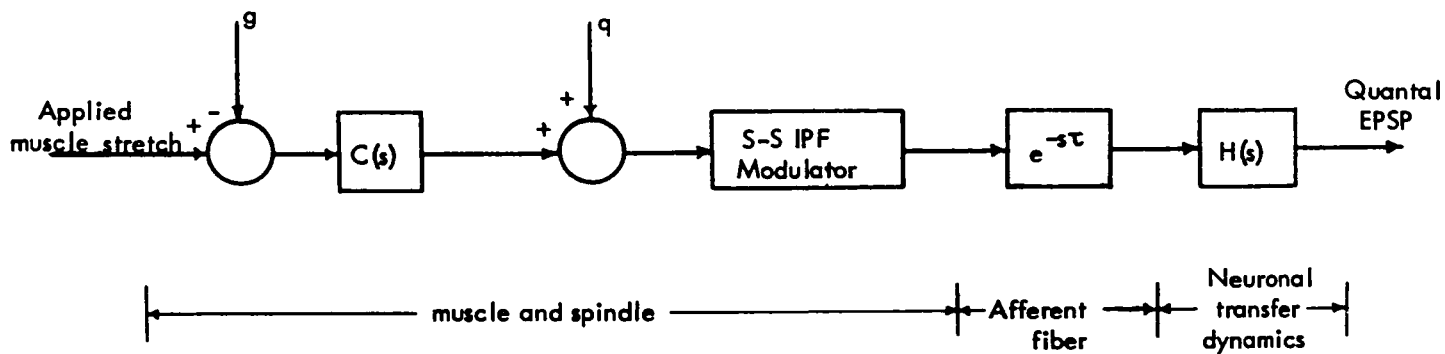


Fig. 5-7. A Model of a Typical Afferent Path in the MSR

time between the onset of the presynaptic pulse and the onset of the resulting quantal EPSP at the neuronal pulse-generating site. For the present analysis, we can and shall lump this delay time with that of the afferent fiber without introducing error. Thus we shall henceforth represent the neuronal transfer dynamics by a linear element containing no time delay.

The complete model for a typical afferent path in the MSR is shown in Figure 5-7. We have pointed out in Section 5.3 that the intrinsic properties of each afferent path differ from those of the others. These properties are represented in the model by  $C(s)$ ,  $H(s)$ , the delay time  $\tau$ , and the input  $q$ . Variation in the stretch-threshold of the spindles in the muscle is described by the variation in the gain of  $C(s)$ , where a higher value of the gain implies a lower threshold and greater sensitivity. The distribution of conduction velocities of the afferent fibers is described by the distribution of delay time  $\tau$ , where a larger value of  $\tau$  denotes a smaller conduction velocity. Variation in the size and shape of quantal EPSP's at the axon hillock of the MN is represented by the variation in the pulse response of  $H(s)$ . In addition to these, the phase characteristic of  $C(s)$  and the input  $q$  may vary from one path to another because of variations in the dynamics of mechanical coupling between the muscle and the spindle, the spindle properties, and the  $\gamma$ -efferent stimulation.

One component and two inputs in the model are considered as invariant for all paths. As we have pointed out in Section 5.3, the change in muscle length is a signal common to all paths. Hence, the applied stretch and the  $\alpha$ -efferent input  $g$ , are invariant from one path to another. The remaining invariant component is the S-S IPFM modulator which represents the neural encoder in the spindle. In reality the encoder of different spindles may have different sensitivities. However, this possible varia-

tion can equally well be embedded in the stretch-threshold variation which has been described by the variation in the gain of  $C(s)$ . Hence it appears reasonable to assume that the S - S IPFM modulator is identical for all paths.

With the model of a typical path thus determined, we may now formulate a multipath model of the muscle-to-motoneuron communication link, as shown in Figure 5-8. In this figure the change in muscle length is a signal common to all paths as already noted. Then at the end of these paths, the quantal EPSP's are assumed to summate linearly in the axon hillock of the motoneuron to produce the signal which is considered to carry the information in this communication link. Note that the S - S IPF modulator is now represented by its functional model (Figure 2-5), and that its pulse-shaping element  $P_i(s)$  has been lumped with the neuronal transfer dynamics  $H_i(s)$  in the  $i$ th path. It should also be noted that the input of  $P_i H_i$  consists of impulses of magnitude  $d$  for all values of  $i$ . Thus, the quantal excitatory postsynaptic potential (EPSP) at the output of the  $i$ th path is given by the impulse response of  $P_i H_i$ , and consequently its Laplace transform is  $d \cdot P_i(s) \cdot H_i(s)$ .

## 5.6 Statistical Analysis of the Muscle-to-Motoneuron Communication System

### 5.6.1 Statistical Formulation

We now proceed to analyze the muscle-to-motoneuron communication link as represented by the model shown in Figure 5-8. Let us, for the present, make the simplifying assumption that the quantal EPSP's all have the same temporal waveform, but may have different amplitudes. Thus, let the Laplace transform at the quantal EPSP in the  $i$ th path

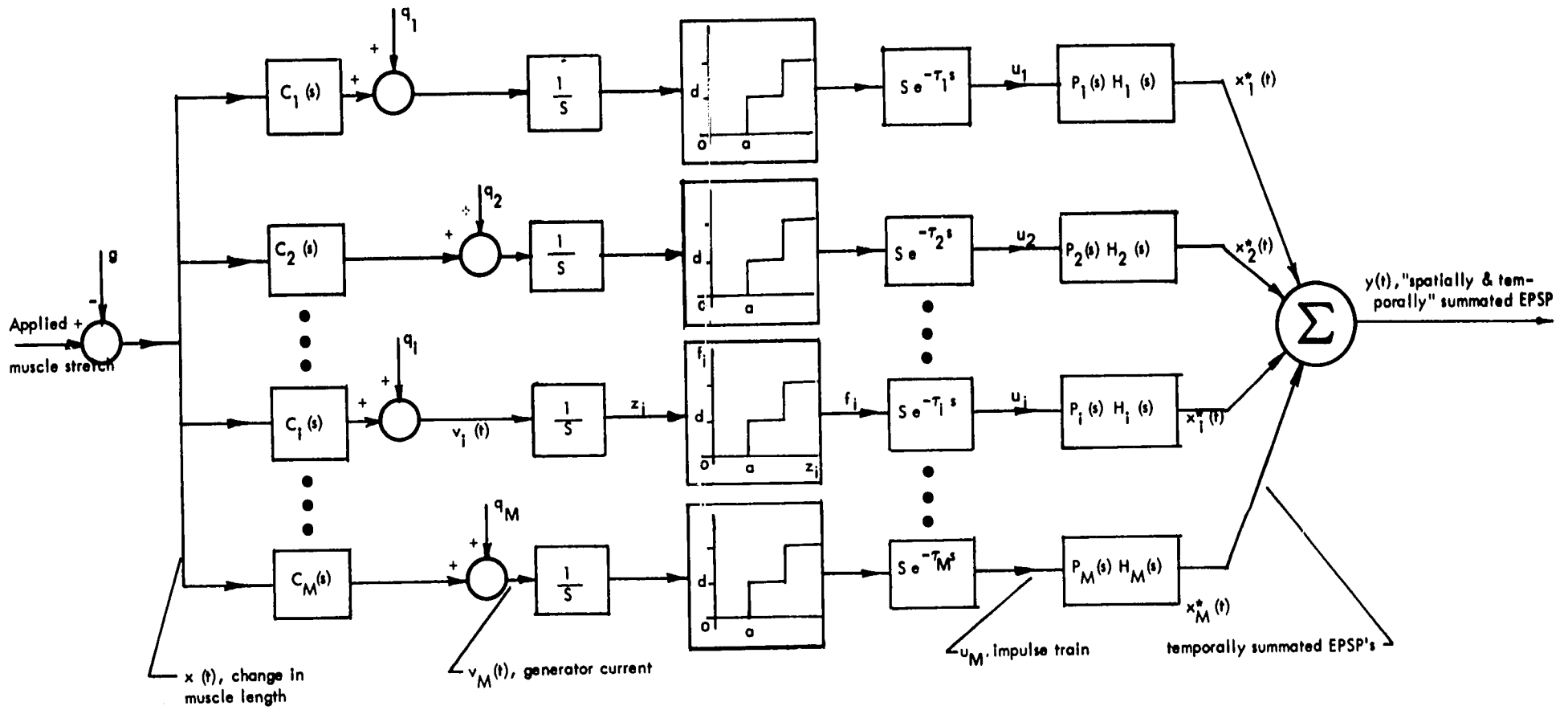


FIGURE 5-8 . A MULTIPATH MODEL OF THE MUSCLE - MOTONEURON COMMUNICATION LINK .

be  $b_i F(s)$ , where  $F(s)$  is invariant for all paths, but the constant  $b_i$  may vary from one path to another. For the special situation described in the previous section, the change in muscle length from its resting length is

$$x(t) = X_o + U \cos \omega_1 t - g, \quad (5-10)$$

where  $X_o$ ,  $U$ ,  $\omega_1$  and  $g$  are constant. Thus, if  $c_i$  and  $\theta_i$  are respectively the gain and phase of  $C_i(s)$  at the frequency  $\omega_1$ , and  $c_{oi}$  is the gain of  $C_i(s)$  at zero frequency, then in the steady state, the summated generator current developed in the primary endings of the  $i$ th spindle is

$$v_i(t) = (X_o - g) \cdot c_{oi} + U \cdot c_i \cos(\omega_1 t + \theta_i) + q_i. \quad (5-11)$$

Assuming that the inputs to the multipath system are such that  $v_i(t) \geq 0$  for all  $i$ , we can readily obtain, by using Equations (3-25) to (3-27) in Chapter III, an expression for the sequence  $x_i^*(t)$  of superposed quantal EPSP at the output of the  $i$ th path. Thus, defining

$$a_i = (X_o - g) c_{oi}, \quad (5-12)$$

we then have,

$$x_i^*(t) = \frac{b_i d}{a} [ (a_i + q_i) A(o) + U c_i A(\omega_1) \cos(\omega_1 t + \theta_i + Q(\omega_1) - \omega_1 \tau_i) ] + N_i(t) \quad (5-13)$$

where

$$N_i(t) = \frac{b_i d}{a} \sum_{k=1}^{\infty} \sum_{n=-\infty}^{\infty} \frac{2 J_n(\beta_i) \lambda_i}{k \omega_0} A(\lambda_i) \cos(\lambda_i t + \varphi_i + Q(\lambda_i) - \lambda_i \tau_i); \quad (5-14)$$

$$\lambda_i = k \omega_0 (\alpha_i + q_i) + n \omega_1, \quad (5-15)$$

$$\varphi_i = n \theta_i - \beta_i \sin \theta_i; \quad (5-16)$$

$$\beta_i = k \omega_0 U c_i / \omega_1, \quad (5-17)$$

$A(\omega)$  and  $Q(\omega)$  are respectively the amplitude and phase characteristics of  $F(s)$  associated with the waveform of the quantal EPSP's, and all other symbols are as previously defined.

Therefore, the "spatially and temporally" summated EPSP is

$$y(t) = \sum_{i=1}^M x_i^*(t) = M \cdot \left[ \frac{1}{M} \sum_{i=1}^M x_i^*(t) \right]. \quad (5-18)$$

As we have noted in Section 5.3, the number of paths in the system is equal to the number of monosynaptic knobs connected to the afferent fibers arising from the spindles under consideration. Since this number is large and since the parameters  $a$ ,  $c$ ,  $b$ ,  $\theta$ ,  $\tau$  and  $q$  vary from path to path, the arithmetic average in Equation (5-18) can be accurately approximated by a statistical average.<sup>78</sup> Thus,

$$y(t) \approx M \cdot E [x^*(t)], \quad (5-19)$$

where  $x^*(t)$  is a member function of the ensemble of pulse sequences

$\{x_i^*(t)\}$ ;  $E[\cdot]$  denotes "the statistical average of", and the average is taken with respect to  $\alpha$ ,  $c$ ,  $b$ ,  $\theta$ ,  $\tau$  and  $q$ , which are now considered as random variables.

Recall that the random variable  $q$  represents the increase in the summated generator current due to constant  $\gamma$ -efferent stimulation,  $\tau$  corresponds to the transmission time between the spindle and the pulse-generating site of the  $\alpha$ -motoneuron, and  $b$  describes the size of the quantal EPSP. There is no known data to indicate whether these three variables are statistically dependent, but we can reasonably assume that they are independent. On the other hand, the variables,  $\alpha$ ,  $c$  and  $\theta$ , being all dependent on  $C(s)$ , are likely to be correlated. Further, a recent report indicates that  $\alpha$  and  $c$  may be correlated with  $\tau$  also.<sup>79</sup> As a result, the statistical average in Equation (5-19) is extremely difficult, if not impossible, to evaluate analytically. In order, therefore, to facilitate the present analysis, we assume that these random variables are all statistically independent. However, as we shall show in the computer simulation study, the main conclusions to be deduced will not be grossly affected by any such dependence described above.

#### 5.6.2 The Signal and Noise Components of the "Spatially and Temporally" Summated EPSP

By dropping the subscript  $i$  in Equation (5-13) and substituting the result into Equation (5-19), we have the following expression for the "spatially and temporally" summated EPSP at the pulse generating site of the  $\alpha$ -motoneuron.

$$y(t) \approx \frac{M d}{a} \cdot E [ b (\alpha + q) A(o) + b U c \cdot A(\omega_1) \cdot \cos(\omega_1 t + \theta + Q(\omega_1) - \omega_1 \tau) ] + M \cdot E [ N(t) ], \quad (5-20)$$

where  $N(t)$  is given by Equation (5-14) with the subscript  $i$  omitted.

The first term of this equation is proportional to the ensemble average of the signal components of the sequences of the quantal EPSP's, while the second term is proportional to the ensemble average of the corresponding noise components. Hence, we define as the signal component  $S(t)$  of the spatially and temporally summated EPSP, the first term of Equation (5-20), and as the noise component  $N_f(t)$ , the second term of that equation. It should be recalled here that the noise component arises from the neural encoding process which converts the summated generator current into the afferent pulse train.

Let us first consider the signal component  $S(t)$ . Since the random variables are assumed statistically independent, we have from Equation (5-20),

$$S(t) = \frac{M d}{a} \cdot \bar{b} \cdot \left\{ (\bar{\alpha} + \bar{q}) A(o) + U \cdot \bar{c} \cdot A(\omega_1) \cdot E [ \cos(\omega_1 t + Q(\omega_1) + \theta - \omega_1 \tau) ] \right\}, \quad (5-21)$$

where " $\bar{\quad}$ " denotes the average value. But

$$\begin{aligned} E [ \cos(\omega_1 t + Q(\omega_1) + \theta - \omega_1 \tau) ] &= \text{Re} \left\{ E [ e^{i(\omega_1 t + Q(\omega_1))} \cdot e^{i\theta} \cdot e^{-i\omega_1 \tau} ] \right\} \\ &= \text{Re} \left\{ e^{i(\omega_1 t + Q(\omega_1))} \cdot E [ e^{i\theta} ] \cdot E [ e^{-i\omega_1 \tau} ] \right\} \\ &= \text{Re} \left\{ e^{i(\omega_1 t + Q(\omega_1))} \cdot \Phi_\theta(i) \cdot \Phi_\tau(-i\omega_1) \right\} \end{aligned} \quad (5-22)$$

where  $\Phi_{\tau}(j\omega)$  and  $\Phi_{\theta}(j\omega)$  are respectively the characteristic functions of the probability densities,  $p_{\tau}(\tau)$  and  $p_{\theta}(\theta)$  for  $\tau$  and  $\theta$  respectively. Let

$$\Phi_{\tau}(j\omega) = B_{\tau}(\omega) e^{i\psi_{\tau}(\omega)}, \text{ and} \quad (5-23)$$

$$\Phi_{\theta}(j\omega) = B_{\theta}(\omega) e^{i\psi_{\theta}(\omega)}, \quad (5-24)$$

where  $B_{\tau}$ ,  $B_{\theta}$ ,  $\psi_{\tau}$  and  $\psi_{\theta}$ , are real functions of  $\omega$ . Then from Equation (5-22) we have

$$E[\cos(\omega_1 t + Q(\omega_1) + \theta - \omega_1 \tau)] = B_{\tau}(-\omega_1) \cdot B_{\theta}(1) \cdot \cos(\omega_1 t + Q(\omega_1) + \psi_{\tau}(-\omega_1) + \psi_{\theta}(1)). \quad (5-25)$$

Therefore, substituting this result into Equation (5-21), we have for the signal component of the summated EPSP,

$$S(t) = \frac{Md}{a} \cdot \bar{b} \cdot [(\bar{\alpha} + \bar{q}) \cdot A(0) + U \cdot \bar{c} \cdot A(\omega_1) \cdot B_{\tau}(-\omega_1) \cdot B_{\theta}(1) \cdot \cos(\omega_1 t + Q(\omega_1) + \psi_{\tau}(-\omega_1) + \psi_{\theta}(1))] \quad (5-26)$$

Equation (5-26) shows that the signal component of the summated EPSP at the  $\alpha$ -motoneuron contains a constant and a sinusoid. The constant is linearly related to the average muscle length and  $\gamma$ -efferent stimulation, while the sinusoidal component is linearly proportional to the variation of muscle length. It should be noted that the amplitude

and phase of the sinusoidal component are respectively dependent on the amplitude and phase characteristics of  $F(s)$ ,  $\Phi_T(-j\omega)$ , and  $\Phi_O(j\omega)$ .

Now, consider the noise component  $N_f(t)$  of the summated excitatory postsynaptic potential (EPSP). From Equation (5.20) we have

$$N_f(t) = M \cdot E [N(t)], \quad (5-27)$$

where  $N(t)$  is described by Equation (5-14) with the subscript  $i$  omitted. As we have shown in Sub-section 3.2.2, the series representing  $N(t)$  may be truncated without introducing significant error, provided that a sufficiently large number of terms are retained.

Thus

$$N_f(t) = M \cdot E \left[ \frac{bd}{a} \sum_{k=1}^K \sum_{n=-N_1}^{N_1} \frac{2}{k\omega_0} \cdot J_n(\beta) \cdot \lambda \cdot A(\lambda) \cdot \cos(\lambda t + \varphi + Q(\lambda) - \lambda \tau) \right], \quad (5-28)$$

where  $\lambda$ ,  $\varphi$ , and  $\beta$  are related to the random variables  $\alpha$ ,  $q$ ,  $\theta$  and  $c$ , and are defined by Equations (5-15) to (5-17) with the subscript  $i$  removed. Taking the average with respect to  $b$  and interchanging the order of summation and averaging, we have

$$N_f(t) = \frac{Md}{a} \cdot \bar{b} \cdot \sum_{k=1}^K \sum_{n=-N_1}^{N_1} \frac{2}{k\omega_0} \cdot E [J_n(\beta) \cdot \lambda \cdot A(\lambda) \cdot \cos(\lambda t + \varphi + Q(\lambda) - \lambda \tau)]. \quad (5-29)$$

Examining this expression in conjunction with Equation (5-26), we see that both the signal and noise components are attenuated by  $\bar{b}$ . Therefore, statistical variation in the size of the numerous quantal EPSP's arising from the multiple paths does not affect the signal - to-noise ratio of the summated EPSP.

Next we take the average with respect to the transmission time  $\tau$ . Since  $\lambda$ ,  $\varphi$  and  $\beta$  are not related to  $\tau$ , we may approach the problem as in the derivation of Equation (5-25) and obtain

$$N_t = \frac{M d}{a} \cdot \bar{b} \cdot \sum_{k=1}^K \sum_{n=-N_1}^{N_1} \frac{2}{k \omega_0} \cdot E [ J_n(\beta) \cdot \lambda \cdot A(\lambda) \cdot B_\tau(-\lambda) \cdot \cos(\lambda t + \varphi + Q(\lambda) + \psi_\tau(-\lambda)) ] , \quad (5-30)$$

where  $B_\tau(\omega)$  and  $\psi_\tau(\omega)$  are respectively the amplitude and "phase" of the characteristic function  $\Phi_\tau(j\omega)$  defined in Equation (5-23). This equation shows that the amplitude and phase of each spectral component of  $N_t(t)$  is dependent on the amplitude and phase characteristics of  $\Phi_\tau(-j\omega)$  respectively. The significance of this result will be discussed in the next sub-section.

We recall that  $\theta$  represents the phase shift introduced into the sinusoidal component of the summated generator current after the signal representing muscle length variation has passed through the dynamics of the whole muscle and the spindle under consideration. It is reasonable to assume that the variation in  $\theta$  is small. Hence, from Equation (5-16), we have

$$\varphi \approx (n - \beta) \theta . \quad (5.31)$$

Substituting this into Equation (5-30) and taking the average with respect to  $\theta$  by the method used in deriving Equation (5-26), we have

$$N_t \approx \frac{M d}{a} \cdot b \cdot \sum_{k=1}^K \sum_{n=-N_1}^{N_1} \frac{2}{k \omega_0} E [J_n(\beta) \cdot \lambda \cdot A(\lambda) \cdot \beta_\tau(-\lambda) \cdot B_\theta(n-\beta) \cdot \cos(\lambda t + Q(\lambda) + \psi_\tau(-\lambda) + \psi_\theta(n-\beta))], \quad (5-32)$$

where  $B_\theta(\omega)$  and  $\psi_\theta(\omega)$  are respectively the amplitude and "phase" of the characteristic function  $\Phi_\theta(j\omega)$  defined in Equation (5-24). Note that, as in the result of averaging with respect to  $\tau$ , the amplitude and phase of each sinusoidal component of  $N_t(t)$  are dependent on the amplitude and "phase" of  $\Phi_\theta(j\omega)$  respectively.

Up to this point in our consideration of the noise component, we have evaluated the statistical average with respect to three of the six random variables involved. The remaining random variables are  $q$ ,  $\alpha$  and  $c$ , which appear in the expressions for  $\lambda$  and  $\beta$ . (See Equations (5-15) and (5-17)). Unfortunately, because of the functional complexities involved, it is not possible, at present, to evaluate the average in Equation (5-32) with respect to these variables. However, we shall examine this effect on the noise component in a computer simulation study which is presented in the next section.

### 5.6.3 Significance of the Analytical Results

In order to examine the significance of the analytical results obtained above, we shall first obtain an expression of the "spatially and temporally" summated EPSP for the

hypothetical case in which all paths of information transmission are identical. For this case, the sequences of quantal EPSP's are synchronous, and thus the resulting summated EPSP is simply the sequence of quantal EPSP's in a single path multiplied by the number of paths in the system. Let the signal and noise components of this summated EPSP be denoted by  $S_o(t)$  and  $N_o(t)$  respectively. Then, from Equations (5-13), (5-14), and (5-18), we have

$$S_o(t) = \frac{M d}{a} \cdot b \cdot [ (\alpha + q) A(o) + U \cdot c \cdot A(\omega_1) \cdot \cos(\omega_1 t + Q(\omega_1) + \theta - \omega_1 \tau) ] , \quad (5-33)$$

and

$$N_o(t) \approx \frac{M d}{a} \cdot b \cdot \sum_{k=1}^K \sum_{n=-N_1}^{N_1} \frac{2}{k \omega_o} \cdot J_n(\beta) \cdot \lambda \cdot A(\lambda) \cdot \cos(\lambda t + Q(\lambda) + (n - \beta) \theta - \lambda \tau) \quad (5-34)$$

where in the latter equation we have truncated the series and approximated  $\varphi$  by  $(n - \beta) \theta$ , as we have done in the above analysis.

Now, consider the more realistic case in which the parameters  $b$ ,  $\tau$ , and  $\theta$  vary from path to path but the parameters  $c$ ,  $a$ , and  $q$  remain invariant. For this case, the expressions for the signal and noise components can be readily derived from Equations (5-26) and (5-32) respectively. Thus,

$$S(t) = \frac{M d}{a} \cdot \bar{b} \cdot [ (\alpha + q) \cdot A(o) + U \cdot c \cdot A(\omega_1) \cdot B_\tau(-\omega_1) \cdot B_\theta(1) \cdot \cos(\omega_1 t + Q(\omega_1) + \psi_\tau(-\omega_1) + \psi_\theta(1)) ] , \quad (5-35)$$

and

$$N_t(t) = \frac{M d}{a} \cdot \bar{b} \cdot \sum_{k=1}^K \sum_{n=-N_1}^{N_1} \frac{2}{k \omega_0} \cdot J_n(\beta) \cdot \lambda \cdot A(\lambda) \cdot$$

(5-36)

$$B_T(-\lambda) \cdot B_\theta(n-\beta) \cdot \cos(\lambda t + Q(\lambda) + \psi_\theta(n-\beta) + \psi_T(-\lambda)).$$

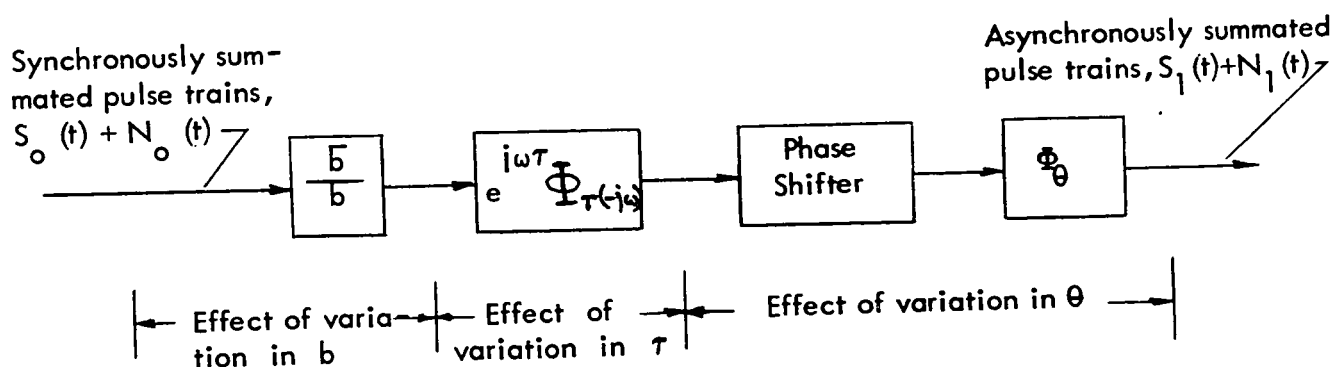


FIGURE 5-9. ILLUSTRATING THE EFFECT OF VARIATIONS IN  $b$ ,  $\tau$ , AND  $\theta$ .  
(SEE TEXT FOR DETAILS OF INTERPRETATION).

Comparing  $S_o(t)$  and  $N_o(t)$  with  $S(t)$  and  $N_t(t)$  respectively, and noting that  $\Phi_T(0) = \Phi_\theta(0) = 1$ , we see that the effect of variations in  $b$ ,  $\tau$  and  $\theta$  is equivalent to the effect of passing the synchronously summated sequences of quantal EPSP's through a system of filters as illustrated in Figure 5-9. The effect of variation in the size  $b$  of the quantal EPSP's is simply that of a pure gain or attenuator, and does not affect the spectral characteristics of the summated EPSP. Further, as noted

previously, the variation in  $b$  does not affect the signal-to-noise ratio of the received signal at the  $\alpha$ -motoneuron.

The variation in the transmission time  $\tau$  is equivalent to filtering the synchronously summated sequences by a filter whose system function is  $e^{j\omega\tau} \Phi_{\tau}(-j\omega)$ . The factor  $e^{j\omega\tau}$  is included to compensate for the phase shift due to  $\tau$  in  $S_o(t)$  and  $N_o(t)$ , since the phase shift  $\omega\tau$  appearing in  $S_o(t)$  and  $N_o(t)$  does not appear in the expression for  $S(t)$  and  $N_t(t)$ . The frequency characteristics of  $\Phi_{\tau}(-j\omega)$  then modify the amplitude and phase of the spectral components of the resulting signal to yield the input to the next phase shifter.

Finally, the effect of variation in the phase shift  $\theta$  is similar but not identical to that of the variation in  $\tau$ . In Figure 5-9, the block entitled "phase shifter" has such a characteristic that the phase shift due to  $\theta$  in  $S_o(t)$  and  $N_o(t)$  becomes zero at its output;  $\Phi_{\theta}$ , on the other hand, further modifies the amplitude and phase of the spectral components of  $S_o(t)$  and  $N_o(t)$  to yield finally the asynchronously summated sequences of quantal EPSP's,  $S(t) + N_t(t)$ . It should be noted, however, that  $\Phi_{\theta}$  is not a linear filter in the usual sense because while it modifies the spectral components of its input, this is not done according to their frequencies.

The equivalent filter  $\Phi_{\tau}(-j\omega)$  tends to enhance the signal-to-noise ratio of the "spatially and temporally" summated EPSP. To justify this statement, note that the distribution of  $\tau$  can be closely approximated by a continuous probability density, and hence  $|\Phi_{\tau}(-j\omega)|$  decreases monotonically as  $|\omega|$  increases.<sup>83</sup> Thus, the noise component of the summated EPSP is attenuated, while the signal component, being at a

frequency lower than most of the spectral frequencies of the noise component, is not as much attenuated. Consequently, the signal-to-noise ratio is generally improved.

As an example, consider the experimentally-observed histograms of the transmission time shown in Figure 5-10. The distributions shown have been computed using experimental data from Reference 80 for the medial gastrocnemius and soleus of the cat. The time axis indicates the time required for transmission from the muscle nerve to the dorsal root. Each of these histograms can be well approximated by either a gamma or a chi-square probability density with appropriate time shift and parameters. However, in order to obtain the total time  $\tau$  required to transmit a signal from the spindle to the pulse-generating site of the  $\alpha$ -motoneuron, we must add the conduction time from the spindle to the muscle nerve, together with the so-called synaptic delay, to the transmission time from the muscle-nerve to the dorsal root. These additional transmission times are not negligible because the synaptic delay is from 0.5 to 0.9 msec.<sup>50</sup> and the conduction time from the spindle to the muscle nerve is probably of at least the same magnitude. Actually there is a further point, that since the spindles are spatially distributed within the muscle and since the Ia fibers from these spindles have different conduction velocities, the transmission times from the spindles to a point on the muscle nerve must also be distributed in some manner. Finally, as noted in Section 5.3, the monosynaptic knobs are distributed more or less uniformly on the soma-dendritic complex of the  $\alpha$ -MN. Thus, the synaptic delay must also vary from path to path. At present, we do not know whether these portions of the total transmission time are correlated or not, but it is probably not unreasonable to assume that they are statistically independent. Therefore, by the central limit theorem<sup>78</sup>, the total transmission times  $\tau$  from the spindles to the pulse-generating

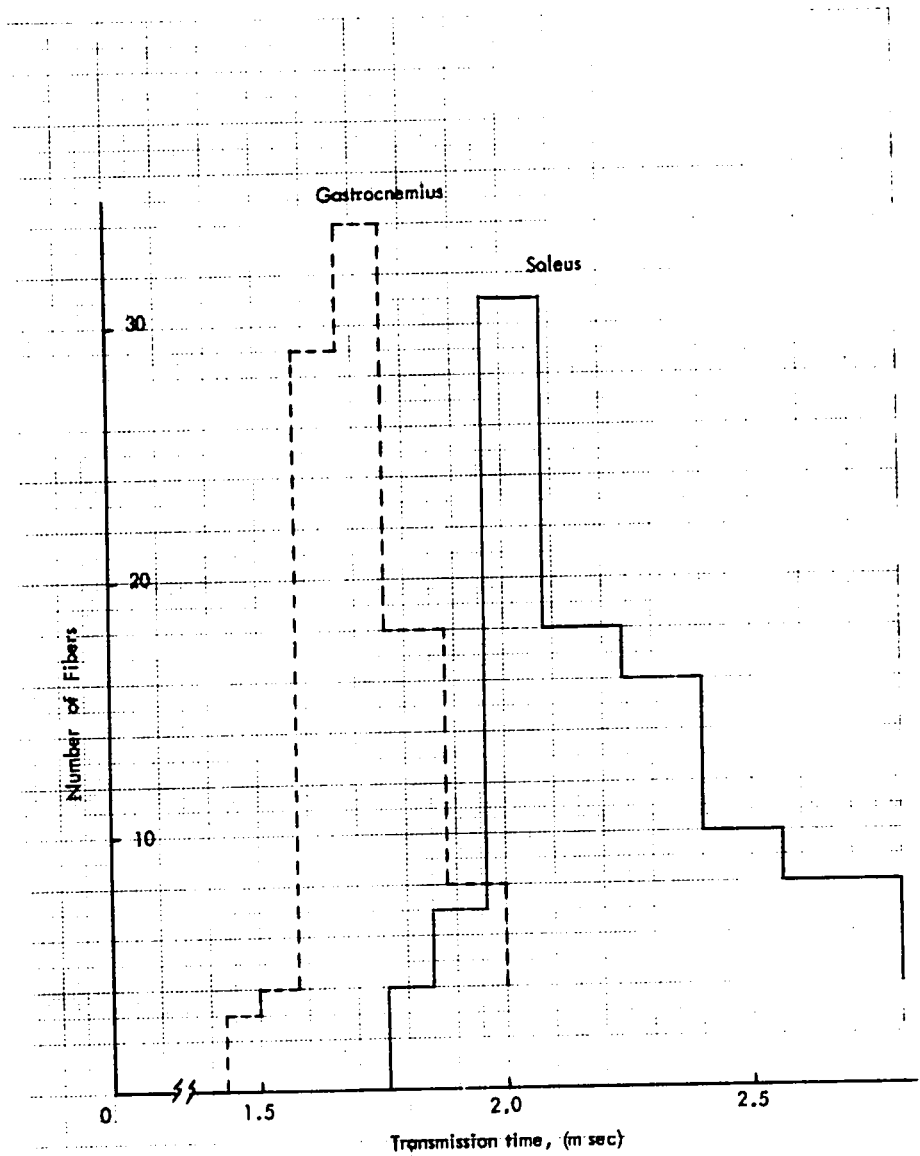


FIGURE 5-10. HISTOGRAMS OF TIME REQUIRED FOR TRANSMISSION FROM MUSCLE NERVE TO DORSAL ROOT.

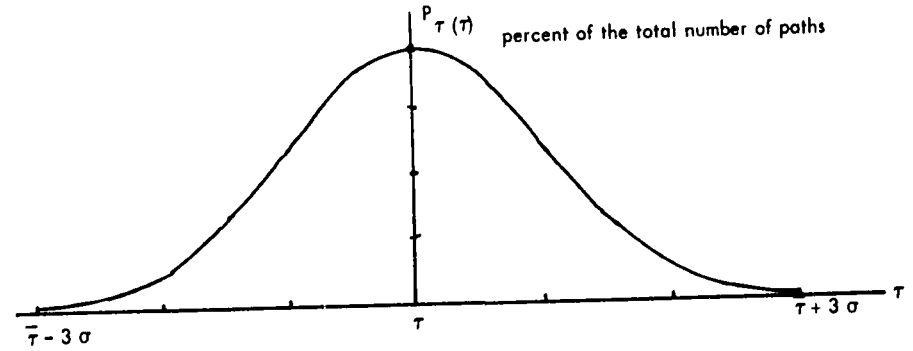


FIGURE 5-11. ASSUMED DISTRIBUTION FOR THE TRANSMISSION TIME,  $\tau$ .

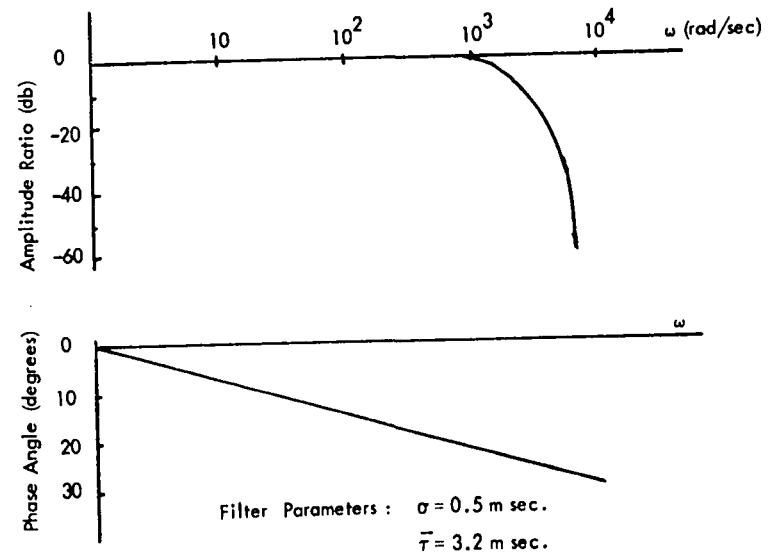


FIGURE 5-12. FREQUENCY RESPONSE OF A GAUSSIAN FILTER.

site of the  $\alpha$ -MN tend to be Gaussian distributed. In fact, because the histograms in Figure 5.10 are already fairly somewhat bell-shaped, (although one shows significant skewness), the distribution of  $\tau$  should be almost Gaussian.<sup>81</sup> Hence, we shall represent the distribution  $p_{\tau}(\tau)$  of  $\tau$  by a truncated Gaussian density as shown in Figure 5-11. The characteristic function of a truncated probability is practically equal to the characteristic function of the original probability density, provided a sufficient portion of the density curve is retained.<sup>82</sup> Thus, if  $p_{\tau}(\tau)$  is truncated at two or more standard deviations, it can be shown that

$$\Phi_{\tau}(-j\omega) \approx e^{-\frac{1}{2} \sigma^2 \omega^2} e^{-j\omega \bar{\tau}} \quad (5-37)$$

where  $\sigma$  is the standard deviation and  $\bar{\tau}$  is the mean transmission time. Equation (5-37) shows that  $\Phi_{\tau}(-j\omega)$  is approximately a Gaussian filter, the frequency response of which is shown in Figure 5-12 for  $\bar{\tau} = 3.2$  msec. and  $\sigma = 0.5$  msec. Clearly, the equivalent filter  $\Phi_{\tau}(-j\omega)$  is a low-pass filter with sharp cutoff characteristic and linear phase; indeed, as we shall show in the computer simulation study, the frequency characteristics of  $\Phi_{\tau}(-j\omega)$  do provide the essential filter in demodulating the afferent pulse trains.

Finally, we consider the filtering effect of the equivalent filter  $\Phi_{\theta}$  which is due to variation of the phase angle  $\theta$  in the summated generator current,  $v(t)$ . (See Equation (5-11)). For the present, let us again postulate that the distribution of  $\theta$  is Gaussian with standard deviation  $\sigma_{\theta}$  and mean  $\bar{\theta}$ . Then,

$$\Phi_{\theta}(j\omega) = e^{-\frac{1}{2} \sigma_{\theta}^2 \omega^2} e^{j\omega \bar{\theta}} \quad (5-38)$$

Using this in Equation (5-35) and (5-36), the expressions for the asynchronously summated sequences of EPSP's become

$$S(t) = \frac{M d}{a} \cdot \bar{b} \cdot [ (\alpha + q) A(0) + U \cdot c \cdot A(\omega_1) \cdot B_{\tau}(-\omega_1) \cdot e^{-\sigma_o^2/2} \cos(\omega_1 t + Q(\omega) + \psi_{\tau}(-\omega_1) + \bar{\theta}) ], \quad (5-39)$$

and

$$N_{\dagger}(t) = \frac{M d}{a} \cdot \bar{b} \cdot \sum_{k=1}^K \sum_{n=-N_1}^{N_1} \frac{2}{k \omega_o} \cdot J_n(\beta) \cdot \lambda \cdot A(\lambda) \cdot B_{\tau}(-\lambda) \cdot e^{-(n-\beta)^2 \sigma_o^2/2} \cdot \cos(\lambda t + Q(\lambda) + \psi_{\tau}(-\lambda) + (n-\beta) \bar{\theta}). \quad (5-40)$$

Comparing these expressions with Equations (5-33) and (5-34) for the synchronously summated sequences of EPSP's, we see that a Gaussian distribution of  $\theta$  does not affect the phase relationship among the spectral components of the summated EPSP, and that the sinusoid in the signal component is attenuated by the factor  $e^{-\sigma_o^2/2}$  which is independent of frequency.

In order to examine the effect of  $\Phi_{\theta}$  on the amplitude of the noise component, we recall from Chapter 3, that this component can be considered as composed of constituents, each of which comprises a set of spectral components. For the noise

component  $N_o(t)$  in the present problem, there are  $K$  significant constituents, and the  $k^{\text{th}}$  constituent has its spectral components at the frequencies,

$$\lambda = k\omega_o (\alpha + q) + n\omega_1 , \quad (5-41)$$

where  $|n| = 0, 1, 2, \dots, N_1$ .

Now consider first the effect of  $\Phi_\theta$  on the  $k^{\text{th}}$  constituent. The amplitude characteristic of  $\Phi_\theta$  is maximum when

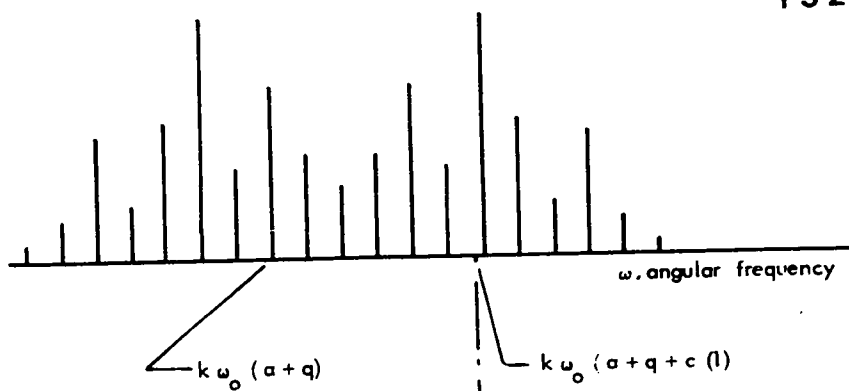
$$n - \beta = n - k\omega_o U c / \omega_1 = 0 , \quad (5-42)$$

that is, when  $n\omega_1 = k\omega_o U c$ . By Equation (5-41), this maximum is located at the frequency,

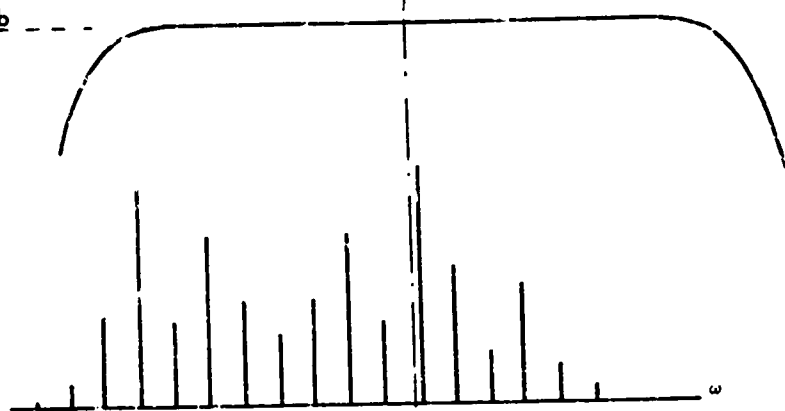
$$\lambda = k\omega_o (\alpha + q + U c) . \quad (5-43)$$

Thus, without loss of generality, if the amplitude spectrum of the  $k^{\text{th}}$  constituent is assumed to be as shown in Figure 5-13 (a), then the resulting amplitude spectrum at the output of  $\Phi_\theta$  is as given in Figure 5-13 (b), if the standard deviation  $\sigma_o$  of the assumed Gaussian distribution for  $\theta$  is small; and as given in Figure 5-13 (c), if  $\sigma_o$  is larger than the previous value. From this illustration, we see that when  $\sigma_o$  is small, the amplitude spectrum of the  $k^{\text{th}}$  noise constituent is essentially unaffected. Since the phase relationship among the spectral components are also unaffected by  $\Phi_\theta$  as we have noted previously, the noise component at the output of  $\Phi_\theta$  remains practically the same as it was at the input of  $\Phi_\theta$ . Turning now to the signal component, we see that for this case of small

(a) Assumed amplitude spectrum of a constituent of the noise component in the synchronously summated sequences of EPSP's .



(b) Amplitude characteristic of  $\Phi_\theta$  with small  $\sigma_c$  and the resulting amplitude spectrum of the noise component,  $N_f(t)$  .



(c) Amplitude characteristic of  $\Phi_\theta$  with large  $\sigma_c$  and the resulting amplitude spectrum of the constituent of the noise component,  $N_f(t)$  .

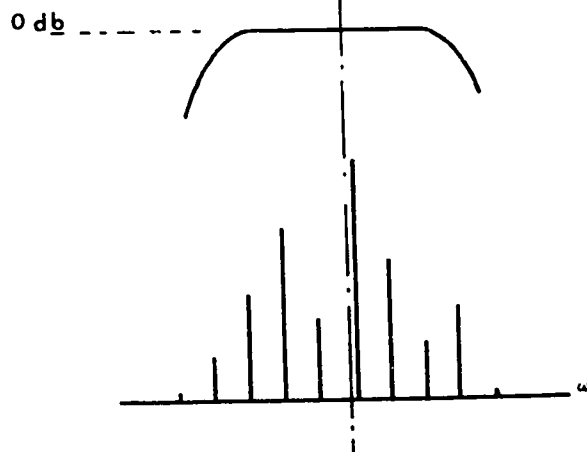


FIGURE 5 - 13. ILLUSTRATING THE EFFECT OF  $\Phi_\theta$  ON THE AMPLITUDE SPECTRUM OF THE NOISE COMPONENT .

$\sigma_o$ , the signal component is not significantly attenuated. Hence, when the distribution of  $\theta$  is Gaussian with a small standard deviation, the variation in  $\theta$  has no significant effect on the signal-to-noise ratio of the summated EPSP.

On the other hand, when the standard deviation  $\sigma_o$  is sufficiently large so that the amplitude spectrum of the  $k^{\text{th}}$  noise constituent is significantly modified as the noise component is passed through  $\Phi_\theta$ , the sinusoid in the signal component will also be significantly attenuated. In this case, whether the signal-to-noise ratio can be improved by the variation in  $\theta$  depends on the relation between several parameters of the transmission system, but especially on  $\sigma_o$  and the system inputs. It is conceivable that the signal-to-noise ratio can even deteriorate as  $\sigma_o$  becomes sufficiently large, since the center frequencies of the noise constituents are not attenuated for any finite value of  $\sigma_o$ , whereas the sinusoid of the signal component is attenuated according to  $e^{-\sigma_o^2/2}$ . However, it should be noted that no valid conclusion can be drawn if  $\sigma_o$  becomes so large as to invalidate the assumption made in obtaining our analytical results.

From the above discussion, we can conclude that small variations in  $\theta$  does not significantly affect the signal-to-noise ratio of the summated EPSP, if the distribution of  $\theta$  is Gaussian. Further, this conclusion is applicable also for other continuous distribution of  $\theta$ , since  $\Phi_\theta(0) = 1$  and since  $|\Phi_\theta(j\omega)|$  decreases monotonically as  $\omega$  increases, as we have noted previously.

#### 5.6.4 Variation in the Waveform of the Quantal EPSP

In the above analysis, we made the simplifying assumption that the quantal EPSP's all have identical pulse shape. We shall now remove this restriction and examine the resulting effects, if any, by allowing the pulse shape to vary from one path to another. For the present, let the neuronal transfer dynamics be represented by a first-order linear system. Thus, let

$$H_i(s) = \frac{1}{1 + T_i s} \quad (5-44)$$

for the  $i^{\text{th}}$  path. We have shown above that the distribution in the transmission time  $\tau$  of the afferent fibers plus subsequent summation in the neuron have the equivalent effect of filtering the synchronously summated sequences of quantal EPSP's, with a filter of frequency characteristic  $\Phi_\tau(-j\omega)$ . Since the spectral characteristics of a single sequence of quantal EPSP's are identical with those of the synchronously summated sequences, let us now consider that each afferent pulse train is filtered by the product  $H_i(j\omega) \Phi_\tau(-j\omega)$ . Further, let the probability density of  $\tau$  be approximated by a Gaussian density with a mean of 3.2 msec. and a standard deviation of 0.5 msec. Then, the amplitude characteristic of  $H_i(j\omega) \Phi_\tau(-j\omega)$  may be plotted as in Figure 5.14 for different values of  $T_i$ . Curves (1), (2), and (3) are the characteristics for which  $T_i = 2$  msec., 4 msec., and 20 msec., respectively. Since the quantal EPSP produced by a synaptic input near the pulse generating site has a shorter delay time than that produced by a synaptic input farther away,<sup>60</sup> we assume that the curve for  $T_i = 2$  msec. is associated with a synapse located nearest to the pulse generating site, while  $T_i = 20$  msec. is associated with one which is located farthest away but still producing a detectable EPSP at the pulse gen-

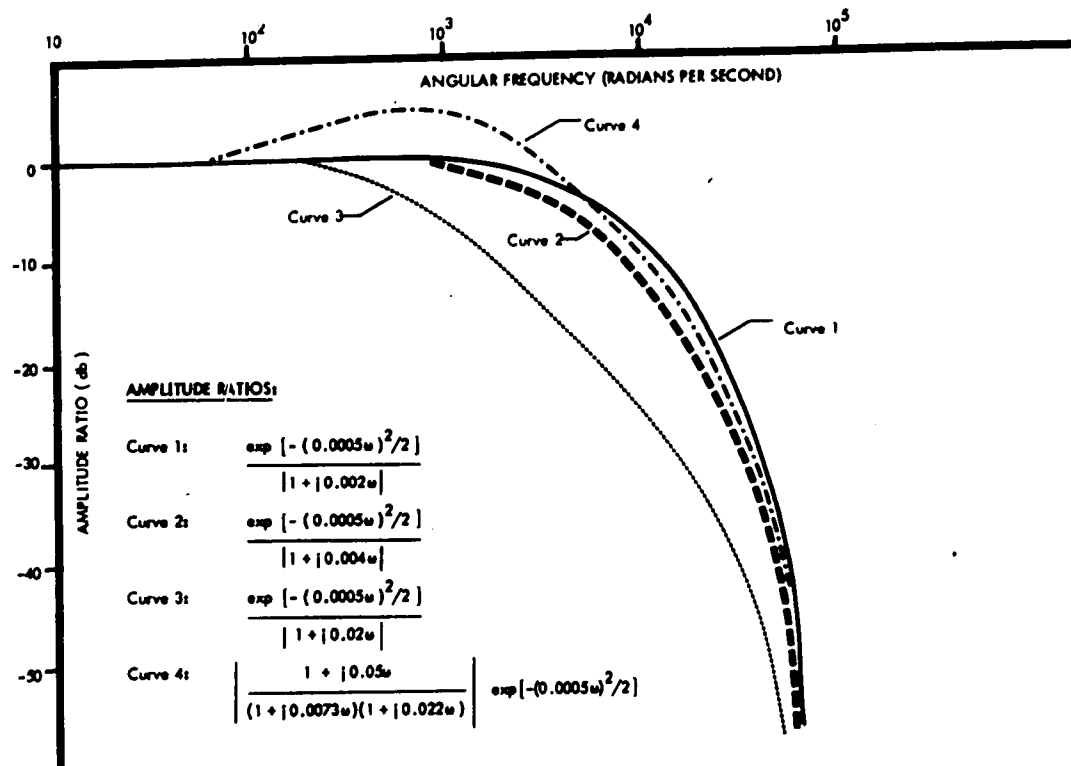


FIGURE 5-14. FREQUENCY RESPONSE OF THE CASCADED NEURAL FILTERS.

erating site. Thus, the amplitude frequency responses of all filters  $H_i(j\omega) \Phi_\tau(-j\omega)$  are bounded by curves (1) and (3), and curve (2) is representative of an intermediate condition with a mean time constant of 4 msec. In fact, recent evidence indicates that the majority of synapses is centered about 400  $\mu$  away from the soma of the MN,<sup>57</sup> and therefore it seems reasonable to assume that the amplitude frequency responses do cluster about the mean response of curve (2) in Figure 5-14. Since the quantal EPSP's produced by synaptic inputs located further away have smaller amplitudes, the contribution to the summated EPSP by the pulse responses of the filters whose frequency characteristics are bounded by curves (2) and (3) is relatively small compared to the contribution made by the others. From these results we may plausibly conclude that the realistic situation in which  $H_i$  varies from path to path, can be analysed without gross error by assuming that all quantal EPSP's have the same shape.

Now, consider the effect of the variation in the filter characteristic. Thus in addition to the frequency responses already considered, we have included in Figure 5-14 a frequency response curve (Curve 4) which describes a subthreshold model of electrotonic conduction in a motoneuron,<sup>67</sup> in cascade with the filter  $\Phi_\tau(-j\omega)$ . We see that while the mid-frequency response varies somewhat, the cutoff characteristic is essentially unchanged from that provided by  $\Phi_\tau(-j\omega)$ . In view of the observations made above and the fact that  $H_i(j\omega)$  does not have an effective cutoff characteristic, it is clear that the filtering of the neural pulse trains is mainly accomplished by  $\Phi_\tau(-j\omega)$ , which is associated with the distribution of the transmission time  $\tau$  of the afferent fibers. Consequently, variation in the subthreshold post-synaptic membrane characteristics, such as time constants, has comparatively little effect on the

signal-to-noise ratio of the summated EPSP. However, it should be noted that this conclusion does not preclude that this variation may be significant for the operation of the overall reflex.

## 5.7 Computer Simulation Study

The muscle-to-motoneuron communication link, as represented by the model shown in Figure 5-8, has been studied by digital computer simulation. The purpose of this study is to verify the theoretically predicted results obtained in the last section, and further, to examine the effects of variations in those system parameters which can not be analytically studied at present.

### 5.7.1 Method

#### (a) Simulating the System

When the change in muscle length from its resting length is a biased sinusoid as described by Equation 5.10, the  $i^{\text{th}}$  path of the communication link, in the steady state, can be represented as shown in Figure 5-15. In this diagram, all symbols and signals are as defined previously. In particular, we recall that the first three blocks together represent the impulse generating mechanism of the neural encoder, the delay unit represents the afferent fiber, and the impulse response of  $P_i H_i$  represents the quantal excitatory postsynaptic potential (EPSP) at the pulse generating site of the  $\alpha$ -motoneuron ( $\alpha$ -MN).

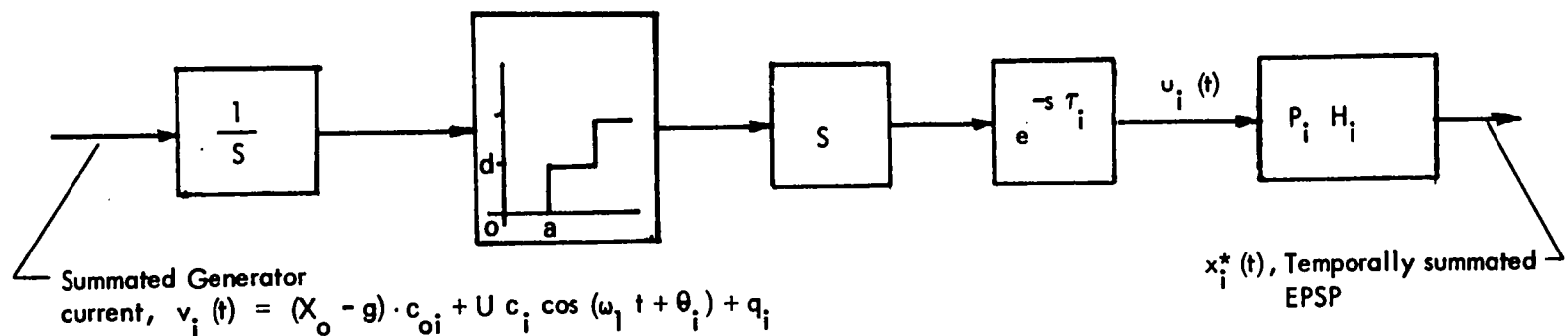


FIGURE 5 - 15 . AN EQUIVALENT REPRESENTATION OF THE  $i$ th PATH IN THE STEADY STATE .

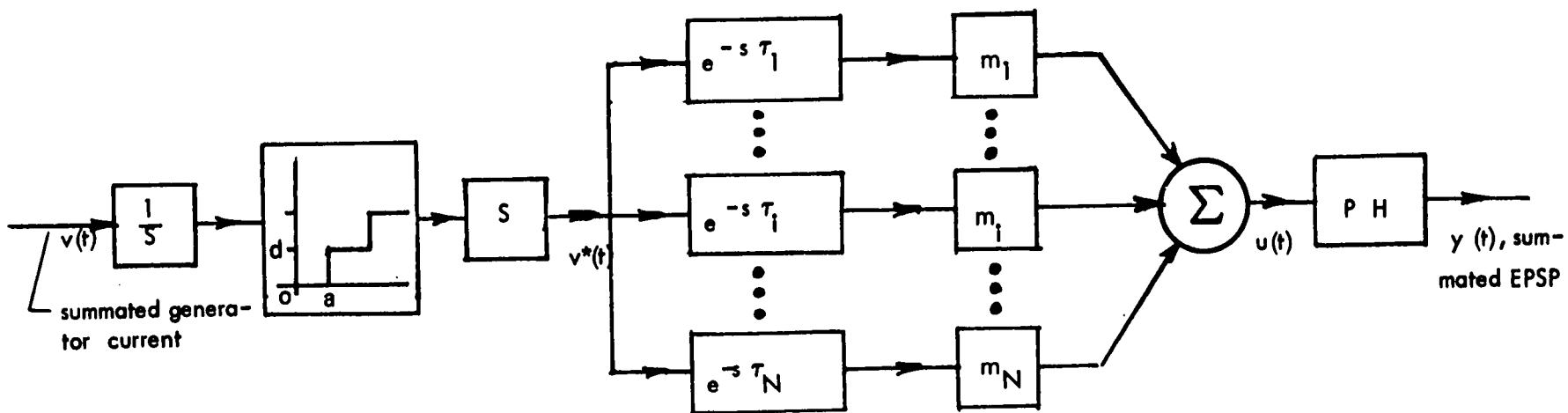


FIGURE 5 - 16. ILLUSTRATING A METHOD FOR SIMULATING THE MUSCLE-TO-MOTONEURON COMMUNICATION LINK. THE BLOCK DIAGRAM REPRESENTS THE SITUATION IN WHICH ONLY THE TRANSMISSION TIME  $\tau$  VARIES FROM PATH TO PATH .

In the present computer simulation study, the impulse generating mechanism is implemented using the following criterion for impulse emission.

$$I_i = \sum_{n=N_{i-1}}^{N_i} v(n \Delta t + \Delta t) \cdot \Delta t \geq a ; \quad (5-45)$$

$$i = 1, 2, 3, \dots; \text{ and } N_0 = 0 ;$$

where  $a$  is a positive constant representing the threshold of the encoder;  $\Delta t$  is the time increment for computation; and  $N_{i-1} \Delta t$  and  $N_i \Delta t$  are the emission times for the  $(i-1)^{\text{th}}$  and the  $i^{\text{th}}$  impulses respectively. It should be noted that this criterion is a numerical representation of the criterion given in Equation (5.3) for pulse emission in S-S IPFM. Whenever Equation (5.45) is satisfied for the smallest value of  $N_i$ , a rectangular pulse of height  $h$  and width  $\Delta t$  is generated at the input of the time-delay unit, and at the same instant,  $I_i$  is reset to zero. Note that the impulse is approximated here by a narrow rectangular pulse. The remaining two blocks in Figure 5-15 are simulated using standard digital computation techniques. The time-delay unit in the simulation has the transfer function,  $e^{-sk \Delta t}$ , where  $k$  is a positive integer; while the input-output relation of  $P_i H_i$  is represented by the convolution summation,

$$X_i(k \Delta t) = \sum_{n=1}^k h_i(n \Delta t) \cdot U_i(k \Delta t - n \Delta t) \cdot \Delta t , \quad (5-46)$$

where  $h_i(t)$  is the unit-impulse response of  $P_i H_i$ .

The simulated model of the complete communication link comprises a set of afferent paths each of which is simulated using the methods just described. Although the multiplicity of paths with different properties can be represented by simply incorporating hundreds of paths into the model and generating random numbers for the parameters that vary from path to path, this requires an excessive amount of computing time. An alternative method therefore has been used. In this alternative method, the communication link is represented by a model with  $N$  different classes of afferent paths, where each class contains only paths with identical properties. Thus, the communication link can be simulated with a model having only  $N$  different pathways whose outputs are weighted according to the number of paths in the class.

As an example, consider the hypothetical case in which only the transmission time  $\tau$  varies from one path to another. Let there be  $M$  paths in the communication link and let there be  $m_i$  paths with the transmission time,  $\tau_i$ , where  $i = 1, 2, \dots, N$ ; and  $M = \sum_{i=1}^N m_i$ . Then, all pulse trains in the paths of the  $i^{\text{th}}$  class are synchronous, and thus the sum of outputs from these paths is equal to the output of a single path in this class multiplied by  $m_i$ . Using this result, and noting that the other properties of the paths are assumed invariant, we can simulate the  $M$ -path system with a model having only  $N$  different pathways as shown in Figure 5-16.

It should be noted that in this alternative method, we treat the parameters of the communication link as discrete random variables. Thus, in the example that we have just presented, the probability density of  $\tau$  can be expressed as

$$p_{\tau}(\tau) = \sum_{i=1}^N p_{\tau_i} \delta(\tau - \tau_i) \quad (5-47)$$

where  $p_{\tau i} = m_i / M$ , and  $\delta(\tau)$  is the unit-impulse function. Thus, in simulating the system for this case, we can equivalently weight the output of the  $i^{\text{th}}$  pathway with  $p_{\tau i}$ .

(b) Statistics and Values of the System Parameters

We recall that in the model of the muscle-to-motoneuron communication link (Figure 5.8) the quantities which vary from path to path are:

1. the static gain  $c_{0i}$  of  $C_i(s)$  which represents the linearized dynamics relating the change in muscle length to the resulting change in summated generator current in the primary nerve endings of the spindle;
2. the dynamic gain  $c_i$  of  $C_i(s)$  at the frequency  $\omega_1$  of the sinusoidal component of the change of muscle length;
3. the phase angle  $\theta_i$  of  $C_i(s)$  at the frequency  $\omega_1$ ;
4. the constant  $q_i$  which represents the increase in the summated generator current produced by constant  $\gamma$ -efferent activity;
5. the time  $\tau_i$  which represents the time required to transmit a pulse from the muscle spindle to the pulse-generating site of the  $\alpha$ -MN; and

6. the transfer function  $P_i(s) H_i(s)$  whose impulse response represents the quantal EPSP at the pulse generating site of the  $\alpha$ -MN.

In order to simulate the communication link it is necessary to specify the statistics and the range of values for these quantities and other system parameters. Unfortunately, with the exception of  $\tau$  and  $P(s) H(s)$ , the required information for the remaining parameters is completely unknown at present. Therefore, in the present simulation study, we can only choose the statistics and the range of values to fit relevant physiological data presently available in the literature.

As we have shown in Sub-section 5.6.3, the probability density  $p_\tau(\tau)$  of  $\tau$  can be reasonably represented by a truncated Gaussian density. In view of the discussion presented in that sub-section, it is reasonable to assume that the transmission time from a leg muscle such as the soleus of the cat to the homonymous  $\alpha$ -MN has a mean of 3.2 msec., a standard deviation of 0.5 msec., and a range of from 1.7 to 4.7 msec. In the present simulation study, this Gaussian density is area-sampled to yield a discrete probability density as shown in Figure 5-17 so that the method of simulation described above can be applied. The error introduced by this area-sampling is negligible for the quantizing size  $\Delta$  used.

In order to obtain a reasonable description of the statistical variations in  $P(s) H(s)$ , let us first consider the distribution of mono-synaptic knobs on the surface of the  $\alpha$ -motoneuron ( $\alpha$ -MN). Recently Terzuolo and Lind, using morphological data, have estimated the distribution of the total synaptic input among different portions of the soma-dendritic complex of a model motoneuron possessing an average dendritic tree.

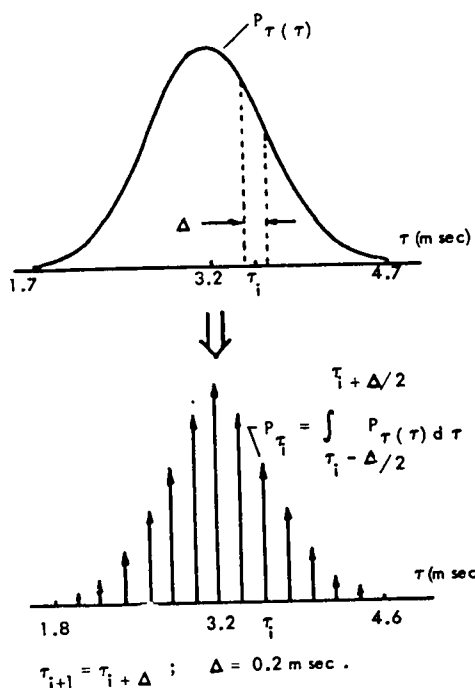


FIGURE 5 - 17. ASSUMED PROBABILITY DENSITY OF TRANSMISSION TIME,  $\tau$ , AND ITS AREA-SAMPLED REPRESENTATION.

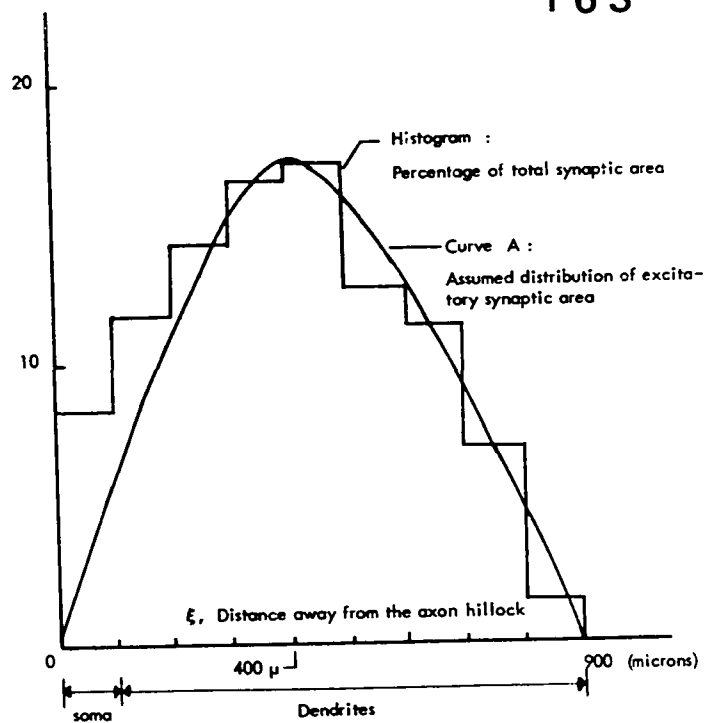


FIGURE 5 - 18. DISTRIBUTION OF SYNAPTIC KNOBS ON A MOTONEURON MODEL (BASED ON DATA FROM REFERENCE 57) .

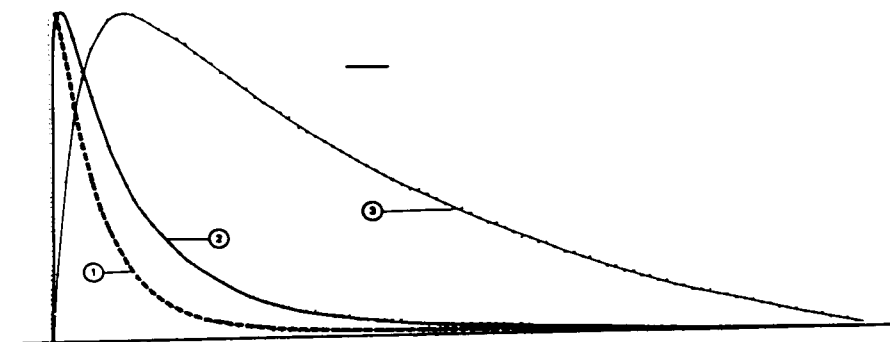


FIGURE 5-19. WAVEFORMS OF EPSP COMPUTED USING EQUATIONS (5-48) AND (5-49). HORIZONTAL BAR DENOTES 2 MSECS.

This distribution is described by the histogram shown in Figure 5-18, wherein the horizontal axis indicates the distance away from the axon hillock. It should be noted that the ordinate of the histogram can be interpreted as the fraction of the total number of synaptic knobs, since it is reasonable to assume that statistical variation in the size of synaptic knob is the same for different portions of the neuronal membrane. There is evidence that the excitatory synaptic knobs are more or less uniformly scattered throughout the soma-dendritic complex, and that the inhibitory inputs are more localized in, or near, the soma.<sup>57</sup> Thus, it is plausible that the distribution of excitatory synaptic knobs is adequately represented by Curve A in Figure 5-18. Since there is also evidence that the monosynaptic inputs are widely distributed over the motoneuronal surface,<sup>56,60</sup> therefore it seems not unreasonable to assume that Curve A in Figure 5-18 also describes the distribution of the synapses from the primary spindle afferents.

With the distribution of the monosynaptic knobs thus postulated, we now turn to the problem of representing the statistical variation in the size and the shape of the quantal EPSP's. A quantal EPSP can be adequately described by the function,

$$h(t) = b \left[ e^{-t/T_1} + e^{-t/T_2} \right], \quad t \geq 0, \quad (5-48)$$

where  $b$ ,  $T_1$ , and  $T_2$  are constants dependent on the location of the synapse. For our present purpose, we postulate some empirical relations for  $b$ ,  $T_1$ , and  $T_2$  as functions of the distance  $\xi$  between the synaptic location and the pulse generating site as follows.

$$b = 500 - 0.159 \pi \xi$$

$$T_1 = 1/b \quad \text{and} \quad T_2 = T_1 / 16 \quad (5-49)$$

where  $\xi$  is in microns.

For these relations, the waveform of a quantal EPSP produced by a synaptic input which is located at the pulse generating site is as shown by Curve 1 in Figure 5-19, whereas the waveform of a quantal EPSP due to a synaptic input located at a site 900 microns away is as shown by Curve 3. Furthermore, if the distribution of monosynaptic inputs is assumed to be given by Curve A in Figure 5-18, then the waveform of the sum of all quantal EPSP's is described by Curve 2 in Figure 5-19. Some properties of these responses are given in Table 5-1. The properties of the sum of quantal EPSP's agree closely with the physiological data for an EPSP evoked by a maximal Group Ia volley, while the properties of the quantal EPSP's are similar to those reported in the literature.<sup>58</sup>

TABLE 5-1.      COMPARISON OF EPSP'S .

TYPE	SYNAPTIC LOCATION	TIME TO PEAK (msec)	DECAY TIME CONSTANT (msec)	RELATIVE AMPLITUDE
Quantal EPSP	Pulse generating site	0.37	2.0	1.0
	900 microns away from the pulse generating site	3.7	20.0	0.083
Sum of quantal EPSP's		0.80	4.0	

Therefore, in the present simulation study, we assume that the quantal EPSP's are described by Equations (5-48) and (5-49), and that the distribution of the synaptic inputs is given by Curve A in Figure 5-18.

The statistics for the remaining parameters are neither available nor deducible from the physiological literature at present. Thus, in the present simulation study, we assume that the probability densities for  $c_o$ ,  $e$ ,  $q$  and  $\theta$  are truncated Gaussian densities. The range of values for all system parameters including the input signal, are chosen in such a manner that the following conditions are not violated.

1. The summated generator current  $v_i(t)$ , as given by Equation (5-11), is non-negative for all  $t$  and all  $i$ .
2. The afferent pulse frequencies lie within the range of from 0 to 120 pulses/sec.

### 5.7.2 Results and Discussions

The results of the present computer simulation study can be separated into two groups: The first group shows the effects of variations in each parameter individually while the second group shows the effect of simultaneous variations in two or more parameters. The present investigation is concerned only with the situation in which the change of muscle length is sinusoidal about a suitable mean length. Thus, in all the simulation results that we shall present below, this change of muscle length is given by

$$x(t) = 10 + 5 \cos 25 t . \quad (5-50)$$

Similarly, the threshold "a" of the neural encoder is kept constant at the value, 0.2, for all the cases studied. For convenience of comparison, the sinusoidal component of  $x(t)$  is plotted in each graph of the summated EPSP, with the curves appropriately scaled to give equal range of variation. The curve composed of points designated by the symbol "o" in Figures 5-20 to 5-29 is the sinusoidal component of  $x(t)$ , while the other curve (symbol "x") represents the summated EPSP which is the output of the communication link.

a. Effect of Variation in Each Parameter Individually

In this part of the simulation study, the waveforms of the quantal EPSP's are assumed invariant with respect to path, but their sizes may vary. Thus, the time constants  $T_1$  and  $T_2$  in Equation (5-48) are set at 4.0 and 0.25 msec. respectively, whence the resulting waveform is as shown by Curve 2 in Figure 5-19.

As a reference for the system's performance we first obtain the curve which results when all parameters in the communication link are invariant with respect to path so that all paths are identical. In this case the summated EPSP at the output of the link is as shown in Figure 5-20. Here, the noise power in the output is so great that the signal component is not even discernible. In the following, we shall examine the effect of variation in each parameter individually, with all other parameters held invariant.

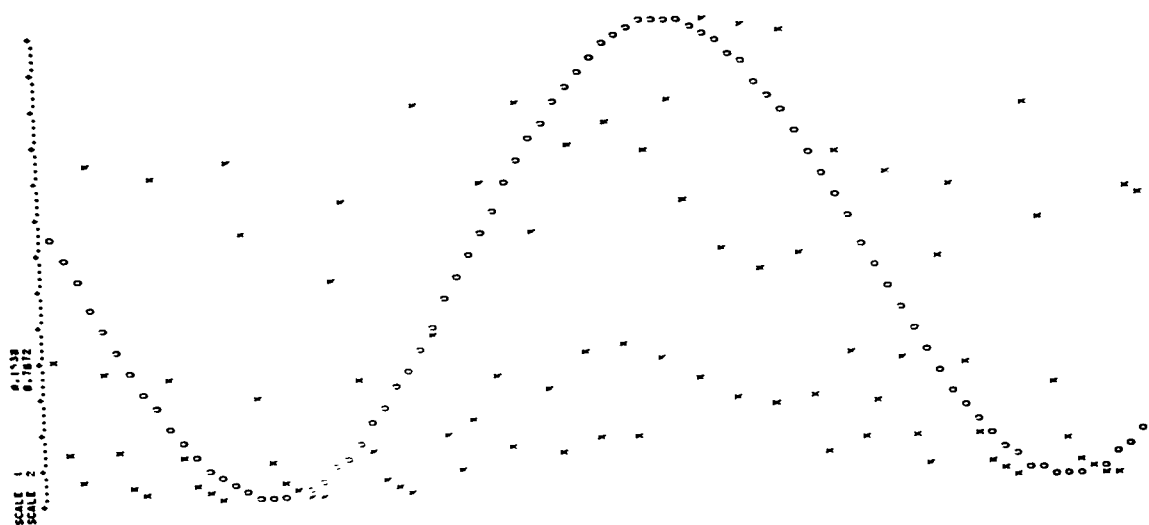


FIGURE 5-20. SUMMATED EPSP WHEN ALL TRANSMISSION PATHS ARE IDENTICAL.

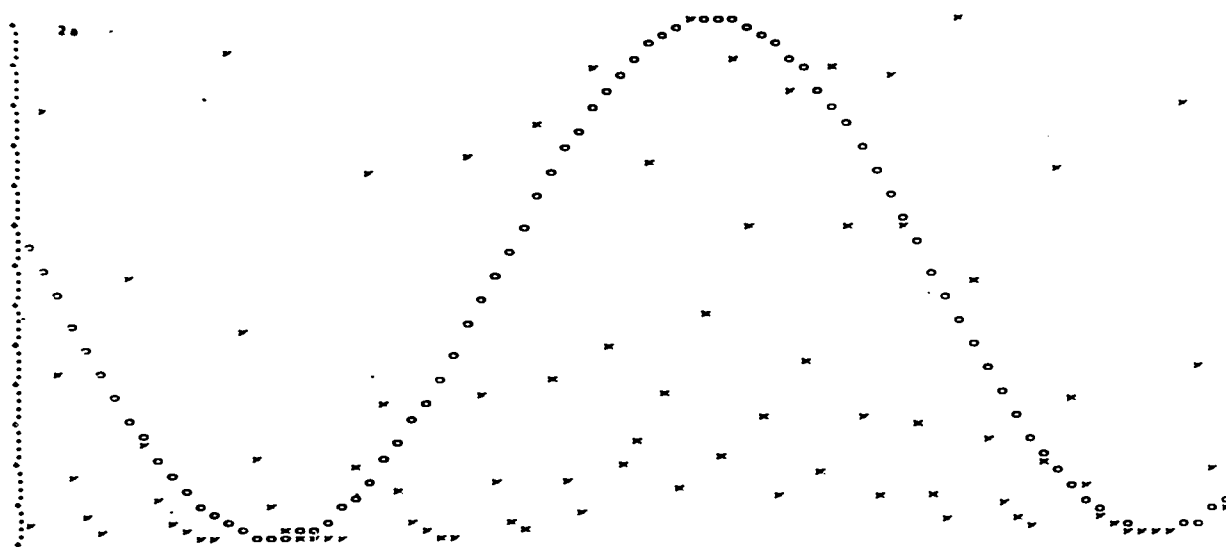


FIGURE 5-21. SUMMATED EPSP WHEN ONLY THE SIZE OF EPSP VARIES.

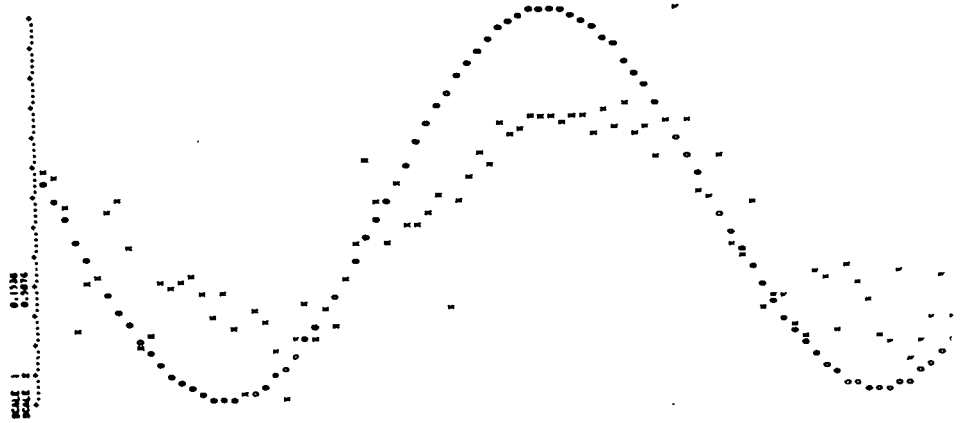


FIGURE 5-22. SUMMATED EPSP WHEN ONLY THE TRANSMISSION TIME,  $\tau$ , VARIES.

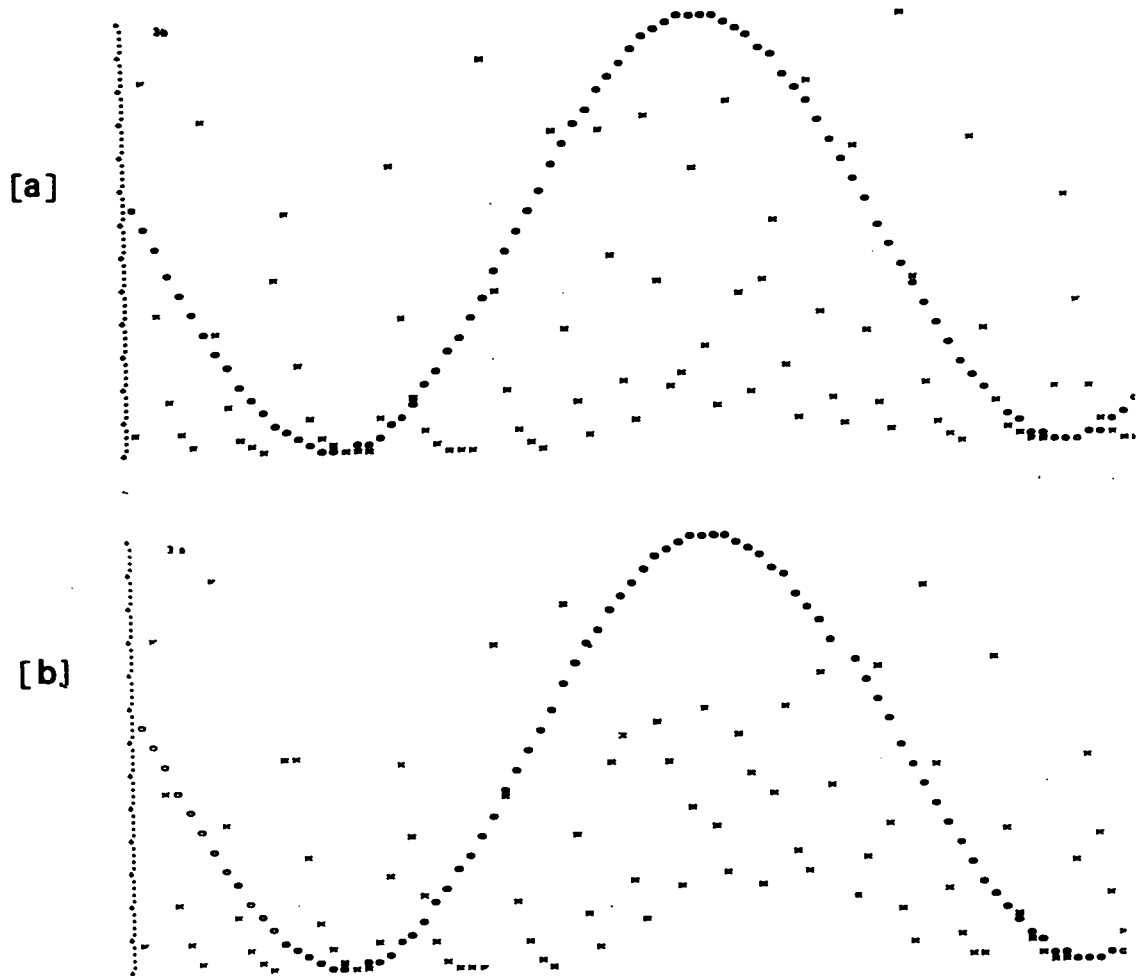


FIGURE 5-23. SUMMATED EPSP WHEN ONLY THE PHASE ANGLE  $\theta$  VARIES.

(i) Variation in the Size of the Quantal EPSP's

The size of a quantal EPSP is represented by the constant  $b$  in Equation (5-48). This constant varies from path to path in the manner described by Equation (5-49). Assuming that the distribution of Group I<sub>a</sub> synaptic inputs on the somadendritic complex of the  $\alpha$ -MN is given by Curve A in Figure 5-18, then the summated EPSP is as shown in Figure 5-21. Comparing this output with that shown in Figure 5-20, we see that variation in the size of the quantal EPSP's alone, has no discernible effect on the noise content of the summated EPSP. This observation agrees with the theoretically predicted result given in Sub-section 5.6.2.

(ii) Variation in the Transmission Time  $\tau$ 

When  $\tau$  alone varies from path to path and the probability density of  $\tau$  is as given in Figure 5-17(b), the summated EPSP is as shown in Figure 5-22. The noise content of this output is significantly less than that for the case of identical transmission paths, (Figure 5-20). In Sub-section 5.6.3, we have shown theoretically that this reduction in noise content is accomplished by the equivalent filter,  $\Phi_{\tau}(-j\omega)$ , which is due to the distribution in  $\tau$ . This conclusion can also be established as follows, by examining the block diagram in Figure 5-16 which has been used to simulate the communication link for the present case.

Let the output of the differentiator in Figure 5-16 be  $v^*(t)$  and let the input of the block PH be  $u(t)$ . Then, the input-output relation for the system of parallel

paths between  $v^*(t)$  and  $u(t)$  is given by

$$u(t) = M \sum_{i=1}^N p_{\tau_i} v^*(t - \tau_i) \quad (5-51)$$

where  $p_{\tau_i} = \frac{m_i}{M}$ . When  $p_{\tau_i}$  is re-defined as given in Figure 5-17 and  $\tau_i = i\Delta$ ,

$$u(t) \approx M \sum_{i=1}^N p_{\tau}(i\Delta) \cdot v^*(t - i\Delta) \cdot \Delta, \quad (5-52)$$

where  $N\Delta = 4.6$  msec. For digital computation, we can set  $t = k\Delta$  without loss of generality. Thus, Equation (5-52) becomes a numerical representation of the input-output relation of a linear system whose unit-impulse response is  $M p_{\tau}(\tau)$ . In other words, the system of parallel paths is a linear digital filter which approximates a linear continuous filter whose system function is

$$M \int_{-\infty}^{\infty} p_{\tau}(\tau) e^{-j\omega\tau} d\tau = M \cdot \Phi_{\tau}(-j\omega). \quad (5-53)$$

On the basis of this observation and of the analytical result derived previously, we now note that the system of different afferent paths, which connect the muscle spindles to the pulse-generating site of the  $\alpha$ -motoneuron, apparently operates in a manner similar to a delay-line synthesizer<sup>86</sup> and a transversal filter.<sup>87</sup>

(iii) Variation in the Phase Angle  $\theta$ 

In simulating the communication link for this case, the probability density of  $\theta$  has been assumed to be a truncated Gaussian density. For the output shown in Figure 5-23(a), the mean,  $\bar{\theta}$ , of  $\theta$  is  $-10^\circ$ , the standard deviation  $\sigma_\theta$  is  $45^\circ$ , and the range of variation is from  $-1^\circ$  to  $-19^\circ$ . For this case of small variation, the noise content in the summated EPSP is essentially as large as that for the case of identical paths. This observation verifies the theoretical prediction given in Sub-section 5.6.3. When  $\bar{\theta}$ ,  $\sigma_\theta$ , and the range of variation are doubled, the resulting output is as shown in Figure 5-23(b). For this case, the noise content is reduced somewhat, but the signal component is still not discernible. From these simulation results and the analytical results obtained previously, we may conclude that the effect of variation in  $\theta$  on the noise content of the summated EPSP is much less than the effect of variation in  $\tau$ .

(iv) Variation in the Static Gain  $c_0$ 

The results, together with the assumed distributions of  $c_0$ , are shown in Figure 5-24. The mean value of  $c_0$  yields a pulse frequency of 60 pulses/sec. or equivalently, about 15 pulses per period of the sinusoidal change in muscle length. The range of variation in  $c_0$  corresponds to the range of pulse frequencies from 10 to 110 pulses/sec. The graphs in Figure 5-24 show that the noise content of the summated EPSP can be significantly reduced by variation in  $c_0$ . This observation agrees with the theoretical result recently reported by Bayly in a study of "neural" pulse frequency

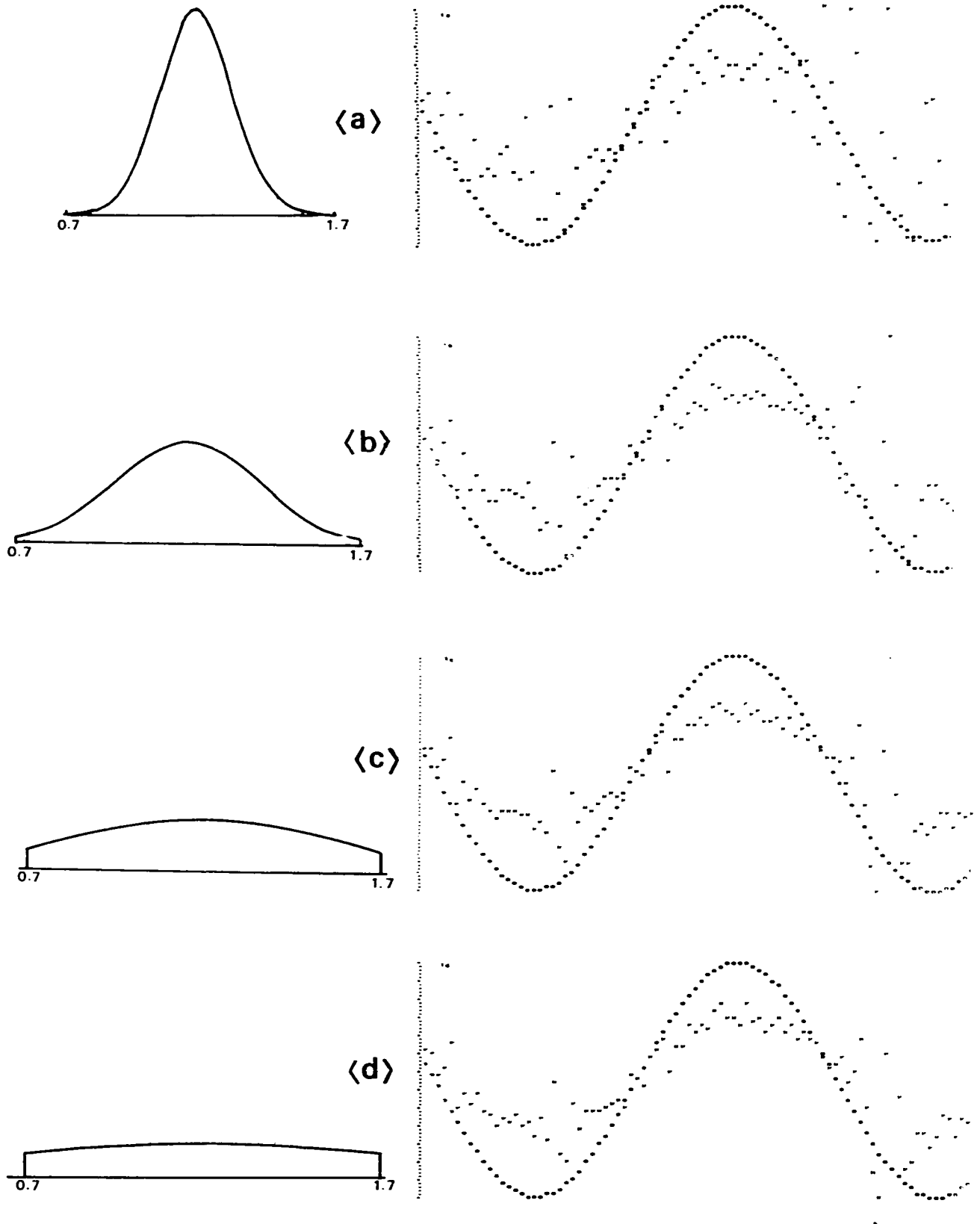


FIGURE 5-24. SUMMATED EPSP WHEN ONLY THE STATIC GAIN  $C_0$  VARIES.

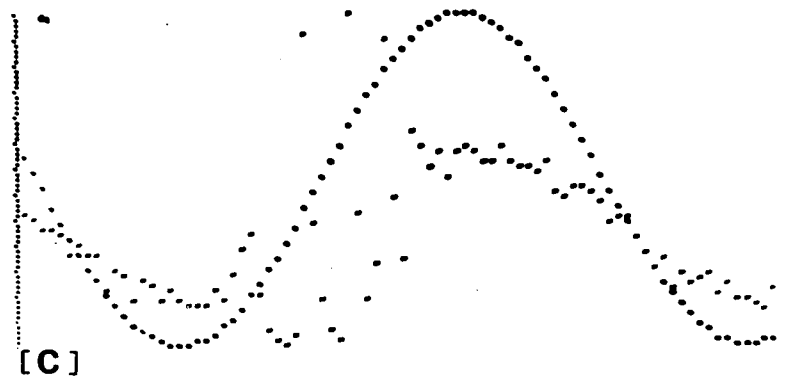
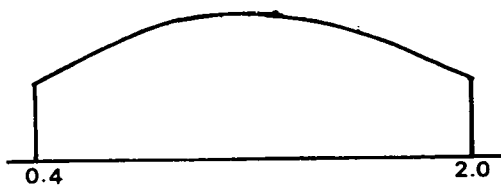
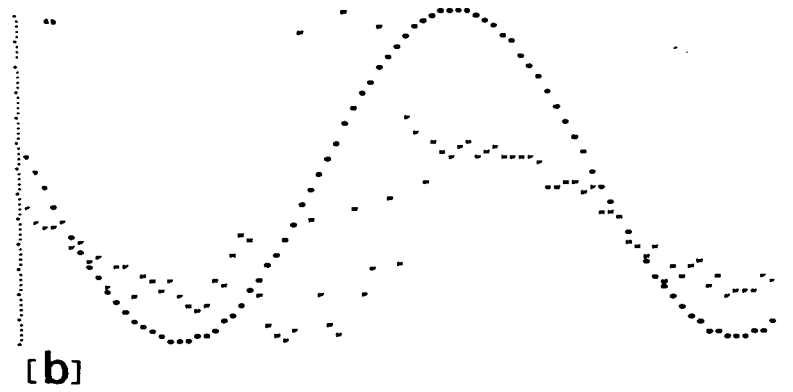
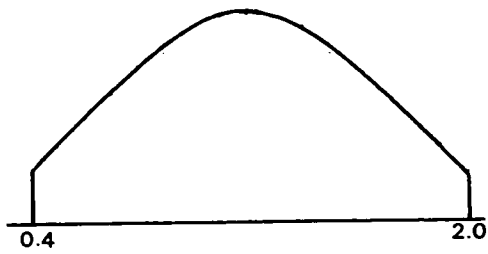
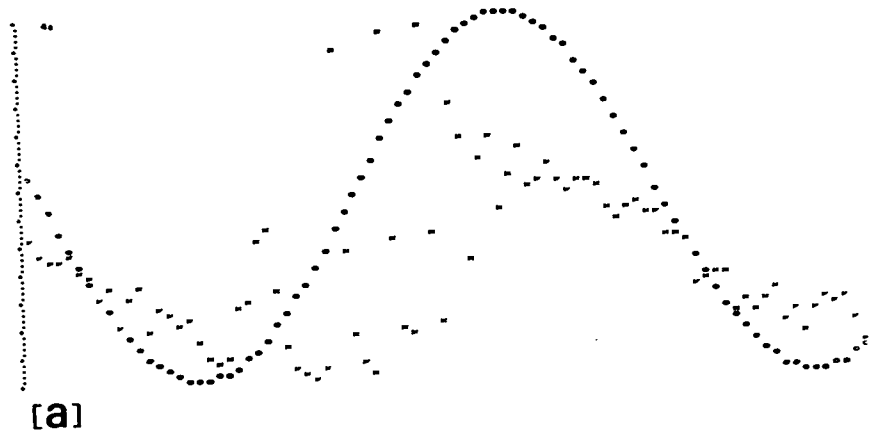
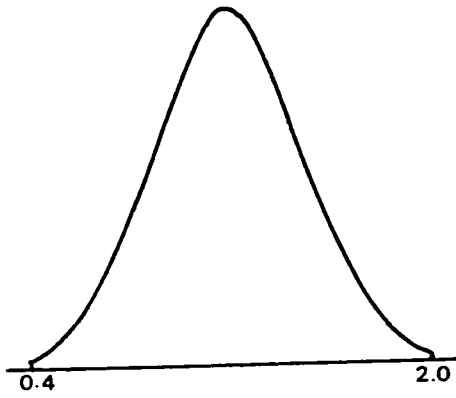


FIGURE 5-25. SUMMATED EPSP WHEN ONLY THE DYNAMIC GAIN C VARIES.

modulation.<sup>26</sup> It is interesting to note that the change in distribution of  $c_o$ , shown in the graphs from (b) to (d), does not significantly affect the noise content of the output.

(v) Variation in the Dynamic Gain,  $c$

When  $c$  alone varies from path to path, the noise content of the summated EPSP is also less than that for the case of identical paths, as shown by the simulation results in Figure 5-25. The distribution of  $c$ , shown beside each graph in the figure, yields a range of pulse frequencies from 0 to 100 pulses/sec. As in the case of variation in  $c_o$ , the change in the distribution of  $c$  apparently has little effect on the noise content of the output.

(vi) Variation in the Constant  $q$

The effect of variation in  $q$  is identical with that due to variation in the static gain  $c_o$ , since both  $q$  and  $c_o$  affect only the constant component of the summated generator current. (See Equation (5-11)). Indeed, if we define  $10 c_o$  as  $q$  in case (iv) presented above, the graphs in Figure 5-24 will illustrate the effect of variation in  $q$ . Thus, we can conclude that variation in  $q$  can also reduce the noise content of the summated EPSP.

In this part of the computer simulation study, we have examined the effect of variation in each random parameter of the communication link. In particular, we have demonstrated that individual variations in  $\tau$ ,  $c_o$ ,  $c$ , and  $q$  can significantly reduce the noise content of the summated EPSP, and that, on the other hand, variations in  $b$  and  $\theta$  have little or no such effect. In the next part, we shall examine the effect of simultaneous-variations in two or more parameters of the communication link.

b. Effect of Simultaneous Variation in the Parameters

As we have noted in Sub-section 5.6.1, the parameters  $c_o$ ,  $c$ , and  $\theta$ , being all dependent on the muscle-and-spindle dynamics, are correlated with one another. Further, we have pointed out there that there is physiological evidence that  $c_o$  and  $c$  are also correlated with the transmission time  $\tau$ . However, in order to facilitate mathematical analysis, we assumed that the parameters were all statistically independent. Now, in this part of the computer simulation study we shall examine whether the noted correlations will significantly affect the conclusions, which we have drawn in the above analysis. We shall study first the case in which  $c_o$ ,  $c$ , and  $\theta$  are correlated, and then the case in which  $c_o$ ,  $c$ , and  $\tau$  are correlated. Finally, in concluding the present simulation study, we shall demonstrate that simultaneous variations in both the size and the shape of the quantal EPSP's has no significant effect on the noise content of the summated EPSP.

(i)  $c_0$ ,  $c$ , and  $\theta$  Deterministically Related

When  $c = 0.9 c_0$  and both of them vary from path to path according to the distribution of  $c_0$  given in Figure 5-24(b), the resulting output of the communication link is as shown in Figure 5-26. If, in addition, we set  $\theta = -0.3 c - 0.1$  which yields a range of variation from  $-16.6^\circ$  to  $-32^\circ$ , then the summated EPSP is as shown in Figure 5-27. Hence we see that the noise content in the output is significantly reduced by variations in the gains  $c_0$  and  $c$  of the muscle-and-spindle dynamics, while additional variation in the phase angle  $\theta$  does not produce any significant further reduction of the noise content. Thus, correlation among these parameters does not affect the conclusions that we have drawn concerning the effect of their variations.

(ii) Simultaneous Variations in  $c_0$ ,  $c$ , and  $\tau$ 

Recently, Carpenter and Hennaman reported that, out of 100 pairs of unselected primary spindle afferents of the cat examined, the unit with lower stretch threshold in 74 pairs had the more slowly conducting axon.<sup>79</sup> This experimental finding indicates that, in our model of communication link, the path with larger transmission time,  $\tau$ , is more likely associated with larger values for the gains  $c_0$  and  $c$ . In other words,  $c_0$  and  $c$  are correlated with  $\tau$  with a positive correlation coefficient. The simulation result for the correlation coefficient,  $r = +0.7$ , is shown in Figure 5-28(a). The summated EPSP's for  $r = 0$  and  $r = -0.7$  are shown in Figure 5-28(b) and (c) respectively. The noise content in the output for these three different cases is

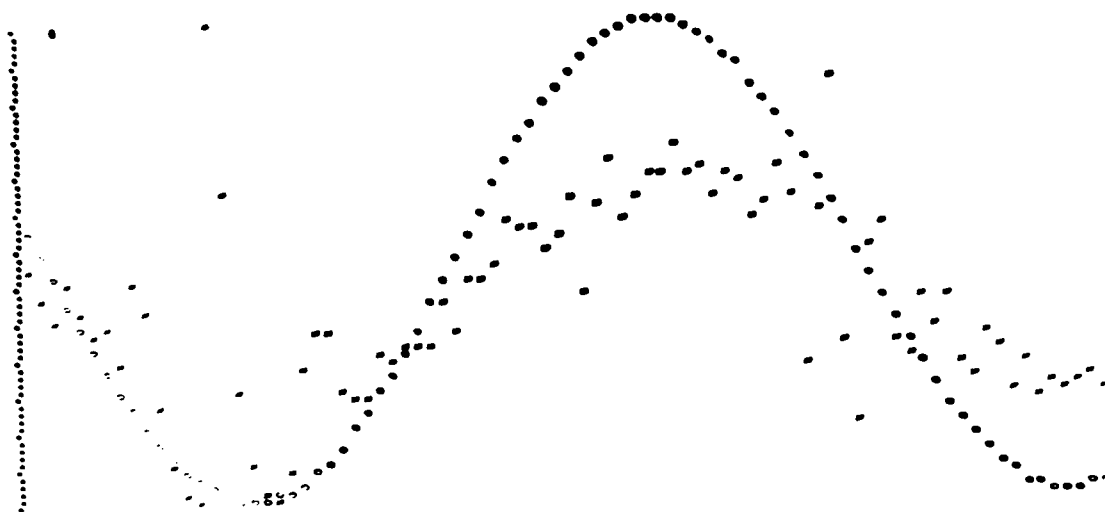


FIGURE 5-26. SUMMATED EPSP WHEN BOTH THE DYNAMIC AND STATIC GAINS VARY SIMULTANEOUSLY.

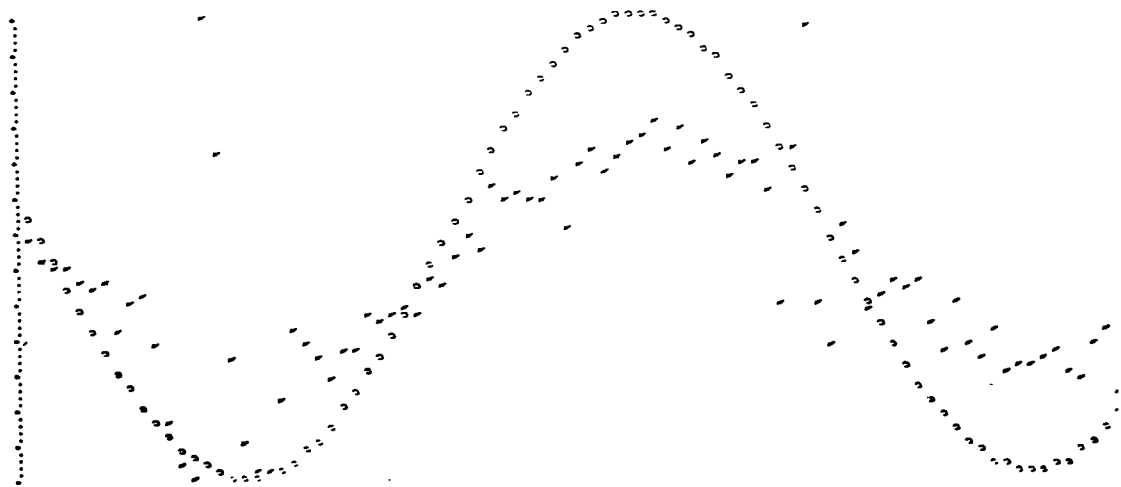


FIGURE 5-27. SUMMATED EPSP WHEN THE GAINS AND THE PHASE ANGLE VARY SIMULTANEOUSLY.

ASSUMED JOINT DISTRIBUTIONS

SUMMATED EPSP

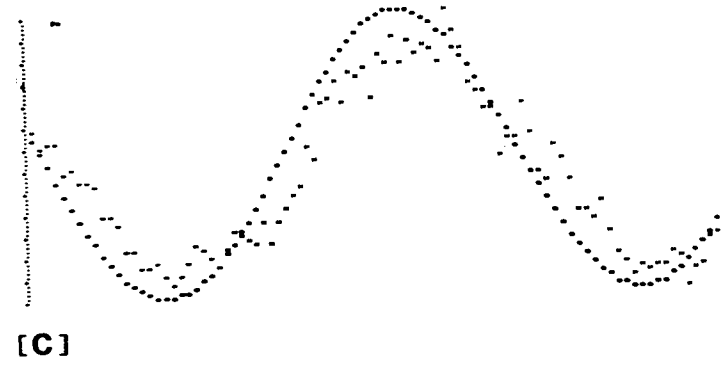
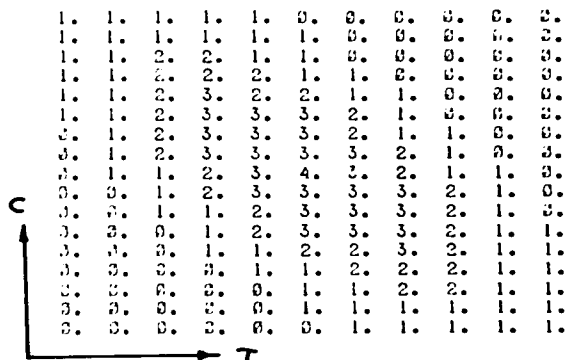
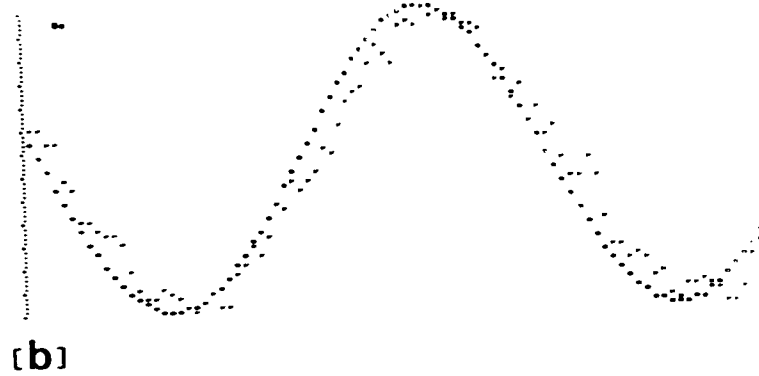
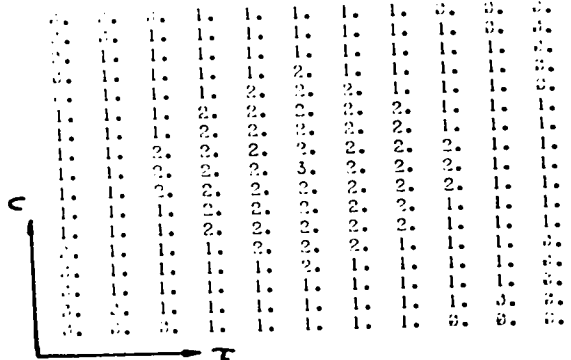
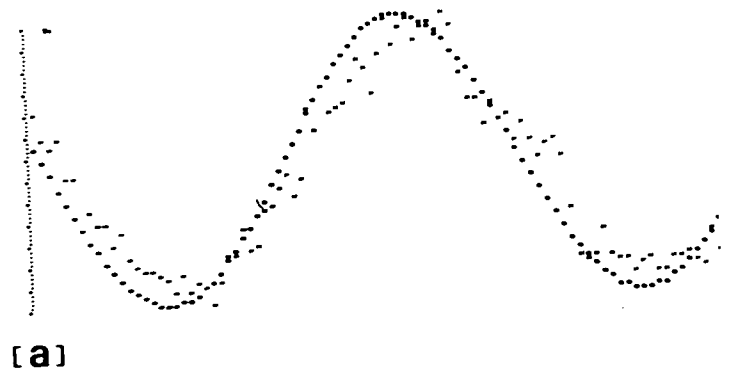
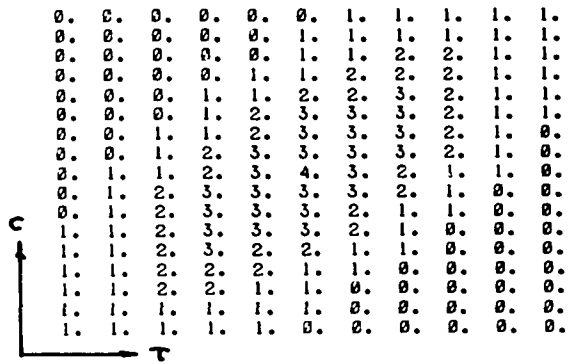


FIGURE 5-28. SUMMATED EPSP WHEN THE GAINS AND THE TRANSMISSION TIME VARY SIMULTANEOUSLY.

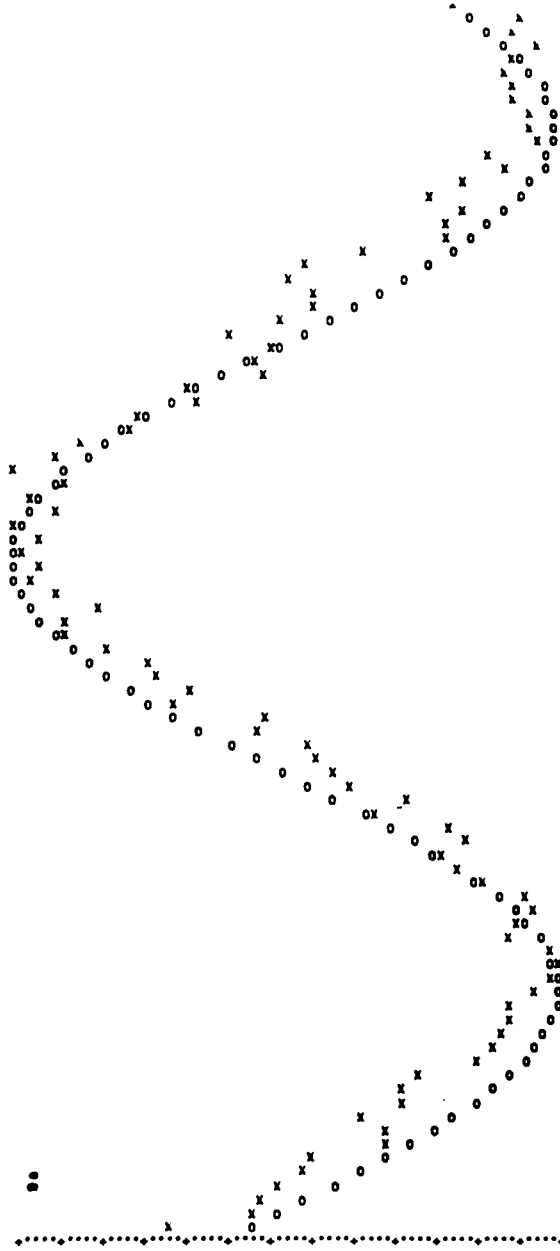


FIGURE 5-29. SUMMATED EPSP WHEN ALL PARAMETERS EXCEPT  $q$  VARY SIMULTANEOUSLY .

very much less than that for the case of identical paths. (Figure 5-20). Further, the results demonstrate that correlation between the transmission time and the gains has little effect on the noise reduction property of the variations in  $c_o$ ,  $c$ , and  $\tau$ .

(iii) Simultaneous Variations in  $c_o$ ,  $c$ ,  $\theta$ ,  $\tau$ , and the Quantal EPSP.

In simulating this more realistic situation,  $c_o$ ,  $c$ , and  $\theta$  are assumed to vary from path to path as described in (i) above, while  $\tau$  and the gains,  $c_o$ , and  $c$ , are assumed correlated with a correlation coefficient of 0.7 as illustrated in Figure 5-28(a). Further, the size and the shape of the quantal EPSP are assumed to vary in the manner described by Equations (5-48) and (5-49), and by Curve A in Figure 5-18 which describes the distribution of synaptic inputs. The parameter  $q$  is set equal to zero since its effect is similar to that of  $c_o$ . The summated EPSP for this more realistic representation of the communication link is shown in Figure 5-29. Comparing this output with that shown in Figure 5-28(a), we see that the noise content in this output is of essentially the same magnitude as the noise content for the case in which all quantal EPSP's are assumed identical. Thus, the variations in the size and the shape of the quantal EPSP do not introduce any noticeable additional reduction in the noise content of the output. This result confirms our conclusion in Sub-section 5.6.4.

In the present computer simulation study, we have verified the theoretical predictions given in Section 5.6. In particular, we have confirmed that the distribution

in the transmission time  $\tau$ , plus the summation of pulse trains in the  $\alpha$ -MN, constitute a filter whose low-pass characteristic is essential for accurate demodulation. Further, we have shown that the noise content of the spatially and temporally summated EPSP can be significantly reduced by variations in the gains,  $c_o$  and  $c$ , of the muscle-and-spindle dynamics, or by variation in the constant,  $q$ , which represents constant  $\gamma$ -efferent activity. The combined effect of variations in  $c_o$ ,  $c$ , and  $\tau$  produces a summated EPSP which is an excellent representation of the change in muscle length.

## 5.8 Discussion and Conclusions

In the present chapter, we have investigated, analytically and by computer simulation, the transmission of a sinusoidal signal from the muscle to a single  $\alpha$ -motoneuron ( $\alpha$ -MN) in the monosynaptic spinal reflex (MSR). The transmission system examined consists of many sensory units and paths whose properties vary from one path to another. In modelling the system, we have made the following major assumptions:

- (a) The summated generator current in the primary nerve endings is a precursor to neural pulse generation, and is linearly related to sinusoidal change in muscle length, within the normal physiological range.
- (b) The neural encoding mechanism in the primary afferent of the muscle spindle is adequately represented by single-signed integral pulse frequency modulation (S-S IPFM).

- (c) The quantal excitatory postsynaptic potentials (EPSP's) summate linearly at the pulse generating site of the motoneuron (MN).
- (d) The "spatially and temporally" summated EPSP carries the intended information for the MN.

Assumptions (a) and (d) are based on known physiological evidence<sup>71,72,53</sup> while assumptions (b) and (c) are simplifications made mainly to ensure a sufficiently tractable mathematical formulation that analytical results may be obtained. In any case, we believe that the model based on these assumptions retains the main features of the physiological system and thus is a reasonably good representation of the real situation. In particular, as we have shown in Section 5.4, the present S-S IPFM model and the actual neural encoding mechanism of the spindle have many similar properties. Further, assumption (c) agrees quite closely with known physiological data: There is evidence that under certain relatively general situations, quantal EPSP's arising from different synaptic inputs summate linearly in the soma of the  $\alpha$ -MN.<sup>58,60</sup>

In Sections 5.6 and 5.7, we have successfully analysed the multi-unit multipath model of the muscle-to-motoneuron communication link, and obtained a number of results concerning the functional significance of the variations in the properties of the transmission paths. In particular, we have shown that variation in the gain of the muscle-and-spindle dynamics tends to reduce the noise content in the output of the system. This result indicates that variation in the stretch threshold of the spindles in

the muscle can improve the signal-to-noise ratio of the "spatially and temporally" summated EPSP at the  $\alpha$ -MN. In addition, we have also shown that the distribution in the transmission time  $\tau$ , plus subsequent summation of the afferent pulse trains in the  $\alpha$ -MN, together constitute a filter whose impulse response is the probability density of  $\tau$ . This latter result agrees with the result recently reported by Williams in his theoretical study of peripheral nerve bundles.<sup>85</sup> The low-pass characteristic of this filter provides the essential filtering characteristic needed for accurate demodulation. The general picture which emerges from the results of the present study is that the combined effect of variations in  $\tau$  and in the gain of the muscle-and-spindle dynamics provides the essential mechanism to achieve fidelity of signal transmission from the muscle to the  $\alpha$ -MN. Recently, Poppele and Terzuolo<sup>53</sup> reported that the changes in the summated EPSP in the MN, evoked by sinusoidal stretches applied to the homonymous muscle, followed the sinusoidal input more closely than did signals derived from individual afferent pulse trains by low-pass filtering. This experimental observation can be explained satisfactorily on the basis of neural filtering which we have just described.

The present analysis has been entirely concerned with the transmission of one sinusoid through the multi-unit multipath system. However, while the results are strictly applicable only to this particular class of signals, they may be used as an indication of the transmission properties for signals of more general nature. In any case, the method presented above may be directly extended to analyze the transmission of a signal comprising a number of sinusoids of different frequencies which may approximate arbitrary input waveforms. A mathematical expression for a single sequence of superposed quantal EPSP's can be readily obtained using the results that we have derived in Section 3.2.3.

Then, the expression for the "spatially and temporally" summated EPSP can be derived and analysed using the approach developed in Section 5.6.

The analysis presented in this chapter can also be extended to investigate the transmission of signals from the  $\gamma$ -efferents to the  $\alpha$ -motoneuron ( $\alpha$ -MN). Recently, Andersson, et.al. have reported that the transfer characteristics between  $\gamma$ -efferent pulse frequency and the spindle afferent pulse frequency is linear, provided the  $\gamma$ -efferent pulse frequencies lie within a certain range, and provided the muscle length is kept constant.<sup>77</sup> In their experiment, single  $\gamma$ -efferent fibers are stimulated by an electrical pulse train from a pulse-frequency modulator which is essentially a single-signed integral pulse frequency (S-S IPF) modulator. Thus, if we stimulate the whole efferent nerve leading to the muscle by a pulse train from a S-S IPF modulator, and selectively block the  $\alpha$ -fibers by compression<sup>84</sup>, while the muscle length is simultaneously kept constant, then the population of spindles in the muscle will have only one time-varying common input, namely, the  $\gamma$ -efferent pulse train. Because the degree of  $\gamma$ -efferent innervation varies from spindle to spindle<sup>50</sup> and because spindle dynamics may also vary from one spindle to another, the dynamics relating the  $\gamma$ -efferent input to the summated generator current in the primary nerve endings are expected to vary from one path of information transmission to another. Hence, the signal transmission system in this case can be represented by a model similar to that shown in Figure 5-8, and consequently, this system can also be analysed using the method developed in Section 5.6.

In the present work, we have only considered the transmission of information from the muscle to a single  $\alpha$ -motoneuron. However, as noted in Section 5.3,

the afferent limb of the MSR consists of a number of these communication links. Thus, in the homonymous  $\alpha$ -motoneuron pool, each MN receives similar information in the manner described in this analysis. Now if we treat all the  $\alpha$ -MN of the pool, in the same way as we have treated the spindles in the muscle, it may be feasible to extend the present analysis to include signal transmission in the efferent limb of the MSR. However, this extension could prove to be mathematically intractable because of the interaction among MN's provided by the feedback paths of the Renshaw cells, with their largely unknown synaptic connections.

In conclusion the present analysis demonstrates that the multi-unit multipath characteristic is essential for fidelity of transmission of information in the afferent limb of the monosynaptic spinal reflex. The method of analysis developed here can be applied to study other multi-unit multipath systems in the monosynaptic spinal reflex. In particular the following conclusions can be drawn :

1. The dispersion in conduction speeds of afferent nerve fibers, plus the summation of afferent pulse trains in the neuron, together constitute an effective low-pass filter which significantly reduces the noise content that would otherwise appear in the summated EPSP ;
2. The dispersion in spindle stretch thresholds also reduces the noise content of the summated EPSP;

3. Variation in postsynaptic membrane characteristics, such as time constants, has comparatively little effect on the signal-to-noise ratio of the summated EPSP.

## CHAPTER VI

### CONCLUSION

#### 6.1 Summary of Results

The present work is concerned with the theory and applications of integral pulse frequency modulation (IPFM). It comprises essentially three parts: The first part deals mainly with the spectral analysis of IPFM, while the second part is concerned with the application to analogue computation. In the third part, single-signed integral pulse frequency modulation (S-S IPFM) is utilized as a model of the neural encoding mechanism for investigating the multi-unit multipath characteristic of neural communication.

The preliminary results of the first part are presented in Chapter II, wherein some of the fundamentals of IPFM are reviewed and re-examined. In particular, S-S IPFM is shown to be equivalent to a well-known method of pulse modulation, which has been generally referred to in the literature as pulse frequency modulation, but has been called continuous pulse frequency modulation (CPFM) in the present work in order to differentiate it from the larger overall class of modulation methods which includes CPM. This equivalence of S-S IPFM and CPM, apparently not established before, effectively broadens the knowledge of IPFM in the sense that what is known about CPM is applicable to S-S IPFM, and vice versa. Another interesting result of the preliminary study is that IPFM can be implemented exactly by means of a feedback system which operates in many ways similar to the neural pulse generating mechanism. Finally, demodulation of IPFM using analogue and digital filters is discussed and is shown to be a summation of pulses in the time domain.

The main results of the first part are presented in Chapter III. Here, a general method for the spectral analysis of S-S IPFM is developed. In this method, the modulating signal is incorporated into a function  $e_k(t)$  which represents a frequency-modulated sinusoidal carrier. A spectral representation of the output pulse train can be readily derived by using this method, provided that the function  $e_k(t)$  can be expressed in terms of its spectral components. The spectral characteristics of the pulse train have been examined in detail for a class of modulating signals comprising one or more sinusoids. The output of the modulator contains a signal component and a noise component, where the latter is produced in the modulating process. The signal component is linearly proportional to the modulating signal as modified by the filtering effect associated with the pulse shape, while the noise component has an amplitude spectrum of theoretically infinite bandwidth, which always overlaps the spectrum of the signal component. However, the significant bandwidth of the noise component is finite and can be shifted outside the signal band by proper choice of the modulator threshold  $a$  and of the biasing constant  $X_0$  in the modulating signal. Based on this result, criteria for selecting these parameters have been derived. These criteria can be expressed in terms of the number of pulses per period of the highest significant frequency in the message signal.

In concluding the first part of the present study, we represent double-signed integral pulse frequency modulation (D-S IPFM) approximately by a simplified model, and then perform a spectral analysis using the method developed for S-S IPFM. The spectral characteristics of a pulse train produced by single-tone modulation is examined in detail. As in S-S IPFM, the output pulse train contains a noise component and a signal component, of which the latter is proportional to the modulating signal.

However, the noise component produced by the present modulation comprises spectral frequencies which are the fundamental and higher harmonics of the modulating signal frequency. Its amplitude spectrum is bounded by a curve which is proportional to the amplitude characteristic of the pulse-shaping element  $P(s)$  in cascade with a differentiator. By using this result, a criterion is derived for selecting the modulator threshold so that the demodulated signal has a signal-to-noise ratio greater than a pre-specified bound.

The second part of the present study is concerned with the application of IPFM to analogue computation. The results are presented in Chapter IV. A method for implementing multipliers using  $S - S$  IPFM is formulated and studied. In addition, the method of pulse frequency modulation originally proposed by Goldberg can be closely represented in terms of  $S - S$  IPFM. An upper bound for the error introduced by the representation is derived. Finally, Goldberg's method of pulse frequency modulation is used to implement analogue dividers.

In the third and last part,  $S - S$  IPFM is used to investigate the functional significance of the multiplicity of sensory units and neural paths employed in peripheral neural communication in physiological systems. In particular, the signal transmission in the afferent limb of the monosynaptic spinal reflex (MSR) of the neuro-muscular system has been examined for the present purpose in Chapter V.

The afferent limb of the MSR is shown to comprise a set of similar communications links in parallel between the muscle and the homonymous motoneuronal pool. Each link connecting the muscle and a single  $\alpha$ -motoneuron consists of numerous

paths whose transmission properties vary with respect to path. The typical link is represented by a multi-unit multipath model which takes into consideration, particularly, the distribution of spindle stretch thresholds, the dispersion of conduction speeds in the afferents, and the effect of spatial distribution of synaptic inputs.

The neural encoding mechanism in the primary afferent endings is represented by a single-signed integral pulse frequency modulator. Indeed, the neural encoder and the modulator are shown to have many similar functional properties. The remaining components in the neural communication system are then modelled so that the main functional features of the biological system are retained.

The transmission of a sinusoidal signal from the muscle to one homonymous motoneuron through the typical communication link is investigated analytically and by computer simulation. A number of results concerning the functional significance of multi-unit multipath characteristic is obtained. In particular, the variation in the spindle thresholds can reduce the noise content of the "spatially and temporally" summated excitatory postsynaptic potential (EPSP), where this noise has been introduced into the afferent pulse trains by the sensory encoding process. Further, the distribution in transmission time of afferent paths, plus subsequent summation of the afferent pulse trains in the  $\alpha$ -motoneuron, together constitute an effective low-pass filter whose frequency characteristics are essential for accurate demodulation. The system function of this equivalent filter is the characteristic function of the probability density of the transmission time; or equivalently, its impulse response is the distribution of the number of afferent paths with respect to the transmission time. The general picture which emerges from the results of the present study is that the combined effect of variations in these

properties of the large number of paths provides the essential mechanism to achieve fidelity of signal transmission in the sinusoidal steady-state from the muscle to the motoneuron.

Finally, the spatial distribution of synaptic inputs is shown to have little effect on the noise content of the summated EPSP. The noise reduction effect is also negligible for variation in the characteristics of the sub-threshold neuronal membrane, such as time constants.

## 6.2 Areas for Further Research

As a result of the present work, several areas are seen to need further research. These are now briefly described and discussed:

### 1. Analysis of IPFM with Random Modulating Signals

In the present study, we have derived a number of useful results from the spectral analysis of IPFM with message signals comprising one or more sinusoids. However, in reality, information-carrying signals are random. Thus, it is desirable to determine the information transfer characteristics of IPFM for random modulating signals. With the modulators represented by the models utilized in the present work, the statistical theory of amplitude quantization can be profitably employed for this purpose.<sup>88,89</sup>

## 2. Spectral Analysis of a Generalization of S-S IPFM

In Section 5.4, we have noted that the neural encoding mechanism can be more realistically represented by replacing the integrator with a "leaky integrator" in the feedback implementation of S-S IPFM (Figure 2-6). The resulting system can be represented by a feedback system which contains the model of D-S IPF modulator given in Figure 2-2<sup>9</sup>. It appears feasible to develop a method of spectral analysis for this type of modulation by using the approximate model for the D-S IPF modulator. The method can then be profitably applied to theoretical studies of neural communication.

## 3. Evaluation of the Performance of Prototype Multipliers and Dividers

In the present work, we have formulated methods for implementing analogue multipliers and dividers using pulse frequency modulation; however, the performance of these devices has not been evaluated in comparison with the commonly available multipliers and dividers. The multiplier using IPFM appears to have all the advantages possessed by the time-division multiplier. Further, since the self-excited time-division multiplier utilizes both pulse-width and pulse-frequency modulations, whereas the multiplier using IPFM uses only pulses of fixed width, the latter may be more versatile and more accurate. Hence, it would be of interest to compare their performance by constructing prototype devices.

#### 4. Extension of the Analysis on Neural Communication

As noted in Section 5.8, the method of statistical analysis of neural communication developed in Section 5.6 can be extended to include a more general input signal. Since the transfer dynamics from  $\gamma$ -efferent pulse trains to the spindle afferent signal have been shown to be linear,<sup>77</sup> it would be interesting to investigate the transmission of a general signal from the  $\gamma$ -efferents to the  $\alpha$ -motoneuron. In addition to this, it is desirable to extend the analysis to include signal transmission in the efferent limb of the monosynaptic spinal reflex. Recently, Poppele and Terzuolo have reported an experimental finding that the averaged electromyogram produced in a muscle by a motoneuron population is sinusoidal for sinusoidal input amplitudes greatly exceeding the limits at which linear behaviour ceases for primary endings and single motoneurons.<sup>53</sup> This physiological observation can probably be satisfactorily explained in terms of neural filtering.

#### 5. Experimental Verification of the Theoretical Results on Neural Communication

We have noted in Section 5.8 that the theory developed in Chapter 5 can satisfactorily explain the experimental observation that the summated EPSP in the motoneuron, evoked by sinusoidal stretches applied to the homonymous muscle, follows the sinusoidal input more closely than do signals derived from individual afferent pulse trains by low-pass filtering.<sup>53</sup> This experimental observation implicitly confirms the theory.

However, it is desirable that this theory be verified by further physiological experiments specially designed to test the significance of the multi-unit multipath characteristic of neural communication.

APPENDIX A

AN ALTERNATIVE DERIVATION OF A MATHEMATICAL EXPRESSION  
OF THE OUTPUT IMPULSE TRAIN FOR SINGLE-SIGNED  
INTEGRAL PULSE FREQUENCY MODULATION (S - S IPFM)

Equation (3-7) is a mathematical expression of the output impulse train for S - S IPFM. However, in order to provide some physical insight, we derive this expression again using a more heuristic approach. Let the output pulses of the modulator in Figure 3-1 be rectangular with height  $hd$  and width  $\tau$ . Since  $v(t)$  consists of impulses of strength  $d$ , for this waveform of the output pulse, we must have

$$P(s) = h \cdot \frac{1 - e^{-\tau s}}{s} \quad (A-1)$$

Lumping the differentiator and  $P(s)$  together we obtain

$$sP(s) = h(1 - e^{-\tau s}) \quad (A-2)$$

Based on this result, we can represent the modulator as shown in Figure A-1. According to this representation, the staircase function  $p_2(t)$  at the output of the quantizer is delayed by a time  $\tau$  and then is subtracted from the same but undelayed signal to produce the rectangular output pulses as illustrated in Figure A-2. Thus, the output of the modulator is

$$x^*(t) = [p_2(t) - p_2(t - \tau)] h \quad (A-3)$$

Now, substituting Equation (3-5) into Equation (3-2), we have

$$p_2(t) = \frac{d}{a} \left[ z(t) - \frac{a}{2} + \sum_{k=1}^{\infty} \frac{2}{k\omega_0} \sin k\omega_0 z(t) \right]. \quad (\text{A-4})$$

Since convergent series can be subtracted term by term,<sup>40</sup> we may substitute this equation into Equation (A-3) and then simplify to obtain

$$x^*(t) = \frac{hd\tau}{a} \left[ \frac{z(t) - z(t-\tau)}{\tau} + \sum_{k=1}^{\infty} \frac{2}{k\omega_0} \frac{\sin k\omega_0 z(t) - \sin k\omega_0 z(t-\tau)}{\tau} \right]. \quad (\text{A-5})$$

Now let  $\tau$  approach zero while keeping  $h\tau = 1$ . Then, in the limit, the output pulses become impulses of magnitude "d", and in addition, using the definition of the derivative we have

$$\begin{aligned} x^*(t) &= \frac{d}{a} \left[ \frac{dz}{dt} + \sum_{k=1}^{\infty} \frac{2}{k\omega_0} \frac{d}{dt} \sin k\omega_0 z(t) \right] \\ &= \frac{d}{a} \left[ \dot{x}(t) + \sum_{k=1}^{\infty} \frac{2}{k\omega_0} \frac{d}{dt} \sin k\omega_0 z(t) \right]. \end{aligned} \quad (\text{A-6})$$

This expression represents the modulator output when  $P(s) = 1$ , since Equation (A-1) can be re-written as

$$P(s) = \frac{h}{s} \left[ s\tau - \frac{(s\tau)^2}{2!} + \frac{(s\tau)^3}{3!} - \dots \right] \quad (\text{A-7})$$

which approaches one as  $\tau$  approaches zero while keeping  $h\tau = 1$ . Therefore, it also represents the impulse train  $v(t)$ . Clearly, with  $x^*(t) = v(t)$  in Equation (A-6) it is identical with Equation (3-7).

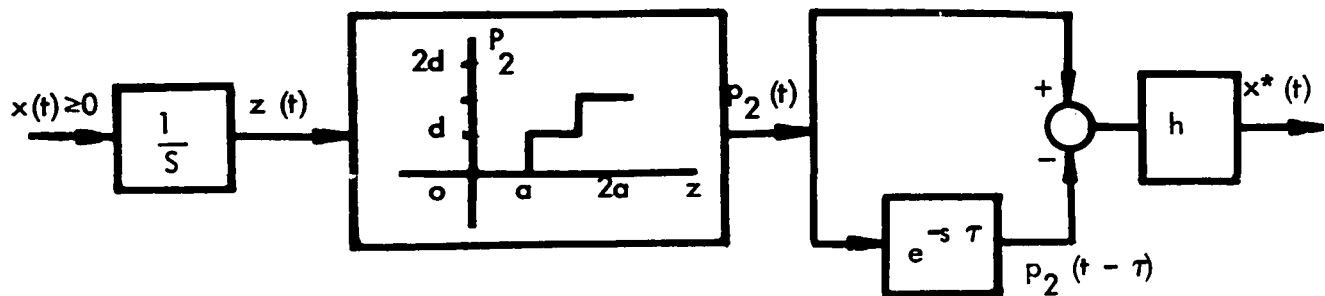


FIGURE A-1. S - S IPFM WITH RECTANGULAR OUTPUT PULSES.

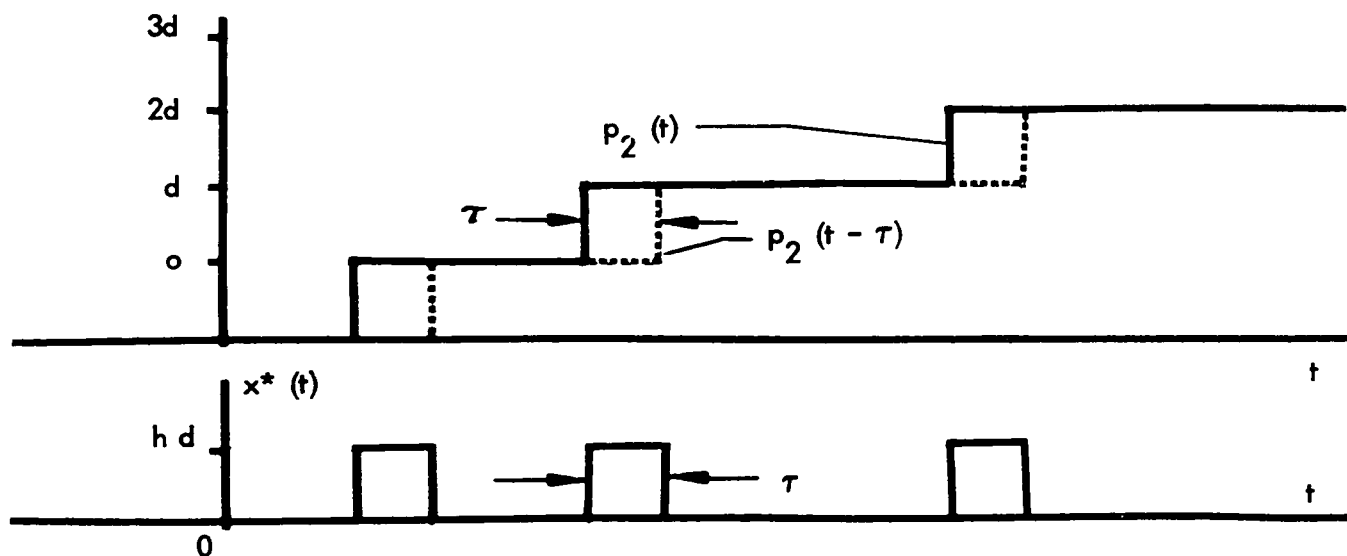


FIGURE A-2. ILLUSTRATING THE GENERATION OF A S-S IPF PULSE TRAIN .

## APPENDIX B

### DERIVATION OF A MODEL FOR THE NEURAL ENCODER FROM A PARTICULAR NEURON MODEL

Recently a mathematical model of the neuron has been developed by Roberge for the study of small neuron networks.<sup>67</sup> This functional model represents realistically many essential features of the spike-initiation and synaptic loci of the neuron. In a simplified version, these two loci are lumped together to yield a simpler model which incorporates essentially the spike-initiation locus and the subthreshold properties of the synaptic locus. The block diagram of this simpler model is shown in Figure B1. In this diagram,  $G_1(s)$  describes the subthreshold current-voltage characteristics of the synaptic locus, with its input coming from the summing point in the forward path which represents the additive property known as temporal summation. The inputs to this summing point represent ionic currents, while the output of  $G_1(s)$  represents the transmembrane potential of the synaptic locus. The subsystem in the feedback path, comprising  $G_2$ ,  $G_3$  and the threshold device, corresponds to the lumped pulse-generating mechanism of both loci, and incorporates into the model both absolute and relative refractoriness in addition to a fixed threshold. When the output of  $G_1(s)$  is sufficiently large to activate the threshold device in the subsystem, a pulse is generated and fed back positively to the input of  $G_1(s)$ . This pulse, after passing through  $G_1(s)$ , becomes a replica of the neural action potential. In analogy to the neuronal mechanism, the feedback pulse corresponds to the transmembrane ionic current at the synaptic locus during the action potential.

In Section 5.4, we have defined that the neural encoder is the mechanism which converts the summated generator current into an afferent pulse train. The neuron

model described above also converts current into a neural pulse train. Since it is reasonable to assume that the general characteristics of the nerve membrane are invariant for different types of neurons, the neuron model so described can very well be considered as a model for the neural encoder. In the following, we shall show that this neuron model is indeed equivalent to a simple generalization of a single-signed integral pulse frequency (S-S IPF) modulator.

The block diagram of the neuron model (Figure B1) can be re-drawn as shown in Figure B2(b) through the intermediate step shown in Figure B2(a). The transfer function  $G_4(s)$  in Figure B2(b) is given by

$$G_4(s) = \frac{G_3(s)}{G_1(s) G_2(s)} - 1$$

$$= 0.458 + \frac{1650(1 + 5.32 \times 10^{-3} s)(1 + 23.4 \times 10^{-3} s)}{s(1 + 50 \times 10^{-3} s)(1 + 1.2 \times 10^{-3} s)} \quad (B-1)$$

The frequency characteristics of the second term of  $G_4(s)$  is shown in Figure B3. Since most of the frequency components of the action potential are greater than 250 rads./sec (see Reference 67 Appendix 5), we have, as indicated in Figure B3,

$$G_4(s) \approx 0.458 + \frac{4.14}{1 + 1.2 \times 10^{-3} s} = \frac{4.6(1 + 0.12 \times 10^{-3} s)}{1 + 1.2 \times 10^{-3} s} \quad (B-2)$$

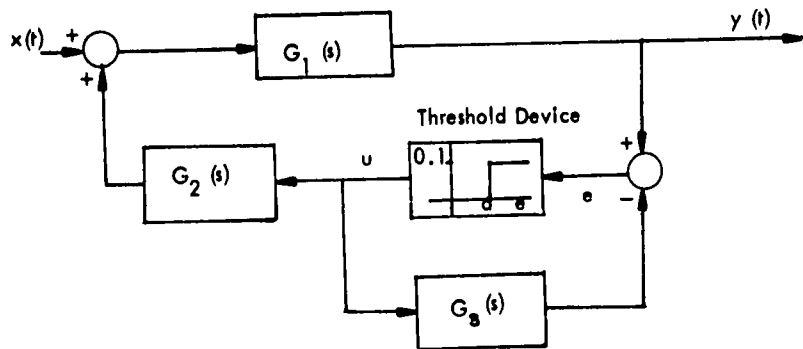
The block diagram of Figure B2(b) shows that the action potential  $y(t)$  at the neuronal pulse generating site is the superposition of the subthreshold response of

the membrane and the propagated pulse itself. Since the output of the neural encoder is the afferent pulse train, the subthreshold response at the output of this model carries no information and thus can be neglected. Hence, the model of our neural encoder can be simplified, by eliminating the forward path containing  $G_1(s)$  alone, to that shown in Figure B4, wherein  $x(t)$  represents the ionic current due to distortion of the afferent nerve endings, while  $x^*(t)$  represents the afferent pulse time.

The model shown in Figure B4 is a simple generalization of the S-S IPF modulator given in Figures 2.6 and 5.4(a). In Figure B4, the signal fed back to the input is a pulse whose Laplace transform is

$$\frac{G_2(s) G_4(s)}{s} [1 - e^{-s\tau}],$$

where  $\tau$  is the time interval in which the threshold device remains activated. Thus, if the block  $G_1(s)$  is replaced by an integrator, the resulting system will be a S-S IPF modulator. In other words, the model given in Figure B4 is a simple generalization of a S-S IPF modulator, and conversely, the S-S IPF modulator is an idealization of a realistic model of the neural encoder.



$$G_1(s) = \frac{5.5(1 + 0.05s)}{(1 + 0.0225s)(1 + 0.0073s)}$$

$$G_2(s) = \frac{0.033s}{1 + 0.00033s}$$

$$G_3(s) = \frac{300}{1 + 0.0012s}$$

FIGURE B-1. BLOCK DIAGRAM OF A NEURON MODEL.

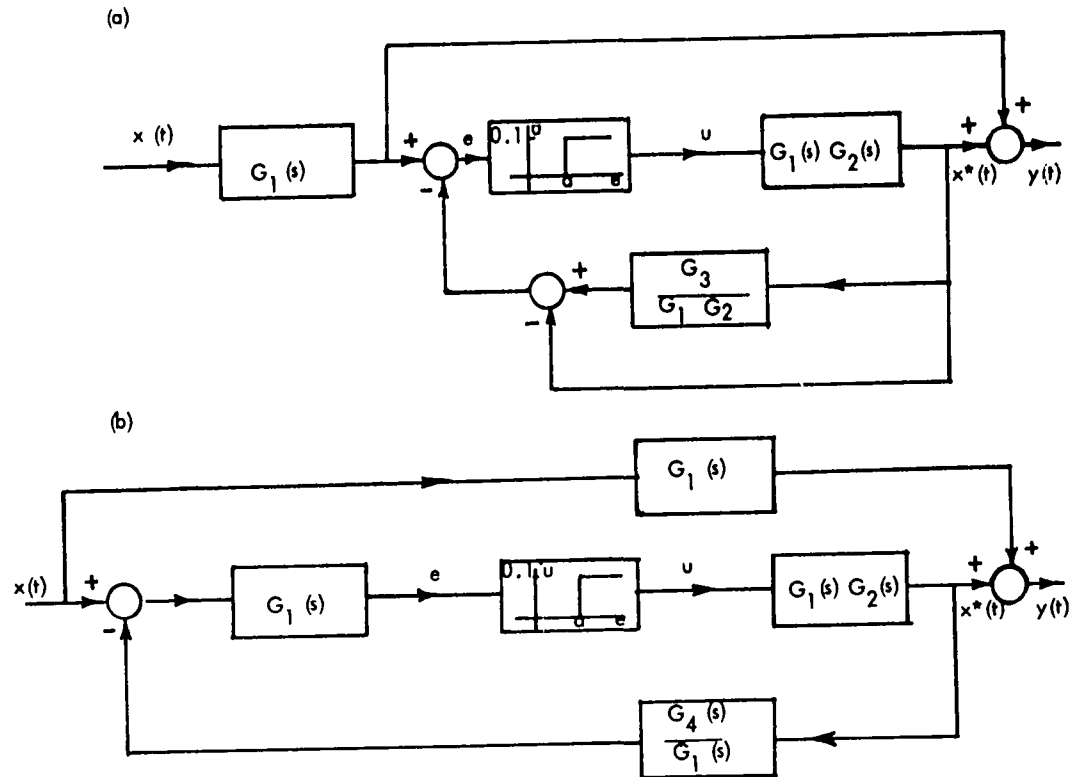
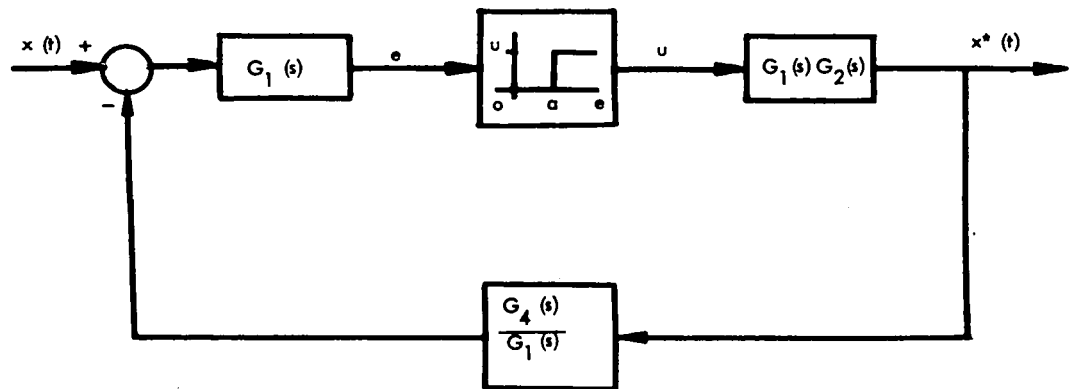
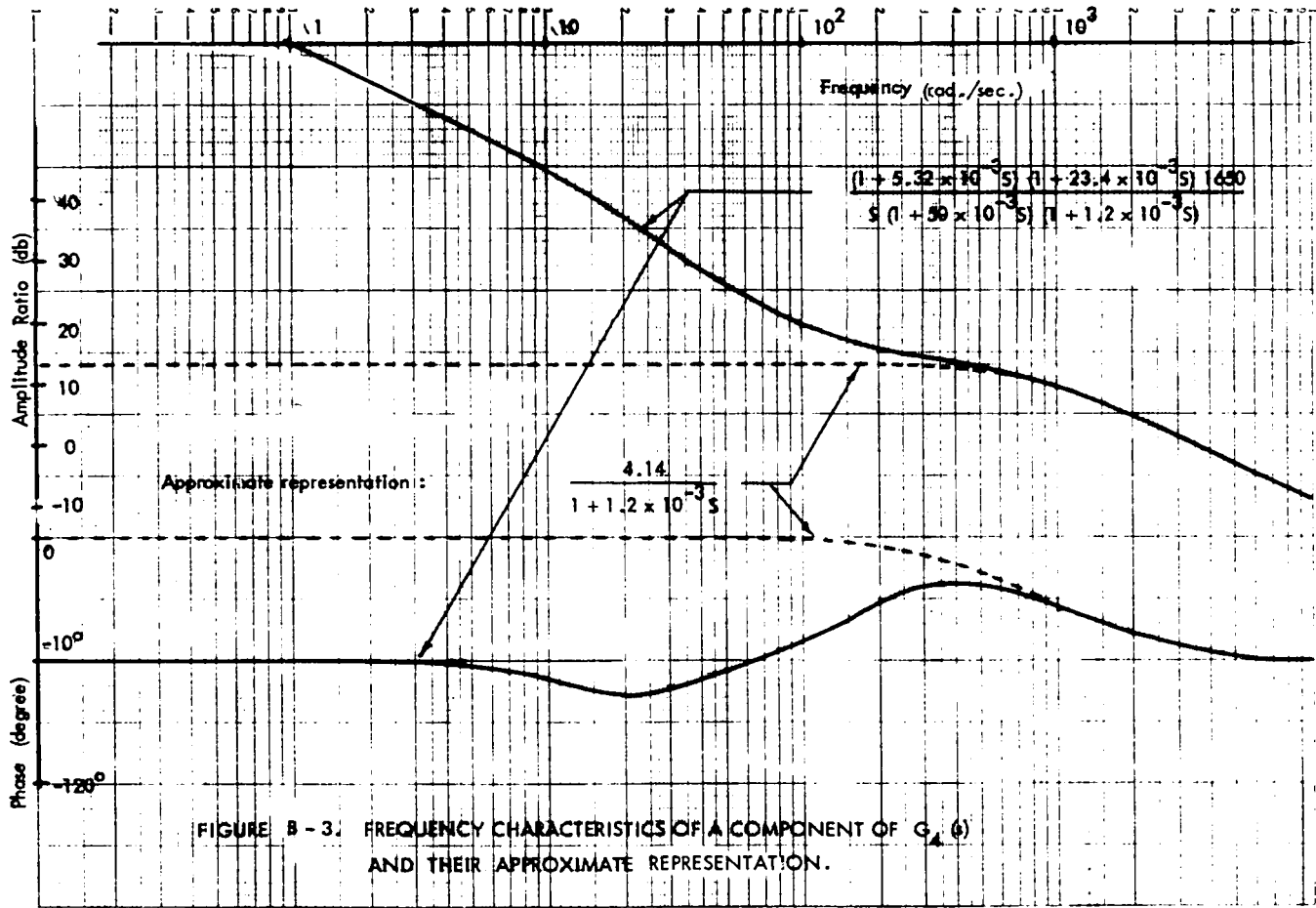


FIGURE B-2. EQUIVALENT BLOCK DIAGRAMS OF A NEURON MODEL.

SEMI-LOGARITHMIC 358-91  
 STIFFLE & ASSOCIATES  
 3075 15th Avenue S.W.



$$G_1(s) = \frac{5.5(1 + 0.05s)}{(1 + 0.022s)(1 + 0.0073s)}$$

$$G_2(s) = \frac{0.033s}{1 + 0.00033s}$$

$$G_4(s) = \frac{4.6(1 + 0.12 \times 10^{-3}s)}{1 + 1.2 \times 10^{-3}s}$$

FIGURE B - 4. A MODEL OF THE NEURAL ENCODER.

REFERENCES

1. Panter, P.F.: "Modulation, Noise, and Spectral Analysis", McGraw-Hill Book Company, 1965.
2. Schwartz, M., Bennett, W.R. and Stein, S. "Communication Systems and Techniques", McGraw-Hill Book Company, 1966.
3. Korn, G.A. and Korn, T.M. "Electronic Analogue and Hybrid Computers", McGraw-Hill Book Company, 1964.
4. Rochelle, R.W. Pulse Frequency Modulation, IRE Trans. Space Electronics and Telemetry, pp. 107-111 ; 1962.
5. Davidson, M., Joseph, H., and Zucker, N. Using Markerless Pulse Trains to Communicate, Electronics, pp. 89-91 ; November 21, 1958.
6. Pshenichnikov, A.M. Choice of Frequency Range for Industrial Pulse Frequency Telemetry System Devices, Automatika i Telemekhanika, Vol. 21, No. 4, pp. 525-529, (English translation : pp. 361-363) ; April, 1960.
7. Pozin, N.V. Concerning the Noise Stability of Pulse Frequency Telemetry, Automatika i Telemekhanika, Vol. 19, p. 968, (English translation : pp. 948-956) ; October, 1958.
8. Li, C.C. "Integral Pulse Frequency Modulated Control Systems". Ph.D. Dissertation, Northwestern University, Illinois, U.S.A. ; 1961.
9. Meyer, A.U. "Pulse Frequency Modulation and Its Effect in Feedback Systems", Ph.D. Dissertation, Northwestern University, Illinois, U.S.A. ; 1961.
10. Farrenkopf, R.L., Sabroff, A.E. and Wheeler, P.C. Integral Pulse Frequency On-Off Attitude Control, "Guidance and Control II, Progress in Astronautics and Aeronautics Series", Vol. 13, pp. 185-230, R.C. Langford and C.J. Mundo (Ed.), Academic Press, New York ; 1964.

11. Ciscato, D. and Mariani, L. On Increasing Sampling Efficiency by Adaptive Sampling, *IEEE Trans. Automatic Control*, p. 318 ; June, 1967.
12. Murphy, G. and West, K.L. The Use of Pulse Frequency Modulation for Adaptive Control, *Proc. of the N.E.C.*, Chicago, Illinois, Vol. 18, pp. 271-277 ; October 8, 1962.
13. Clark, J.P.C. "An Analysis of Pulse Frequency Modulated Control Systems", Ph.D. Thesis, University of Washington, U.S.A., 1965.
14. Onyshko, S. "Optimized Pulse Frequency Modulated Control Systems", Ph.D. Thesis, University of Washington, U.S.A. ; 1966 .
15. Pavlidis, T. and Jury, E.I. Analysis of a New Class of Pulse Frequency Modulated Feedback System, *IEEE Trans. Automatic Control*, pp.35-43 ; 1965.
16. Pavlidis, T. "Analysis and Synthesis of Pulse Frequency Modulation Feedback System", Ph.D. Thesis, University of California, Berkeley, California, U.S.A. ; 1964.
17. Jury, E.I. and Blanchard, J.G. A Nonlinear Discrete System Equivalence of Integral Pulse Frequency Modulation Systems, *IEEE Trans. Automatic Control*, Vol. AC-12, pp. 415-422, August 1967.
18. Blanchard, J.G., "Theory and Applications of Pulse Frequency Modulated Systems", Ph.D. Thesis, University of California, Berkeley, California, U.S.A. ; 1966.
19. Bombi, F. and Ciscato, D. Noise Effects in Integral Pulse Frequency Modulators, *Proc. IFAC Symposium on Pulse Rate and Pulse-Number Signals in Automatic Control*, Budapest, Hungary ; April, 1968.
20. Aida, S. Theory and Applications of Imictron : A Control Element having Mechanisms of a Living Neuron, Report of the Institute of Industrial Science, University of Tokyo, Japan , Vol. 17, No. 5 (Serial No. 112) ; March, 1967.

21. Pavlidis, T. A New Model for Simple Neural Nets and its Application in the Design of a Neural Oscillator, *Bull. Math. Biophysics*, 27 : 215-229 ; 1966.
22. Jones, R.W., Li, C.C., Meyer, A.U. and Pinter, R.B. Pulse Modulations in Physiological Systems, Phenomenological Aspects, *I.R.E. Trans. Bio-Med. Electronics*, pp. 56-67 ; January 1961.
23. Li, C.C. and Jones, R.W. Integral Pulse Frequency Modulated Control System, *Proc. 2nd. Congress of International Federation of Automatic Control*, Basle, Switzerland ; 1963.
24. Partridge, L.D. A Possible Source of Nerve Signal Distortion Arising in Pulse Rate Encoding of Signal, *J. Theoret. Biol.*, 11 : 257-281 ; 1966.
25. Partridge, L.D. Modification of Neural Output Signals by Muscles : A Frequency Response Study, *J. App. Physiol.*, 20 : 150-156 ; 1965.
26. Bayly, E.J. Spectral Analysis of Pulse Frequency Modulation in the Nervous System , *IEEE Trans. Bio-Med. Eng.*, Vol. BME-15, No. 4, pp.257-265.; October, 1968.
27. Goldberg, Harold. Report on Pulse Modulation, an unpublished Stromberg-Carlson Report, December 27, 1944. (See Reference 28).
28. Ross, A.E. Theoretical Study of Pulse Frequency Modulation, *Proc. I.R.E.* 37 : 1277-86 ; November, 1949.
29. Inose, H. and Yasuda, Y. A Unity Bit Coding Method by Negative Feedback, *Proc. IEEE*, pp. 1524-1535 ; November 1963.
30. Mishkin, E. and Braun, L., Jr. "Adaptive Control Systems". McGraw-Hill ; 1961.
31. C.R.C. Standard Mathematical Tables, 13<sup>th</sup> Ed., The Chemical Rubber Co. ; 1964.

32. Fitch, E. The Spectrum of Modulated Pulses, J. IEE, London, Vol. 94, Pt. 3A, pp. 556-564 ; 1947.
33. Seeley, S.W., Kimball, C.N. and Bargo, A.A. Generation and Detection of Frequency Modulated Waves, RCA Review, Vol. 6, pp. 269-286 ; 1941-1942.
34. Scroggie, M.G. Low Distortion FM Discriminator, Wireless World, pp. 158-162 ; April, 1956.
35. Millman, J. and Taub, H. "Pulse, Digital, and Switching Wave-forms", McGraw Hill Book Co. ; 1965.
36. Landee, R.W., Davis, D.C. and Albrecht, A.P. "Electronic Designers' Handbook", McGraw Hill Book Co. ; 1957.
37. Rader, C.M. and Gold, B. Digital Filter Design Techniques in the Frequency Domain, Proc. IEEE, pp. 149-171 ; February, 1967.
38. Wylie, C.R., Jr. "Advanced Engineering Mathematics"; 2nd, Ed. McGraw-Hill Book Co. ; 1960.
39. Erdelyi, A. From delta function to distributions, in "Modern Mathematics for Engineers", 2<sup>nd</sup> Series, E.F. Beckenback (Ed.), Chapter 1, p. 36, McGraw Hill Book Co. ; 1961.
40. Sokolnickoff, I.S. and Redheffer, R.M. "Mathematics of Physics and Modern Engineering", McGraw Hill Book Co. ; 1958.
41. Baghdady, E.J. Analog Modulation Systems, in "Lectures on Communication System Theory", E.J. Baghdady (Ed.), McGraw Hill Book Co. ; 1961.
42. Corrington, M.S. Variation of Bandwidth with Modulation Index in Frequency Modulation , Proc. IRE, pp. 1013-1020 ; 1947.

43. Giacoletto, L.J. Generalized Theory of Multitone Amplitude and Frequency Modulation, Proc. IRE, pp. 680-693 ; July, 1947.
44. Salvadori, M.G. and Schwarz, R.J. "Differential Equations in Engineering Problems", p. 304, Prentice Hall Book Co. ; 1954.
45. Morrill, C.D. Electronic Multipliers and Related Topics, in H.D. Huskey. and G.A. Korn , "Computer Handbook", McGraw Hill, New York ; 1962.
46. Maslav, A.A. Survey and Classification of Multiplying Devices, Automatika i Telemekhanika, VI. 21 ; October, 1960.
47. Monroe, A.J., "Digital Processes for Sampled Data Systems", John Wiley and Sons, Inc. ; 1962.
48. Mountcastle, V.B. The problem of sensing and the neural coding of sensory events, in "The Neurosciences". Ed. by G.C. Quanton, et al. The Rockefeller Univ. Press, New York ; 1967.
49. Perkel, D.H. and Bullock, T.H. Neural Coding. Neurosciences Research Program Bulletin, Vol. 6, No. 3, pp. 227-348.; December, 1968.
50. Ruch, T.C. and Patton, H.D. "Physiology and Biophysics", 19<sup>th</sup> Ed., W.B. Saunders Co. ; 1965.
51. Matthews, P.B.C. Muscle Spindles and Their Motor Control. Physiol. Rev. 44: 219-288 ; 1964.
52. Guyton, A.C. "Medical Physiology", 3rd.Ed., W.B. Saunders Co. ; 1966.
53. Poppele, R.E. and Terzuolo, C.A. Myotatic Reflex: Its Input-output Relations. Science 159:743-745 ; February 1968.
54. Maffei, L. Spatial and Temporal Averages in Retinal Channels, J. Neurophysiol, 31: 283-287 ; March, 1968.

55. Mendell, L.M. and Henneman, E. Terminals of Single Ia Fibers: Distribution with a Pool of 300 Homonymous Motor Neurons, *Science* 160: 96-98 ; April, 1968.
56. Rall, W. Branching Dendritic Trees and Motoneuron Membrane Sensitivity, *Exp. Neurol.* 1: 491-527 ; 1959.
57. Terzuolo, C.A. and Llinas, R. Distribution of Synaptic Inputs in the Spinal Motoneurone and Its Functional Significance. "Nobel Symp. I, Muscular Afferents and Motor Control", R. Granit (Ed.), John Wiley and Sons, N.Y., pp. 373-384 ; 1966.
58. Burke, R.E. Composite Nature of the Monosynaptic Excitatory Postsynaptic Potential, *J. Neurophysiol.* 30: 1114-1137 ; September, 1967.
59. Rall, W. Theoretical Significance of Dendritic Trees for Neuronal Input-output Relations, "Neural Theory and Modeling", R.F. Reiss, (Ed.), Stanford University Press ; 1964.
60. Rall, W., Burke, R.E., Smith, T.G., Nelson, P.G. and Frank, K. Dendritic Location of Synapses and Possible Mechanisms for the Monosynaptic EPSP in Motoneurons, *J. Neurophysiol.* 30: 1169-1193 ; September, 1967.
61. Lippold, O.C.J., Nichols, J.G. and Redfeam, J.W.T. Electrical and Mechanical Factors in the Adaptation of a Mammalian Muscle Spindle, *J. Physiol.* 153: 209-217 ; 1960.
62. Edwards, C. Changes in the Discharge from a Muscle Spindle Produced by Electrotonus in the Sensory Nerve, *J. Physiol.* 127: 636-640.
63. Katz, B. Depolarization of Sensory Terminals and the Initiation of Impulses in the Muscle Spindle, *J. Physiol.* 111: 261-282 ; 1950.

64. Shepherd, G.M. and Ottoson, D. Response of the Isolated Muscle Spindle to Different Rates of Stretching, "Sensory Receptors", Cold Spring Harbor Symp. on Quantitative Biology, Vol. 30 ; 1965.
65. Ottoson, D. and Shepherd, G.M. Receptor Potentials and Impulse Generation in Isolated Spindle during Controlled Extension, "Sensory Receptors", Cold Spring Harbor Symp. on Quantitative Biology, Vol. 30 ; 1965.
66. Harmon, L.D. and Lewis, E.R. Neural Modeling, *Physiol. Rev.* 46: 513-591 ; 1966.
67. Roberge, F.A. "A Neuron Model for the Study of Small Neuron Pools", Ph.D. Thesis, Department of Electrical Engineering, McGill University, Canada ; 1964.
68. Devanandan, M.S. and Eccles, R.M. Single Motor Units of Mammalian Muscle, *J. Physiol.* 178: 359-367 ; 1965.
69. Granit, R. (Ed.), "Nobel Symposium I, Muscular Afferents and Motor Control", John Wiley and Sons, New York ; 1966.
70. Pringle, J.W.S. Models of Muscle, in "Models and Analogues in Biology". Symp. Soc. Exp. Biol. 14: 41-68 ; 1960.
71. Houk, J.C., Sanchez, V. and Wells, B.F. Frequency Response of a Spindle Receptor, Quarterly Progress Report No. 67, Res. Lab. of Electronics, M.I.T., pp. 223-227 ; 1962.
72. Lennerstrand, G. and Thoden, U. Dynamic Analysis of Muscle Spindle Endings in the Cat Using Length Changes of Different Length-time Relations, *Acta Physiol. Scand.* 73, pp. 234-250 ; 1968.
73. Lennerstrand, G. Position and Velocity Sensitivity of Muscle Spindles in the Cat. I, Primary and Secondary Engings Deprived of Fusimotor Activation, *Acta Physiol. Scand.* 73, pp. 281-299 ; 1968.

74. Lennerstrand, G. and Thoden, U. Position and Velocity Sensitivity of Muscle Spindles in the Cat. II. Dynamic Fusimotor Single-fibre Activation of Primary Endings, *Acta Physiol. Scand.* 74, pp. 16-29 ; 1968.
75. Lennerstrand, G. and Thoden, U. Position and Velocity Sensitivity of Muscle Spindles in the Cat. III. Static Fusimotor Single-fibre Activation of Primary and Secondary Engings, *Acta Physiol. Scand.* 74 , pp. 30-49 ; 1968.
76. Lennerstrand, G. Position and Velocity Sensitivity of Muscle Spindles in the Cat. IV. Interaction Between Two Fusimotor Fibres Converging on the Same Spindle Ending, *Acta Physiol. Scand.* 74, .pp. 257-273 ; 1968.
77. Andersson, B.F., Lennerstarnd, G. and Thoden, U. Response Characteristics of Muscle Spindle Endings at Constant Length to Variations in Fusimotor Activation, *Acta Physiol. Scand.* 74, pp. 301-318 ; 1968.
78. Papoulis, A. "Probability, Random Variables, and Stochastic Processes", McGraw Hill Book Co. ; 1965.
79. Carpenter, D.O. and Henneman, E. A Relation Between the Threshold of Stretch Receptor in Stretched Muscle and the Diameter of Their Axons, *J. Neurophysiol.* 29: 353-368 ; 1966.
80. Hunt, C.C. Relation of Function to Diameter in Afferent Fibers of Muscle Nerves, *J. Gen. Physiol.* 38: 117-131 ; 1955.
81. Bennett, C.A. and Franklin, N.L. "Statistical Analysis in Chemistry and the Chemical Industry", p. 90, John Wiley and Sons ; 1954.
82. Papoulis, A. "The Fourier Integral and Its Application", McGraw Hill Book Co. ; 1962 .

83. Paynter, H.M. On an Analogy Between Stochastic Processes and Monotone Dynamic Systems, Proc. Conf. on Control Technology, Heidelberg, Germany ; September, 1956.
84. Leksell, L. The Action Potential and Excitatory Effects of the Small Ventral Root Fibres to Skeletal Muscle, Acta Physiol. Scand. 10, Suppl. 31 ; 1965.
85. Williams, W.J. Bio-cybernetic Aspects of Latency Dispersion in Peripheral Nerve Bundles, Record of the 1968 IEEE Systems Science and Cybernetics Conf., San Francisco ; 1968.
86. Goodman, T.P. Theory and Application of a Tapered Electronic Delay-line Synthesizer, in "Automatic and Remote Control", Proc. 1<sup>st</sup> IFAC, Moscow, 1960 ; Ed. J.F. Coales, et.al. Butterworths, London, Vol. III, pp. 102-108 ; 1961.
87. Zadeh, L.A. and Desoer, C.A. "Linear System Theory", McGraw Hill Book Co., p. 447 ; 1963.
88. Widrow, B. "Statistical Analysis of Amplitude Quantized Sampled-data Systems," Tech. Report No. 2103-1, Stanford Electronics Lab.; Stanford Univ., California, U.S.A. ; May, 1960.
89. Kosyakin, A.A. The Statistical Theory of Amplitude Quantization, Automation and Remote Control, (Avtomatika i Telemekhanika) Vol. 22, No. 6, pp. 624-630 ; June, 1961.